

**A systems biology approach for investigating
oral squamous cell carcinoma (OSCC)**

**A thesis submitted to the University of
Manchester for the degree of**

PhD in Chemistry

**In the Faculty of Chemical Engineering and
Analytical Sciences**

2012

Paul Wilcock

School of Chemistry

Table of Contents

Table of Contents	1
List of Figures.....	6
List of Tables	8
Abstract	9
Declaration	10
Copyright Statement.....	12
Acknowledgments	13
List of Abbreviations	14
Chapter 1: Introduction	22
1.2 Introduction	23
1.2.1 OSCC and its Incidence.....	23
1.2.1.1 Genomic factors involved in OSCC	24
1.2.1.2 Phosphodiesterase 4D	25
1.2.2 Environmental effects	34
1.2.2.1 The Warburg effect.....	34
1.2.2.2 The role of the transcription factors HIF-1 and CREB.....	41
1.2.2.3 Mimicking the effects of hypoxia using cobalt chloride	44
1.2.2.4 The glutamate shunt.....	49
1.2.3 Systems biology.....	52
1.2.3.1 Systems biology for advancing cancer knowledge	52
1.2.3.2 High throughput technology and the ‘omics’ revolution.....	53
1.2.3.2.1 Metabolomics	55

1.2.3.2.2 Liquid chromatography mass spectrometry and gas chromatography mass spectrometry	57
1.2.3.2.3 Chemometrics	61
1.2.3.2.3.1 Principal component analysis.....	61
1.2.3.2.3.2 Principal component-discriminant function analysis	62
1.2.3.2.3.3 Parallel factor analysis	62
1.2.3.2.3.4 Clustergram analysis.....	62
1.2.3.3 Modelling in cancer.....	63
1.2.4 Aims and objectives of the project	64
1.3 References.....	65

Chapter 2: A metabolomics investigation into the suitability of cobalt chloride as a substitute for hypoxia in eukaryotic cells

2.1 Abstract.....	93
2.2 Introduction	93
2.3 Materials and Methods.....	96
2.3.1 Cell culture of hTERT cells.	96
2.3.2 Quantification of the HIF-1 α protein using ELISA.	97
2.3.3 Assessment of ATP	97
2.3.4 Condition exposure and metabolite extraction.	98
2.3.5 GC-MS analysis for metabolite detection.....	98
2.3.6 UHPLC-MS analysis for metabolite detection.	99
2.3.7 GC-MS and UHPLC-MS metabolite identification.....	99
2.3.8 Data processing and data analysis.	100
2.4 Results and Discussion.....	103
2.4.2 Assessment of ATP.	104

2.4.3 Assessment of lactic acid.....	106
2.4.4 PARAFAC of central metabolism metabolites from GC-MS.....	106
2.4.5 Clustergram of GC-MS metabolites.	108
2.4.6 PC-DFA of GC-MS, LC-MS positive and LC-MS negative data.	110
2.4.7 Box and whisker plots - typical metabolite behaviour.....	113
2.5 Concluding remarks	115
2.6 Acknowledgements	116
2.7 References.....	117
2.8 Supplementary Information	124
Chapeter 3: The phenotypic and metabolic effects of phosphodiesterase type 4D (PDE4D) knockdown in the oral squamous cell carcinoma (OSCC) cell line BicR16.....	136
3.1 Abstract.....	137
3.2 Introduction	137
3.3 Materials and Methods.....	139
3.3.1 Cell culture.....	139
3.3.2 Control and target shRNAs.	140
3.3.3 Transformations, maxi-prep and quality assurance of shRNAs.	140
3.3.4 Puromycin kill curve for BicR16 cells.	140
3.3.5 KD of PDE4D in BicR16 cells.....	140
3.3.6 Taqman design for qPCR.	141
3.3.7 Reverse-transcriptase PCR (RT-PCR).	141
3.3.8 Taqman gene expression assay for relative PDE4D quantification.	142
3.3.9 Verification of shRNA insert through end point PCR.....	142
3.3.10 Efficiency of the PDE4D KDs verified through Western blotting....	142

3.3.11 MTT assay to assess cell proliferation.	143
3.3.12 Clonogenic assay to assess radiation resistance.....	143
3.3.13 Scratch assay to assess migration.....	143
3.3.14 Metabolic analysis of PDE4D KD using GC-MS.	143
3.3.15 Data processing and data analysis.	144
3.4 Results	145
3.4.1 Stable KD of PDE4D in BicR16 cells.	145
3.4.2 PDE4D KD increases proliferation, migration and ability to withstand radiation.	146
3.4.3 PDE4D KD causes a metabolic reconfiguration.....	148
3.4.4 The combined effects of CREB and HIF-1 on central metabolism..	150
3.5 Discussion.....	152
3.6 Concluding Remarks.....	156
3.7 Acknowledgements.....	156
3.8 References.....	157
3.9 Supplementary Information	165
Chapter 4: Kinetic model of cellular metabolism and the affects of Hypoxia Inducible Factor 1 (HIF-1).....	171
4.1 Abstract.....	172
4.2 Introduction	172
4.3 Materials & Methods	174
4.3.1 Constructing the model.	174
4.3.2 Rate laws of the model.	184
4.3.3 Model assumptions.	184
4.3.4 Parameter estimation.....	184

4.3.5 Model optimisation.....	185
4.3.6 Production of the hypoxic state.....	186
4.3.7 Model validation using concentrations and V_{max} values.....	187
4.3.8 Model validation though flux and steady state analyses and comparison of experimental data and data from the literature.....	187
4.3.9 Fluctuation of external glucose, glutamine and sensitivity analysis.	188
4.4 Results and Discussion.....	189
4.4.1 Time course of the models post optimisation.....	189
4.4.2 Optimisation – regular start values vs. random start values.....	191
4.4.3 Comparison of initial and steady state concentrations.....	192
4.4.4 Model Validation.....	194
4.4.5 The predicted effects from altering external glucose concentrations on cellular metabolism.....	198
4.4.6 The predicted effects from altering glutamine concentrations on cellular metabolism.....	201
4.4.7 Sensitivity analysis to determine potential target intermediates.....	203
4.5 Concluding Remarks.....	206
4.6 References.....	207
4.7 Supplementary Information.....	210
Chapter 5:.....	213
General Discussion and Conclusions.....	213
5.1 General Discussion.....	214
5.2 Concluding Remarks.....	224
5.3 References.....	225

List of Figures

Figure 1.1 Examples of the two varying types of precursor oral lesions (POLs)	24
Figure 1.2 A schematic illustrating the various forms of Phosphodiesterases (PDEs).....	27
Figure 1.3 HIF dependent regulation of transcription.....	42
Figure 1.4 HIF independent regulation of transcription.....	43
Figure 1.5 HIF-1 α Degradation During Normoxia.	45
Figure 1.6 Activated HIF-1 α During Hypoxia.	47
Figure 1.7 CoCl ₂ as a Hypoxia Mimicker.	48
Figure 1.8 Glutaminolysis Modifications in Cancer Cells	50
Figure 1.9 General flow chart for Mass Spectrometry	59
Figure 2.1 Total HIF-1 α concentrations determined through ELISA	103
Figure 2.2 GC-MS PARAFAC - Central Metabolism Only	107
Figure 2.3 Clustergram of Correlated GC-MS Metabolites for CoCl ₂ Analysis	109
Figure 2.4 PC-DFA of (a) GC-MS, (b) LC-MS negative and (c) LC-MS positive data	111
Figure 2.5 Box and whisker plots displaying typical behaviour of metabolites	114
Figure.3.1 End Point PCR to Verify the Incorporation of the shRNA	145
Figure 3.2 Relative Quantification of Gene Expression for total PDE4D in Stably Transfected BicR16 Cells	146
Figure 3.3 Phenotypic assays comparing stable PDE4D KDs with control and WT BicR16 cells	148
Figure 3.4 Preliminary GC-MS PCA scores and loadings plots. A) PCA scores plot highlighting separation of the WT/controls and the PDE4D KD Samples	149
Figure 3.5 Full GC-MS PCA scores and loadings plots. A) PCA scores plot showing separation of the PDE4D KD and control cells under hypoxia or normoxia.....	151

Figure 4.1 Schematic of the mathematical model comprising of glycolysis, the TCA cycle, glutaminolysis and cell energetics.....	176
Figure 4.2 Time course of the models	190
Figure 4.3 Model validation using behavioural aspects from the literature	198
Figure 4.4 The predicted effects of altering external glucose concentration on central metabolism under normoxia and hypoxia	199
Figure 4.5 The model predicted effects of altering glutamine concentration on central metabolism under normoxia and hypoxia	202
Figure 4.6 Sensitivity analysis of the normoxic model	204
Figure 4.7 Sensitivity analysis of the hypoxic model.....	205

List of Tables

Table 1.1 Common terminologies utilised in metabolomics.	56
Table 4.1 Metabolites and initial concentrations	177
Table 4.2 Model Reactions	180
Table 4.3 Parameter Values of the Model.....	183
Table 4.4 Parameters and values used in the parameter estimation function	185
Table 4.5 Steady state concentrations used to create a hypoxic state in the model.....	186
Table 4.6 Comparison of parameter estimation values from regular start values and random start values for the normoxic and hypoxic models.....	192
Table 4.7 Modelling of initial and steady state concentrations of metabolites	193
Table 4.8 Comparison of normoxic and hypoxic fluxes.....	196
Table 5.1 Summary of central metabolite alterations: PDE4D KD, hypoxia exposure, combined KD and hypoxia exposure and CoCl ₂ exposure	218

Abstract

A systems biology approach was adopted in order to assess various aspects of the disease oral squamous cell carcinoma. Three main aims were addressed; assess the ability of CoCl_2 to mimic the hypoxic response in a eukaryotic cell line, assess the role of PDE4D in oral squamous cell carcinoma (OSCC) and the construction of a normoxic/hypoxic mathematical model to identify therapeutic targets.

Cancer cells often acquire a revised metabolism which aids in initiation, survival and progression of the tumour. This is predominantly due to the transcription factor HIF-1 which is activated under hypoxic conditions. Certain compounds such as cobalt chloride (CoCl_2) have been used extensively to inhibit the degradation of HIF-1 α and simulate hypoxia. CoCl_2 is likely to have off-target effects on metabolism; these effects were examined when exposing human telomerase reverse transcriptase (hTERT) cells to 100 μM CoCl_2 . Gas chromatography-mass spectrometry (GC-MS), liquid chromatography-mass spectrometry (LC-MS) based metabolomics were utilised in combination with ELISA assays for HIF-1 α and ATP. Central metabolism was accurately mimicked when hTERT cells were subjected to 100 μM CoCl_2 , however; it was apparent that this concentration of CoCl_2 does not induce an equal extent of hypoxia as 1% oxygen. A number of off-target effects of CoCl_2 were observed in secondary metabolism, specifically in lipids and fatty acids. In conclusion, CoCl_2 should be used with caution as a hypoxic mimicker with the caveat that interpretation of results should be restricted to its effects on central metabolism.

The transcription factor CREB has the ability to regulate approximately 4000 genes, a number of which are associated with cancer initiation and progression. Cyclic adenosine monophosphate (cAMP) is required to activate CREB and is partially regulated through its degradation via the enzyme phosphodiesterase type 4D (PDE4D). A homozygous deletion of PDE4D has been associated with OSCC; however; the exact consequence of this deletion has not been fully

elucidated. PDE4D was knocked down in the OSCC cell line BicR16 and cellular proliferation, migration, resistance to ionising radiation and central metabolism was investigated using MTT, scratch, clonogenic and GC-MS, respectively. The knockdown resulted in an increase in proliferation, migration and radiation resistance suggesting the role of PDE4D as a TSG. Amino acids, cholesterol, fatty acids, carbohydrates and TCA intermediates were found to be altered in concentration.

A mathematical model of glycolysis, TCA and glutaminolysis under normoxia and hypoxia was constructed through the amalgamation of two established models from the literature. New reactions, parameters and metabolite concentrations were added and unnecessary entities were deleted. COmplex PATHway Simulator (COPASI) was utilised to construct the model before validating the model using experimental data from the literature and steady state and flux analyses. Sensitivity analysis and a reduction in external glucose and glutamine were mimicked and the alterations in hypoxic and normoxic metabolism analysed. The reactions vCSII, vGS, vPGK and vGII were identified as potential therapeutic targets which may affect metabolism in hypoxia only. However, certain validation methods proved unsuccessful and hence the model requires further work before attempting the analyses again.

Declaration

I, Paul Wilcock, declare that no portion of the work referred to in the dissertation has been submitted in support of an application for another degree or qualification of this or any other university or other institute of learning.

Copyright Statement

i. The author of this thesis (including any appendices and/or schedules to this thesis) owns any copyright in it (the “Copyright”) and s/he has given The University of Manchester the right to use such Copyright for any administrative, promotional, educational and/or teaching purposes.

ii. Copies of this thesis, either in full or in extracts, may be made **only** in accordance with the regulations of the John Rylands University Library of Manchester. Details of these regulations may be obtained from the Librarian. This page must form part of any such copies made.

iii. The ownership of any patents, designs, trademarks and any and all other intellectual property rights except for the Copyright (the “Intellectual Property Rights”) and any reproductions of copyright works, for example graphs and tables (“Reproductions”), which may be described in this thesis, may not be owned by the author and may be owned by third parties. Such Intellectual Property Rights and Reproductions cannot and must not be made available for use without the prior written permission of the owner(s) of the relevant Intellectual Property Rights and/or Reproductions.

iv. Further information on the conditions under which disclosure, publication and exploitation of this thesis, the Copyright and any Intellectual Property Rights and/or Reproductions described in it may take place is available from the Head of School of (*insert name of school*) (or the Vice-President) and the Dean of the Faculty of Life Sciences, for Faculty of Life Sciences’ candidates.

Acknowledgments

I would like to thank my supervisors Prof Roy Goodacre, Prof Nalin Thakker, Dr Ian Hampson, Dr Lynne Hampson and Prof Pedro Mendes for their constant advice and support throughout my work. I would also like to thank Dr William Allwood for running the mass spectrometry samples and his advice and support and Dr Susan Greenwood for the use of her hypoxic chamber. Furthermore, I thank Dr Gavin Batman and Thomas Walker for their practical advice and support, Dr David Wedge, Dr Elon Correa and Dr Andrew Vaughan for their aid in data processing and analysis and also Dr Xiaotong He for his expertise advice. Finally, I would like to show my appreciation to the BBSRC and the EPSRC for their financial support throughout my PhD along with the DTC for Systems Biology at the University of Manchester and my family for their continued support throughout.

List of Abbreviations

2PG/3PG	2-Phosphoglyceric acid/3-Phosphoglyceric acid
5'AMP	5 [Prime] adenosine mono phosphate
5'GMP	5 [Prime] guanosine mono phosphate
AC	Adenylate cyclase
ADP	Adenosine diphosphate
AKT	Protein kinase B
α -KG	[alpha]-ketoglutaric acid
AMP	Adenosine monophosphate
AMPK	AMP activated protein kinase
ATP	Adenosine triphosphate
β 2M	Beta-2-microglobulin
Bak	Bcl-2 homologous antagonist/killer
Bax	Bcl-2 associated X protein
Bcl-2	B-cell lymphoma 2
cAMP	Cyclic adenosine mono phosphate
CBP	CREB binding protein
CCA	Canonical correlation analysis
CCN1/CYR61	Cyclin-A2/cysteine-rich angiogenic inducer 61
CDKN2A	Cyclin-dependent kinase inhibitor 2A

cDNA	Copy deoxyribose nucleic acid
CE	Capillary electrophoresis
cGMP	Cyclic guanosine mono phosphate
C-MYC	Cellular myelocytomatosis
CNA	Copy number alteration
CoCl ₂	Cobalt chloride
COPASI	Complex pathway simulator
COPD	Chronic obstructive pulmonary disease
COSMIC	Catalogue of somatic mutations in cancer
COX	Cytochrome C oxidase
Cr	Creatine
CRE	cAMP response element
CREB	cAMP response element binding
CSMD1	CUB and sushi domain 1
DAG	Diacylglycerol
DF	Discriminant function
DFO	Desferrioxamine
DHAP	Dihydroxyacetone phosphate
DMEM	Dulbecco's modified eagle medium
DNA	Deoxyribose nucleic acid

DPG	Diphosphoglycerate
EAC	Esophageal adenocarcinoma
EAC	Oesophageal adenocarcinoma
ELISA	Enzyme linked immunosorbent assay
EMSC	Extended multiplicative signal correction
ERK	Extracellular signal regulated kinase
ESI	Electrospray ionisation
F ₁ , 6P ₂	Fructose-1-6-bisphosphate
F ₂ , 6P ₂	Fructose-2-6-bisphosphate
F6P	Fructose 6-phosphate
FBS	Foetal bovine serum
FDG-PET	18F-2-fluorodeoxyglucose - positron emission tomography
FDP	Fructose diphosphate
FIH	Factor inhibiting HIF
FT-ICR-MS	Fourier transform ion cyclotron resonance mass spectrometry
G6P	Glucose 6-phosphate
GA3P	Glyceraldehyde 3-phosphate
GAPDH	Glyceraldehyde 3-phosphate dehydrogenase
GC	Gas chromatography
GLUT	Glucose transporter

GMD	Max Plank Institute molecular plant physiology database
GMP	Guanosine mono phosphate
HAP	Hypoxia associated protein
HARBS	High affinity rolipram binding site
HD	Homozygous deletion
HEPES	4-(2-hydroxyethyl)-1-piperazineethanesulfonic acid
HIF-1 α /2 α	Hypoxic inducible factor type 1 [alpha] / type 2 [alpha]
HK	Hexokinase
HNSCC	Head and neck squamous cell carcinoma
HPLC	High performance liquid chromatography
HRE	Hypoxia response element
hTERT	Human telomerase reverse transcriptase
IAP2	Inhibitor of apoptosis 2
IMP	Inosine monophosphate
iNOS	Inducible nitric oxide synthase
IS1/2	Internal standard 1/2
KD	Knockdown
KEGG	Kyoto encyclopaedia of genes and genomes
LARBS	Low affinity rolipram binding site
LC	Liquid chromatography

LDHA	Lactate dehydrogenase A
LIT	Linear ion trap
LR	Linking region
LSCC	Larynx squamous cell carcinoma
LTQ	Linear trap quadrupole
MALDI	Matrix-assisted laser desorption/ionization
MAPK	Mitogen Activated Protein Kinase
MATLAB	Matrix laboratory
MDM2	Murine double minute
MeOH	Methanol
MIAME	Minimum information about a microarray experiment
MIAPE	Minimum information about a protein experiment
MIF	Migration inhibitory factor
mRNA	Messenger ribose nucleic acid
MS	Mass spectrometry
MSI	Metabolomics standards initiative
mTOR	Mammalian target of rapamycin
MTT	(3-(4,5-Dimethylthiazol-2-yl)-2,5-diphenyltetrazolium bromide
NAD ⁺	Nicotinamide adenine dinucleotide
NADH	Nicotinamide adenine dinucleotide (reduced)

NADP+	Nicotinamide adenine dinucleotide phosphate
NADPH	Nicotinamide adenine dinucleotide phosphate (reduced)
NIPALS	Non-linear iterative partial least squares
NO	Nitric oxide
NSLCC	Non small cell lung cancer
OAA	Oxaloacetic acid
OD	Optical density
ODD	Oxygen dependent degradation
OMM	Outer mitochondrial membrane
OSCC	Oral squamous cell carcinoma
OTSCC	Oral tongue squamous cell carcinoma
PA	Monoacyl-glycerophosphates
PARAFAC	Parallel factor analysis
PBS	Phosphate buffered saline
PC	Principal component
PC	Phosphocholine
PCA	Principal component analysis
PC-DFA	Principal component - discriminant function analysis
PCR	Polymerase chain reaction
PCr	Phosphocreatine

P-CREB	Phosphorylated cAMP response element binding
PDE(4D)	Phosphodiesterase(4D)
PDH	Pyruvate dehydrogenase
PDK	Pyruvate dehydrogenase kinase
PEP	Phosphoenolpyruvic acid
PFK	Phosphofructokinase
PHD	Prolyl hydroxylase
PI3K	Phosphatidylinositol 3 kinase
PK	Pyruvate kinase
PKA	Protein kinase A
PLS	Partial least squares
POL	Precursor oral lesion
PRPP	Phosphoribosyl pyrophosphate
PVDF	Polyvinylidene fluoride
pVHL	Product of von hippel-lindau
Q	Quadrupole
qPCR	Quantitative polymerase chain reaction
RAS	Rat sarcoma viral oncogene homolog
RD	Random decamers
RFU	Relative fluorescence units

RNA	Ribose nucleic acid
RNase	Ribonuclease
ROS	Reactive oxygen species
RT-PCR	Reverse transcriptase - polymerase chain reaction
RUNX	Runt-related transcription factor
SCLC	Small cell lung carcinoma
SFM	Serum free medium
shRNA	Short hairpin ribose nucleic acid
TCA	Tricarboxylic acid cycle
TEV	Total explained variance
TF	Transcription factor
TIGAR	TP53 induced glycolysis and apoptosis regulator
TOF	Time of flight
TS/TSG	Tumor suppressor/tumor suppressor gene
UCR	Upstream conserved region
UHPLC	Ultra high performance liquid chromatography
VDAC	Voltage dependent anion channel
VEGF	Vascular endothelial growth factor
VHL	Von hippel-lindau
WT	Wild-type

Chapter 1:

Introduction

1.2 Introduction

1.2.1 OSCC and its Incidence

Oral squamous cell carcinoma (OSCC) is the sixth most common cancer in the United States of America (Park *et al.*, 2009) and worldwide accounts for around 275,000 new cases and >120,000 deaths per annum (Kujan *et al.*, 2006). Hence, it is more common than lymphoma, malignant melanoma and metastatic neoplasms (of liver, lung, breast, etc) and accounts for ~3% of total cancer cases worldwide (Scully & Felix, 2006). Current prognosis is poor with a 5 year survival rate of ~50% and has remained at a constant level for the past 30 years (Park *et al.*, 2006). Both incidence and mortality rates are increasing (Kujan *et al.*, 2005), which in Western societies is a direct impact of modern luxuries such as tobacco and alcohol (Lee *et al.*, 2007).

Early diagnosis is paramount to a healthy prognosis (Liu *et al.*, 2009). Fedele (2009) estimated that 40,000 deaths may be prevented if detection of the disorder occurs during the early stages of the disease and therapeutics such as surgery and radiation are administered soon thereafter.

OSCC falls into a larger category known as head and neck squamous cell carcinomas (HNSCCs). This collection constitutes all squamous carcinomas of the oral cavity, larynx, pharynx and oesophagus (Guha *et al.*, 2007) of which OSCC is the most common (da Silveria *et al.*, 2008). Communally, HNSCC accounts for approximately 10% of all newly diagnosed cases of cancer globally (Guha *et al.*, 2007). This bleak outlook for OSCC is the rationale which justifies further investigation.

OSCC is characterised by a cancerous tissue growth of the epithelial cells of the oral cavity which show signs of squamous cell differentiation. This disorder is brought about by an array of genomic abnormalities which may have developed over a period of time (Sparano *et al.*, 2006). It is well documented that the vast majority of all OSCCs are preceded by the formation of precursor oral lesions (POLs) (Fedele, 2009). POLs are visible disfigurement within the

oral cavity of leukoplakia (white) or erythroplakia (red) patches (Kujan *et al.*, 2006; Roz *et al.*, 1996) (see Figure 1.1). It is estimated that between 3-6% of POLs develop into OSCCs but this is largely dependent on various factors including size of POL, type of POL and the extent of the dysplasia (Roz *et al.*, 1996).

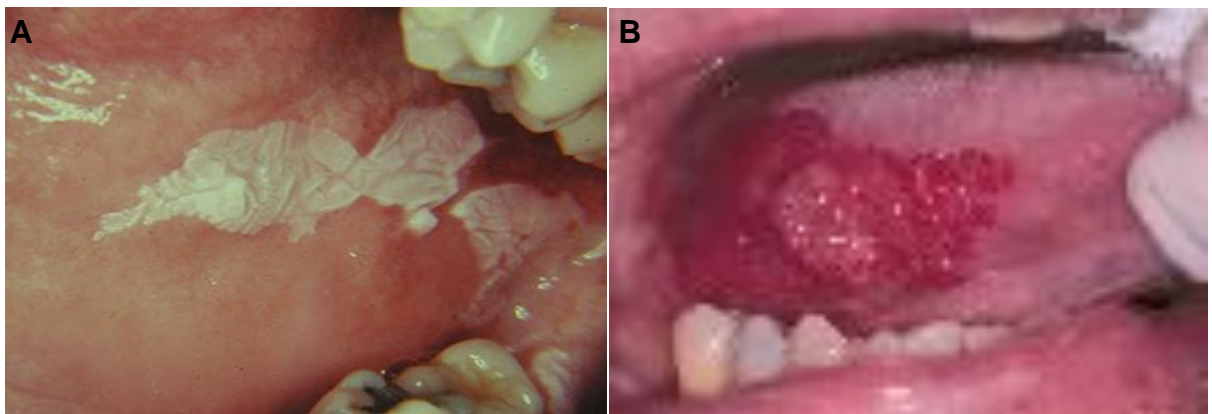


Figure 1.1 Examples of the two varying types of precursor oral lesions (POLs). (A) A photograph of a leukoplakia (white) disfigurement of the oral cavity. (B) A photograph of erythroplakia (red) disfigurement of the oral cavity.

1.2.1.1 Genomic Factors Involved in OSCC

Cancer, including that of OSCC, is a complex disease (Gath & Brakenhoff, 1999; Kato *et al.*, 2006) which by definition comprises a multitude of factors, originating from both genetic and environmental means, resulting in the onset of the disorder (Johnson and Todd, 2000). There is an abundance of genomic factors in the literature which are believed to be associated with OSCC including *Cub and Sushi Multiple Domain 1 (CSMD1)* (Baldwin *et al.*, 2005; Sparano *et al.*, 2005; Sparano *et al.*, 2006; Toomes *et al.*, 2003), *Cyclin Dependent Kinase 2A (CDKN2A)* – which encodes the proteins $p16^{INK4A}$ and $p19^{ARF}$ (Kato *et al.*, 2006; Ohta *et al.*, 2009; Wu *et al.*, 1999), *CyclinD1* (Baldwin *et al.*, 2005; Matta *et al.*, 2007) but to name a few. This list is by no means complete and not all factors are currently known. One gene which is not included in this list, but has potential to be included, is that of *phosphodiesterase type 4D (PDE4D)* and is discussed below.

1.2.1.2 Phosphodiesterase 4D (PDE4D)

The PDEs (phosphodiesterases) are a relatively large family of enzymes which are involved in degrading cAMP (cyclic adenosine monophosphate) to 5'AMP and cGMP (cyclic guanosine monophosphate) to 5'GMP (Ong *et al.*, 2009). The PDEs mode of function is via cleaving the phosphodiester bond of the nucleic acids. cAMP and cGMP are nucleotides which operate as secondary messengers within the cell (Houslay & Adams, 2003). They have a number of essential roles within the cell including gene expression, the cell cycle, cytoskeletal function, metabolism and proliferation (McCahill *et al.*, 2008). cAMP is produced from ATP (via the enzyme adenylate cyclase (AC)) at the plasma membrane of the cell (McCahill *et al.*, 2008) and the concentration of this and cGMP are under strict regulation via the PDEs (Lugnier, 2006). The only method of reducing cAMP concentration in the cell is via its degradation utilising PDEs (Houslay & Adams, 2003).

The PDE super-family constitutes of 11 members (Huang *et al.*, 2001) with an associated 25 known PDE genes (Ong *et al.*, 2009) with 50 different PDE products which may be formed via alternative splicing (Lugnier, 2006). The nomenclature of PDEs are based on their varying substrates (e.g. cAMP), kinetics, localisation, tissue distribution, allosteric regulation, etc (Beavo, 1995; Pyne & Furman, 2003).

The sub-family PDE4 is cAMP specific (Houslay & Baillie, 2005; Huang *et al.*, 2001) and is insensitive to cGMP (Lugnier, 2006). This family is of vital importance to cAMP signalling and compartmentalisation within the cell (Houslay & Adams, 2003; Houslay & Baillie, 2005; Ong *et al.*, 2009). The PDE4 family encompasses four genes, A, B, C and D with in excess of 20 isoforms (Huston *et al.*, 2006; Ong *et al.*, 2009). Each of these isoforms vary in the sense that they possess a unique N-terminal domain (Houslay & Adams, 2003), which defines the specific function of the protein (Houslay & Baillie, 2005).

The PDE4s are present in rich concentrations in immune cells, inflammatory cells, brain cells and in cardiovascular and airway smooth muscle cells, but are in low concentrations in platelets (Huang *et al.*, 2001; Lugnier, 2006). They are able to degrade cAMP only with a K_m value of 2-4 μ M (Lugnier, 2006). In order to regulate the levels of cAMP efficiently, the cell also requires tight regulation of the PDE4s themselves, and this is achieved through phosphorylation (McCahill *et al.*, 2008); stringent promoter control (Houslay & Adams, 2003); binding of protein or modifier and proteolysis (Lugnier, 2006).

This set of enzymes has potential therapeutic targets for a broad range of disorders (Houslay & Baillie, 2005). These include type II diabetes (Ong *et al.*, 2009), erectile dysfunction (Lugnier, 2006), asthma and chronic obstructive pulmonary disease (COPD) (Huang *et al.*, 2001), amongst others. However, limitations have been met as these enzyme-based therapeutics initiate nausea and emesis (Houslay & Adams, 2003; McCahill *et al.*, 2008; Ong *et al.*, 2009). Of these enzymes, PDE4D has attracted much attention of the pharmaceutical companies and researchers, but as with the related family members, the side effects still present a hurdle which needs to be overcome if PDE4D is to become a viable therapeutic target (McCahill *et al.*, 2008).

The PDE4D gene is found at locus 5q11.2, is >1.5Mbp (1,513,407bp) and is composed of 17 exons (Smith *et al.*, 2006). There are nine isoforms of PDE4D which are brought about via alternative splicing and/or the utilisation of various promoters (Rahrmann *et al.*, 2009; Huston *et al.*, 2006). The PDE4s (including PDE4D) are present in various forms; long form (PDE4D 3, 4, 5, 7, 8 and 9) (Rahrmann *et al.*, 2009); short form (PDE4D 1, 2 and 6) (Rahrmann *et al.*, 2009); super-short form; and “dead-short” form (Figure 1.2) (Houslay & Adams, 2003; Houslay, Baillie & Maurice, 2007). The long form is composed of the upstream conserved region 1 and 2 (UCR1 and UCR2, respectively), linker region 1 (LR1) which connects UCR1 and UCR2, linker region 2 (LR2) which joins UCR1 and the catalytic region and the C-terminal domain, the role of which is currently unknown (Houslay & Adams, 2003). The short form is

deficient of the UCR1 (Lugnier, 2006). The super-short form also lacks the UCR1 and has a truncated UCR2 (Houslay & Adams, 2003) whilst the “dead-short” form has both a truncated N and C regions and as a result is inactive (Houslay, Baillie & Maurice, 2007). The mode of function of the PDEs is brought about via the interaction of the UCR1 and UCR2 regions, which in turn coordinates the phosphorylation by ERK (extracellular signal regulated kinase) and PKA (protein kinase A) (Huston *et al.*, 2006; Houslay & Adams, 2003).

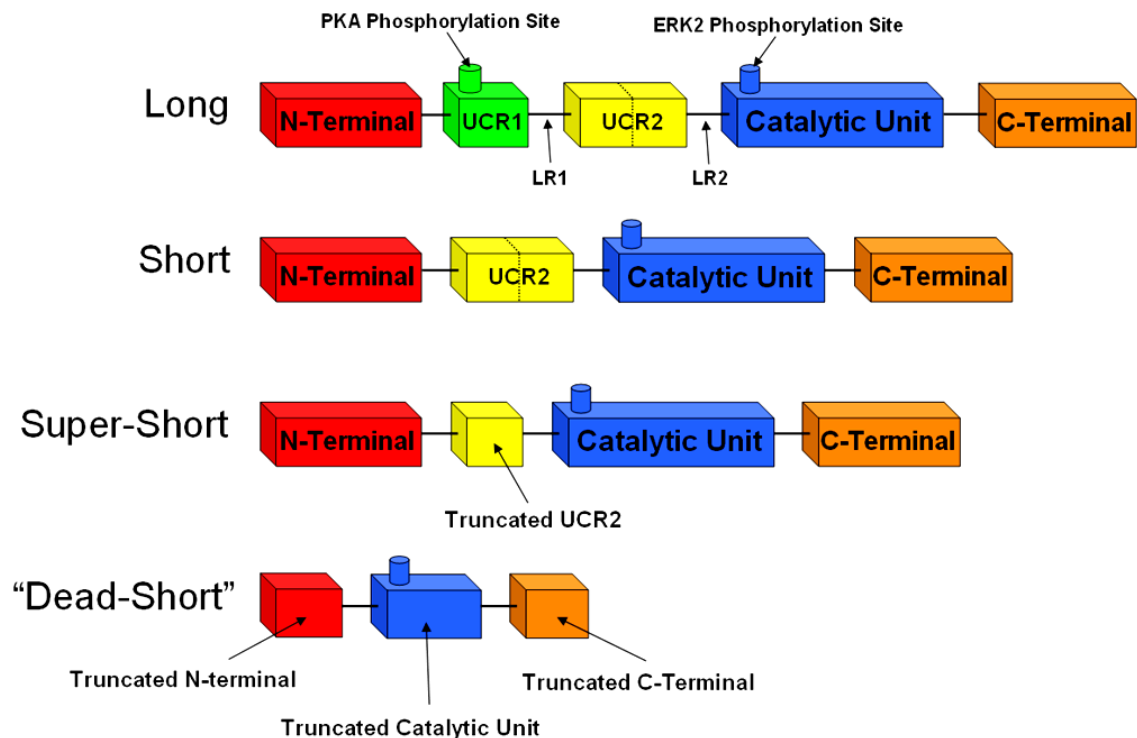


Figure 1.2 A schematic illustrating the various forms of Phosphodiesterases (PDEs). PDE forms: long; short; super-short; and “dead-short”. The red sections indicate the N-terminal domain, the green signifies UCR1, yellow shows UCR2, the blue specifies the catalytic unit and the orange the C-terminal domain. Other important sites and regions are also indicated including LR1, LR2 and the PKA and ERK2 phosphorylation sites.

Conti and co-workers (1991) provided evidence suggesting that prolonged, elevated cAMP concentrations cause an upregulation of the short form of PDE4D (PDE4D 1, 2 and 6). PDE4D regulation has also been linked to PDE4A

and PDE4B concentrations, as a down regulation in these two proteins causes an upregulation in PDE4D in endothelial cells (Keravis, Komasa & Lugnier, 2000). In brain tissue Miro *et al.* (2002) found that when PDE4A is upregulated, PDE4B and PDE4D are downregulated. Therefore, it appears that the control of the PDE gene products and hence cAMP and cGMP is a profoundly complex, interacting system.

The PDE4 sub-family are distributed throughout the cell, dependant on the classification and hence function of the enzyme. It has been documented that localisation may occur at the sarcolemma (Okruhlicova, Vrbjar, & Lugnier, 1998), the nuclear envelope (Lugnier *et al.*, 1999) and the plasma membrane (i.e. the same location to where cAMP is produced (Houslay & Adams, 2003)). Alterations of PDE4 distribution has been linked to the cell signalling revision of the cell (Lugnier, 2006).

A number of experiments have taken place in order to identify the chief roles of the PDE4 sub-family within the cell. For example, PDE4D knockout mice exhibited an anti-depressant behaviour which may then be linked back to the role of cAMP in depression (Zhang *et al.*, 2002). Jin *et al.* (1999) produced mice exhibiting depleted levels of PDE4D which resulted in traits such as deferred growth and female fertility issues. Finally, those mice with a deleted PDE4D gene exhibited an emesis characteristic (Robichaud *et al.*, 2002) which could well be linked to the failed clinical trials of the PDE4D inhibitors. For example, one inhibitor of PDE4D is rolipram – a potential drug for depression; however, for reasons discussed above, rolipram failed clinical trials due to the adverse side effects including that of emesis (Lugnier, 2006).

In addition to the disorders discussed previously, the PDE super-family has acquired attention from oncology researchers. Consequently, there is a broad array of literature attempting to relate the PDE enzymatic family to various forms of cancer in an effort to utilise them as therapeutic targets (Marko *et al.*, 2000; Weber, 2002 and Nancarrow *et al.*, 2008).

In a number of instances, cAMP is found in depleted concentrations in cancer cells in comparison to non-cancerous cells (Marko *et al.*, 2000). This situation arises due to the relative activities of two enzymes involved with cAMP homeostasis, namely adenylate cyclase (AC) and the PDE family (Conti & Jin, 1999; Weber, 2002). The function of AC is the synthesis of cAMP at the plasma membrane and as discussed previously, the role of the PDEs is the degradation of the cAMP. Therefore, it is evident that the activity ratio between AC and PDE, and hence the concentration of cAMP, is the relevant factor. The 'normal' activities of AC and PDE are heavily dependent on the cellular location within the organism. For example, at the cell membrane of a liver cell, the ratio of AC to PDE is relatively equal, whereas in the cytosol of the liver and hepatomas, there is significantly more activity from PDE enzymes than AC (Weber, 2002), the consequence of which is reduced concentrations of cAMP.

In 2002, Weber published a paper regarding gene expression in cancer cells. One intriguing revelation was in relation to hepatocellular carcinoma. Weber found a correlation between the growth rate of the tumor and associated increase in PDE activity and decrease in AC activity. Furthermore, in the more severe and aggressive cases of hepatocellular carcinoma, the PDE activity increase was close to the region of 10 fold and the AC activity declined by up to a fifth. Hence, Weber proposed that this PDE/AC ratio (and thus the intracellular cAMP concentration) may be directly correlated to the growth rate of the tumor, the higher the ratio, the lower the concentration of cAMP and the more aggressive the tumor. This would suggest PDE4D to be an oncogene.

Correspondingly, Marko and co-workers (2000) found increased PDE activity and hence decreased cAMP concentrations in lung cancer in both cell lines and solid tumors. Of the PDE super-family, it was found that sub-family PDE4 attained the greatest activity of which PDE4D exhibited the utmost enzymatic activity. They also examined alterations in PDE activity/cAMP concentration and the extent of malignancy between mouse primary keratinocytes and benign papilloma cell lines. They found no differences between the two sample types.

However, when they analysed differences in CarB cell lines (an extremely malignant cell line), they found much elevated levels of PDE and as a result depleted concentrations of cAMP. In consensus with Weber, this data implies that PDE4D is an oncogene.

Conversely, Jarvinen *et al.* (2008) and Nancarrow *et al.* (2008) more recently reported homozygous deletions (HDs) of PDE4D (5q12) in oral tongue squamous cell carcinoma (OTSCC)/larynx squamous cell carcinoma (LSCC) and oesophageal adenocarcinoma (EAC), respectively. Whilst Jarvinen and co-authors discovered no physical change in PDE4D expression levels, Nancarrow and colleagues determined from this HD, that PDE4D is likely to be a Tumor Suppressor Gene (TSG). Further evidence to this is provided by Weir *et al.* (2007) who found similar HDs of PDE4D in lung adenocarcinoma, again suggesting its role as a TSG.

Therefore, there is contradicting evidence for the role of PDE4D in cancer. Paradoxically, there is compelling support for the role of PED4D as a TSG and as an oncogene. One solution to this apparent paradox is that cAMP activities are cell type specific and so the effects of raised/decreased cAMP and hence PDE4D activity vary from cell to cell, depending on their place of origin within the organism.

Hirsh *et al.* (2004) suggest that elevated concentrations of cAMP in *in vivo* cancer cells may initiate a cellular response and terminate the functions of the cell, thereby killing the cell. There have been a number of attempts to produce drugs which are able to promote the levels of intracellular cAMP within cancer cells in order to induce apoptosis. As mentioned above, issues with toxicity to healthy cells have presented a barrier to cancer drug designers (Bhat *et al.*, 2002). Recent interest has focussed on PDE inhibitors (which function via increasing cAMP levels) for the combat against prostate, ovarian and lung cancer (Hirsh *et al.*, 2004). Two drugs which fit this description and are currently utilised as a therapeutic agent for asthma are a group of substances known as methylated xanthines (methylxanthines), for example, theophylline and

aminophylline (i.e. they have passed clinical trials and are currently on the market) (Hirsh *et al.*, 2004). These substances were tested for their ability to induce apoptosis as a solitary drug and in conjunction with other administered anti-cancer drugs. The results indicated that theophylline was effective independently and when combined with other substances, and it was suggested that the latter would be the preferred therapy. Conversely, aminophylline was not successful at inducing apoptosis at a relatively low drug concentration.

Other *in vitro* studies have taken place for exploring the use of the PDE4 inhibitor, theophylline in small cell lung carcinoma (SCLC) (Hirsh *et al.*, 2004). This resulted in reduced cell viability and inhibition of DNA synthesis and hence non-function ability of the cell. Similarly, the use of methylxanthines has also been publicised in non-small lung carcinoma cells (NSLCC) (Hirsh *et al.*, 2004). The results were in accordance with that of SCLC as theophylline was an effective inducer of apoptosis in the cancer cells, particular when combined with other drugs such as gemcitabine. In unpublished data, the same authors also found theophylline plus gemcitabine to be promising for prostate cancer cells (Hirsh *et al.*, 2004).

Methylxanthines (including that of theophyllines) mode of action as a therapeutic agent is currently vague. There are a number of related hypotheses. Firstly, methylxanthine may increase the levels of cAMP by inhibiting the PDEs involved with cAMP homeostasis. This will effect downstream events including the inhibition of RAS activity (Stork & Schmitt, 2002) and hence MAPK (mitogen activated protein kinase), which in turn leads to arrest of the cell cycle during the G₀/G₁ phase (post mitotic phase) (Favot, Keravis & Lugnier, 2004). This is a result of inhibition of PDE4 (Favot, Keravis & Lugnier, 2004). Alternatively, the increase in cAMP may result in a decline in the expression of Bcl2 (Yoshida *et al.*, 2000), an anti-apoptosis protein, and inhibition of MDM2 (Shmueli & Oren, 2004), which is an inhibitor of the apoptotic p53 protein. These two cellular modifications vastly increase the chance of apoptosis and decrease cell growth (Hirsh *et al.*, 2004).

Rolipram is also a very well documented inhibitor of the PDE4 group. It is a specific inhibitor of PDE4 and is insensitive to cGMP (Lugnier, 2006). It is able to bind to the PDE4 molecule at two different sites aptly named the low affinity rolipram binding site (LARBS) and the high affinity rolipram binding site (HARBS) (Houslay, Schafer & Zhang, 2005). Evidence suggests that the interaction between the PDE4 LARBS and the rolipram results in the positive effects of the drug, i.e. anti-inflammatory characteristics (Lugnier, 2006) which has potential for the treatment of asthma (Huang *et al.*, 2001). However, it is the interaction between the HARBS segment of PDE4 and rolipram which reaps the repercussions of utilising the drug, i.e. emesis and nausea (McCahill *et al.*, 2008; Houslay, Schafer & Zhang, 2005). The affinity of interactions between LARBS/HARBS and rolipram is not necessarily constant or consistent and varies on a number of factors including; PDE4 subtype; Mg²⁺ bound enzyme (Houslay, Schafer & Zhang, 2005); dimerisation of the PDE4 molecule through UCR1 and UCR2 (McCahill *et al.*, 2008); plus the interaction of other molecules including RACK1:PDE4D5 which increases the affinity of rolipram (McCahill *et al.*, 2008).

The intracellular introduction of rolipram results in a concentration shift of the PDE4 family and any interacting proteins (Terry *et al.*, 2003). This in turn will significantly affect the localised distribution of cAMP throughout the cell, with an obvious overall effect of elevated cAMP concentration (Ong *et al.*, 2009). Eventually, as a consequence of the introduction of the PDE4 inhibitor rolipram, cellular arrest and programmed cell death will follow (Kowalczyk *et al.*, 2009; Houslay, Schafer & Zhang, 2005)

The link between cAMP concentration (and hence PDE activity) and apoptosis is not yet understood. Fryknäs *et al.* (2006) proposed a number of propositions which require further investigation. Firstly, they hypothesised the involvement of the PKA pathway and associated molecules such as nitric oxide (NO). Prior studies have suggested that NO may be coupled with the inducement of apoptosis (Karpuzoglu & Ahmed, 2006; Zheng, Sinniah & Hsu, 2006). NO is

under gene regulation via inducible nitric oxide synthetase (iNOS), which in turn may be activated by PDEs (Fryknäs *et al.*, 2006). Hence, an upregulation of PDE may have a sequential downstream upregulation of NO which may result in an apoptotic activity. Secondly, they suggested the contribution of calcium concentration within the cell. If a cell was to surpass the intracellular threshold concentration of calcium, the cell would undergo cell death (Olofsson *et al.*, 2008). There is a complex relationship between cAMP and intracellular calcium concentrations; however, it is believed that cAMP encourages export of calcium from the cell and ensures that localisation of intracellular calcium is controlled (Vajanaphanich *et al.*, 1995). Therefore, as PDE regulates cAMP levels, further downstream it will also regulate intracellular calcium concentrations. The third and final proposal, once again includes the PKA pathway. The mechanisms of the PKA pathway result in a downstream activation of ERK1, ERK2 and p38 (Chio *et al.*, 2004). The ERK molecules and p38 are associated with cell death and reduced cell growth and hence, if these molecules are activated by the lack of upstream activities from the PDE family, apoptosis will occur (Fryknäs *et al.*, 2006). Conversely, if a situation arises whereby PDE activity is elevated causing a reduction in cAMP, ERK/p38 will not be activated and apoptosis cannot occur.

The literature associating PDE4D (and other PDEs) with OSCC is limited and only mentioned in brief. For example, Fushimia *et al.* (2008) found PDE4D to be a genetic factor associated with the disease but do not elaborate further on their claim. This suggests that this link is not fully elucidated, and hence, requires further investigation.

1.2.2 Environmental Effects

1.2.2.1 The Warburg Effect

In 1927, Otto Warburg and co-workers released evidence of a phenomenon which was to revolutionise the current view on the onset and development of tumorigenesis (Warburg, 1930; 1956; 1965; Warburg, Posener & Negelein, 1924 and Warburg, Wind & Negelein, 1927). When healthy mammalian cells are subjected to normoxic conditions, the preferred route for generating ATP is via oxidative phosphorylation in the mitochondria of the cells. This is the most efficient means of a cell to produce ATP; yielding 31 or 29.5 molecules of ATP per glucose molecule depending on NADH shuttling into the mitochondria. Under the same conditions, glycolysis (which takes place in the cytoplasm of the cell) is a significantly less efficient method of producing ATP, gaining just two molecules of ATP per glucose molecule. In healthy cells, glycolysis is only preferred to oxidative phosphorylation under hypoxic conditions. Warburg discovered a metabolic shift in the manner cancer cells produce energy, finding that they predominantly utilise glycolysis, even in the presence of oxygen (this is known as the Warburg effect or aerobic glycolysis). Hence, a paradoxical situation arises, as a cancer cell requires elevated levels of ATP to grow and develop, yet the mode in which the cell gathers ATP is subordinate to its counter-method. The scientific community believe that this switch from oxidative phosphorylation to glycolysis is paramount for tumor development and progression (Bartrons & Caro, 2007).

There are currently six established characteristics which are shared by cancerous cells: unprecedented ability to grow and multiply; evade apoptosis; ability to invade proximate and distant tissues; angiogenesis; and capability of producing and acting upon growth signals (Gogvadze, Orrenius & Zhivotovsky, 2009). There is now current debate within the oncological field as to whether a seventh should be added to the list involving the requisite of glycolysis within cancer cells (Gogvadze, Orrenius & Zhivotovsky, 2009). This pronouncement is

ambiguous for a number of reasons. Firstly, there is speculation as to whether aerobic glycolysis is essential in all tumors; there is currently no evidence advocating or disputing this statement. Secondly, it is yet to be determined whether this observed Warburg effect is a systematic symptom of other effectors causing the onset of tumorigenesis or whether it is the foundation on which tumorous growth is formed (Ashrafian, 2006). These factors are contributing to the scrutiny which is being received regarding aerobic glycolysis.

However, experts in the field are unable to disregard the advancement in which this revelation has brought about and the constructive aid this has provided. For example, diagnosis and prognosis enhancements (through the stage of the cancer) has been made through the use of ^{18}F -2-fluorodeoxyglucose (a glucose analogue) - Positron emission tomography (FDG-PET) imaging (Suzuki *et al.*, 2009a). This enables one to measure the glucose metabolism spatially *in vivo*, which in general, have a strong positive correlation with tumorigenesis and the stage of development of the tumor.

The underlying mechanisms behind this mysterious divergence from oxidative phosphorylation to glycolysis within tumors remain ambiguous. Warburg explained the occurrence by dysfunctional mitochondria and since this is where oxidative phosphorylation should occur and may no longer do so, glycolysis retains ATP production control. However, more recent evidence suggests that mitochondria originating from tumor cells are still able to function sufficiently, disproving Warburg's hypothesis (Nakashima *et al.*, 1984; Frezza and Gottlieb, 2009). Although the mechanisms behind aerobic glycolysis are extremely complex and not yet understood, the following attempts to outline a number of the relevant factors involved.

So, how is aerobic glycolysis possible? Through an intricate system of interactions, productions and inhibitions including gene amplifications of oncogenes, repression of tumor suppressor genes and post translational modifications (Altenberg & Greulich, 2004), a number of which are discussed below. In order for cancerous cells to survive, this system must provide an

enhanced supply of glucose (or other energy source) to sustain the ability to grow and divide.

The regular glycolysis process converts glucose to pyruvate, whereas aerobic glycolysis i.e. the Warburg effect converts glucose to lactate (Bartrons & Caro, 2007). The initial step of glycolysis is the conversion of glucose to glucose-6-phosphate (G6P) and is controlled by the enzyme hexokinase (HK) (Mathupala, Ko & Pedersen, 2009). There are 4 various isoforms of HK (HK1-4) and evidence suggests that HK-2 is the predominant isoform in most cancer cells (Nakashima *et al.*, 1986) and in comparison, this isoform is scarce within healthy cells (Mathupala, Ko & Pedersen, 2009). This overexpression of HK-2 is a direct result of upregulation from: HIF-1 (Frezza & Gottlieb, 2009); c-Myc (Kondoh, 2008) and p53 (Kondoh, 2008). This is further supported, as the transcription factors HIF-1 and p53 binding sequences have been found on the promoter region of HK-2 (Mathupala *et al.*, 1997). Evidence suggests that this upregulation of HK-2 plays a major role within cancer cells. HK-2 binds to mitochondria at the voltage dependent anion channel (VDAC) at the outer mitochondrial membrane (OMM) (Gogvadze, Orrenius & Zhivotovsky, 2009). This is advantageous to the cancerous cell for a number of reasons. Firstly, this contributes anti-apoptotic properties. Mitochondria are involved with the apoptosis procedure as the pro-apoptotic molecules Bax (Bcl-2 associated X protein) and Bak (Bcl-2 homologous antagonist/killer) are signalled to bind to the OMM which in turn initiates a release of cytochrome c which downstream instigates apoptosis (Robey & Hay, 2009). The binding site of the Bax/Bak molecules at the OMM is the same site that HK-2 binds and therefore, in cancer cells, competitive inhibition takes place (Pastorino, Shulga & Hoek, 2002). Hence, apoptosis is inhibited. Furthermore, binding of HK-2 to the OMM may be promoted through factors which are elevated in cancer cells such as Akt (Robey & Hay, 2009). Secondly, the binding of HK-2 to the OMM grants the HK-2 exclusive access to a continuous flow of ATP molecules which may be used to phosphorylate glucose to G6P, hence glucose metabolism becomes relentless in the cancerous cell (Zhivotovsky & Orrenius, 2009).

Arguably, HIF-1 is the most important factor involved in the Warburg effect. HIF-1 is found to be abundant in many cancer cells (Bartrons & Caro, 2007) and has a number of advantageous effects for the tumor. In healthy cells, HIF-1 is activated under hypoxic conditions in order to cope with the stress the cell is subjected to whilst lacking oxygen (Bartrons & Caro, 2007). When hypoxia is relieved, the α -subunit of HIF-1 is rapidly degraded with the aid of von Hippel-Lindau (VHL) protein (Minchenko *et al.*, 2002). The VHL initiates the degradation of the α -subunit of HIF-1 via the ubiquitin degradation pathway. Cancerous cells are not necessarily hypoxic, but yet still frequently overexpress the HIF-1 α protein.

So how is HIF-1 α able to survive in the presence of oxygen? At present, this is still vague, but evidence suggests that other factors are able to prolong the half life of HIF-1 α even in the presence of oxygen (King, Selak, & Gottlieb, 2006). For example, a mutation may cause the production of a dysfunctional VHL protein which results in an inhibition of degradation of HIF-1 α and hence a prolonged HIF-1 α half life (Semenza, 2009). Furthermore, the activation of the PI3K, Akt, and mTOR pathways are believed to promote stabilisation of HIF-1 α (Jiang *et al.*, 2001; Martinive *et al.*, 2009). In many cases, tumor cells are subjected to hypoxia, chiefly due to an inadequate oxygen supply through the vascular system (HelmLinger *et al.*, 1997). When these situations arise, HIF-1 concentrations may be sustained as there is no oxygen to promote the degradation of the HIF-1 α subunit.

There are a number of means by which HIF-1 promotes glycolysis and enhances survival and growth of the tumor. Firstly, HIF-1 upregulates a host of genes associated with glycolysis (Kondoh, 2008) and initiates metabolic reprogramming. Glucose transporter expression is upregulated in order to increase the flux of glucose into the cell which in turn will increase glycolysis (Frezza & Gottlieb, 2009). These transporters include glucose transporter-1 (GLUT1) and glucose transporter-3 (GLUT3) (Bartrons & Caro, 2007). Furthermore, HK/HK2 activity is increased, elevating the initial step of glycolysis

and the conversion of glucose to G6P (Frezza & Gottlieb, 2009). Regulation between oxidative phosphorylation and glycolysis is under the control of the activity of two enzymes, namely, pyruvate dehydrogenase kinase (PDK) and lactate dehydrogenase A (LDHA) (Gogvadze, Orrenius & Zhivotovsky, 2009). Under hypoxic conditions these are regulated by the HIF-1 transcription factor and hence, this is believed to be a key player behind the mechanisms involved in tumorigenesis (Frezza & Gottlieb, 2009). Secondly, mitochondria activity is reduced (the activity location of oxidative phosphorylation), and in order to compensate, the glycolytic activity in the cytoplasm of the cell is increased (Zhivotovsky & Orrenius, 2009). In association with the mitochondria is the enzyme cytochrome c oxidase (COX) (or Complex IV) which is regulated by HIF-1 (Fukuda *et al.*, 2007). The regulation of the COX4-2 enzyme isoform is of particular importance for a cell to undergo efficient respiration under hypoxic conditions (Semenza, 2009). Thirdly, HIF-1 has the ability to promote angiogenesis as an attempt to relieve the hypoxic stress the cell/tumor is subjected to (Hsu & Sabatini, 2008). Consequently, the tumorous cell is able to enhance the intake of glucose and oxygen, which is paramount for the cells survival. Fourthly, this upregulation in glycolysis (which is partially the responsibility of HIF-1) results in an overproduction of lactic acid (Kim, Gardner & Dang, 2005). This leads to acidosis, which has recently been associated with elevated ability of invasiveness (Nijsten & van Dam, 2009) and the capability of enhanced growth (providing p53 dysfunction) (Gatenby & Gillies, 2004). Evidence suggests that lactate may also be recycled as an energy source for the cell. Finally, HIF-1 activates a number of oncogenes including Akt, c-Myc (Kim, Gardner & Dang, 2005) and Ras (Chen *et al.*, 2001) further promoting tumorigenesis.

AMP activated protein kinase (AMPK) is a cellular component which has a responsibility for monitoring and acting upon cellular energy stores, e.g. ATP and glucose (Kahn *et al.*, 2005). AMPK is sensitive to 5'AMP and is inhibited by ATP and glycogen (Ashrafian, 2006) and through this has the ability to regulate the cellular energy. When energy levels are depleted, glucose and fatty acid

metabolism is stimulated by AMPK in order to raise energy levels and GLUT-1 and GLUT-4 translocation are utilised to increase glucose uptake into the cell (Ashrafian, 2006). When the cell is subjected to stress (e.g. hypoxia), AMPK may be activated which in turn promotes cell metabolism. Due to the varying requirements between early tumors and late tumors, a paradox arises regarding the expression of AMPK. An advantage to early tumors would be inhibition of AMPK in order to allow anabolic processes to occur such as proliferation (Ashrafian, 2006). Inhibition is brought about via the mTOR pathway (Swinnen *et al.*, 2005). Conversely, in latter stages of tumorigenesis, evidence suggests that elevated levels of glycolysis is paramount and so, AMPK activation is required in order to contribute to raising glucose metabolism (Buzzai *et al.*, 2005). Robey & Hay (2009) suggested that Akt has some indirect control over AMPK activity, which is an important aspect of activating the mTOR pathway (Hahn-Windgassen *et al.*, 2005).

Alongside hexokinase (HK) and phosphofructokinase (PFK), pyruvate kinase (PK) is believed to be amongst the most controlling steps in glycolysis (Weber *et al.*, 1966). Therefore, one would assume that these rate controlling steps may play a major role in the Warburg effect. PK is the catalyst for the irreversible reaction of phosphoenolpyruvate (PEP) to pyruvate (Hsu & Sabatini, 2008) and is present in a number of isoforms dependent upon cellular location and activity; Liver (PKL); Erythrocyte (PKR); Muscle-1 (PKM1) and Muscle-2 (PKM2). The predominant isoform in many cancers is PKM2 and a correlation has been suggested between the concentration of PKM2 and the extent of the malignancy (Eigenbrodt *et al.*, 1997). Unexpectedly, the isoform PKM2 is less efficient than its counterpart PKM1 (Mazurek *et al.*, 2005) but yet, PKM2 is still beneficial to the tumor. One reason for this is that intermediates from the glycolytic pathway are diverted and used for advancement in tumor growth and development caused by PKM2 (Ferguson & Rathmell, 2008). Furthermore, PKM2 promotes cancer metabolism and growth signalling (Christofk *et al.*, 2008). PKM2 is under regulation by a number of factors including deactivation

by oncogenes (Eigenbrodt *et al.*, 1992) and an increase under hypoxic conditions (through HIF-1) (Kress *et al.*, 1998).

It is now under popular belief that PFK is the rate limiting enzyme in glycolysis (Kondoh, 2008; Robey & Hay, 2009). PFK-1 catalyses the reaction of fructose-6-phosphate (F6P) to fructose-1-6-bisphosphate (F1-6P₂) and PFK-2 catalyses the reaction F6P to fructose-2-6-bisphosphate (F2-6P₂). PFK-1 is allosterically activated by F2-6P₂ (Minchenko *et al.*, 2002), which is promoted by AMP and inhibited by ATP and citrate (Frezza and Gottlieb, 2009). Hence, the activity of PFK-1 is dependent on intermediates associated with the glycolytic pathway. Sequentially, if cellular levels of F6P are elevated, PFK-2 produces F2-6P₂ which stimulates PFK-1 which converts the F6P into F1-6P₂. The relative activities of PFK have been found to differ in cancerous cells in comparison to their healthy counter-parts, which ultimately would have an effect on glycolysis. There are a number of methods by which PFK activity is altered. Hypoxia may elevate the concentration of PFK-1 which is a direct result of the activation of HIF-1 (Bartrons & Caro, 2007). An alternative method which has been documented is the activation of oncogenes such as *Ras* (Kole *et al.*, 1991), *Src* (Durante *et al.*, 1999) and *c-Myc* (Kondoh, 2008) in cell lines. Chesney *et al.* (1999) found that PFK-2 is expressed constitutively in cancer cell lines which results in an amplified level of F2-6P₂, which successively activates PFK-1 and hence improved flux of glycolysis. Conversely, flux through glycolysis may be depleted due to suppressions via TP53 and TIGAR on F2-6P₂ and hence PFK-1 (Bensaad *et al.*, 2006). Akt has also been documented to effect levels of PFK-1 and hence glycolysis in tumorigenesis (Robey & Hay, 2009). In this case, Akt activates PFK-2 which in turn, activates F2-6P₂ and then PFK-1 inducing increased glycolysis activity.

1.2.2.2 The Role of the Transcription Factors HIF-1 and CREB

HIF-1 and cAMP response element binding (CREB) are transcription factors (TFs) which regulate particular genes in a cell specific and gene specific manner (O'Reilly *et al.*, 2006; Dimova *et al.*, 2007). The TFs bind to the hypoxia response element (HRE) (Baugh *et al.*, 2006) and cAMP response element (CRE) binding domains, respectively (Dimova *et al.*, 2007), binding in the 5' flanking region of various genes. Once bound these TFs upregulate or repress the transcription of genes in an intricate fashion.

HIF-1 is activated under hypoxic conditions within the cell; however it may also be present in an active form in cancer cells under normoxia. A consensus belief within the scientific community is that the activation of HIF-1 in cancer cells provides a major contribution to the progression and severity of cancer through its selective regulation of genes (Abramovitch *et al.*, 2004; Breit *et al.*, 2008; Suzuki *et al.*, 2009b).

The secondary messenger cAMP causes the release of the catalytic subunit of PKA (protein kinase A) (Suzuki *et al.*, 2009b) which sequentially phosphorylates CREB at residue serine 133, thereby activating it (Abramovitch *et al.*, 2004). P-CREB is then able to recruit a number of cofactors, forming a complex which binds to the *cis* binding site CRE, resulting in CREB regulation of the gene. CRE is found in the promoters of ~4000 genes (Suzuki *et al.*, 2009b). The CREB distribution between tissues is relatively generic, but regulation by CREB is heavily dependent on numerous factors including the methylation state of the *cis* region and the selective recruitment of the cofactors (Zhang *et al.*, 2005).

The interaction between the TFs and *cis* regions is multifaceted and may function via numerous mechanisms. These may be categorised as HIF dependent and HIF independent regulation. The two dominant mechanisms from the literature are briefly discussed below.

In one model, Firth and co-workers (1995) suggested that the TF HIF-1 cannot exclusively regulate gene expression, requiring adjacent binding domains to be

simultaneously stimulated (see Figure 1.3) (Breit *et al.*, 2008). In this case, HIF-1 stimulation is essential but sufficient to activate transcription without adjacent binding of other TF such as CREB. In addition, further cofactors are necessary such as the CREB binding protein (CBP)/p300 complex and the recruitment of the transcriptional machinery.

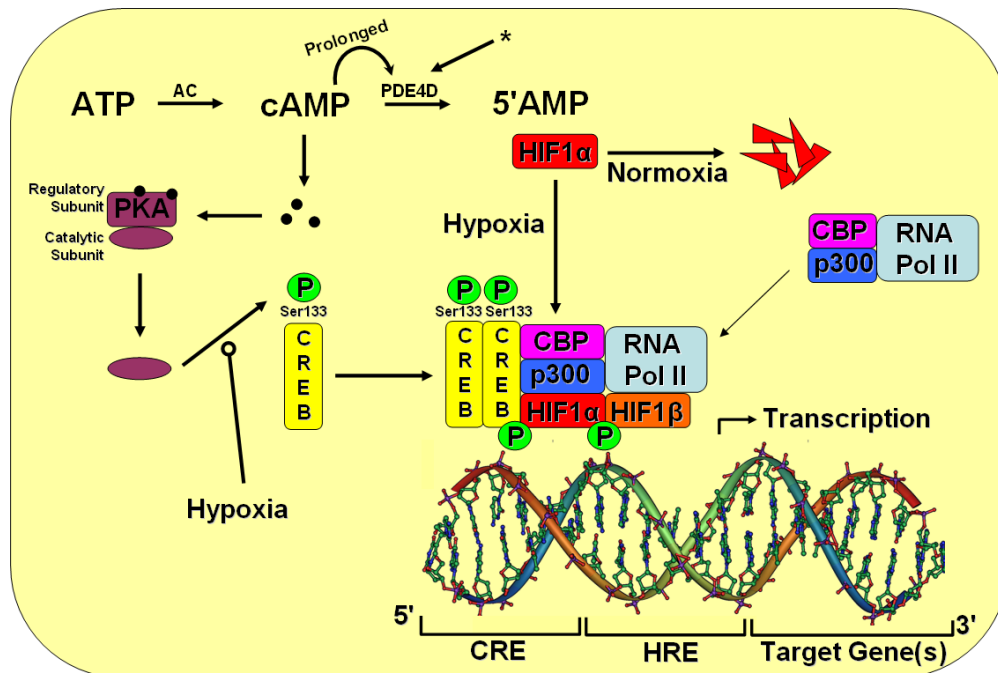


Figure 1.3 HIF dependent regulation of transcription. cAMP concentrations are regulated by the enzymes AC (cAMP production) and PDE4D (cAMP degradation). The asterisk indicates the regulation of PDE4D through post-translational modification, promoter control, proteolysis, etc. cAMP binds to PKA, releasing the catalytic subunit which sequentially phosphorylates CREB at Ser133. The P-CREB, already bound to CRE, selectively recruits the cofactors p300/CBP in addition to the transcriptional machinery. Meanwhile, under hypoxic conditions, HIF forms a complex which simultaneously binds to HRE. p300/CBP are scaffolding proteins.

In a further model termed HIF independent regulation (Dimova, Jakubowska & Kietzmann, 2007; O'Reilly *et al.*, 2006), CREB regulates gene expression, regardless of the aid from HIF (see Figure 1.4). CREB is activated via the same means as the previous model, recruits CBP/p300 and RNA polymerase II to

form a complex, and initiates transcription of the target gene(s). A point of interest in both models is the enhancement of CREB functions through hypoxia, for example the phosphorylation of CREB from PKA is augmented (Dimova, Jakubowska & Kietzmann, 2007) as is the transcription of CREB and CBP (Freeland, Boxer & Latchman, 2001).

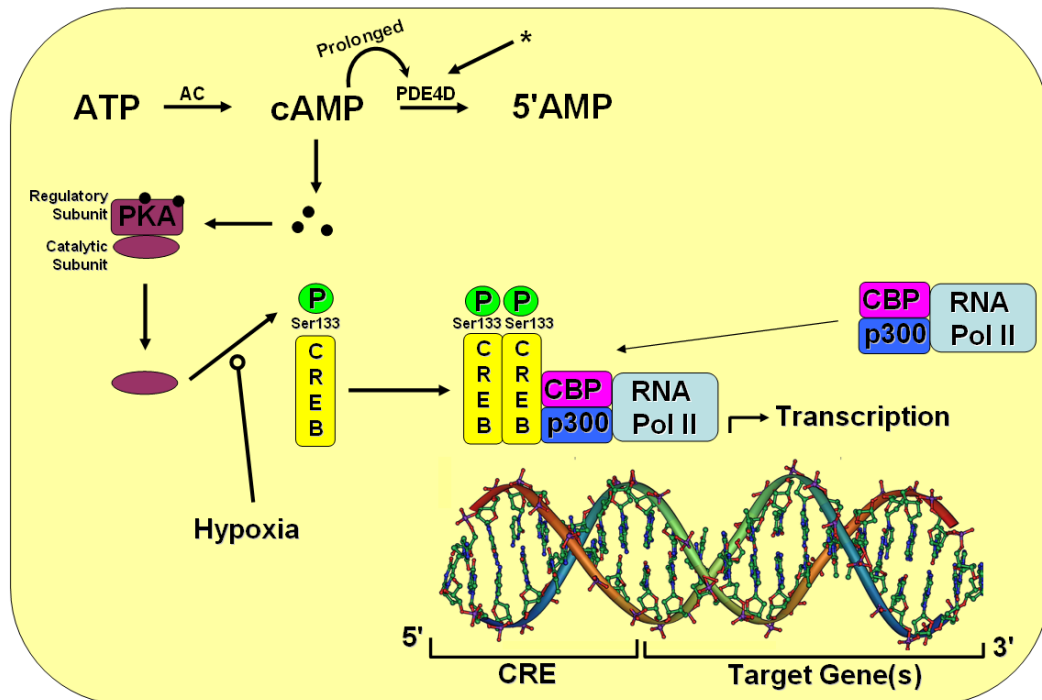


Figure 1.4 HIF independent regulation of transcription. cAMP concentrations are regulated by AC (cAMP production) and PDE4D (cAMP degradation). The asterisk indicates the regulation of PDE4D through post-translational modification, promoter control, proteolysis, etc. cAMP binds to PKA, releasing the catalytic subunit which sequentially phosphorylates CREB at Ser133. The P-CREB, already bound to CRE, selectively recruits the cofactors p300/CBP in addition to the transcriptional machinery.

To add further complexity to the issue, CRE and HRE are interchangeable, i.e. HIF may bind to the CRE binding domain and CREB may bind to the HRE *cis* region (Dimova *et al.*, 2007; O'Reilly *et al.*, 2006). Moreover, both HIF and CREB may simultaneously bind to a solitary HRE or CRE domain and hence do not compete for binding sites. The binding of both TFs to a sole *cis* domain

permits supplementary regulation beyond the binding of a single TF (Abramovitch *et al.*, 2004).

It may prove useful to investigate which genes are influenced by these TFs in OSCC and may also provide insight on how these mechanisms contribute to the Warburg effect. Potential genes which may be influenced by such mechanisms include VEGF (Abramovitch *et al.*, 2004; Meyuhas *et al.*, 2008), LDH (Abramovitch *et al.*, 2004), Bcl-2 (Freeland *et al.*, 2001), CCN1/CYR61 (Meyuhas *et al.*, 2008), IAP2 (Abramovitch *et al.*, 2004), COX-2 (Park *et al.*, 2005), macrophage migration inhibitory factor (MIF) (Baugh *et al.*, 2006), iNOS (Fryknäs *et al.*, 2006), CyclinD1 (Abramovitch *et al.*, 2004) and CyclinA (Abramovitch *et al.*, 2004). This array of gene control ultimately results in regulation of cancerous characteristics such as cellular growth, angiogenesis, anti-apoptotic behaviour, proliferation, enhanced mitotic index, etc.

Literature searches indicate that co-activation of transcription by HIF-1 and CREB has not been investigated in OSCC cells and, since regulation is cell type specific, it may establish some significant factors and may shed light on the underlying mechanisms behind OSCC. An interesting factor which has recently come to light is that frequently a HD of PDE4D is found in OSCC. This disables the cell from degrading the majority of cAMP which sequentially results in elevated cAMP levels, enhanced PKA activation, increased CREB phosphorylation and potentially an escalation of gene regulation.

1.2.2.3 Mimicking the Effects of Hypoxia using Cobalt Chloride (CoCl₂)

It is well documented that subjecting a cell to CoCl₂ under normoxic conditions has similar effects to that of hypoxia (An *et al.*, 1998; Guo *et al.*, 2006; Wang & Semenza, 1993). This is achieved via the activation of hypoxia related pathways through the increased expression and/or stabilisation of the HIF-1 α and HIF-2 α proteins (Ho and Bunn, 1996; Yuan *et al.*, 2003; Chachami *et al.*, 2004). The underlying mechanisms by which this occurs have been under much debate. During normoxia the α -subunit of the HIF protein is degraded by pVHL

(Figure 1.5) whereas under hypoxic conditions, HIF-1 α is present in its active form (Figure 1.6). One proposal suggested for the hypoxic mimicking capabilities of CoCl₂ is due to the cobalt (Co) competitively inhibiting the oxygen dependent degradation (ODD) site of the HIF-1 α which results in the inability of pVHL to bind and hence HIF-1 α may not be degraded (Yaun *et al.*, 2003) (Figure 1.7).

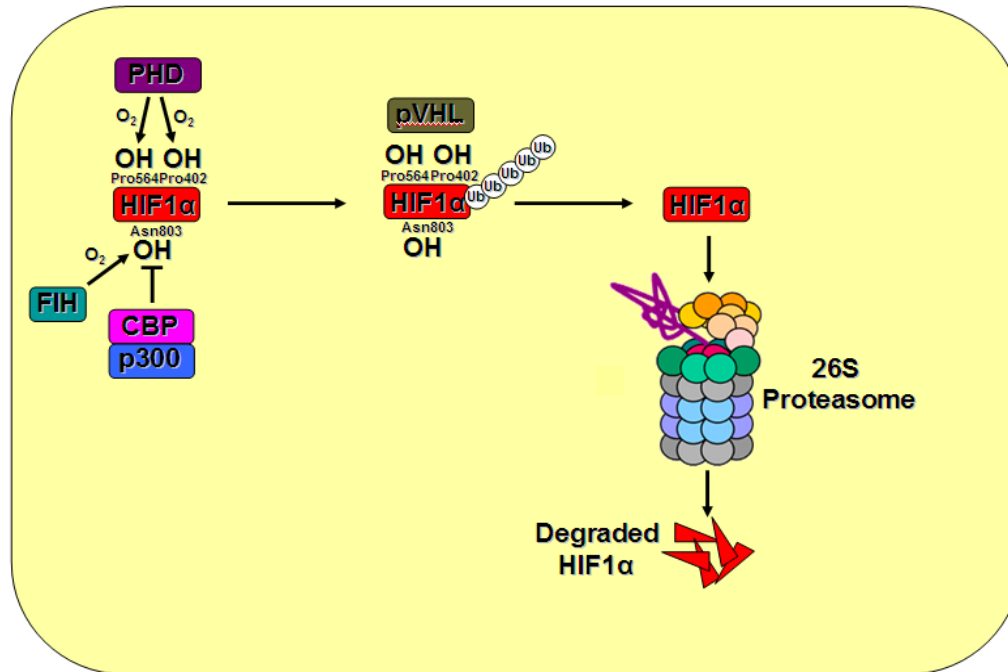


Figure 1.5 HIF-1 α Degradation During Normoxia. HIF proline residues 402 and/or 564 are hydroxylated which is catalysed by the enzyme Prolyl Hydroxylase (PHD) (Ke and Costa, 2006). This process is O₂ and iron (Fe²⁺) dependent. The asparagine at residue 803 is also hydroxylated by Factor Inhibiting HIF (FIH) (in the presence of O₂) and inhibits CREB Binding Protein (CBP/p300 complex binding/recruitment to HIF-1 α under normoxic conditions. This post-translational modification acts as an ‘insurance policy’, ensuring that any HIF-1 α which evades normoxic degradation is inhibited of its hypoxic duties. Subsequent to this, HIF-1 α is multi-ubiquitinated by the von Hippel-Lindau gene product, pVHL. pVHL is an E3 ubiquitin ligase and also a TSG. The final stage of the procedure is initiated by the multi-ubiquitination and is the degradation of the HIF-1 α via the 26S proteasome. It is noteworthy that the half-life of HIF-1 α during normoxia is approx 5-8 min (Berra *et al.*, 2001).

Chachami and co-workers (2004) suggest that this behaviour is observed due to an upregulation in the translation of the HIF-1 α protein which is brought about via the phosphatidylinositol 3 kinase (PI3K) pathway. This activation of the PI3K pathway is the normal mode of action for inducing the protein synthesis of HIF-1 α under hypoxic conditions, and the results from this experiment provide evidence that this was also the case when subjecting the cells to CoCl₂. The view of this activation of the PI3K pathway is shared by Kim *et al.* (2006). It is known that reactive oxygen species (ROS) are involved during hypoxia and CoCl₂ infliction, and their role was elucidated by Chandel *et al.* (1998). ROS are initially formed as superoxide (O₂⁻), before being converted to hydrogen peroxide (H₂O₂) before their degradation to water (H₂O). The work established distinctions in ROS behaviour between hypoxia and CoCl₂ subjected cells. Under hypoxia, mitochondria signalling induces ROS elevation and results in an upregulation of translation. Conversely, CoCl₂ promotes ROS production which in turn upregulates translation and hence, does not require the utilisation of mitochondrial signalling. This highlights the fact that subjecting cells to CoCl₂ merely imitates hypoxia and does not literally induce the hypoxic response.

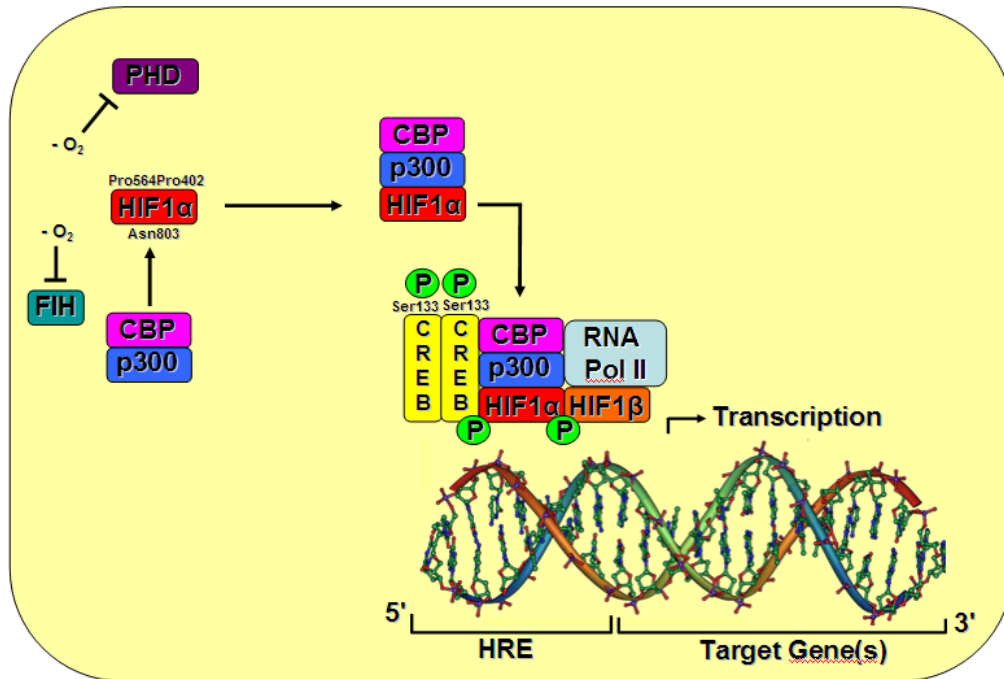


Figure 1.6 Activated HIF-1 α During Hypoxia. In the absence of oxygen (hypoxia), PHD and FIH are inhibited resulting in no hydroxylation of the proline and asparagine residues of the HIF-1 α protein. Subsequently, pVHL is incapable of ubiquitination of the HIF-1 α protein and therefore, the 26S proteasome is unable to degrade HIF-1 α . This results the binding of HIF-1 α to the *cis* regions and hence regulating transcription.

These discrepancies in hypotheses may be due to the variations in cell types used in the experiments, for example Chachami utilised smooth muscle rabbit trachea cells whereas Yuan exploited rat pheochromocytoma and chinese hamster ovary cells. That is to say differences in organisms and cell origins may cause the observed variations in behaviour between the experimental groups. It is also noteworthy that other hypoxia mimicking substances are known such as desferrioxamine (DFO) (Guo *et al.*, 2006) and nickel (Ho & Bunn, 1996) and these may produce the hypoxic imitating effects through varying mechanisms.

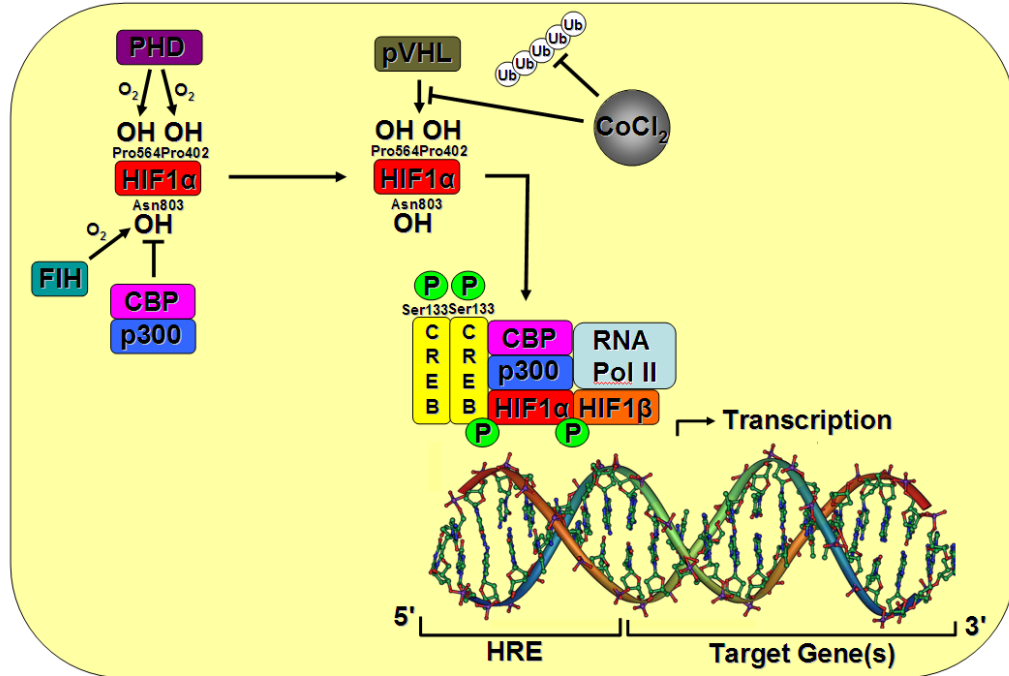


Figure 1.7 CoCl₂ as a Hypoxia Mimicker. CoCl₂ interferes with HIF-1α at the pVHL stage of degradation. This inhibition of degradation could be a result of the CoCl₂ inhibiting the interaction between pVHL and HIF-1α (LaManna, Pichiule & Chavez, 2007) and/or the prevention of ubiquitination of HIF-1α by the pVHL (Ohh *et al.*, 2000). Regardless, either mechanism results in escalated HIF-1α concentrations, which may then dimerise with HIF-1β, recruit the remaining members of complex and induce transcription of genes containing the HRE *cis* region.

From the model presented in Figure 1.7, it is important to note that CoCl₂ is indeed a hypoxic *mimicker* and should not be confused as a hypoxic *inducer*. As can be seen in the models presented in Figures 1.5 – 1.7 above, the mechanisms behind hypoxia and CoCl₂ induced hypoxia are significantly distinct. In addition, CoCl₂ may have severe off target effects which are yet to be analysed in detail. Part of the aims of this work is to investigate these questions further.

1.2.2.4 The Glutamate Shunt

Tumorous cells display a number of characteristics which are different to their healthy counterparts including that of a modified glutaminolysis (Diaz-Ruiz *et al.*, 2009). Glutaminolysis is a term used to describe the conversion of glutamine to glutamate (glutamic acid), aspartate, ammonia (NH₃) and CO₂ (Brand, 1985) and is catalysed by the enzyme glutaminase (Kovacevic & McGivan, 1983) (see Figure 1.8). The eventual product of this process is pyruvate and/or lactate via malate of the TCA (Baggetto, 1992). This reaction is reversible and occurs in the mitochondria of the cell (DeBerardinis *et al.*, 2008).

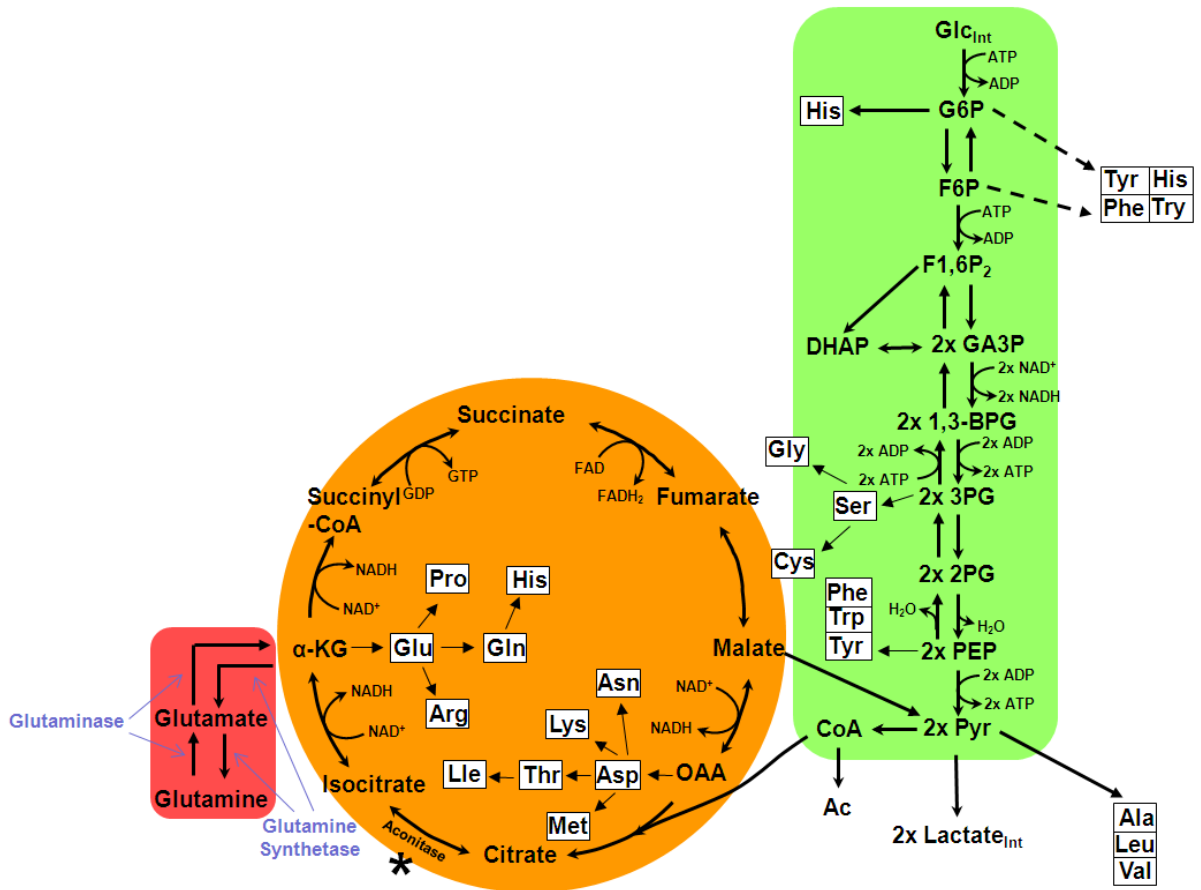


Figure 1.8 Glutaminolysis Modifications in Cancer Cells. The green section signifies glycolysis, orange the TCA cycle, pink highlights glutaminolysis, the white boxes indicate amino acids and the blue labels denotes enzymes. Cancer cells often have compromised aconitase enzymatic activity (which catalyses the reaction of citrate to isocitrate and is highlighted by the asterisk (*)) as a result of increased ROS concentration. In order for continuation of the TCA, glutamine enters at α -KG where it proceeds to malate and is eventually converted to pyruvate. This is termed the truncated Krebs cycle (Baggetto, 1992).

Evidence suggests that cancerous cells rely on the forward reaction (i.e. conversion of glutamine to glutamate) which is achieved via the hyper expression of the glutaminase enzyme or the inhibition/suppression of glutamine synthetase (DeBerardinis *et al.*, 2008). This became apparent as many cancer cells exhibit elevated concentrations of glutamate, aspartate, etc than their counterparts (Fan *et al.*, 2008) and a subsequent lower concentration of glutamine (Kovacevic & McGivan, 1983). This glutamate shunt is beneficial

for tumorous cells for a number of reasons. Primarily, glutamine is a copious amino acid in *Homo sapiens* (Feron, 2009) and may be utilised as a carbon source which may enter the TCA cycle via the conversion to glutamate and subsequently α -ketoglutarate (Hitchler & Domann, 2009). This is advantageous to cancer cells as the enzyme aconitase (which catalyses the reaction citrate to isocitrate in the TCA cycle) is compromised resulting in the inhibition of the TCA cycle. The ability of glutamine to enter the TCA via glutamate and then α -ketoglutarate enables a continuation of the TCA cycle. This modification has been termed the truncated Krebs cycle by Baggetto (1992). In addition, a number of by-products are produced during the TCA cycle via glutaminolysis including; the amino acids proline, aspartate, arginine and asparagine (Frezza & Gottlieb, 2009) which are beneficial for cancer progression; the energy source NADPH from NADP⁺ (Feron, 2009) which again is an important factor in tumor advances in order to produce fatty acids and nucleotides for growth. Furthermore, the truncated TCA cycle results in the final product of lactate which is believed to be utilised as an energy source by cancer cells (Feron, 2009).

Due to the innovative input of glutamine to the TCA cycle in cancer cells, acetyl CoA is now focussed into synthesising fatty acids and cholesterol which further aid the tumor (Feron, 2009). Additionally, evidence suggests that fatty acids and glutamate may aid in the defence of attacks from the host's immune system, i.e. they are immunosuppressive (Eck, Drings & Driige, 1989; Jiang, Bryce & Hoorobin, 1998). As discussed above, ROS are produced in cancerous cells and may be highly abundant. It is therefore important that the process of glutaminolysis is not detrimentally affected by ROS production if the tumor is to progress. It is noteworthy that lower glutamine concentrations (Kovacevic & McGivan, 1983), elevated glutamate concentrations, increased implications of the Warburg effect and elevated lactate (Nijsten, & van Dam, 2009) concentration are correlated to the aggressiveness of the tumor.

1.2.3 Systems Biology

1.2.3.1 Systems Biology for Advancing Cancer Knowledge

As previously mentioned, cancer is a complex disease which by definition involves an accumulation of natural (genomic) and environmental implications upon the cell (Pfeifer, 2010). A relatively novel approach to investigate such convoluted disorders is via systems biology (Hornberg *et al.*, 2006). Systems biology incorporates a multi-disciplinary nature in which biologists, chemists, mathematicians, physicists and computer specialists unite in order to achieve a communal, biological goal. Traditionally, biologists have investigated complex cellular behaviour by means of a reductionist approach. This involves studying complex biological behaviour by investigating specific molecules and interactions within a system. The contemporary systems approach investigates the system as a whole (holism), looking at all interacting molecules within the system simultaneously. The belief is that “the whole is greater than the sum of its parts” (Aristotle), i.e. one cannot study sole interactions and expect to understand how the whole system functions. This is due to behaviour which arises due to the complex interacting nature of the system which would not be normally observed whilst utilising a reductionist approach. These are known as emergent properties. Obviously, this systems biology course of action would not be possible without the knowledge gained from prior experiments on the relatively simple single interactions. For a systems biology review, please refer to Chuang *et al.* (2010). So, what does systems biology involve? What tools are utilised to advance systems biology?

1.2.3.2 High Throughput Technology and the ‘Omics’ Revolution

‘Omics’ is the study of biological organisms using a set of tools which are utilised in order to produce a large quantity of semi-/quantitative data. For this reason, these are known as high-throughput technologies. The ‘omics’ include genomics – the study of the genome; transcriptomics – the study of transcripts; proteomics – the study of proteins; and metabolomics – the study of the metabolites. Such relatively novel approaches are of great use when investigating cancer. There are a number of reasons for this.

Firstly, this enables the investigator to elucidate potential biomarkers (Johnson & Todd, 2000) and highlight altered pathways within the cancer cell (Patel *et al.*, 2009). This is achieved via a high resolution, comprehensive comparison between a healthy and cancerous cell at any instance in time (Hornberg *et al.*, 2006). The advanced ability of these platforms enables the identification of oncogenes and TSG which provide further understanding to the underlying mechanisms behind the disorder (Edgren *et al.*, 2007). Furthermore, as this comparison is instantaneous, an investigation may take place to study the onset and development of a cancerous growth; i.e. the cancer may be studied at various stages (Patel *et al.*, 2009), which in turn may provide further insight. Edgren and co-authors (2007) suggested that copy number alterations (CNAs) and somatic mutations are the underlying reasons for the onset of cancers and on these grounds, a comprehensive investigation may be undertaken using such platforms (Pinkel & Albertson, 2005).

Secondly, this is a systems approach which therefore results in the incorporation of emergent properties (Laubenbacher *et al.*, 2009) which would not arise if the study was to look at single interactions or pathways. That is to say, the complete interacting network is investigated concurrently (Nagaraj, 2009) which is advantageous as it enables the investigator to construct a cancer signature which may be utilised in the future as a diagnostic and prognostic tool (Eschrich *et al.*, 2009). Additionally, Nagaraj (2009) proposed

that a number of targets simultaneously require perturbation to combat the disease efficiently. In order to establish these combinations of targets, a systems approach is required. Further advantages include; no dissection of the sample is required (as this would cause obvious damage to the cells and proteins/metabolites may be lost) and also, whilst using specific platforms, no prior knowledge of protein composition is necessary (Patel *et al.*, 2009).

The high-throughput technologies with respects to the 'omics' are ever evolving. The various platforms each have associated advantages and disadvantages. For example, the study of the proteome is made possible through numerous platforms, and has the ability to elucidate biomarkers related with the disease (Srinivas *et al.*, 2002), has potential as a diagnostic and prognostic tool (Zhang *et al.*, 2009), and may provide some insight into the underlying mechanisms involved with the cancer (Nagaraj, 2009). Mass spectrometry (MS) is a useful tool within proteomics and is compatible to work in conjunction with other techniques such as 2D gel electrophoresis, for further analysis (Nagaraj, 2009) and with other omics technologies (Johnson & Todd, 2000). MS based proteomics has the capability of creating a map of the proteins within a sample (Gagné *et al.*, 2005) which is valuable when comparing cancerous and non-cancerous samples and for future reference. A large number of analytes may be simultaneously determined in a single experiment providing a sensitive analysis whilst covering a broad range of chemistries including peptides, polypeptides and tri-glycerides (Walch *et al.*, 2008).

In terms of disadvantages of high throughput technologies, Nagaraj (2009) stated that integration and standardisation is still an issue and validation against accepted clinical and pathology techniques is still necessary.

1.2.3.2.1 Metabolomics

The metabolomics field is becoming increasingly popular within the scientific community as a means of investigating cellular behaviour and function. Metabolomics is the quantitative evaluation of all low molecular weight molecules (metabolites) of the cell under a set of defined conditions at a specific point in time (Goodacre *et al.*, 2004). It is complementary to the other 'omics' and has associated advantages. Firstly, the metabolome is the final product of the cell and is a result of the interactions between the genes, mRNA and proteins (Nordström and Lewensohn, 2010). Hence, quantitating the metabolome is generally considered more closely related to assessing the phenotype of the organism than the other 'omics' (Ellis *et al.*, 2007). Diseased states will therefore be evident within the metabolome of biological systems (Ellis *et al.*, 2007). Secondly, minute alterations in the levels of proteins and mRNA may not be detected when measuring directly. However, these variations may significantly alter the concentrations of an array of metabolites which may then be identified and quantified (Urbanczyk-Wochniak *et al.*, 2003). Furthermore, a range of metabolites can be identified and quantified simultaneously with a degree of accuracy and precision (Ellis *et al.*, 2007).

Conversely, metabolism is extremely complex, with *Homo sapiens* possessing tens (and possibly hundreds) of thousands of metabolites (Spratlin *et al.*, 2009; Goodacre *et al.*, 2004). At present, it is not possible to identify and quantify all of these metabolites as a result of lack in technology (Goodacre *et al.*, 2004), although, this is a goal which is currently been worked towards. In addition, there are other issues concerning the methodology for metabolomics experiments including quenching (Faijes *et al.*, 2007) and extraction (Goodacre *et al.*, 2004).

The terminology of metabolomics may be confusing and is occasionally misused (Goodacre *et al.*, 2004). Table 1.1 defines the terms commonly used in metabolomics.

Table 1.1 Common terminologies utilised in metabolomics.

Term	Definition	Reference
Metabolomics	Identification and quantification of all metabolites within an organism. At present, this is not possible.	Goodacre <i>et al.</i> (2004)
Metabonomics	The quantitative measurement of the dynamic multiparametric metabolic response of living systems to pathophysiological stimuli or genetic modification.	Nicholson <i>et al.</i> (1999)
Metabolome	A quantitative analysis of all metabolites in a given sample	Ellis <i>et al.</i> (2007)
Metabolite target analysis	Quantitative analysis of a set of specific metabolites which are of interest.	Goodacre <i>et al.</i> (2004)
Metabolic/metabolite profiling	Analysis of a set of related metabolites within a sample. These may be related structurally (e.g. amino acids), or originate from a specific pathway	Fiehn (2001); Goodacre <i>et al.</i> (2004)
Metabolic fingerprinting	Is a top down approach. The high-throughput global analysis of the intracellular metabolome. The aim is to create a metabolic signature which will change upon perturbation of the system and thus maybe compared.	García-Pérez <i>et al.</i> (2008); Ellis <i>et al.</i> (2007)
Metabolic footprinting	The high throughput analysis of the extracellular metabolome. This assesses the metabolites secreted/excreted into the external environment. This generally requires no quenching or extraction of metabolites.	Goodacre <i>et al.</i> (2004)

1.2.3.2.2 Liquid Chromatography Mass Spectrometry (LC-MS) and Gas Chromatography Mass Spectrometry (GC-MS)

Chromatography techniques such as gas chromatography (GC) and liquid chromatography (LC) are frequently linked to mass spectrometry (MS) and utilised in order to determine and quantify analytes in a given sample. The measurements are then used to elucidate the molecular structure properties of an analyte or establish the elements which compose the sample (Watson & Sparkman, 2008). This is achieved through mass to charge (m/z) measurements of the analytes performed by the mass spectrometer. In biological terms, MS is applicable for metabolomics, proteomics and lipidomics (Griffiths & Wang, 2009).

GC-MS combines two analytical techniques which work in conjunction with each other. The GC performs the separation of the components of the sample predominantly based on volatility and chemistry and the MS is utilised for identification purposes. Once the GC separates the compounds within the sample, the mass spectrometer is able to identify and quantify each compound, thereby providing quantified values for each compound (Watson & Sparkman, 2008). GC-MS may be utilised for volatile, low molecular weight substances (Ekman *et al.*, 2009), such as fatty acids and metabolites (Bedair & Sumner, 2008) after derivatisation through methyl esterification. Derivatisation is a chemical process which modifies a chemical structure into a derivative which possesses more desirable attributes such as volatility, solubility or polarity. GC is beneficial in comparison to LC as is it relatively undemanding, the separation procedure is more rapid, the columns are more efficient than those of HPLC (Ekman *et al.*, 2009) and it is relatively inexpensive (Bedair & Sumner, 2008).

As with GC-MS, LC-MS is also a combination of two analytical practices, the LC for the separation and the MS for the identification and quantification of the compounds. Conversely to GC-MS, LC-MS is employed for the analysis of non-volatile and non-polar compounds which cannot be analysed via GC-MS

(Watson & Sparkman, 2008). LC-MS is also a very popular technique for metabolomics analysis (Bedair & Sumner, 2008). Advantages of LC-MS over GC-MS include reduced operating temperatures which enable the analysis of metabolites which are degraded at GC-MS temperatures and improved sample preparation requirements; i.e. no derivatisation is generally required (Bedair & Sumner, 2008).

The MS instrumentation comprises of three main components; the ionisation source, the mass analyser and the ion detector (see Figure 1.9). First, the metabolites are separated in terms of volatility, polarity and charge via GC, LC or capillary electrophoresis (CE). GC functions through heating of the sample whereby metabolites elute in order of volatility, the most volatile metabolite first since they will vaporise at a lower temperature. However, as mentioned previously, metabolites which are sensitive to heat will not be detected. In addition, the GC separation is also dependent on the column chemistry as metabolites will interact with the column differently. When utilising LC for separation, the sample is diluted in an appropriate solvent at low temperatures (and hence volatility is not a factor) and separation is generally based due to polarity of the analytes under investigation. However, the metabolites must be ionised if they are to be detected during MS.

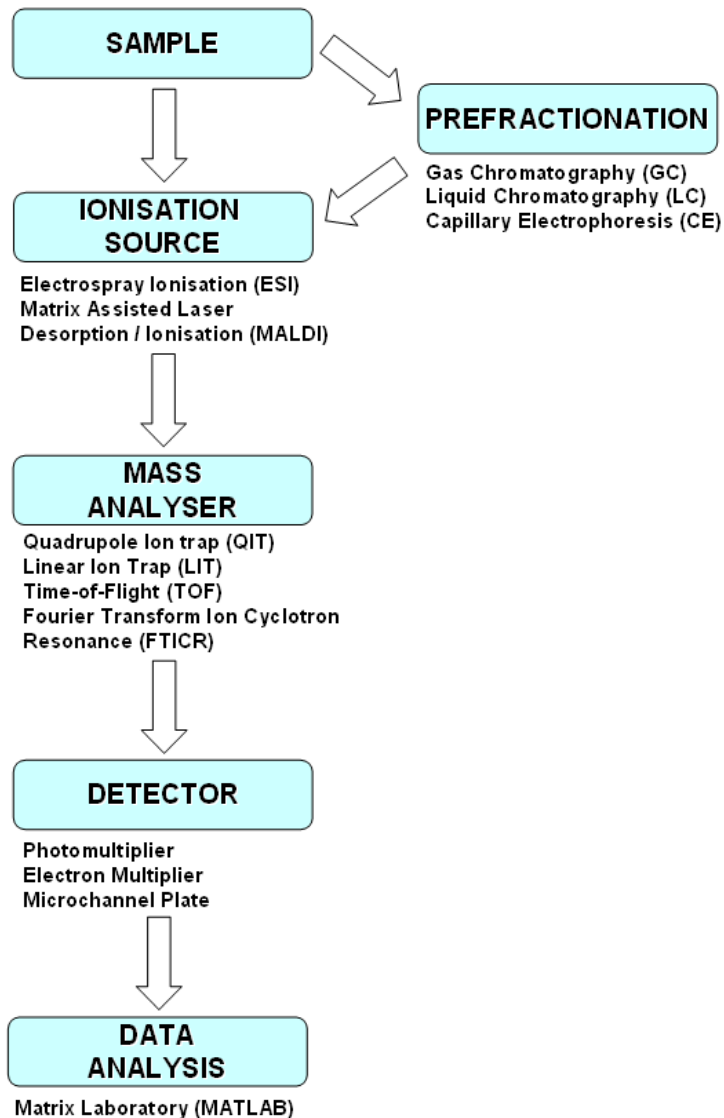


Figure 1.9 General flow chart for Mass Spectrometry
(Feng *et al.*, 2008).

The subsequent stage is ionisation of the sample. Only a recent enhancement in technology has resulted in advanced techniques which have allowed mass spectrometry to become an everyday use for biologists. These developments included that of electropray ionisation (ESI) (Fenn *et al.*, 1989) and matrix assisted laser desorption/ionisation (MALDI) (Karas & Hillenkamp, 1988; Tanaka *et al.*, 1988) both of which result in ‘softer’ ionisation of the sample (Prokai *et al.*, 1996; Feng *et al.*, 2008).

Once the sample has been ionised the mass analyser separates the ions according to their mass-to-charge ratio (m/z). Again, there are variations within mass analysers including quadrupole (Q), linear ion trap (LIT), Fourier transform ion cyclotron resonance-mass spectrometry (FTICR), Orbitrap and time-of-flight (TOF). Linear TOF-MS is a common approach adopted for the analysis of variety of analytes (including metabolites). This variation involves a flight tube in which an electric field is utilised to accelerate metabolites through the tube to the detector. The mass of the ion is proportional to the arrival time of the metabolite (analyte) through the flight tube to the detector; the metabolites reach the detector in order of m/z (Guilhaus *et al.*, 1997; Allwood & Goodacre 2010). The Orbitrap device is the most recent development for an ion trapping m/z analyser (Watson & Sparkman, 2008). In this system, ions are trapped and maintained in a potential well about a central spindle electrode (Hu *et al.*, 2005; Ekman *et al.*, 2009). Rather than ejecting the ions for detection, the oscillatory frequency of the ions are measured (and this behaviour is based on the m/z ratio of the ions) (Bedair & Sumner, 2008). The result is an increased resolution and improved mass accuracy (Bedair & Sumner, 2008; Ekman *et al.*, 2009).

As promising as MS may appear, there are still drawbacks to its use. Primarily, there is a distinct lack of standards relating to the methodology including sample preparation (predominantly in proteomics) (Calvano *et al.*, 2010; Nagaraj, 2009). Also, there is a lack of analytical standards for natural compounds that allow identification. Another major issue relates to the bioinformatics tools available for analysing the vast quantity of data produced with these high throughput technologies (van Wieringen, van de Wiel & Ylstra, 2007). However, such bioinformatics tools are rapidly evolving and databases containing a wealth of information are being developed such as the COSMIC (catalogue of somatic mutations in cancer). In addition, legislations are being brought into play such as the minimum information about a microarray experiment (MIAME); the minimum information about a proteomics experiment (MIAPE) and the metabolomics standards initiative (MSI) which ensure that

scientists supply as much information as possible to their peers in order of reference to aid in further advancing current knowledge (Sumner *et al.*, 2007). Metabolite identification is a major factor in metabolomics based experiments and the MSI states that published data should elaborate upon each metabolite reported. This should include the status of the identification and whether this is definite, putative or unknown based upon physiochemical properties and/or spectral similarities with public databases.

1.2.3.2.3 Chemometrics

Chemometrics is a tool used in chemistry based science to extract information using techniques from mathematics, statistics and computer sciences. The aim is to optimise the data (such as that obtained from metabolomics experiments) through elucidating relationships which may previously not be so obvious. Techniques include principal components analysis (PCA), partial least squares (PLS) and discriminant function analysis (DFA), some of which are elaborated on below. For a more in-depth review on chemometrics, please refer to Workman *et al.* (2006) and/or Madsen *et al.* (2010).

1.2.3.2.3.1 Principal Component Analysis (PCA)

PCA is a widely exploited, unsupervised, multivariate analysis technique which is used to analyse data sets with large numbers of variables (Jolliffe, 1986). The aim of PCA is to reduce the complexity of the data whilst maintaining the greatest variance of the data set. This is achieved by the algorithm (in this case, non-linear partial least squares (NIPALS) (Wold, 1966)) explaining the variance-covariance structure of a data set via a few linear combinations of these variables. The data are displayed by a small number of principal components (PCs), with PC1 attaining the greatest quantity of variance, PC2 the second greatest and so on and so forth. This reduced data may then be visualised on a PCA scores plot in addition to a loadings plot, which depicts the origin of the variance observed. Nevertheless, PCA does not always exhibit the desired

relationship and so, the PC scores may be used as an intermediate step to further analyses such as PC-DFA (principal component-discriminant function analysis).

1.2.3.2.3.2 Principal Component-Discriminant Function Analysis (PC-DFA)

Depending on the data set, PCA may not always correctly represent the data and so other methods are needed to extract the relevant information. One option is PC-DFA (Manly, 1994), which is another multivariate analysis technique. PC-DFA is supervised which requires *a priori* information which is fed into the algorithm; this aids in discriminating the various classes. The algorithm uses this information and maximises the distance between classes and minimises the distance amongst classes, which in effect causes tighter, more defined clusters. However, since this is a supervised technique, validation is required which uses trained and test data to ensure that the model is not over-fitting the data.

1.2.3.2.3.3 PARAllel FACtor (PARAFAC) Analysis

PARAFAC (Bro, 1997) is a modified version of PCA, which basically adopts PCA at multiple tensors (such as time points) (Kroonenberg, 2008). This analysis is displayed in the form of a manifold of PCA scores plots, each exhibiting different tensors. This is useful when there is a large array of data taken over various time points and sheds light on the behaviour over the specified time.

1.2.3.2.3.4 Clustergram Analysis

A further analysis technique used during these studies was a clustergram, which is a hybrid of a heat map and a dendrogram. The purpose of a clustergram is to represent variables (such as metabolites) which are behaving in a similar fashion in an aesthetically pleasing manner. It is expected that related variables will cluster together on the clustergram, providing experimental

validity to the data. If this is the case, one can also assume that variables which have not been assessed will, by and large, behave in an analogous fashion also.

1.2.3.3 Modelling in Cancer

Once such vast amounts of data have been collected through high throughput technologies, one possibility is to input the information into a computational representation as a means of attempting to understand the complex behaviour. A model may be constructed in such a manner, that it may predict an outcome utilising a set of equations and defined parameters which have been derived from experimental work.

Modelling cancer is an extremely challenging prospect due to its unpredictable nature and the vast quantity of genes, proteins, molecules etc involved (for a review on modelling in cancer refer to Hornberg *et al.*, 2006). Furthermore, by definition, cancer is a multi-cellular disorder, which further complicates the modelling process. In addition, the model has to be made aware of cellular processes such as apoptosis, all integrated feedback loops involved with associated components, etc. The complexity of a cancer network is currently incomprehensible.

The overall aim of a mathematical model in cancer is to elucidate therapeutic targets within the cell which can be utilised to combat the disease or to expose biomarkers specific to that cancer. It is also possible to construct models which can predict the behaviour of the system following perturbation; for example, exposure to cancer drugs which would highlight the system wide effects of the drug. Models provide a valuable tool which can present insight into a complex system such as cancer behaviour, and thus, utilised in conjunction with complimentary methods such as high throughput technologies, may lead to the understanding of cancer.

1.2.4 Aims and Objectives of the Project

The general aims and objectives of this project are:

- To elucidate the capability of CoCl_2 as a hypoxic mimicker in hTERT cells and to assess (if any) those effects caused by CoCl_2 exposure which are not associated with the hypoxic response. Explicitly, to investigate any limitations with using CoCl_2 as a hypoxic mimicker.
- To investigate the effects of a PDE4D knock down on BicR16 cells and hence its potential influence on cancer initiation and progression. Phenotypic effects and central metabolism will be a main focus.
- To create a validated mathematical model of central metabolism and the effects of the transcription factor HIF-1 with practical predictive capabilities.

CoCl_2 will be found to be an inappropriate hypoxic mimic in eukaryotic cells due to its undesirable effects seen in metabolism. Although the hypoxic response will be mimicked in terms of central carbon metabolism when exposed to $100\mu\text{M}$ CoCl_2 ; these off-target effects should be noted and the substance should be avoided where possible and substituted for the genuine hypoxic environment.

PDE4D will play a role in cancer associated attributes and will have an effect on central metabolism in the OSCC cell line BicR16. These effects will be synergetic through the transcription factors HIF-1 and CREB. PDE4D will be elucidated as a TSG as the knockdown in expression will result in an increased proliferation, migration and glycolytic flux.

Tumorous central metabolism contains weak points which may be targeted for therapeutic benefit. These targets will be a component of glycolysis since this pathway is enhanced through hypoxia and if targeted, these therapeutic agents will have less of an effect on healthy cells. Glutaminolysis associated enzymes will be a target for therapeutic benefit since cancerous cells are heavily reliant on glutamine as an energy source and this will be elucidated in the model.

1.3 References

Abramovitch, R. Tavor, E. Jacob-Hirsch, J. Zeira, E. Amariglio, N. Pappo, O. Rechavi, G. Galun, E. and Honigman, A. (2004). A Pivotal Role of Cyclic AMP-Responsive Element Binding Protein in Tumor Progression. *Cancer Research*, **64**: 1338-1346.

Allwood, J. W. and Goodacre, R. (2010). An introduction to liquid chromatography-mass spectrometry instrumentation applied in plant metabolomic analyses. *Phytochemical Analysis*, **21**: 33-47.

Altenberg, B. and Greulich, K, O. (2004). Genes of glycolysis are ubiquitously overexpressed in 24 cancer classes. *Genomics*, **84**: 1014-1020.

An, W, G. Kanekal, M. Simon, M, C. Maltepe, E. Blagosklonny, M, V. and Meckers, L, M. (1998). Stabilization of wild-type p53 by hypoxia-inducible factor 1alpha. *Nature*, **392**: 405-408.

Ashrafian, H. (2006). Cancer's sweet tooth: the Janus effect of glucose metabolism in tumorigenesis. *Lancet*, **367**: 618-621.

Baggetto, L, G. (1992). Deviant energetic metabolism of glycolytic cancer cells. *Biochimie*, **74**: 959-974.

Baldwin, C. Garnis, C. Zhang, L. Rosin, M, P. and Lam, W, L. (2005). Multiple Microalterations Detected at High Frequency in Oral Cancer. *Cancer Research*, **65**: 7561-7567.

Bartrons, R. and Caro, J. (2007). Hypoxia, glucose metabolism and the Warburg's effect. *Journal of Bioenergetics and Biomembranes*, **39**: 223-229.

Baugh, J, A. Gantier, M. Li, L. Byrne, A. Buckley, A. Donnelly, S, C. (2006). Dual regulation of macrophage migration inhibitory factor (MIF) expression in hypoxia by CREB and HIF-1. *Biochemical and Biophysical Research Communications*, **347**: 895-903.

Beavo, J, A. (1995). Cyclic nucleotide phosphodiesterases: functional implications of multiple isoforms. *Physiological Reviews*, **75**: 725-748.

Bedair, M. and Sumner, L, W. (2008). Current and emerging mass-spectrometry technologies for metabolomics. *Trends in Analytical Chemistry*, **27**: 238-250.

Bensaad, K. Tsuruta, A. Selak, M, A. Vidal, M, N. Nakano, K. Bartrons, R. Gottlieb, E. and Vousden, K, H. (2006). TIGAR, a p53-inducible regulator of glycolysis and apoptosis. *Cell*, **126**: 107-120.

Berra, E. Roux, D. Richard, D, E. Pouyssegur, J. (2001). Hypoxia-inducible factor-1 α (HIF-1 α) escapes O₂-driven proteasomal degradation irrespective of its subcellular localization: nucleus or cytoplasm. *EMBO Reports*, **2**: 615-620.

Bhat, S, G. Mishra, S. Mei, Y. Nie, Z. Whitwort, C, A. Rybak, L, P. and Ramkumar, V. (2002). Cisplatin up-regulates the adenosine A1 receptor in the rat kidney. *European Journal of Pharmacology*, **442**: 251-264.

Brand, K. (1985). Glutamine and glucose metabolism during thymocyte proliferation. Pathways of glutamine and glutamate metabolism', *Biochemical Journal*, **228**: 353-361.

Breit, J, F. Ault-Ziel, K. Al-Mehdi, AB. and Gillespie, M, N. (2008). Nuclear protein-induced bending and flexing of the hypoxic response element of the rat vascular endothelial growth factor promoter. *The FASEB Journal*, **22**: 19-29.

Bro, R. (1997). PARAFAC. Tutorial and applications. *Chemometrics and intelligent laboratory systems*, **38**: 149-171.

Buzzai, M. Bauer, D, E. Jones, R, G. DeBerardinis, R, J. Hatzivassiliou, G. Elstrom, R, L. and Thompson, C, B. (2005). The glucose dependence of Akt-transformed cells can be reversed by pharmacologic activation of fatty acid [beta]-oxidation. *Oncogene*, **24**: 4165-4173.

Calvano, C, D. Aresta, A. Iacovone, M. DeBenedetto, G, E. Zambonin, C, G. Battaglia, M. Ditonno, P. Rutigliano, M. and Bettocchi, C. (2010). Optimization of analytical and pre-analytical conditions for MALDI-TOF-MS human urine protein profiles. *Journal of Pharmaceutical and Biomedical Analysis*, **51**: 907-914.

Chachami, G. Simos, G. Hatziefthimiou, A. Bonanou, S. Molyvdas, PA. and Paraskeva, E. (2004). Cobalt Induces Hypoxia-Inducible Factor-1 α Expression in Airway Smooth Muscle Cells by a Reactive Oxygen Species– and PI3K-Dependent Mechanism. *American Journal of Respiratory Cell and Molecular Biology*, **31**: 544-551.

Chandel, N, S. Maltepe, E. Goldwasser, E. Mathieu, C, E. Simons, M, C. and Schumacker, P, T. (1998). Mitochondrial reactive oxygen species trigger hypoxia-induced transcription. *Cell Biology*, **95**: 11715-11720.

Chen, C. Pore, N. Behrooz, A. Ismail-Beigi, F. and Maity, A. (2001). Regulation of glut1 mRNA by hypoxia-inducible factor-1. Interaction between H-ras and hypoxia. *Journal of Biological Chemistry*, **276**: 9519-9525.

Chesney, J. Mitchell, R. Benigni, F. Bacher, M. Spiegel, L. Al-Abed, Y. Han, J. H. Metz, C. and Bucala, R. (1999). An inducible gene product for 6-phosphofructo-2-kinase with an AU-rich instability element: role in tumor cell glycolysis and the Warburg effect. *Proceedings of the National Academy of Sciences*, **96**: 3047-3052.

Chuang, HY. Hofree, M. and Ideker, T. (2010). A Decade of Systems Biology. *Annual Review of Cell and Developmental Biology*, **26**: 721-744.

Chio, CC. Chang, YH. Hsu, YM. Chi, KH. and Lin, WW. (2004). PKA-dependent activation of PKC, p38 MAPK and IKK in macrophage: implication in the induction of inducible nitric oxide synthase and interleukin-6 by dibutyryl cAMP. *Cellular Signalling*, **16**: 565-575.

Christofk, H, R. Vander Heiden, M, G. Harris, M, H. Ramanathan, A. Gerszten, R, E. Wei, R. Fleming, M, D. Schreiber, S, L. and Cantley, L, C. (2008). The M2 splice isoform of pyruvate kinase is important for cancer metabolism and tumour growth. *Nature*, **452**: 230-233.

Conti, M. Jin, S, L. Monaco, L. Repaske, D, R. and Swinnen, J, V. (1991). Hormonal regulation of cyclic nucleotide phosphodiesterases. *Endocrine Reviews*, **12**: 218-234.

Conti, M. and Jin, SL, C. (1999). The molecular biology of cyclic nucleotide phosphodiesterases', *Progress in Nucleic Acid Research and Molecular Biology*, **63**: 1-38.

da Silveira, É, J, D. Oliveira, M, C. de Moraes, M, L, S, A. Queiroz, L, M, G. Costa, A, L, L. (2008). nm23 protein expression in metastatic and non-metastatic tongue squamous cell carcinoma. *Brazilian Journal of Otorhinolaryngology*, **74**: 356-359.

DeBerardinis, R, J. Sayed, N. Ditsworth, D. and Thompson, C, B. (2008). Brick by brick: metabolism and tumor cell growth. *Current Opinion in Genetics & Development*, **18**: 54-61.

Diaz-Ruiz, R. Uribe-Carvajal, S. Devin, A. and Rigoulet, M. (2009). Tumor cell energy metabolism and its common features with yeast metabolism. *Biochimica et Biophysica Acta*, **1796**: 252-265.

Dimova, E, Y. Jakubowska, M, M. and Kietzmann, T. (2007). CREB binding to the hypoxia-inducible factor-1 responsive elements in the plasminogen activator inhibitor-1 promoter mediates the glucagon effect. *Journal of Thrombosis and Haemostasis*, **98**: 296-303.

Durante, P. Gueuning, MA. Darville, M, I. Hue L. and Rousseau, G, G. (1999). Apoptosis induced by growth factor withdrawal in fibroblasts overproducing fructose 2,6-bisphosphate. *FEBS letters*, **448**: 239-243.

Eck, HP. Drings, P. and Driige, W. (1989). Plasma glutamate levels, lymphocyte reactivity and death rate in patients with bronchial carcinoma. *Journal of Cancer Research and Clinical Oncology*, **115**: 571-574.

Edgren, H. Wolf, M. Kallioniemi, O. Nees, M. (2007). Cancer genome analysis: a landscape seen from many angles. *Drug Discovery Today: Disease Mechanisms*, **4**: 269-276.

Eigenbrodt, E. Basenau, D. Holthusen, S. Mazurek, S. and Fischer, G. (1997). Quantification of tumor type M2 pyruvate kinase (Tu M2-PK) in human carcinomas. *Anticancer Research*, **17**: 3153-3156.

Eigenbrodt, E. Reinacher, M. Scheefers-Borchel, U. Scheefers, H. and Friis, R. (1992). Double role for pyruvate kinase type M2 in the expansion of phosphometabolite pools found in tumor cells. *Critical Reviews in Oncogenesis*, **3**: 91-115.

Ekman, R. (Ed), Silberring, J. (Ed), Brinkmalm, A, M. (Ed), Desiderio, D, M. Nibbering, N, M. (2009). *Mass Spectrometry: Instrumentation, Interpretation, and Applications*. Wiley.

Ellis, D, I. Dunn, W, B. Griffin, J, L. Allwood, J, W. Goodacre, R. (2007). Metabolic fingerprinting as a diagnostic tool', *Pharmacogenomics*, **8**: 1243-1266.

Eschrich, S. Zhang, H. Zhao, H. Boulware, D. Lee, JH. Bloom, G. and Torres-Roca, J, F. (2009). Systems biology modelling of the radiation sensitivity network: A biomarker discovery platform. *International Journal of Radiation, Oncology, Biology, Physics*, **75**: 497-505.

Faijes, M. Mars, A, E. and Smid, E, J. (2007). Comparison of quenching and extraction methodologies for metabolome analysis of *Lactobacillus plantarum*. *Microbial Cell Factories*, **6**: 27.

Fan, T, W. Kucia, M. Jankowski, K. Higashi, R, M. Ratajczak, J. Ratajczak, M, Z. Lane, A, N. (2008). Rhabdomyosarcoma cells show an energy producing anabolic metabolic phenotype compared with primary myocytes. *Molecular Cancer*, **7**: 79.

Favot, L. Keravis, T. and Lugnier, C. (2004). Modulation of VEGF-induced endothelial cell cycle protein expression through cyclic AMP hydrolysis by PDE2 and PDE4. *Thromb Haemost*, **92**: 634-645.

Fedele, S. (2009). Diagnostic aids in the screening of oral cancer. *Head & Neck Oncology*, **1**: 5.

Feng, X. Liu, X. Luo, Q. and Liu, B. (2008). Mass Spectrometry in Systems Biology: An Overview. *Mass Spectrometry Reviews*, **27**: 635-660.

Fenn, J, B. Mann, M. Meng, C, K. Wong, S, F. and Whitehouse, C, M. (1989). Electrospray ionization for mass spectrometry of large biomolecules. *Science*, **246**: 64-71.

Fiehn, O. (2001). Combining genomics, metabolome analysis, and biochemical modelling to understand metabolic networks. *Comparative and Functional Genomics*, **2**: 155-168.

Ferguson, E, C. and Rathmell, J, C. (2008). New roles for pyruvate kinase M2: working out the Warburg effect. *Trends in Biochemical Sciences*, **33**: 359-362.

Feron, O. (2009). Pyruvate into lactate and back: From the Warburg effect to symbiotic energy fuel exchange in cancer cells. *Radiotherapy and Oncology*, **92**: 329-333.

Firth, J, D. Ebert, B, L. and Ratcliffe, P, J. (1995). Hypoxic Regulation of Lactate Dehydrogenase A. Interactions between hypoxia-inducible factor 1 and cAMP response elements. *The Journal of Biological Chemistry*, **270**: 21021-21027.

Freeland, K. Boxerb, L, M. Latchman, D, S. (2001). The cyclic AMP response element in the Bcl-2 promoter confers inducibility by hypoxia in neuronal cells. *Molecular Brain Research*, **92**: 98-106.

Frezza, C. and Gottlieb, E. (2009). Mitochondria in cancer: Not just innocent bystanders. *Seminars in Cancer Biology*, **19**: 4-11.

Fryknäs, M. Rickardson, L. Wickström, M. Dhar, S. Lövborg, H. Gullbo, J. Nygren, P. Gustafsson, M. G. Isaksson, A. and Larsson, R. (2006). Phenotype-Based Screening of Mechanistically Annotated Compounds in Combination with Gene Expression and Pathway Analysis Identifies Candidate Drug Targets in a Human Squamous Carcinoma Cell Model. *Journal of Biomolecular Screening*, **11**: 457-468.

Fukuda, R. Zhang, H. Kim, J. W. Shimoda, L. Dang, C. V. and Semenza, G. L. (2007). HIF-1 regulates cytochrome oxidase subunits to optimize efficiency of respiration in hypoxic cells. *Cell*, **129**: 111-122.

Fushimia, K. Uzawaa, K. Ishigamia, T. Yamamotof, N. Kawatab, T. Shibaharaf, T. Itob, H. Mizoe, J. Tsujiie, H. Tanzawaa, H. (2008). Susceptible genes and molecular pathways related to heavy ion irradiation in oral squamous cell carcinoma cells. *Radiotherapy and Oncology*, **89**: 237-244.

Gagné, JP. Gagné, P. Hunter, J. M. Bonicalzi, ME. Lemay, JF. Kelly, I. Le Page, C. Provencher, D. Mes-Masson, AM. Droit, A. Bourgeois, D. and Poirier, G. G. (2005). Proteome profiling of human epithelial ovarian cancer cell line TOV-112D. *Molecular and Cellular Biochemistry*, **275**: 25-55.

García-Pérez, I. Vallejo, M. García, A. Legido-Quigley, C. and Barbas, C. (2008). Metabolic fingerprinting with capillary electrophoresis', *Journal of Chromatography A*, **1204**: 130-139.

Gatenby, R. A. and Gillies, R. (2004). Why do cancers have high aerobic glycolysis? *Nature Reviews Cancer*, **4**: 891-899.

Gath H, J. and Brakenhoff, R. H. (1999). Minimal residual disease in head and neck cancer. *Cancer and Metastasis Reviews*, **18**: 109-126.

Gogvadze, V. Orrenius, S. and Zhivotovsky, B. (2009). Mitochondria as targets for cancer chemotherapy. *Seminars in Cancer Biology*, **19**: 57-66.

Goodacre, R. Vaidyanathan, S. Dunn, W, B. Harrigan, G, G. and Kell, D, B. (2004). Metabolomics by numbers: acquiring and understanding global metabolite data. *Trends in Biotechnology*, **22**: 245-252.

Griffiths, W, J. and Wang, Y (2009). Mass spectrometry: from proteomics to metabolomics and lipidomics. *Chemical Society Reviews*, **38**: 1882-1896.

Guha, N. Boffetta, P. Filho, V, W, Neto, J, E. Shangina, O. Zaridze, D. Curado, M, P. Koifman, S. Matos, E. Menezes, A. Szeszenia-Dabrowska, N, Fernandez, L. Mates, D. Daudt, A, W. Lissowska, J. Dikshit, R and Brennan P. (2007). Oral Health and Risk of Squamous Cell Carcinoma of the Head and Neck and Esophagus: Results of Two Multicentric Case-Control Studies. *American Journal of Epidemiology*, **166**: 1159-1173.

Guilhaus, M. Mlynski, V. and Selby, D. (1997). Perfect timing: Time-of-flight mass Spectrometry. *Rapid Communications in Mass Spectrometry*, **11**: 951-962.

Guo, M. Song, LP. Jiang, Y. Liu, W. Yu, Y. and Chen, GQ. (2006). Hypoxia-mimetic agents desferrioxamine and cobalt chloride induce leukemic cell apoptosis through different hypoxia-inducible factor-1 α independent mechanisms. *Apoptosis*, **11**: 67-77.

Hahn-Windgassen, A. Nogueira, V. Chen, C, C. Skeen, J, E. Sonenberg, N. and Hay, N. (2005). Akt activates the mammalian target of rapamycin by regulating cellular ATP level and AMPK activity. *Journal of Biological Chemistry*, **280**: 32081-32089.

Hardie, D, G. (2004). The AMP-activated protein kinase pathway – new players upstream and downstream. *Journal of Cell Science*, **117**: 5479-5487.

HelmLinger, G. Yuan, F. Dellian, M. and Jain, R, K. (1997). Interstitial pH and pO₂ gradients in solid tumors in vivo: high-resolution measurements reveal a lack of correlation. *Nature Medicine*, **3**:177-182.

Hirsh, L. Dantesa, A. Suhb, BS. Yoshidac, Y. Hosokawac, K. Tajimac, K. Kotsujic, F. Merimskyd, O. and Amsterdama, A. (2004). Phosphodiesterase inhibitors as anti-cancer drugs. *Biochemical Pharmacology*, **68**: 981-988.

Hitchler, M, J. and Domann, F, E. (2009). Metabolic defects provide a spark for the epigenetic switch in cancer. *Free Radical Biology & Medicine*, **47**: 115-127.

Ho, V, T. and Bunn, H, F. (1996). Effects of transition metals on the expression of the erythropoietin gene: Further evidence that the oxygen sensor is a heme protein. *Biochemical and Biophysical Research Communications*, **223**: 175-180.

Hornberg, J, J. Bruggemana, F, J. Westerhoff, H, V. and Lankelma, J. (2006). Cancer: A Systems Biology disease. *BioSystems*, **83**: 81-90.

Houslay, M, D. and Adams, D, R. (2003). PDE4 cAMP phosphodiesterases : modular enzymes that orchestrate signalling cross-talk, desensitization and compartmentalization. *Biochemical Journal*, **370**: 1-18.

Houslay, M, D. and Baillie, G, S. (2005). β -Arrestin-recruited phosphodiesterase-4 desensitizes the AKAP79/PKA-mediated switching of β 2-adrenoceptor signalling to activation of ERK. *Biochemical Society Transactions*, **33**: 1333-1336.

Houslay, M, D. Schafer, P. and Zhang, K, Y, J. (2005). Keynote review: Phosphodiesterase-4 as a therapeutic target. *Drug Discoveries and Therapeutics*, **10**: 1503-1519.

Houslay, M, D. Baillie, G, S. and Maurice, D, H. (2007). cAMP specific phosphodiesterase-4 enzymes in the cardiovascular system: a molecular toolbox for generating compartmentalised cAMP signalling. *Circulation Research*, **100**: 950-966.

Hsu, P, P. and Sabatini, D, M. (2008). Cancer Cell Metabolism: Warburg and Beyond. *Cell*, **134**: 703-707.

Hu, Q. Noll, R, J. Li, H. Makarov, A. Hardman, M. and Cooks, R, G. (2005). The Orbitrap: a new mass spectrometer', *Journal of Mass Spectrometry*, **40**: 430-443.

Huang, Z. Ducharme, Y. Macdonald, D. and Robichaud, A. (2001). The next generation of PDE4 inhibitors. *Current Opinion in Chemical Biology*, **5**: 432-438.

Huston, E. Houslay, T, M. Baillie, G, S. and Houslay, M, D. (2006). cAMP phosphodiesterase-4A1 (PDE4A1) has provided the paradigm for the intracellular targeting of phosphodiesterases, a process that underpins compartmentalized cAMP signalling. *Biochemical Society Transactions*, **34**: 504-509.

Jarvinen, AK. Autio, R. Kilpinen, S. Saarela, M. Leivo, I. Grenman, R. Makitie, A, A. and Monni, O. (2008). High-Resolution Copy Number and Gene Expression Microarray Analyses of Head and Neck Squamous Cell Carcinoma Cell Lines of Tongue and Larynx. *Genes, Chromosomes & Cancer*, **47**: 500-509.

Jiang, B, H. Jiang, G. Zheng, J, Z. Zhimin, L. Hunter, T. and Vogt, P, K. (2001). Phosphatidylinositol 3-kinase signalling controls levels of hypoxia-inducible factor 1. *Cell Growth and Differentiation*, **12**, pp. 363-369.

Jiang, W, G. Bryce, R, P. and Hoorobin, D. (1998). Essential fatty acids: molecular and cellular basis of their anti-cancer action and clinical implications. *Critical Reviews in Oncology/Hematology*, **27**: 179-209.

Jin, S, L. Richard, F, J. Kuo, W, P. D'Ercole, A, J. and Conti, M. (1999). Impaired growth and fertility of cAMP-specific phosphodiesterase PDE4D-deficient mice. *Proceedings of the National Academy of Sciences USA*, **96**: 11998-12003.

Johnson, G, C, L. and Todd, J, A. (2000). Strategies in complex disease mapping. *Current Opinion in Genetics & Development*, **10**: 330-334.

Jolliffe, I. (1986). 'Principal Component Analysis', NewYork, Springer-Verlag.

Jones, R, G. Plas, D, R. Kubek, S. Buzzai, M. Mu, J. Xu, Y. Birnbaum, M, J. and Thompson, C, B. (2005). AMP-activated protein kinase induces a p53-dependent metabolic checkpoint. *Molecular Cell*, **18**: 283-293.

Kahn, B, B. Alquier, T. Carling, D. and Hardie, D, G. (2005). AMP-activated protein kinase: ancient energy gauge provides clues to modern understanding of metabolism. *Cell Metabolism*, **1**: 15-25.

Karas, M. and Hillenkamp, F. (1988). Laser desorption ionization of proteins with molecular masses exceeding 10,000 daltons. *Analytical Chemistry*, **60**: 2299-2301.

Karpuzoglu, E. and Ahmed, S, A. (2006). Estrogen regulation of nitric oxide and inducible nitric oxide synthase (iNOS) in immune cells: Implications for immunity, autoimmune diseases, and apoptosis. *Nitric Oxide*, **15**: 177-186.

Kato, K. Hara, A. Kuno, T. Mori, H. Yamashita, T. Toida, M. and Shibata, T. (2006). Aberrant promoter hypermethylation of p16 and MGMT genes in oral squamous cell carcinomas and the surrounding normal mucosa. *Journal of Cancer Research and Clinical Oncology*, **132**: 735-743.

Ke, Q. and Costa, M. (2006). Hypoxia-Inducible Factor-1 (HIF-1). *Molecular Pharmacology*, **70**: 1469-1480.

Keravis, T. Komasa, N. and Lugnier, C. (2000). Cyclic nucleotide hydrolysis in bovine aortic endothelial cells in culture: differential regulation in cobblestone and spindle phenotypes. *Journal of Vascular Research*, **37**: 235-249.

Kim, JW. Gardner, L, B. and Dang, C, V. (2005). Oncogenic alterations of metabolism and the Warburg effect. *Drug Discovery Today: Disease Mechanisms*, **2**: 233-238.

Kim, K, S. Rajagopal, V. Gonsalves, C. Johnson, C. and Kalra, V, K. (2006). Chemokine in Human Endothelial Hypoxia-Mediated Expression of IL-8 Factor in Cobalt Chloride- and A Novel Role of Hypoxia-Inducible cells. *Journal of Immunology*, **177**: 7211-7224.

King, A. Selak, M, A. and Gottlieb, E. (2006). Succinate dehydrogenase and fumarate hydratase: linking mitochondrial dysfunction and cancer', *Oncogene*, **25**: 4675-4682.

Kole, H, K. Resnick, R, J. Van Doren, M, and Racker, E. (1991). Regulation of 6-phosphofructo-1-kinase activity in ras-transformed rat-1 fibroblasts. *Archives of Biochemistry and Biophysics*, **286**: 586-590.

Kondoh, H. (2008). Cellular life span and the Warburg effect. *Experimental Cell Research*, **314**: 1923-1928.

Kovacevic, Z and McGivan, J, D. (1983). Mitochondrial Metabolism of Glutamine and Glutamate and Its Physiological Significance. *Physiological Reviews*, **63**: 547-605.

Kowalczyk, P. Kinjo, T. Kowalczyk, M. Walaszek, Z. Hanausek, M. Slaga, T, J. (2009). Effect of phosphodiesterase antagonists on glucocorticoid mediated growth inhibition in murine skin cell lines. *European Journal of Pharmacology*, **610**: 29-36.

Kress, S. Stein, A. Maurer, P. Weber, B. Reichert, J. Buchmann, A. Huppert, P. and Schwarz, M. (1998). Expression of hypoxia-inducible genes in tumor cells. *Journal of Cancer Research and Clinical Oncology*, **124**: 315-320.

Kroonenberg, P, M. (2008). Applied multiway data analysis. Wiley Series in Probability and Statistics, Wiley-Interscience.

Kujan, O. Glenny, A, M. Duxbury, J. Thakker, N. and Sloan, P. (2005). Evaluation of Screening Strategies for Improving Oral Cancer Mortality: A Cochrane Systematic Review. *Journal of Dental Education Journal of Dental Education*, **69**: 255-265.

Kujan, O. Oliver, R. Roz, L. Sozzi, G. Ribeiro, N. Woodward, R. Thakker, N, and Sloan, P. (2006). Fragile Histidine Triad Expression in Oral Squamous Cell Carcinoma and Precursor Lesions. *Clinical Cancer Research*, **12**: 6723-6729.

Laubenbacher, R. Hower, V. Jarrah, A. Torti, S, V. Shulaev, V. Mendes, P. Torti, F, M. and Akman, S. (2009). A systems biology view of cancer. *Biochimica et Biophysica Acta*, **1796**: 129-139.

Lee, CH. Wu, DC. Lee, JM. Wu, IC. Goan, YG. Kao, EL. Huang, HL. Chan, TF. Chou, SH. Chou, YP. Lee, CY. Chen, PS. Ho, CK. He, J. and Wu, MT. (2007). Carcinogenetic impact of alcohol intake on squamous cell carcinoma risk of the oesophagus in relation to tobacco smoking' *European Journal of Cancer*, **43**: 1188-1199.

LaManna, J, C. Pichiule, P. and Chavez, J, C. (2007). 7.2 Genetics and Gene Expression of Glycolysis. IN *Handbook of Neurochemistry and Molecular Neurobiology*. Springer-Verlag Berlin Heidelberg.

Liu, HS. Lu, HH. Lui, MT. Yu, EH. Shen, W. Chen, YP. Chang, KW. And Tu, HF. (2009). Detection of copy number amplification of cyclin D1 (CCND1) and cortactin (CTTN) in oral carcinoma and oral brushed samples from areca chewers. *Oral oncology*, **12**: 1032-1036.

Lugnier, C. (2006). Cyclic nucleotide phosphodiesterase (PDE) superfamily: A new target for the development of specific therapeutic agents. *Pharmacology & Therapeutics*, **109**: 366-398.

Lugnier, C. Keravis, T. Le Bec, A. Pauvert, O. Proteau, S. and Rousseau, E. (1999). Characterization of cyclic nucleotide phosphodiesterase isoforms associated to isolated cardiac nuclei. *Biochim Biophys Acta*, **1472**: 431-446.

Madsen, R. Lundstedt, T. and Trygg, J. (2010). Chemometrics in metabolomics- A review in human disease diagnosis. *Analytica Chimica Acta*, **659**: 23-33.

Manly, B, F, J. (1994). *Multivariate Statistical Methods: A Primer*. London, Chapman & Hall.

Marko, D. Pahlke, G. Merz, KH, and Eisenbrand, G. (2000). Cyclic 3', 5'-Nucleotide Phosphodiesterases: Potential Targets for Anticancer Therapy. *Chemical Research in Toxicology*, **13**: 944-948.

Martinive, P. Defresne, F. Quaghebeur, E. Daneau, G. Crockart, N. Grégoire, V. Gallez, B. Dessy, C. and Feron, O. (2009). Impact of cyclic hypoxia on HIF-1alpha regulation in endothelial cells - new insights for anti-tumor treatments. *FEBS Journal*, **276**: 509-518.

Mathupala, S, P. Heese, C. and Pedersen, P, L. (1997). Glucose catabolism in cancer cells. The type II hexokinase promoter contains functionally active response elements for the tumor suppressor p53. *Journal of Biological Chemistry*, **272**: 22776-22780.

Mathupala, S, P. Ko, Y, H. and Pedersen, P, L. (2009). Hexokinase-2 bound to mitochondria: Cancer's stygian link to the "Warburg effect" and a pivotal target for effective therapy. *Seminars in Cancer Biology*, **19**: 17-24.

Matta, A. Bahadur, S. Duggal, R. Gupta, S, D. and Ralhan, R. (2007). Over-expression of 14-3-3zeta is an early event in oral cancer. *BMC Cancer*, **7**: 169.

Mazurek, S. Boschek, C, B. Hugo, F. and Eigenbrodt, E. (2005). Pyruvate kinase type M2 and its role in tumor growth and spreading. *Seminars in Cancer Biology*, **15**: 300-308.

McCahill, A, C. Huston, E. Li, X. and Houslay, M, D. (2008). PDE4 Associates with Different Scaffolding Proteins: Modulating Interactions as Treatment for Certain Diseases. IN Klusmann, E. Scott, J. (eds.) *Protein-Protein Interactions as New Drug Targets*, **186**: 125-166.

Meyuhas, R. Pikarsky, E. Tavor, E. Klar, A. Abramovitch, R. Hochman, J. Lago, T, G. and Honigman, A. (2008). A Key Role for Cyclic AMP-Responsive Element Binding Protein in Hypoxia-Mediated Activation of the Angiogenesis Factor CCN1(CYR61) in Tumor Cell. *Molecular Cancer Research*, **6**: 1397-1409.

Minchenko, A. Leshchinsky, I. Opentanova, I. Sang, N. Srinivas, V. Armstead, V. and Caro, J. (2002). Hypoxia-inducible Factor-1-mediated Expression of the 6-Phosphofructo-2-kinase/fructose-2,6-bisphosphatase-3 (PFKFB3) Gene. *Journal of Biological Chemistry*, **277**: 6183-6187.

Miro, X. Perez-Torres, S. Artigas, F. Puigdomenech, P. Palacios, J, M. and Mengod, G. (2002). Regulation of cAMP phosphodiesterase mRNAs expression in rat brain by acute and chronic fluoxetine treatment. An in situ hybridization study. *Neuropharmacology*, **43**: 1148-1157.

Nagaraj, N, S. (2009). Evolving 'omics' technologies for diagnostics of head and neck cancer. *Briefings in Functional Genomics and Proteomics*, **8**: 40-59.

Nakashima, R, A. Paggi, M, G. and Pedersen, P, L. (1984). Contributions of glycolysis and oxidative phosphorylation to adenosine 5'-triphosphate production in AS-30D hepatoma cells. *Cancer Research*, **44**: 5702-5706.

Nakashima, R, A. Mangan, P, S. Colombini, M. and Pedersen, P, L. (1986). Hexokinase receptor complex in hepatoma mitochondria: evidence from N, N'-dicyclohexylcarbodiimide-labeling studies for the involvement of the pore-forming protein VDAC. *Biochemistry*, **25**: 1015-1021.

Nancarrow, D, J. Handoko, H, Y. Smithers, M. Gotley, D, C. Drew, P, A. Watson, D, I. Clouston, A, D. Hayward, N, K. and Whiteman, D, C. (2008). Genome-Wide Copy Number Analysis in Esophageal Adenocarcinoma Using High-Density Single-Nucleotide. *Cancer Research*, **68**: 4163-4172.

Nicholson, J, K. Lindon, J, C. and Holmes, E. (1999). 'Metabonomics': understanding the metabolic responses of living systems to pathophysiological stimuli via multivariate statistical analysis of biological NMR spectroscopic data. *Xenobiotica*, **29**: 1181-1189.

Nijsten, M, W, N. and van Dam, G, M. (2009). Hypothesis: Using the Warburg effect against cancer by reducing glucose and providing lactate. *Medical Hypotheses*, **73**: 48-51.

Nordström, A. and Lewensohn, R. (2010). Metabolomics: Moving to the Clinic. *Journal of Neuroimmune Pharmacology*, **5**: 4-17.

O'Reilly, S, M. Leonard, M, O. Kieran, N. Comerford, K, M. Cummins, E. Pouliot, M. Lee, S, B and Taylor, C, T. (2006). Hypoxia induces epithelial amphiregulin gene expression in a CREB-dependent manner. *American Journal of Cell Physiology*, **290**: 592-600.

Ohh, M. Park, C, W. Ivan, M. Hoffman, M, A. Kim, TY, Huang, L, E. Pavletich, N. Chau, V. and Kaelin Jr., W, G. (2000). Ubiquitination of HIF requires direct binding to the beta-domain of the von Hippel-Lindau protein. *Nature Cell Biology*, **2**: 423-427.

Ohta, S. Uemura, H. Matsui, Y. Ishiguro, H. Fujinami, K. Kondo, K. Miyamoto, H. Yazawa, T. Danenberg, K. Danenberg, P, V. Tohnai, I. and Kubota, Y. (2009). Alterations of p16 and p14ARF genes and their 9p21 locus in oral squamous cell carcinoma. *Oral and Maxillofacial Pathology*, **107**: 81-91.

Okruhlicova, L. Vrbjar, N. and Lugnier, C. (1998). Characterization of type 4 cyclic nucleotide phosphodiesterase (PDE4) in cardiac sarcolemma. *Experimental and Clinical Cardiology*, **3**: 188-192.

Olofsson, M, H. Havelka, A, M. Brnjic, S. Shoshan, M, C. and Linder, S. (2008). Charting calcium-regulated apoptosis pathways using chemical biology: role of calmodulin kinase II. *BMC Chemical Biology*, **8**: 2.

Ong, W, K. Gribble, F, M. Reimann, F. Lynch, M, J. Houslay, M, D. Baillie, G, S. Furman, B, L. and Pyne, N, J. (2009). The role of the PDE4D cAMP phosphodiesterase in the regulation of glucagon-like peptide-1 release', *British Journal of Pharmacology*, **157**: 633-644.

Patel, S, A. Barnes, A. Loftus, N. Martin, R. Sloan, P. Thakkerchand, N. Goodacre, R. (2009). Imaging mass spectrometry using chemical inkjet printing reveals differential protein expression in human oral squamous cell carcinoma. *Analyst*, **134**: 301-307.

Park, N, J. Zhou, H. Elashoff, D. Henson, B, S. Kastratovic, D, A. Abemayor, E. and Wong, D, T. (2009). Salivary microRNA: Discovery, Characterization, and Clinical Utility for Oral Cancer Detection. *Clinical Cancer Research*, **15**: 5473-5477.

Park, S. Ku, Y, K. Seo, M, J. Kim, D, Y. Yeon, J, E. Lee, K, M. Jeong, SC. Yoon, W, K. Harnic, C, H. and Kim, H, M. (2006). Principal component analysis and discriminant analysis (PCA–DA) for discriminating profiles of terminal restriction fragment length polymorphism (T-RFLP) in soil bacterial communities. *Soil Biology and Biochemistry*, **38**: 2344-2349.

Pastorino, J, G. Shulga, N. and Hoek, J, B. (2002). Mitochondrial binding of hexokinase II inhibits Bax-induced cytochrome c release and apoptosis. *Journal of Biological Chemistry*, **277**: 7610-7618.

Pfeifer, G, P. (2010). Environmental exposures and mutational patterns of cancer genomes. *Pfeifer Genome Medicine*, **2**: 54.

Pinkel, D. and Albertson, D, G. (2005). Array comparative genomic hybridization and its applications in cancer. *Nature Genetics*, **37**: S11-S17.

Prokai, L. Ramanathan, R. Nawrocki, J. and Eyler, J. (1996). Electrospray ionization mass spectrometry of cyclodextrin complexes of amino acids and peptides. *Journal of Inclusion Phenomena and Macrocyclic Chemistry*, **25**: 117-120.

Pyne, N, J. Furman, B. (2003). Cyclic nucleotide phosphodiesterases in pancreatic islets. *Diabetologia*, **46**: 1179-1189.

Rahrmann, E, P. Collier, L, S. Knutson, T, P. Doyal, M, E. Kuslak, S, L. Green, L, E. Malinowski, R, L. Roethe, L. Akagi, K. Waknitz, M. Huang, W. Largaespada, D, A. and Marker, P, C. (2009). Identification of PDE4D as a Proliferation Promoting Factor in Prostate Cancer Using a Sleeping Beauty Transposon-Based Somatic Mutagenesis Screen. *Cancer Research*, **69**: 4388-4397.

Robey, R, B. and Hay, N (2009). Is Akt the “Warburg kinase”? - Akt-energy metabolism interactions and oncogenesis. *Seminars in Cancer Biology*, **19**: 25-31

Robichaud, A. Stamatiou, P, B. Jin, S, L. Lachance, N. MacDonald, D. Laliberte', F. Liu, S. Huang, Z. Conti, M. and Chan, C, C. (2002). Deletion of phosphodiesterase 4D in mice shortens alpha(2)-adrenoceptor-mediated anesthesia, a behavioural correlate of emesis. *Journal of Clinical Investigation*, **110**: 1045-1052.

Roz, L. Wu, C, L. Porter, S. Scully, C. Speight, P. Read, A. Sloan, P. and Thakker, N (1996). Allelic Imbalance on Chromosome 3p in Oral Dysplastic Lesions: An Early Event in Oral Carcinogenesis. *Cancer Research*, **56**: 1228-1231.

Scully, C. and Felix, D, H. (2006). Oral Medicine - Update for the dental practitioner Oral Cancer. *British Dental Journal*, **200**: 13-17.

Semenza, G, L. (2009). Regulation of cancer cell metabolism by hypoxia-inducible factor 1. *Seminars in Cancer Biology*, **19**: 12-16.

Shmueli, A. and Oren, M. (2004). Regulation of p53 by Mdm2: fate is in the numbers. *Molecular Cell*, **13**: 4-5.

Smith, D, I. Zhua, Y. McAvoya, S. and Kuhn, R. (2006). Common fragile sites, extremely large genes, neural development and cancer. *Cancer Letters*, **232**: 48-57.

Sparano, A. Quesnelle, K, M. Kumar, M, S. Wang, Y. Sylvester, A, J. Feldman, M. Sewell, D, A. Weinstein, G, S. and Brose, M, S. (2006). Genome-Wide Profiling of Oral Squamous Cell Carcinoma by Array-Based Comparative Genomic Hybridization. *Laryngoscope*, **116**: 735-741.

Sparano, A. Kumar, M, S. Quesnelle, K, M. and Brose, M, S. (2005). Gene Copy Number Alterations Involving CSMD1 in Oral Squamous Cell Carcinoma. *Otolaryngology-Head and Neck Surgery*, **133**: 141-142.

Spratlin, J, L. Serkova, N, J. and Eckhardt, S, G. (2009). Clinical Applications of Metabolomics in Oncology: A Review. *Clinical Cancer Research*, **15**: 431-440.

Srinivas, P, R. Verma, M. Zhao, Y. and Srivastava, S. (2002). Proteomics for Cancer Biomarker Discovery. *Clinical Chemistry*, **48**: 1160-1169.

Stork, P, J. and Schmitt, J, M. (2002). Crosstalk between cAMP and MAP kinase signaling in the regulation of cell proliferation. *Trends in Cell Biology*, **12**: 258-266.

Sumner, L, W. Amberg, A. Barrett, D. Beale, M, H. Beger, R. Daykin, C, A. Fan, T, WM. Fiehn, O. Goodacre, R. Griffin, J, L. Hankemeier, T. Hardy, N. Harnly, J. Higashi, R. Kopka, J. Lane, A, N . Lindon, J. C. and Marriott, P. (2007). Proposed minimum reporting standards for chemical analysis Chemical Analysis Working Group (CAWG) Metabolomics Standards Initiative (MSI). *Metabolomics*, **3**: 211-221.

Suzuki, H. Fukuyama, R. Hasegawa, Y. Tamaki, T. Nishio, M. Nakashima, T. and Tatematsu, M. (2009a). Tumor thickness, depth of invasion, and Bcl-2 expression are correlated with FDG-uptake in oral squamous cell carcinomas. *Oral Oncology*, **45**: 891-897.

Suzuki, M. Shinohara, F. Endo, M. Sugazaki, M. Echigo, S. and Rikiishi, H. (2009b). Zebularine suppresses the apoptotic potential of 5-Xuorouracil via cAMP/PKA/CREB pathway against human oral squamous cell carcinoma cells. *Cancer Chemotherapy Pharmacology*, (2009b), **64**: 223-232.

Swinnen, J, V. Beckers, A. Brusselmans, K. Organe, S. Segers, J. Timmermans, L. Vanderhoydonc, F. Deboel, L. Derua, R. Waelkens, E. De Schrijver, E. Van de Sande, T. Noël, A. Fougelle, F. and Verhoeven, G (2005). Mimicry of a cellular low energy status blocks tumor cell anabolism and suppresses the malignant phenotype. *Cancer Research*, **65**: 2441-2448.

Tanaka, K. Waki, H. Ido, Y. Akita, S. Yoshida, Y. Yoshida, T. and Matsuo, T. (1988). Protein and polymer analyses up to m/z 100,000 by laser ionization time-of-flight mass spectrometry. *Rapid Communications in Mass Spectrometry*, **2**: 151-153.

Terry, R. Cheung, Y, F. Praestegaard, M. Baillie, G, S. Huston, E. Gall, I. Adams, D, R. and Houslay, M, D. (2003). Occupancy of the catalytic site of the PDE4A4 cyclic AMP phosphodiesterase by rolipram triggers the dynamic redistribution of this specific isoform in living cells through a cyclic AMP independent process. *Cell Signal*, **15**: 955-971.

Teusink, B. Passarge, J. Reijenga, C, A. Esgalhado, E. van der Weijden, C, C. Schepper, M. Walsh, M, C. Bakker, B, M. van Dam, K. Westerhoff, H, V. Snoep, J, L. (2000). Can yeast glycolysis be understood in terms of in vitro kinetics of the constituent enzymes? Testing biochemistry. *European Journal of Biochemistry*, **267**: 5313-5329.

Toomes, C. Jackson, A. Maguire, K. Wood, J. Gollin, S. Ishwad, C. Paterson, I. Prime, S. Parkinson, K. Bell, S. Woods, G. Markham, A. Oliver, R. Woodward, R. Sloan, P. Dixon, M. Read, A. and Thakker, N. (2003). The Presence of Multiple Regions of Homozygous Deletion at the CSMD1 Locus in Oral Squamous Cell Carcinoma Question the Role of CSMD1 in Head and Neck Carcinogenesis. *Genes, Chromosomes & Cancer*, **37**: 132-140.

Urbanczyk-Wochniak, E. Luedemann, A. Kopka, J. Selbig, J. Roessner-Tunali, U. Willmitzer, L. & Fernie, A. R. (2003). Parallel analysis of transcript and metabolic profiles: a new approach in systems biology. *EMBO Reports*, **4**: 989-993.

Vajanaphanich, M. Schultz, C. Tsien, R. Y. Traynor-Kaplan, A. E. Pandol, S. J. and E, K. (1995). Cross-Talk between Calcium and cAMP-dependent Intracellular Signaling Pathways. Implications for Synergistic Secretion in T84 Colonic Epithelial Cells and Rat Pancreatic Acinar Cells. *Barrett journal of clinical investigation*, **96**: 386-393.

van Wieringen, W, N. van de Wiel, M, A. and Ylstra, B. (2007). Normalized, Segmented or Called aCGH Data? *Cancer Informatics*, **3**: 331-337.

Walch, A. Rauser, S. Deininger SO. and Höfler, H. (2008). MALDI imaging mass spectrometry for direct tissue analysis: a new frontier for molecular histology. *Histochemistry and Cell Biology*, **130**: 421-434.

Wang, G, L. Semenza, G, L. (1993). Characterization of hypoxia-inducible factor 1 and regulation of DNA binding activity by hypoxia. *The Journal of Biological Chemistry*, **268**: 21513-21518.

Warburg, O. Posener, K. and Negelein, E, U. (1924). On metabolism of tumors. *Biochemical Magazine*, **152**: 319-344.

Warburg, O. Wind, F, and Negelein, E. (1927). The metabolism of tumors in the body. *The Journal of General Physiology*, **8**: 519-530.

Warburg, O. (1930). The metabolism of tumours Constable: London.

Warburg, O. (1956). On the origin of cancer cells. *Science*, **123**: 309-314.

Warburg, O. (1965). On respiratory impairment in cancer cells. *Science*, **124**: 269-270.

Watson, J. T. and Sparkson, O. D. (2008). Introduction to Mass Spectrometry. 4th Ed, Wiley.

Weber, G. Singhal, R. L. Stamm, N. B. Lea, M. A. and Fisher, E. A. (1966). Synchronous behaviour pattern of key glycolytic enzymes: glucokinase, phosphofructokinase and pyruvate kinase. *Advances in Enzyme Regulation*, **4**: 59-81.

Weber, G. (2002). Reciprocal regulation: recognition of pattern of gene expression in cancer cells', *Advanced Enzyme Regulation*, **42**, pp. 83-100

Weir, B. A. Woo, M. S. Getz G, Perner, S. Ding, L. Beroukhim, R. Lin, W. M. Province, M. A. Kraja, A. Johnson, L. A. Shah, K. Sato, M. Thomas, R. K. Barletta, J. A. Borecki, I. B. Broderick, S. B. Chang, A. C. Chiang, D. Y. Chirieac, L. R. Cho, J. Fujii, Y. Gazdar, A. F. Giordano, T. Greulich, H. Hanna, M. Johnson, B. E. Kris, M. G. Lash, A. Lin, L. Lindeman, N. Mardis, E. R. McPherson, J. D. Minna, J. D. Morgan, M. B. Nadel, M. Orringer, M. B. Osborne, J. R. Ozenberger, B. Ramos, A. H. Robinson, J. Roth, J. A. Rusch, V. Sasaki, H. Shepherd, F. Sougnez, C. Spitz, M. R. Tsao, MS. Twomey, D. Verhaak, R. G. W. Weinstock, G. M. Wheeler, D. A. Winckler, W. Yoshizawa, A. Yu, S. Zakowski, M. F. Zhang, Q. Beer, D. G. Wistuba, I. I. Watson, M. A. Garraway¹, L. A. Ladanyi, M. Travis, W. D. Pao, W. Rubin, M. A. Gabriel, S. B. Gibbs, R. A. Varmus, H. A. Wilson, R. K. Lander, E. S. and Meyerson, M. (2007). Characterizing the cancer genome in lung adenocarcinoma. *Nature*, **450**: 893-898.

Wold, H. (1966). Estimation of principal components and related models by iterative least squares. *Multivariate Analysis*: 391-420.

Workman Jr. J. J. Mobley, P, R. Kowalski, B, R. and Bro, R. (1996). Review of Chemometrics Applied to Spectroscopy: 1985-95, Part I. *Applied Spectroscopy Reviews*, **31**: 73-124.

Wu, C, L. Roz, L. McKown, S. Sloan, P. Read, A, P. Holland, S. Porter, S. Scully, C. Paterson, I. Tavassoli, M. and Thakker, N. (1999). DNA Studies Underestimate the Major Role of CDKN2A Inactivation in Oral and Oropharyngeal Squamous Cell Carcinomas. *Genes, Chromosomes & Cancer*, **25**: 16-25.

Yoshida, Y. Hosokawa, K. Dantes, A. Tajima, K. Kotsuji, F. and Amsterdam, A. (2000). Theophylline and cisplatin synergize in down regulation of BCL-2 induction of apoptosis in human granulosa cells transformed by a mutated p53 (p53 val135) and Ha-ras oncogene. *International Journal of Oncology*, **17**: 227-235.

Yuan, Y. Hilliard, G. Ferguson, T. and Millhorn, D, E. (2003). Cobalt Inhibits the Interaction between Hypoxia-inducible Factor- α and von Hippel-Lindau Protein by Direct Binding to Hypoxia-inducible Factor- α . *The Journal of Biological Chemistry*, **278**: 15911-15916.

Zhang, H, T. Huang, Y. Jin, S, L. Frith, S, A. Suvarna, N. Conti, M. and O'Donnell, J, M. (2002). Antidepressant-like profile and reduced sensitivity to rolipram in mice deficient in the PDE4D phosphodiesterase enzyme. *Neuropsychopharmacology*, **27**: 587-595.

Zhang, X. Odom, D, T. Koo, SH. Conkright, M, D. Canettieri, G. Best, J. Chen, H. Jenner, R. Herbolsheimer, E. Kadam, S. Ecker, J, R. Emerson, B. Hogenesch, J, B. Unterman, T. Young, R, A. and Montminy, M. (2005). Genome-wide analysis of cAMP-response element binding protein occupancy, phosphorylation, and target gene activation in human tissues. *Proceedings of the National Academy of Science of the USA*, **102**: 4459-4464.

Zhang, D, Y. Ye, F. Gao, L. Liu, X. Zhao, X. Che, Y. Wang, H. Wang, L. Wu, J. Song, D. Liu, W. Xu, H. Jiang, B. Zhang, W. Wang, J. and Lee, P. (2009). Proteomics, Pathway Array and Signaling Network-Based Medicine in Cancer. *Cell Division*, **4**: 4-20.

Zheng, L. Sinniah, R. and I-Hong Hsu, S. (2006). Renal cell apoptosis and proliferation may be linked to nuclear factor- κ B activation and expression of inducible nitric oxide synthase in patients with lupus nephritis *Human Pathology*. **37**: 637-647.

Zhivotovsky, B. and Orrenius, S. (2009). The Warburg Effect returns to the cancer stage. *Seminars in Cancer Biology*, **19**: 1-3.

Chapter 2:

A metabolomics investigation into the suitability of cobalt chloride as a substitute for hypoxia in eukaryotic cells

The following chapter is to be submitted as a peer reviewed paper to PloS one early in October 2012.

Royston Goodacre, Nalin Thakker, Ian Hampson and Lynne Hampson contributed through continuous advice and support throughout the project. William Allwood was involved in the operation of mass spectrometry and also various aspects of data analysis. Elon Correa and David Wedge aided with the data analysis and Andrew Vaughan helped with the data processing. Gavin Batman provided support though the wet side of the project including cell culture and ELISA.

2.1 Abstract

The oxygen-labile, hypoxia Inducible transcription factor 1 (HIF-1) plays a pivotal role in the onset and development of many cancers where it regulates genes which are associated with cancer initiation and progression. Furthermore, tumor cells have been found to maintain high levels of HIF-1 α even under normoxic conditions. Cobalt chloride (CoCl₂) is known to inhibit the degradation of HIF-1 α in the presence of O₂, and this has been used extensively to simulate hypoxia. However, even at low concentrations, CoCl₂ is likely to have off-target effects on cellular metabolism. Thus, it was our intention to investigate these off-target effects on human telomerase reverse transcriptase (hTERT) immortalised human keratinocytes by the use of gas chromatography-mass spectrometry (GC-MS), liquid chromatography-mass spectrometry (LC-MS) based metabolomics in combination with ELISA assays for HIF-1 α and ATP. hTERT cells were subjected to normoxia (21% O₂), hypoxia (1% O₂) or 100 μ M CoCl₂ (21% O₂) for 0h, 4h, 8h, 12h, 18h and 24h prior to fingerprint (cellular) and footprint (supernatant) analysis of samples. 100 μ M CoCl₂ induces HIF-1 α and is a good mimicker of hypoxia in terms of central metabolism although it is clear that this treatment does not induce the same level of effect as 1% O₂ for the corresponding exposure time. Furthermore, numerous off-target effects of CoCl₂ were observed in secondary metabolism particularly in lipids and fatty acids. In conclusion, CoCl₂ should be used with caution as a hypoxic mimicker with the caveat that interpretation of results should be restricted to its effects on central metabolism.

2.2 Introduction

Hypoxia Inducible Factor 1 (HIF-1) is a transcription factor which is able to regulate the expression of many genes. This is achieved via its ability to bind to the Hypoxia Response Element (HRE) (Baugh *et al.*, 2006) located in the 5' flanking regions of HIF-1 responsive genes which up or down regulate transcription. HIF-1 is composed of two sub-units: a β -subunit which is

constitutively expressed within the cell, and an α -subunit which is regulated via oxygen concentrations. Under ordinary circumstances, the α -subunit is rapidly degraded in the presence of oxygen resulting in deactivation. Since most tumours are hypoxic, activation of HIF-1 is a common feature of malignant disease which, in turn, de-regulates expression of a variety of genes associated with both progression and prognosis of many cancers (Abramovitch *et al.*, 2004; Breit *et al.*, 2008; Suzuki *et al.*, 2009). Thus, HIF-1 is able to reprogram the cells' metabolism from "regular" primary metabolism that predominantly uses oxidative phosphorylation, to a revised primary metabolic mode of glycolysis. This is known as the Warburg effect (Warburg *et al.*, 1924; 1927; Warburg, 1930; 1956; 1965) and is a common feature of tumour cells.

When healthy mammalian cells are subjected to normoxic conditions, the preferred route for generating ATP is via mitochondrial oxidative phosphorylation which is the most efficient means of energy production yielding approximately 30 molecules of ATP per glucose molecule. Under the same conditions, cytoplasmic glycolysis is far less efficient producing just two molecules of ATP per glucose molecule. In healthy cells, glycolysis only occurs in preference to oxidative phosphorylation under hypoxic conditions. Hence, somewhat paradoxically, although cancer cells require elevated levels of ATP to support their growth they use a very inefficient means of producing this and it is widely believed that this switch from oxidative phosphorylation to glycolysis is crucial for tumor development and progression (Bartrons & Caro, 2007).

Genes regulated by HIF-1 which are associated with the Warburg effect include; glucose transporter-1 (GLUT-1) and glucose transporter-3 (GLUT-3) (Bartrons & Caro, 2007), hexokinase-2 (HK-2) (Frezza & Gottlieb, 2009), pyruvate dehydrogenase kinase (PDK), lactate dehydrogenase A (LDHA) (Gogvadze *et al.*, 2009), cytochrome c oxidase (COX) (or Complex IV) (Fukuda *et al.*, 2007) and pyruvate kinase PKM2 (Kress *et al.*, 1998). The co-ordinate regulation of these genes with angiogenesis (Hsu & Sabatini, 2008), amino acid synthesis (Vander Heiden *et al.*, 2009) and lactic acid production (acidosis)

(Gatenby & Gillies, 2004; Nijsten & van Dam, 2009) illustrates the advantages of the Warburg effect over normal metabolism in cancer and proliferating cells.

Oxygen mediated degradation of the HIF-1 α subunit is ultimately produced by its ubiquitination. During normoxia, HIF-1 α proline residues 402 and/or 564 are hydroxylated by the enzyme prolyl hydroxylase (PHD) (Ke and Costa, 2006) which is O₂ and iron (Fe²⁺) dependent. The asparagine at residue 803 is also hydroxylated by factor inhibiting HIF (FIH) which inhibits creb binding protein (CBP)/p300 complex binding/recruitment to HIF-1 α under normoxic conditions. This post-translational modification acts as an extra level of control to ensure that any HIF-1 α present is prevented from activating hypoxia regulated systems. Subsequent to this, HIF-1 α is multi-ubiquitinated by the von Hippel-Lindau gene product, pVHL which is an E3 ubiquitin ligase which has tumour suppressor activity. The final stage of the procedure is initiated by the multi-ubiquitination and is the degradation of the HIF-1 α via the 26S proteasome. It is noteworthy that the half-life of HIF-1 α during normoxia is approx 5-8 min (Berra *et al.*, 2001).

Conversely, hypoxia inhibits the activity of PHD and FIH which suppresses hydroxylation of the HIF-1 α protein which inhibits pVHL mediated proteasomal degradation. This results in accumulation of HIF-1 α which enables its dimerisation with HIF-1 β and subsequent translocation to the nucleus where it binds to *cis acting* transcriptional regulatory elements.

It has been widely reported that CoCl₂ mimics the effects of hypoxia under normoxic conditions (An *et al.*, 1998; Wang & Semenza, 1993; Guo *et al.*, 2006) whereby its mode-of-action is thought to be via increased expression and/or stabilisation of the HIF-1 α and HIF-2 α proteins (Ho and Bunn, 1996; Yuan *et al.*, 2003; Chachami *et al.*, 2004). However, the precise mechanism for this effect is not clear. It has been suggested that cobalt competitively inhibits the oxygen dependent degradation (ODD) site of the HIF-1 α which prevents the binding of pVHL (Yaun *et al.*, 2003; LaManna, Pichiule & Chavez, 2007) and subsequent ubiquitination (Ohh *et al.*, 2000). Chachami *et al.* (2004) suggested that CoCl₂ upregulates the synthesis of the HIF-1 α protein via activation of the

phosphatidylinositol 3 kinase (PI3K) pathway which is normal means of inducing HIF-1 α under hypoxic conditions. It is also known that reactive oxygen species (ROS) play a role during hypoxia and treatment with CoCl₂ (Chandel *et al.* 1998). Hypoxia requires mitochondria associated signalling which induces a ROS elevation and results in an upregulation of transcription. Conversely, CoCl₂ directly promotes ROS production which, in turn, up-regulates transcription with no requirement for mitochondrial signalling. This indicates that subjecting cells to CoCl₂ imitates hypoxia - it does not induce an exact replica of the hypoxic response. This issue is also illustrated by the observation that the mechanisms behind hypoxia induced and CoCl₂ induced HIF-1 α induction are distinct.

It has been common practice to treat cells with CoCl₂ to mimic hypoxia in preference to the use of genuine hypoxic conditions and it is undeniable that this practice is partly the result of limited access to hypoxic conditions. Furthermore, CoCl₂ also facilitates ease of handling and harvesting cells since it eliminates the problems associated with re-exposure of cells to normoxia which can cause rapid re-oxygenation-related alterations in gene expression. However, In spite of these advantages, it is clear that CoCl₂ is a toxic substance and is likely to affect cells in ways other than those associated with hypoxia.

To date, there have been no studies investigating the accuracy of CoCl₂ as a hypoxic mimicker in eukaryotes in terms of its effects on central metabolism or any unforeseen effects which may occur and we now report an in depth metabolic study on the effects of CoCl₂ in hTERT cells.

2.3 Materials and Methods

2.3.1 Cell Culture of hTERT Cells. Human telomerase reverse transcriptase (hTERT) cells were obtained from INH (St. Mary's hospital, Manchester, UK). Keratinocyte serum free medium (SFM) and HAM F-12 medium were purchased from Invitrogen (Paisley, UK) and fetal bovine serum (FBS) was purchased from Sigma Aldrich (Dorset, UK). Cells were cultured in accordance with Dickson *et al.* (2000). Briefly, the cells were cultured in T150 cell culture flasks and grown to a maximum of 30% confluence in a humidified

incubator at 37°C and 5% CO₂. To sub-culture the cells, the old growth medium was aspirated and the cells were washed in 20mL of phosphate buffered saline (PBS) and aspirated once more. To detach the adhesive cells, 1mL of trypsin/EDTA (0.25% Invitrogen) was added to the T150 and incubated for 3min in a humidified incubator at 37°C and 5% CO₂. The flasks were then observed under a light microscope to ensure the cells were detached. Subsequent to efficient detachment, the trypsin was neutralised using medium containing 9mL of Ham F-12 medium and 1mL of calf serum. The cells were then centrifuged at 8000xg for 5min, the neutralising medium aspirated and the cells re-suspended in 10mL of Keratinocyte SFM. Subsequent to a cell count, the cells were re-seeded at 0.5×10^6 cells per T150 flask.

2.3.2 Quantification of the HIF-1 α protein using ELISA. In order to quantify the concentrations of the active form of the transcription factor HIF-1 α , the DuoSet® IC Human/Mouse Active HIF-1 α ELISA (Enzyme-linked immunosorbent assay) product was purchased from R&D Systems (Abingdon, UK). The supplementary products were purchased and the methodology followed as advised in the manufacturer's protocol. hTERT cells were cultured in 96 well plates and exposed to hypoxia or 100 μ M CoCl₂ for 4h, 8h, 12h, 18h and 24h in triplicate. In addition, a control normoxia sample was prepared in triplicate, which contains no CoCl₂ and was cultured in 21% oxygen for the relevant time. Subsequently, the cells were fixed in 4% formaldehyde, quenched (to prevent further reactions) and blocked (to block any surface which remains uncoated by the protein) before exposure to the primary and secondary antibodies for HIF-1a and cytochrome C determination. The fluorogenic substrates were then added to the samples and the fluorescence was measured on the Molecular Devices, Spectra Max, Gemini XS instrument as described.

2.3.3 Assessment of ATP. The ATP colorimetric/fluorometric assay kit was purchased from Abcam (Cambridge, UK) and the protocol followed as described. In brief, a standard curve was produced utilising the ATP standard buffer supplied with the kit. 1×10^6 cells per sample were lysed in the ATP

assay buffer and flash frozen in liquid nitrogen to inhibit further ATP metabolism. The samples were centrifuged at 15,000xg for 2min, the supernatant retained and 50µL per sample added to a 96 well plate followed by the addition of 50µL of ATP reaction buffer to each sample and subsequent incubation in the dark at room temperature for 30min. The OD was then measured at 540nm in a micro plate reader and the calculation performed as described. The samples were normalised to total protein concentration determined by Nanodrop assessment.

2.3.4 Condition Exposure and Metabolite Extraction. hTERT cells were grown to ~60% confluence in 18x T150 flasks. Prior to condition exposure, fresh warmed hypoxic medium replaced the old medium in the hypoxic condition, and fresh warmed regular medium was used to replace the old medium in the normoxic and CoCl₂ treated conditions. Six replicate samples in flasks were then subjected to each condition: (1) normoxia – 21% oxygen, 5% CO₂ at 37°C; (2) hypoxia – 1% oxygen, 5% CO₂ at 37°C and (3) 100µL of the hypoxic mimicker CoCl₂ at 21% oxygen, 5% CO₂ at 37°C for 4h, 8h, 12h, 18h and 24h. Subsequently, metabolite extraction was performed as described by Sellick *et al.* (2010). The medium was decanted and the cells washed in warmed PBS. To quench the cells, 5mL of -48°C MeOH was added to each T150 flask (on ice), the cells were scraped, followed by flash freezing in liquid nitrogen for 1min. The cells were then vortexed for 30s, thawed on ice and returned to the liquid nitrogen for a further minute. This freeze/thaw/vortex step was repeated a total of four times followed by centrifugation at 4°C at 3000xg for 10min. In addition to the fingerprint samples collected as described, a footprint was also collected for each sample. Subsequent to condition exposure, 1ml of medium was collected and evaporated in a speed vac and stored until analysis. The footprint and fingerprint samples were treated identically from here on.

2.3.5 GC-MS Analysis for Metabolite Detection. 100µL of Internal Standard 2 (IS2) solution was added (IS2 was prepared by diluting 2mL of IS1 in 10mL of HPLC grade H₂O). Internal standard 1 (IS1) was composed of 10mg

succinic- d_4 acid, 10mg glycine- d_5 acid and 10mg malonic- d_2 acid in 10mL of HPLC grade H₂O. IS is used to assess instrument drift throughout the run and derivatisation efficiency of each sample. The samples were then evaporated overnight using a speed vac and stored at -80°C until analysis. The samples were derivatised via methoxylation utilising methoxyamine hydrochloride at 60°C for 30min and silylation via *N*-methyl-*N*-(trimethylsilyl)-trifluoroacetamide (MSTFA) at 60°C for 30min (Lenz and Wilson, 2007). GC-MS analysis followed using an Agilent 6890 gas chromatograph coupled to a Leco Pegasus III TOF mass spectrometer with an Agilent 7893 autosampler and was performed in accordance with the methods of Begley *et al.* (2009). The data were ratioed to the succinic- d_4 acid internal standard (to account for instrument drift and variation in sample derivatisation) and this was based on peak areas (the area under the peak which equivlates to relative concentrations).

2.3.6 UHPLC-MS Analysis for Metabolite Detection. Samples were analysed in concordance with Brown *et al.* (2009, 2011). In brief, all samples were reconstituted in 100µL HPLC H₂O and subsequently run separately in ESI- and ESI+ modes on an Accela UHPLC system (ThermoScientific, Hemel Hempstead, UK) coupled to an electrospray LTQ-Orbitrap XL hybrid mass spectrometry system (ThermoFisher, Bremen, Germany). In terms of UHPLC separation, a linear water-methanol gradient was applied to a stationary phase column (Hypersil GOLD (Fisher Scientific, Loughborough, UK); length 100mm, diameter 2.1mm, particle size 1.2µM). Finally, the data were normalised to total peak area and data analysis performed.

2.3.7 GC-MS and UHPLC-MS Metabolite Identification. The GC-MS metabolites were assigned in accordance with the Metabolomics Standards Initiative for Chemical Analysis (Sumner *et al.*, 2007). Chromatograms were deconvolved in LECO ChromaTOF according to Begley *et al.* (2008) and then library matched against an in-house GC library and the Max Plank Institute Molecular Plant Physiology database (GMD) with 80%+ match score on forward and reverse matching and a retention index error +/- 10. Metabolite features detected in the UHPLC-MS analysis were assigned using an in-house

metabolite ID workflow as described in Brown *et al.* (2011). This involves the generation of elemental compositions based upon accurate mass data and isotopic peaks, the elemental compositions are then matched to a database compiled from a range of external databases including HMDB, KEGG, Chem Spider and PubChem.

2.3.8 Data Processing and Data Analysis. In order to analyse the ELISA of the HIF-1 α , firstly the background relative fluorescence units (RFUs) were subtracted from all samples and the HIF-1 α RFUs were normalised using the cytochrome C RFUs (as Cytochrome C is constitutively expressed at high concentrations with low variability). Finally, the average normoxic values were subtracted from all samples to attain alterations from the normoxic condition.

For certain analyses elaborated below, the negative and positive metabolites for LC-MS were reduced to 150 each, through deducing the most significant metabolites from the data sets. In this instance, significant refers to those metabolites with the lowest p-values (<0.05) when comparing the concentrations of a particular metabolite between the three conditions (i.e. hypoxia, normoxia and CoCl₂). Once the most significant metabolites were obtained, removal of those with no/nonsense identifications or labelled multiply charged ion or isotope commenced, resulting in the significant metabolites which were further analysed.

Box and whisker plots were plotted in MATLAB 2010a for all GC-MS metabolites detected. In addition, only the 300 most significant LC-MS metabolites (150 positive and 150 negative) were plotted in an identical manner. A box and whisker plot graphically displays numeric data through their 5 number summaries: the smallest observation, lower quartile, median, upper quartile, and largest observation. Each box and whisker was devised of a hypoxic, normoxic and CoCl₂ sample showing relative concentrations of a specific metabolite.

PARAllel FACtor (PARAFAC) analysis was performed on the GC-MS data containing only metabolites from central metabolism (glycolysis, TCA and amino acids) including F6P, deoxyglucose, glucose (which potentially may be

galactose), lactic acid, fructose, fumaric acid (which potentially may be maleic acid), malic acid, L-glutamine, pyroglutamic acid, glutamine, valine, leucine, serine, threonine, proline, aspartic acid, cysteine, arginine (which potentially may be citrulline), phenylalanine, tyrosine (which could be tyramine) in accordance with Bro (1997) in R version 2.13.1 (R Foundation for Statistical Computing, Vienna, Austria); the scripts are available from the authors on request. PARAFAC is a multi-way data analysis method which is considered a higher-order generalization of principal component analysis (PCA) applied to tensors (Kroonenberg, 2008). The interpretation of the 2D PARAFAC plots presented here is similar to the interpretation of a 2D PCA scores plot. Component 1 was plotted against Component 2 for each of the time points 4h, 8h, 12h, 18h and 24h alongside a general scores plot and a time model.

A clustergram analysis was also adopted for the analysis of the GC-MS data and contained all 53 metabolites. The most significant metabolites from LC-MS negative (40 metabolites) and LC-MS positive (32 metabolites) data sets were combined to produce a single clustergram (data not shown). All clustergram analyses were performed in R version 2.13.1 using the "heatmap.2" package and the scripts are available from the authors on request. A clustergram is a hybrid of a dendrogram and a heat map, which clusters metabolites which are behaving in a similar fashion. Each metabolite is correlated with all other metabolites and the pattern of the correlations is utilised to cluster those metabolites behaving similarly.

Principal component–discriminant function analysis (PC-DFA) was performed on GC-MS, LC-MS negative and LC-MS positive data sets containing all metabolites detected on the respective platforms as described by Goodacre *et al.* (2003). The objective of PCA is to explain the variance-covariance structure of a set of variables through a few linear combinations of these variables. Much of the original data variability can be accounted for by a small number of principal components (PCs) which are then used for data reduction and visual data interpretation. However, PCA alone does not reveal all the relationships present in the data. Therefore, PCA is often used as an

intermediate step and its PCs are used as inputs to other analysis methods. The present work uses PCA combined with discriminant function analysis (PC-DFA) to examine the data. The objective of DFA is to separate distinct sets of objects (or observations) and allocate new objects to previously defined groups. The PC-DFA code was implemented in R version 2.13.1 and is also available from the authors on request. Firstly, PCA is performed on the full data and the first 15 principal components are extracted. On average these 15 PCs accounted for at least 90% of the data variance and this was the number of PCs that generated the best results during model validation. Secondly, the extracted PCs are used as inputs to perform discriminant function analysis. Finally, the model is validated using a bootstrap cross-validation method according to (Correa *et al.*, 2012) and the confidence interval of the predictions for each class is reported over 1000 independent cross-validations.

2.4 Results and Discussion

2.4.1 Quantification of HIF-1 α . To assess the relative concentrations of the transcription factor HIF-1 α , an ELISA approach was adopted for normoxia (0h), hypoxia and CoCl₂ for 4h, 8h, 12h, 18h and 24h (Figure 2.1). As expected, HIF-1 α was induced when cells were exposed to either CoCl₂ or hypoxia at all time points assessed. It is also clear that the 1% O₂ causes a greater induction of HIF-1 α than 100 μ M CoCl₂ at each time point; although, these results were not significant (Mann Whitney; $p < 0.05$). HIF-1 α concentrations increased for the initial 12h under both the hypoxic and CoCl₂ conditions, and then subsequently diminished. These data indicate that 100 μ M CoCl₂ is mimicking hypoxia with respect to HIF-1 α , although the level of induction was not as marked.

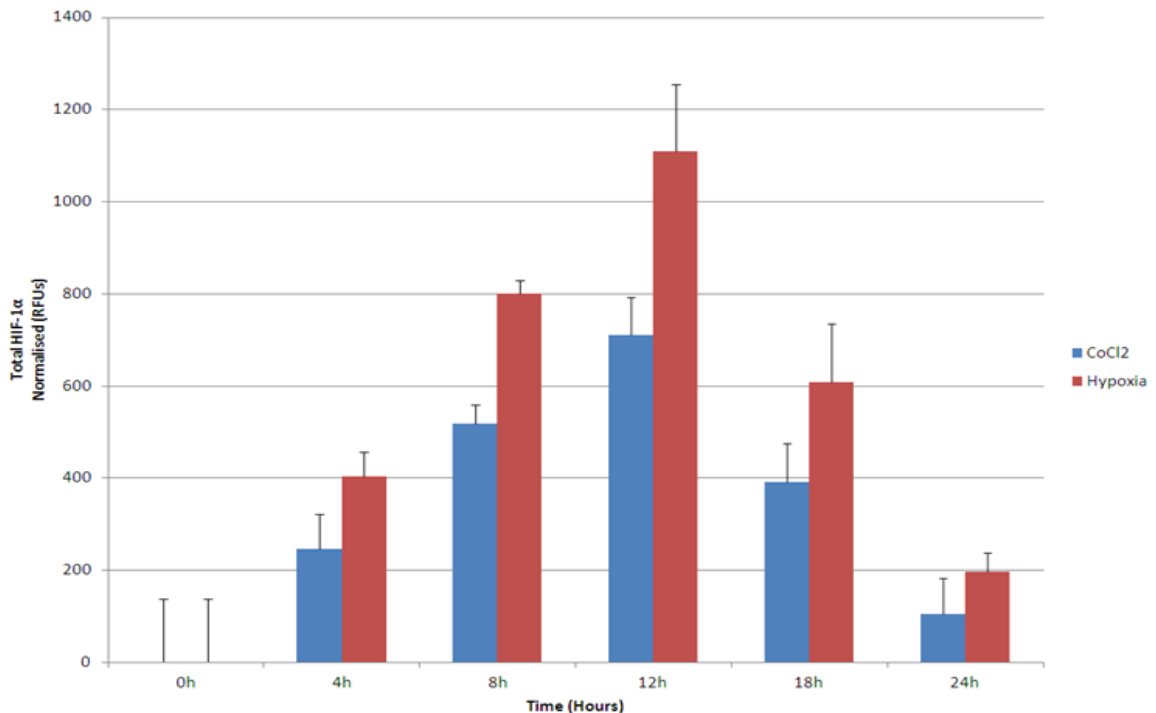


Figure 10 Total HIF-1 α concentrations determined through ELISA for hTERT cells exposed to normoxia, hypoxia, and 100 μ M CoCl₂ for a range of time points between 0h (normoxia) to 24h. Total RFUs are shown following normalisation to cytochrome C for CoCl₂ (blue) and hypoxia (red) after deduction of the normoxic (0h) RFUs. Cytochrome C did not alter drastically between treatments. Means are shown and the error bars display standard deviation from triplicate samples.

The observed fluctuation in HIF-1 α protein levels has been reported previously (Ryan *et al.*, 1998) and these authors suggested this is due to elevated protein stability. In similar findings, Mottet and co-workers (2003) found increased HIF-1 α protein stability for 5h followed by a decrease in concentrations after 16h. They explained this through the PI3K/Akt pathway which they state is required for HIF-1 α stabilisation and since prolonged hypoxia leads to a decrease in Akt phosphorylation, HIF-1 α stabilisation decreases. In terms of CoCl₂ induction of HIF-1 α , Ardyanto *et al.* (2006) discovered similar findings when exposing the human gastric carcinoma cell line MKN-1 to 500 μ M CoCl₂ and HIF-1 α concentrations were increased for 4h and then decreased until 36h. The data presented here further emphasises the point that CoCl₂ is a suitable mimicker of low oxygen tension.

2.4.2 Assessment of ATP. ATP concentrations were measured in order to assess the energy state of cells under hypoxic and CoCl₂ conditions (see Figure 2.S1). It is clear that both treatments produced an initial drop in ATP concentration at 8h followed by a modest increase at 12h which remained stable. However, overall CoCl₂ treated cells had lower levels of ATP than hypoxic cells at the equivalent time points; however, only the 4h time point was significant ($p < 0.05$).

Energy regulation is an important aspect of the hypoxic response as cells convert from oxidative phosphorylation as a means of energy production, to the less-efficient glycolysis. Under normoxic conditions, oxidative phosphorylation produces 31 or 29.5 ATP molecules per glucose molecule depending on NADH shuffling into the mitochondria. Under hypoxic stress, HIF-1 directs a metabolic change whereby glycolysis is preferred yielding just two ATP molecules per glucose molecule. Furthermore, sub-lethal concentrations of CoCl₂ also induce an increase in HIF-1 with the same outcome. Thus, if ATP consumption is considered equal regardless of oxygenation status or CoCl₂ treatment, normoxic cells should, theoretically, have ~15 fold more ATP than either hypoxia or CoCl₂ treated cells. However, in practice, although ATP levels were lower in hypoxia/CoCl₂ treated cells when compared to normoxic cells, this was in the

order of a five-fold reduction in magnitude (from 0.05nmol to 0.01nmol between 0h (normoxia) and the 8h time point). There are two possible explanations for this phenomenon: hypoxic or CoCl₂ treated cells are consuming less ATP than their normoxic counterparts or alternatively they are importing and using more glucose than normoxic cells. Indeed the latter possibility is supported by the observed HIF-1-dependent upregulation of the glucose transporters (GLUT-1 and GLUT-3) (Bartrons and Caro, 2007).

It is also curious that ATP concentrations decreased from 0 - 8h exposure to either hypoxia or CoCl₂ and then increased stabilising at approximately 0.02nmol after 12h. These data suggest either that the cells are stabilising at 12h having become accustomed to the stress, or they are beginning to revert back to a more normoxic state which is consistent with the PARAFAC of the GC-MS metabolites (*vide infra*). The reduction in ATP levels seen after 18-24h exposure to CoCl₂ is in keeping with the cells undergoing toxicity-related apoptosis. Indeed, although ATP concentrations are consistently lower in CoCl₂ treated cells when compared to hypoxia, this is a paradox since the HIF-1 stabilisation data indicate that the latter should have a more pronounced effect on ATP levels. A potential explanation could be that CoCl₂ is interfering with ATP production/usage or is indirectly affecting the levels of ATP through other processes such as oxidative stress. The 8h time point appears to be significant since after this point, the drop in ATP level arrests then increases and subsequently stabilises.

In related terms, the mass spectrometry data highlighted a number of interesting metabolites related to purine metabolism which are associated with energy regulation. This pathway is utilised to recycle nucleotides and bases via a *de novo* and a *salvage* pathway from phosphoribosyl pyrophosphate (PRPP) to ATP and GTP (guanosine triphosphate). Elevated concentrations of IMP (inosine monophosphate), adenine and xanthosine were found in the hypoxic condition relative to that of normoxia and also an increased concentration was found of adenine under CoCl₂ and hypoxic exposure. Hence, in terms of adenine behaviour, CoCl₂ appears to be mimicking the genuine hypoxic

response; however, it does not mimic in relation to IMP and xanthosine as these concentrations remain unchanged from the normoxic condition. This behaviour is potentially indicating the degradation of the ATP pool to its associated derivatives resulting in diminished ATP levels (Björklund *et al.*, 2008) as a consequence of the paradoxical switch from oxidative phosphorylation to glycolysis and the TCA cycle. It is unknown why xanthosine and IMP in the CoCl₂ condition did not yield the same response as the hypoxic condition.

2.4.3 Assessment of Lactic Acid. Relative intracellular and extracellular lactic acid concentrations were assessed by mass spectrometry for normoxia, hypoxia and CoCl₂ exposure between 0 - 24h (Figure 2.S2). The internal and external lactic acid (upper graph and lower graph, respectively) generally display the same pattern, with an initial increase between 4 - 8h, a decrease at 12h followed by an elevation at the 24h time point. Following exposure to hypoxia or CoCl₂, lactic acid replaces pyruvate as the end point of glycolysis. Although this is consistent with the lactate levels found at 24h it is not so for the preceding time points. Overall, the lactic acid concentration in CoCl₂ treated cells was intermediate between that of hypoxic and normoxic conditions for both internal and external lactic acid, which indicates that 100µM CoCl₂ does not impose directly equivalent to hypoxia.

2.4.4 PARAFAC Analysis of Central Metabolism Metabolites from GC-MS. GC-MS was adopted to assess the ability of CoCl₂ to mimic hypoxia in terms of primary metabolism. A PARAFAC analysis was performed on the metabolites from central metabolism (i.e., glycolysis, amino acids and TCA metabolites) to determine the level of variation at the various time points (see Figure 2.2) (Xu *et al.*, 2011). The reasoning for performing the PARAFAC solely on central metabolism intermediates was to investigate whether there was any overlap between the hypoxic and CoCl₂ groups since this would provide central metabolic evidence for the ability of the former to mimic the latter.

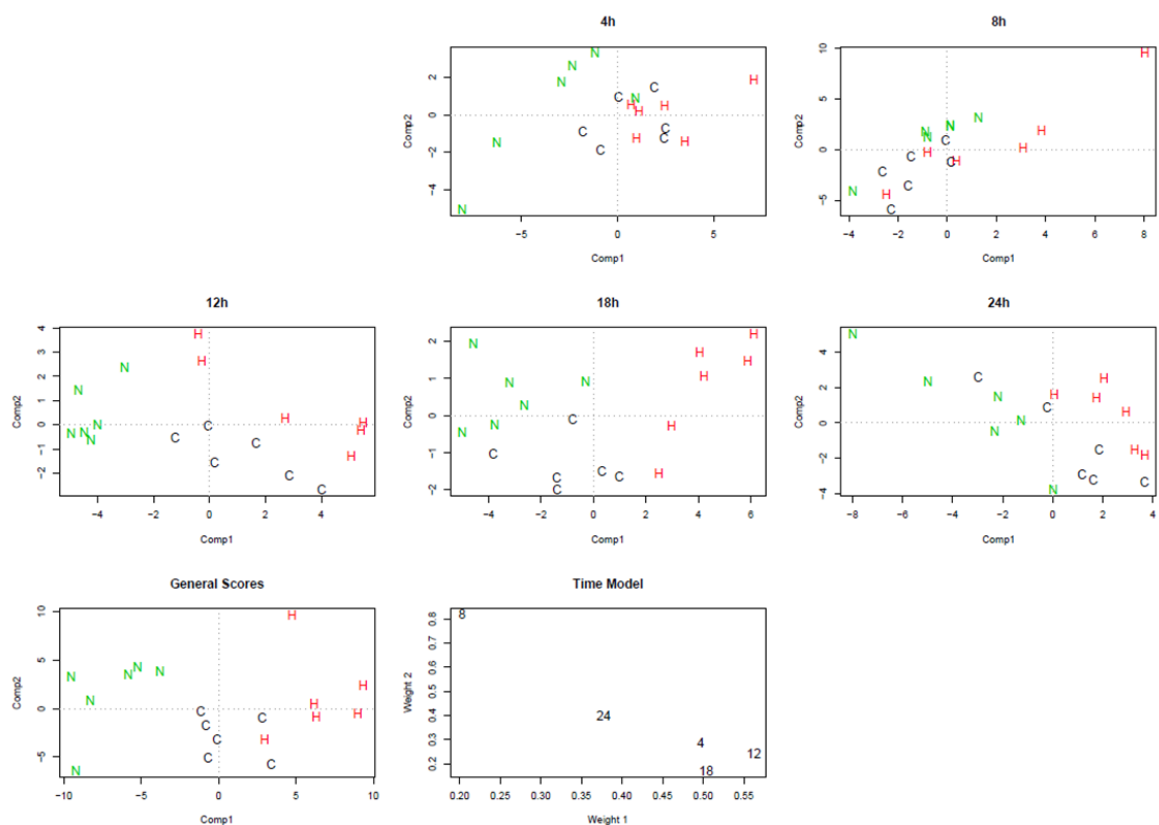


Figure 11 GC-MS PARAFAC - Central Metabolism Only. The metabolites include F6P, deoxyglucose, glucose (which potentially may be galactose), lactic acid, fructose, fumaric acid (which potentially may be maleic acid), malic acid, L-glutamine, pyroglutamic acid, glutamine, valine, leucine, serine, threonine, proline, aspartic acid, cysteine, arginine (which potentially may be citruline), phenylalanine, tyrosine (which could be tyramine). A plot is shown for each time point with Component 1 against Component 2 for each alongside a general scores plot and a time model. The green N's highlight normoxia, the red H's hypoxia and the black C's the CoCl₂ condition. Each number in the time model represents a time point and the plot depicts which of those time points had the greatest influence on Component 1 (Weight 1) and Component 2 (Weight 2).

The 4h time point shows the CoCl₂ and hypoxia conditions completely overlapping, with the normoxia condition separated from the two (except one normoxic sample which has merged). Hence, the early stages of CoCl₂ exposure mimic hypoxia (1% oxygen) extremely accurately in terms of central

metabolism. At 8h all conditions appear to merge although loose clustering of the groups can still be observed. After 12h there is clear separation of the groups, including hypoxia and CoCl_2 yet the CoCl_2 group lies intermediate between hypoxia and normoxia but with closer proximity to hypoxia. The normoxic constituents cluster tightly on the negative of component 1, whilst the CoCl_2 and hypoxic groups, although separated, cluster on the positive of component 1. At 18h the normoxic and CoCl_2 conditions begin to merge, whilst the hypoxic condition retains its distance from both of these. Curiously at 24h, merging of all conditions is observed, with CoCl_2 being located between the other two conditions. This behaviour is potentially a result of reduced HIF-1 α levels in both the hypoxic and CoCl_2 condition (Figure 2.1) since by 24h this is beginning to revert back to levels found under normoxia. The general scores plot shows clustering and separation of the three groups, with CoCl_2 intermediate, lying closer to the hypoxic condition, which is to be expected. The time model for the central metabolism PARAFAC shows the 8h time point is distant from the other time points, having the greatest effect on Component 2 with little effect on Component 1, whereas the time points 4h, 12h and 18h are having a major impact on Component 1 but little impact on Component 2. The 24h time point is having a modest effect on Component 1 and Component 2.

2.4.5 Clustergram of GC-MS Metabolites. Figure 2.3 shows a clustergram of GC-MS variables whereby metabolites which behave in a similar fashion are clustered together. The blue boxes highlight metabolites which cluster together on the x-axis i.e. amino acids, TCA, fatty acids/lipids, glycolysis, sugars and polyols (identifications, and levels thereof are given in the supporting information; Table 2. S1). The amino acids clustering on the immediate left consists of glycine, proline and aspartic acid whilst the amino acid cluster on the far right incorporates pyroglutamic acid, L-glutamine, leucine, tyrosine (which may potentially be tyramine), valine, arginine/citrulline, phenylalanine, serine and threonine. The TCA cluster includes fumaric acid (potentially maleic acid), glutamine and malic acid and the glycolysis grouping contains lactic acid, F6P and glucose (which may be galactose). Glycerol,

cholesterol, hexadecanoic acid, oleic acid and palmitoleic acid cluster in the fatty acid/lipid set, mannose/allose/glucose/galactose (x3), sugar/sugar alcohol and deoxyglucose cluster as a sugar group and the polyol assemblage comprises probable sugar alcohol (x2), threitol and malitol.

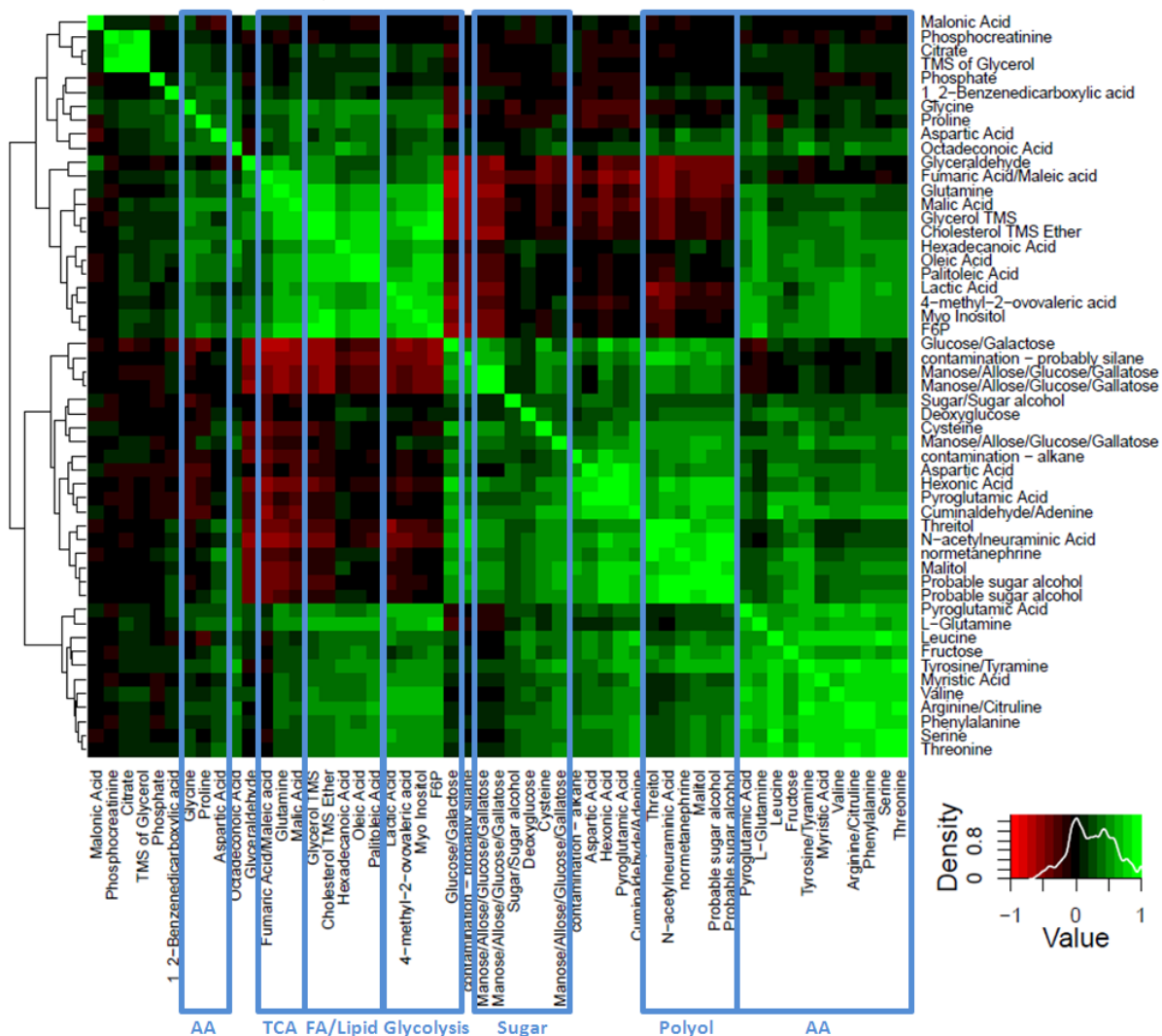


Figure 12 Clustergram of Correlated GC-MS Metabolites for CoCl₂ Analysis. A clustergram is a hybrid of a heat map and a dendrogram. The same metabolites are shown on the x-axis and y-axis of the graph and the y-axis shows the dendrogram tree. Those metabolites which cluster closer together behave in a similar manner. The blue boxes highlight related metabolites which cluster together and from left to right are amino acids, TCA, fatty acids/lipids, glycolysis intermediates, sugars, polyols (sugar alcohols) and amino acids. The green boxes specify a positive correlation, red boxes a negative correlation and dark boxes indicate no correlation; where the stronger the colour, the greater the correlation. The scale on the bottom right of clustergram highlights this.

2.4.6 PC-DFA of GC-MS, LC-MS Positive and LC-MS Negative Data.

PC-DFA was performed on data from all three platforms independently. Figure 2.4A depicts the PC-DFA for all GC-MS metabolites with bootstrapping validation accuracy shown on the right. It is evident that the individual time points cluster, for example, the 4h time points (all conditions) group on the negative of DF1 and marginally on the positive of DF2. In the later time points (>12h), it becomes increasingly difficult to distinguish between the individual times, particularly 18h and 24h which is evident in the 95% confidence intervals. In terms of treatment it is clear that for a specific time point, CoCl₂ is positioned intermediate between hypoxic and normoxic conditions. A good example of this is the 12h time point, where hypoxia is to the extreme positive of DF2, normoxia is clustered at a value of 1 and CoCl₂ is between the two although this is less obvious at earlier time points. For example, at 4h CoCl₂ and normoxia overlap with hypoxia clustering separately whereas at 8h it is difficult to ascribe clustering amongst any of the groups. This is potentially a result of the poor clustering of the 8h hypoxia condition with a confidence level of 11-15% and is also compounded with the poor clustering observed at 8h CoCl₂ with a confidence level of 27-33%.

Figure 2.4B displays the PC-DFA for the LC-MS negative data using the same set up as for the GC-MS PC-DFA, except that DF3 is plotted rather than DF2. The rationale behind this was that the normoxia and hypoxia overlapped in DF1 vs. DF2 and CoCl₂ was separated in the third component. There was clear clustering of the time points with the latter (from 12h onwards) becoming more difficult to differentiate. What is evident from this PC-DFA plot and the associated confidence levels displayed on the right, is that the CoCl₂ is behaving diversely from normoxia and hypoxia with off target effects observed in terms of metabolites detected from negative LC-MS. The PC-DFA for the positive LC-MS data is shown in Figure 2.4C which shows similar findings to the LC-MS negative data with differences observed between CoCl₂ and hypoxia/normoxia. This is illustrated by the plot of DF1 vs. DF2 and also in the confidence scores for post-8h time points which all have 100% accuracy.

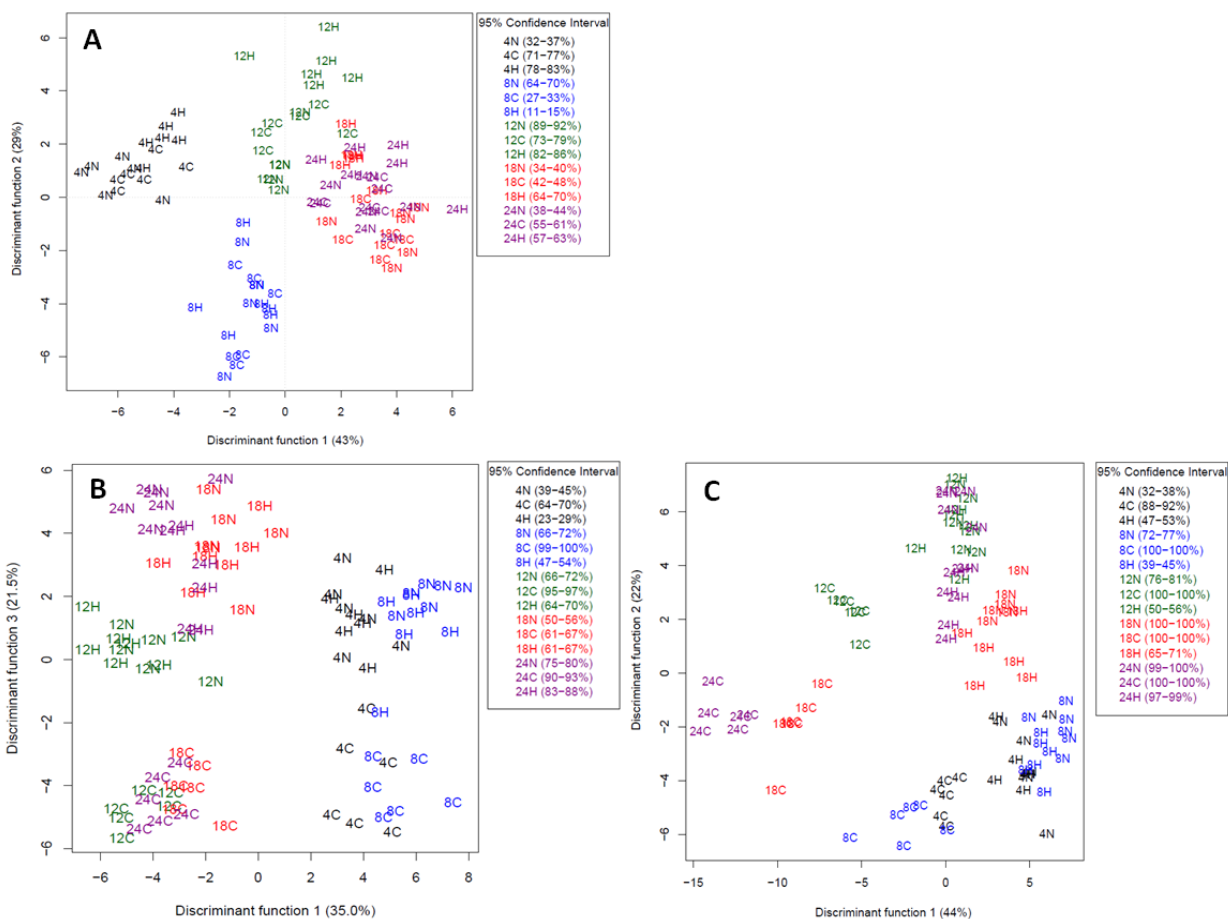


Figure 13 PC-DFA of (a) GC-MS, (b) LC-MS negative and (c) LC-MS positive data. The time points are colour coded and also labelled by number – black signifies 4h, blue highlights 8h, green 12h, red denotes 18h and purple represents the 24h time point. The condition type is indicated by the letter following the time point where H symbolises hypoxia, C implies CoCl₂ exposure and N signifies normoxia. Plots (a) and (c) display Discriminant Function 1 (DF1) vs. Discriminant Function 2 (DF2) where the explained variances are indicated in brackets. Plot (b) shows DF1 vs. DF3. Model validation was performed using bootstrapping of 1000 times and the accuracy of each test sample is displayed in the box on the right hand side of each plot within a 95% confidence interval.

The LC-MS data demonstrated a number of CoCl₂ specific effects which did not mirror that of the hypoxia. The most prominent of these was the group of metabolites related to phospholipids, including diacylglycerols (DAGs), phosphocholines (PCs) and monoacyl-glycerophosphates (PAs); see Tables S2 and S3 for information. Phospholipids are a major constituent of cellular

membranes and sub cellular organelle membranes such as the nucleus, mitochondria, Golgi apparatus and endoplasmic reticulum. Indeed it has previously been reported that exposing cells to CoCl_2 results in lipid peroxidation in both cell culture (Tan *et al.*, 2008) and whole organisms (Christova, Duridanova & Setchenska, 2002; Gonzales *et al.*, 2005). This is most likely the result of CoCl_2 -induced production of ROS (Jung *et al.*, 2007) which subsequently attacks cellular components including membranes (Slater, 1984; Jung *et al.*, 2007).

In addition to their structural properties, lipids have other roles within the cell. For example, they act as secondary messengers (or lipid signaling) with the ability to diffuse freely through membranes. This means that they cannot be stored in vesicles and are only synthesized at specific locations when required. Furthermore, previous studies have shown that CoCl_2 causes an increase in phosphorylated lipid secondary messengers (Anelli *et al.*, 2007; Ryu *et al.*, 2010). Thus, both these CoCl_2 induced effects on lipids may contribute to the observed off-target effects of CoCl_2 . Consistent with this, fatty acid metabolism was also found to be markedly altered by CoCl_2 and yet this was not perturbed by hypoxia. Fatty acids are derived from phospholipids and triglycerides and are used, via beta oxidation, to produce ATP. Therefore, since each phospholipid consists of two fatty acids and these are located in cell membranes, the observed off-target effects on this group of metabolites is likely to be related to those associated with phospholipids as previously discussed.

A further set of metabolites of interest, were those related to vitamins and acetylcholine. The essential vitamin pantothenic acid (vitamin B5) and acetylcholine were both reduced during hypoxia but were found in "regular" concentrations with CoCl_2 . This is significant as they are both major components of acetyl coenzyme A which is essential for normal aerobic functioning of the TCA cycle. Thus, it could be inferred that these metabolites might behave in a similar fashion under hypoxic or CoCl_2 conditions and yet, there was no change with CoCl_2 and a reduction during hypoxia. The observed

reduction could reflect a rapid conversion of acetyl-CoA to citric acid although why this is not observed in the CoCl₂ treatment is not clear.

2.4.7 Box and Whisker Plots Demonstrating Typical Metabolite Behaviour. For each metabolite detected in GC-MS and for all significant metabolites for LC-MS negative and positive data, box and whisker plots were created to highlight differences between the three culture conditions (see Figure 2.5 for examples). These were also produced for each treatment at each time point to highlight the effects on metabolite concentration over time (data not shown). The differences between conditions used were subcategorized into three groups as depicted in Figure 2.5. For central metabolism, the majority of metabolites fell into the first category, where CoCl₂ and hypoxia behaved in a similar fashion suggesting that CoCl₂ accurately mimics hypoxia. In comparison, normoxia produced either elevated or reduced concentrations. The second category consists of metabolites which were altered by hypoxia but not by CoCl₂ or normoxia. Clearly for these metabolites, CoCl₂ does not accurately mimic hypoxia and this was found for vitamins and IMP. The third and final grouping were metabolites which were altered by CoCl₂ but not by hypoxia or normoxia. Examples of these were fatty acids and lipids such as phospholipids, phosphocholines and diacylglycerophosphates. For ease of interpretation, a colour coded KEGG map of metabolism is shown (Figure 2.S3) which highlights the areas of metabolism where CoCl₂ mimics hypoxia and also those pathways where there are off-target effects. Furthermore, this method aids in identifying which metabolites are associated with which groups from typical metabolite behaviour (Figure 2.5).

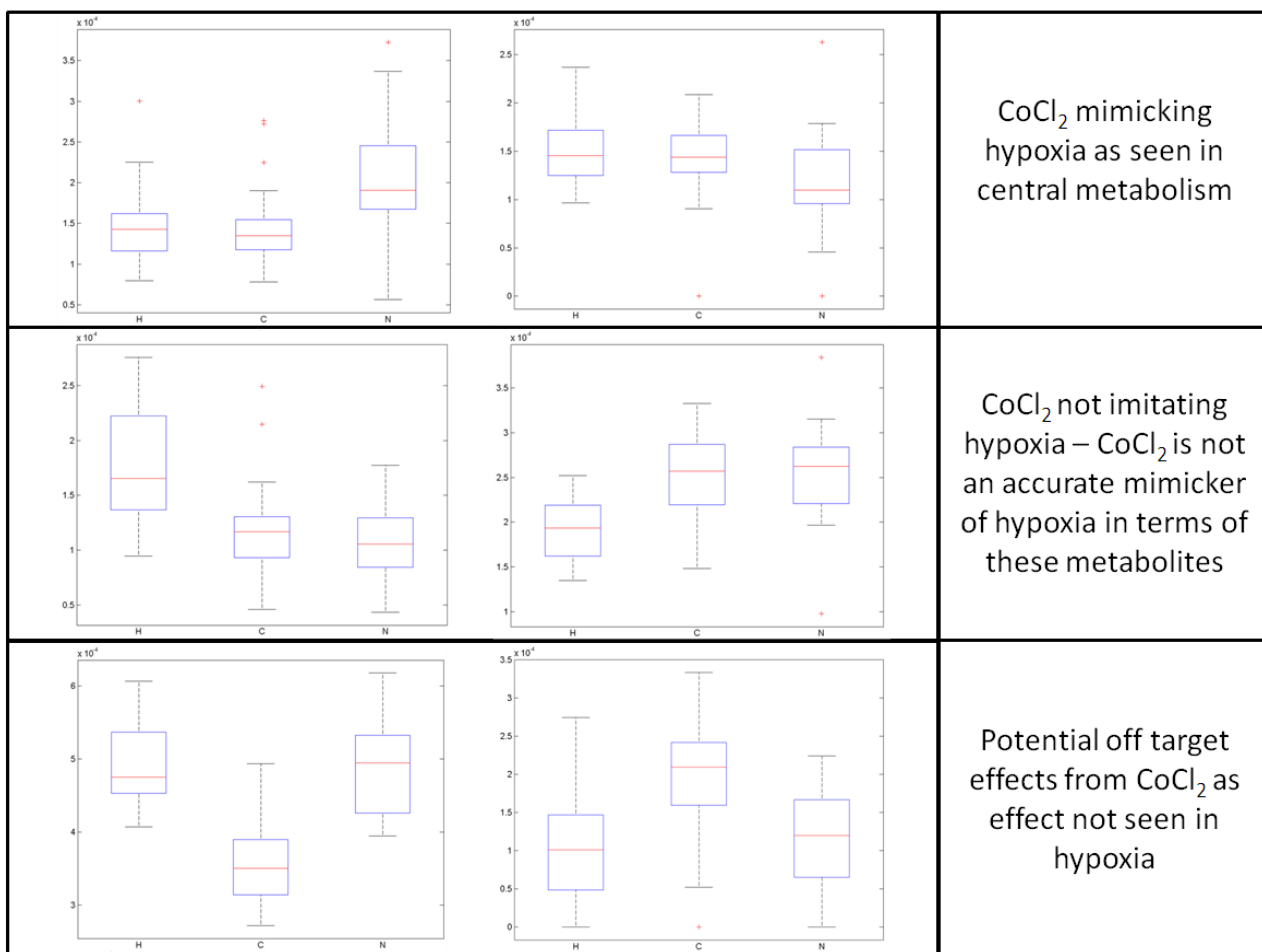


Figure 14 Box and whisker plots displaying typical behaviour of metabolites. For each example, the condition, from left to right is hypoxia (H), CoCl₂ (C) and normoxia (N). The red line indicates the median, the boxes represent the upper (75th percentile) and lower (25th percentile) quartiles, the whiskers signify the minimum and maximum values and the red crosses specify outliers in the data. The box and whisker plots have been categorised into three groups, from top to bottom: CoCl₂ appears to be mimicking hypoxia as seen in central metabolism, CoCl₂ does not appear to be mimicking hypoxia and potential off target effects as CoCl₂ is initiating a response which is not present in the hypoxia condition.

2.5 Concluding remarks

The GC-MS data suggest that CoCl_2 is able to imitate hypoxia in terms of central metabolism, specifically glycolysis, the TCA cycle and amino acid production. This was to be expected and is most likely a direct result of altered levels of the transcription factor HIF-1 α causing this alteration in metabolism in both hypoxia (Denko, 2008) and CoCl_2 (Chandel *et al.*, 1998). However, from our results, it is clear that 100 μM CoCl_2 has an intermediate effect between hypoxia and normoxia which is best exemplified by the PC-DFA of the GC-MS data (Figure 2.4A). In addition, when the GC-MS data are analysed in a univariate fashion (Box and Whisker for typical central metabolites; see Figure 2.5), CoCl_2 does not increase central metabolism intermediates to the same extent as hypoxia.

Clustergram analysis (Figure 2.3) is an unsupervised technique which is a hybrid between a heat map and a dendrogram and clearly shows the expected clustering of similar groups of metabolites. For example, it could be predicted that the majority of glycolysis intermediates would behave in a similar fashion, i.e. all increase during hypoxic and CoCl_2 exposure. Since each metabolite is correlated against all metabolites, those behaving similarly should be clustered together and it is evident that amino acids, TCA intermediates, fatty acids/lipids, glycolysis metabolites, sugars and polyols do this. This illustrates that each set of related metabolites behaves in a similar manner which emphasises the consistent nature of the data.

In conclusion CoCl_2 is able to mimic hypoxia in hTERT cells in terms of central metabolism, but appears to have some off target effects relating to secondary metabolism involving phospholipids and fatty acids. Hence, CoCl_2 should only be used as a hypoxic mimicker when investigating central metabolism and off target effects should be taken into consideration. Consequently, it is clear that, wherever possible, genuine hypoxia should be adopted for such studies.

2.6 Acknowledgements

We would like to thank Dr Susan Greenwood for the use of her hypoxic chamber. JWA, DCW, AAV were funded by Cancer Research UK and the Wolfson Foundation within the Clinical Research Infrastructure Scheme. PW and RG wish to thank BBSRC for financial support of The Manchester Centre for Integrative Systems Biology (BBC0082191). GB was supported by the Margaret Pritchard Memorial Fund which was awarded by the Humane Research Trust. Work in the Gynaecological Research Laboratories was also supported by donations from the Caring Cancer Trust, The Cancer Prevention Research Trust and United-in-Cancer.

2.7 References

- Abramovitch, R. Tavor, E. Jacob-Hirsch, J. Zeira, E. Amariglio, N. Pappo, O. Rechavi, G. Galun, E. and Honigman, A. (2004). A pivotal role of cyclic AMP-responsive element binding protein in tumor progression. *Cancer Research*, **64**: 1338-1346.
- An, W, G. Kanekal, M. Simon, M, C. Maltepe, E. Blagosklonny, M, V. and Meckers, L, M. (1998). Stabilization of wild-type p53 by hypoxia-inducible factor 1alpha. *Nature*, **392**: 405-408.
- Anelli, V. Gault, C, R. Snider, A, J. and Obeid, L, M. (2010). Role of sphingosine kinase-1 in paracrine/transcellular angiogenesis and lymphangiogenesis *in vitro*. *The Federation of American Societies for Experimental Biology Journal*. **24**: 2727-2738.
- Ardyanto, T, W. Osaki, M. Tokuyasu, N. Nagahama, Y. and Ito, H. (2006). CoCl₂-induced HIF-1alpha expression correlates with proliferation and apoptosis in MKN-1 cells: A possible role for the PI3K/Akt pathway. *International Journal of Oncology*. **29**: 549-555.
- Bartrons, R. and Caro, J. (2007). Hypoxia, glucose metabolism and the Warburg's effect. *Journal of Bioenergetics and Biomembranes*. **39**: 223-229.
- Baugh, J, A. Gantier, M. Li, L. Byrne, A. Buckley, A. Donnelly, S, C. (2006). Dual regulation of macrophage migration inhibitory factor (MIF) expression in hypoxia by CREB and HIF-1. *Biochemical and Biophysical Research Communications*. **347**: 895-903.
- Begley, P. Francis-McIntyre, S. Dunn, W, B. Broadhurst, D, I. Halsall, A. Tseng, A. Knowles, J. HUSERMET Consortium, Goodacre, R. and Kell, D, B. (2009). Development and performance of a gas chromatography-time-of-flight mass spectrometry analysis for large-scale nontargeted metabolomic studies of human serum. *Analytical Chemistry*. **81**: 7038-7046.

Berra, E. Roux, D. Richard, D, E, Pouysségur, J. (2001). Hypoxia-inducible factor-1 α (HIF-1 α) escapes O₂-driven proteasomal degradation irrespective of its subcellular localization: nucleus or cytoplasm. *EMBO Reports*. **2**: 615-620.

Björklund, O. Shang, M. Tonazzini, I. Daré, E. and Freholm, B, B. (2008). Adenosine A1 and A3 receptors protect astrocytes from hypoxic damage. *European Journal of Pharmacology*. **596**: 6-13.

Breit, J, F. Ault-Ziel, K. Al-Mehdi, AB. and Gillespie, M, N. (2008). Nuclear protein-induced bending and flexing of the hypoxic response element of the rat vascular endothelial growth factor promoter. *The FASEB Journal*. **22**: 19-29.

Bro, R. (1997). PARAFAC. Tutorial and applications. *Chemometrics and Intelligent Laboratory Systems*. **38**: 149-171.

Brown, M. Dunn, W, B., Dobson, P. Patel, Y. Winder, C, L. Francis-McIntyre, S. Begley, P. Carroll, K. Broadhurst, B. Tseng, A. Swainston, N. Spasic, I. Goodacre, R. and Kell, D.B. (2009). Mass spectrometry tools and metabolite-specific databases for molecular identification in metabolomics. *Analyst*. **134**: 1322-1332.

Brown, M. Wedge, D, C. Goodacre, R. Kell, D, B. Baker, P. N. Kenny, L, C. Mamas, M, A. Neyses, L. and Dunn, W, B. (2011). Automated workflows for accurate mass-based putative metabolite identification in LC/MS-derived metabolomic datasets. *Bioinformatics*. **27**: 1108-1112.

Chachami, G. Simos, G. Hatziefthimiou, A. Bonanou, S. Molyvdas, PA. and Paraskeva, E. (2004). Cobalt Induces Hypoxia-Inducible Factor-1 α expression in airway smooth muscle cells by a reactive oxygen species–and PI3K-dependent mechanism. *American Journal of Respiratory Cell and Molecular Biology*. **31**: 544-551.

Chandel, N, S. Maltepe, E. Goldwasser, E. Mathieu, C, E. Simons, M, C. and Schumacker, P, T. (1998). Mitochondrial reactive oxygen species trigger hypoxia-induced transcription. *Cell Biology*. **95**: 11715-11720.

Christova, T, Y. Duridanova D, B. and Setchenska, M, S. (2002). Enhanced heme oxygenase activity increases the antioxidant defense capacity of guinea pig liver upon acute cobalt chloride loading: comparison with rat liver. *Comparative Biochemical and Physiology. Toxicology Pharmacology*. **131**: 177-184.

Correa, E. Sletta, H., Ellis, D.I., Hoel, S., Ertesvåg, H., Ellingsen, T.E., Valla, S. & Goodacre, R. (2012). Rapid reagentless quantification of alginate biosynthesis in *Pseudomonas fluorescens* bacteria mutants using FT-IR spectroscopy coupled to multivariate partial least squares regression. *Analytical and Bioanalytical Chemistry*. **403**: 2591-2599.

Denko, N, C. (2008). Hypoxia, HIF1 and glucose metabolism in the solid tumour. *Nature Reviews Cancer*. **8**: 705-713.

Dickson, M, A. Hahn, W, C. Ino, Y. Ronfard, V. Wu, J, Y. Weinberg, R, A. Louis, D, N. Li, F, P. and Rheinwald, J. G (2000). Human keratinocytes that express hTERT and also bypass a p16INK4a-enforced mechanism that limits life span become immortal yet retain normal growth and differentiation characteristics. *Molecular and Cellular Biology*. **20**: 13436-1447.

Frezza, C. and Gottlieb, E. (2009). Mitochondria in cancer: Not just innocent bystanders. *Seminars in Cancer Biology*. **19**: 4-11.

Fukuda, R. Zhang, H. Kim, J, W. Shimoda, L. Dang, C, V. and Semenza, G, L. (2007). HIF-1 regulates cytochrome oxidase subunits to optimize efficiency of respiration in hypoxic cells. *Cell*. **129**: 111-122.

Gatenby, R, A. and Gillies, R. (2004). Why do cancers have high aerobic glycolysis? *Nature Reviews Cancer*. **4**: 891-899.

Gogvadze, V. Orrenius, S. and Zhivotovsky, B. (2009). Mitochondria as targets for cancer chemotherapy. *Seminars in Cancer Biology*. **19**: 57-66.

- Goodacre, R., York, E.V., Heald, J.K., Scott, I.M. (2003). Chemometric discrimination of unfractionated plant extracts analyzed by electrospray mass spectrometry. *Phytochemistry*. **62**: 859-863.
- González, R. Romay, C. Borrego, A. Hernández, F. Merino N. Zamora, Z. and Rojas, E. (2005). Lipid peroxides and antioxidant enzymes in Cisplatin-induced chronic nephrotoxicity in rats. *Mediators of Inflammation*. **3**: 139-143.
- Guo, M. Song, LP. Jiang, Y. Liu, W. Yu, Y. and Chen, GQ. (2006). Hypoxia-mimetic agents desferrioxamine and cobalt chloride induce leukemic cell apoptosis through different hypoxia-inducible factor-1 α independent mechanisms. *Apoptosis*. **11**: 67-77.
- Ho, V, T. and Bunn, H, F. (1996). Effects of transition metals on the expression of the erythropoietin gene: Further evidence that the oxygen sensor is a heme protein. *Biochemical and Biophysical Research Communications*, **223**: 175-180.
- Hsu, P, P. and Sabatini, D, M. (2008). Cancer Cell Metabolism: Warburg and Beyond. *Cell*. **134**: 703-707.
- Jung, JY. Mo, HC. Yang, KH. Jeong, YJ. Yoo, HG. Choi, NK. Oh, WM. Oh, HK. Kim, SH. Lee, JH. Kim, HJ. and Kim, WJ. (2007). Inhibition by epigallocatechin gallate of CoCl₂ -induced apoptosis in rat PC12 cells. *Life Sciences*. **80**: 1355-1363.
- Ke, Q. and Costa, M. (2006). Hypoxia-Inducible Factor-1 (HIF-1). *Molecular Pharmacology*. **70**: 1469-1480.
- Kress, S. Stein, A. Maurer, P. Weber, B. Reichert, J. Buchmann, A. Huppert, P. and Schwarz, M. (1998). Expression of hypoxia-inducible genes in tumor cells. *Journal of Cancer Research and Clinical Oncology*. **124**: 315-320.
- Kroonenberg, P, M. (2008). Applied multiway data analysis. Wiley Series in Probability and Statistics, Wiley-Interscience.

LaManna, J, C. Pichiule, P. and Chavez, J, C. (2007). 7.2 Genetics and gene expression of glycolysis IN *Handbook of Neurochemistry and Molecular Neurobiology*. Springer-Verlag Berlin Heidelberg.

Lenz, E, M. and Wilson, I, D. (2007). Analytical strategies in metabolomics. *Journal of Proteome Research*. **6**: 443-458.

Mottet, D. Dumont, V. Deccache, Y. Demazy, C. Ninane, N. Raes, M. and Michiels, C. (2003). Regulation of hypoxia-inducible factor-1alpha protein level during hypoxic conditions by the phosphatidylinositol 3-kinase/Akt/glycogen synthase kinase 3beta pathway in HepG2 cells. *Journal of Biological Chemistry*. **278**: 31277-31285.

Nijsten, M, W, N. and van Dam, G, M. (2009). Hypothesis: Using the Warburg effect against cancer by reducing glucose and providing lactate. *Medical Hypotheses*. **73**: 48-51.

Ohh, M. Park, C, W. Ivan, M. Hoffman, M, A. Kim, TY, Huang, L, E. Pavletich, N. Chau, V. and Kaelin Jr., W, G. (2000). Ubiquitination of HIF requires direct binding to the beta-domain of the von Hippel-Lindau protein. *Nature Cell Biology*. **2**: 423-427.

Ryan,H, E. Lo, J. and Johnson, R, S. (1998). HIF-1a is required for solid tumor formation and embryonic vascularization. *The EMBO Journal*. **17**: 3005-3015.

Ryu, M, H. Park, J, H. Park, J, E. Chung, J. Lee, C, H. and Park, H, R. (2010). Cobalt chloride stimulates phosphoinositide 3-kinase/Akt signaling through the epidermal growth factor receptor in oral squamous cell carcinoma. *Biocell*. **34**: 15-21.

Sellick, C, A. Knight, D. Croxford, A, S. Maqsood, A, R. Stephens, G, M. Goodacre, R. Dickson, A, J. (2010). Evaluation of extraction processes for intracellular metabolite profiling of mammalian cells: matching extraction approaches to cell type and metabolite targets. *Metabolomics*. **6**: 427-438.

Slater, T, F. (1984). Free-radical mechanisms in tissue injury. *Biochemical Journal*. **222**: 1-15.

Sumner, L, W. Amberg, A. Barrett, D. Beger, R. Beale, M, H. Daykin, C, A. Fan, T, WM. Fiehn, O. Goodacre, R. Griffin, J, L. Hardy, N. Higashi, R. Kopka, J. Lindon, J, C. Lane, A, N. Marriott, P. Nicholls, A, W. Reily, M, D. and Viant M. (2007). Proposed minimum reporting standards for chemical analysis: Chemical Analysis Working Group (CAWG) Metabolomics Standards Initiative (MSI). *Metabolomics*. **3**: 211-221.

Suzuki, M. Shinohara, F. Endo, M. Sugazaki, M. Echigo, S. and Rikiishi, H. (2009). Zebularine suppresses the apoptotic potential of 5-Xuorouracil via cAMP/PKA/CREB pathway against human oral squamous cell carcinoma cells. *Cancer Chemotherapy Pharmacology*. **64**: 223-232.

Tan, X, L. Huang, X, Y. Gao, W, X. Zai, Y. Huang, Q, Y. Luo, Y, J. and Gao, Y, Q. (2008). CoCl₂-induced expression of p300 promotes neuronal-like PC12 cell damage. *Neuroscience Letters*. **441**: 272-276.

Vander Heiden, M, G. Cantley, L, C. and Thompson, C, B. (2009). Understanding the Warburg effect: The metabolic requirements of cell proliferation. *Science*. **324**: 1029-1033.

Warburg, O. Posener, K. and Negelein, E, U. (1924). On metabolism of tumors. *Biochemical Magazine*. **152**: 319-344.

Warburg, O. Wind, F, and Negelein, E. (1927). The metabolism of tumors in the body. *The Journal of General Physiology*. **8**: 519-530.

Warburg, O. (1930). The metabolism of tumours' Constable: London.

Warburg, O. (1956). On the origin of cancer cells. *Science*. **123**: 309-314.

Warburg, O. (1965). On respiratory impairment in cancer cells. *Science*. **124**: 269-270.

Xu, Y. Cheung, W. Winder, C, L. Dunn, W, B. and Goodacre, R. (2011). Metabolic profiling of meat: assessment of pork hygiene and contamination with *Salmonella typhimurium*. *Analyst*. **136**: 508-514.

Yuan, Y. Hilliard, G. Ferguson, T. and Millhorn, D, E. (2003). Cobalt inhibits the interaction between Hypoxia-inducible Factor- α and von Hippel-Lindau protein by direct binding to Hypoxia-inducible Factor- α . *The Journal of Biological Chemistry*. **278**: 15911-15916.

2.8 Supplementary Information

Table 2.S1. All GC-MS Metabolites

Metabolite	Confidence	CID Number	Chemical Class	Norm Average (±SE)	Hyp Average (±SE)	CoCl ₂ Average (±SE)	P-Value
1,2-Benzenedicarboxylic acid	Putative	1017	Carboxylic Acid	0.1606 (0.137)	0.1055 (0.077)	0.0681 (0.054)	5.354E-01
4-methyl-2-oxovaleric Acid	Putative	70	Ketone	0.0407 (0.004)	0.0322 (0.003)	0.0349 (0.003)	2.407E-01
Arginine/Citruline	Putative	6322/9750	Amino Acid	0.4777 (0.026)	0.5493 (0.020)	0.4628 (0.020)	3.530E-03
Aspartic Acid	High Confidence	5960	Amino Acid	0.8036 (0.050)	0.6199 (0.032)	0.6226 (0.032)	2.090E-04
C6 Monosaccharide	Putative	N/A	Monosaccharide	0.0623 (0.011)	0.0786 (0.005)	0.0514 (0.004)	6.632E-09
C6 Monosaccharide	Putative	N/A	Monosaccharide	0.0571 (0.009)	0.0701 (0.004)	0.0372 (0.003)	4.592E-05
Cholesterol	Putative	5997	Sterol	0.2330 (0.021)	0.1894 (0.018)	0.1761 (0.015)	2.754E-02
Citrate	High Confidence	31348	Carboxylic Acid	0.0395 (0.017)	0.0220 (0.002)	0.0225 (0.002)	3.046E-01
Cuminaldehyde/Adenine	Putative	326/190	Aldehyde/Nucleo base	0.6131 (0.051)	0.8801 (0.036)	0.6206 (0.034)	5.117E-07
Cysteine	High Confidence	5862	Amino Acid	0.2887 (0.025)	0.3291 (0.013)	0.2091 (0.012)	1.121E-09
Deoxyglucose	Putative	108223	Monosaccharide	0.1620 (0.032)	0.1451 (0.015)	0.1172 (0.009)	8.591E-02
F6P	High Confidence	9062	Monosaccharide	0.0261 (0.002)	0.0239 (0.002)	0.0227 (0.002)	2.977E-01
Fructose	Putative	5984	Monosaccharide	0.0291 (0.002)	0.0320 (0.002)	0.0253 (0.001)	7.758E-03
Fumarate/Maleate	Putative	444972/444266	Dicarboxylic Acid	0.1518 (0.005)	0.1028 (0.007)	0.1486 (0.010)	3.121E-08
Glucose/Galactose	Putative	5793/6036	Monosaccharide	0.6061 (0.081)	0.9154 (0.068)	0.6628 (0.059)	2.892E-04
Glutamine	High Confidence	5961	Amino Acid	1.5133 (0.062)	1.309 (0.070)	1.4760 (0.082)	5.642E-03
Glyceraldehyde	Putative	751	Aldehyde	0.0657 (0.003)	0.0589 (0.003)	0.0646 (0.003)	2.011E-

							01
Glycerol	High Confidence	753	Polyol	0.1058 (0.013)	0.0935 (0.012)	0.1184 (0.013)	1.274E-01
Hexadecanoic Acid	High Confidence	985	Lipid	0.1299 (0.004)	0.1224 (0.004)	0.1229 (0.004)	2.268E-01
Hexonic Acid	Putative	604	Lipid	0.0126 (0.003)	0.0239 (0.002)	0.0105 (0.001)	7.884E-06
Lactic Acid	High Confidence	612	Carboxylic Acid	16.3065(0.854)	14.5208 (0.761)	14.0508 (0.785)	2.693E-02
Leucine	High Confidence	857	Amino Acid	3.9240 (0.263)	4.8235 (0.179)	3.9262 (0.197)	8.711E-04
L-Glutamine	Putative	5961	Amino Acid	0.0394 (0.002)	0.0399 (0.002)	0.0365 (0.002)	2.042E-01
Malate	High Confidence	160434	Dicarboxylic Acid	0.1532 (0.010)	0.0946 (0.010)	0.1364 (0.012)	3.178E-05
Malitol	Putative	3871	Polyol	0.1546 (0.027)	0.2377 (0.018)	0.1503 (0.014)	2.765E-04
Malonate	High Confidence	9084	Dicarboxylic Acid	0.4982 (0.009)	0.5033 (0.007)	0.4959 (0.006)	4.691E-01
Mannose/Allose/Glucose/Galactose	Putative	N/A	Monosaccharide	0.0699 (0.009)	0.0893 (0.005)	0.0672 (0.005)	2.283E-04
Mannose/Allose/Glucose/Galactose	Putative	N/A	Monosaccharide	1.2705 (0.063)	1.4201 (0.056)	1.3332 (0.053)	1.236E-02
Mannose/Allose/Glucose/Galactose	Putative	N/A	Monosaccharide	0.4420 (0.033)	0.4922 (0.026)	0.4606 (0.026)	2.200E-02
Myo Inositol	High Confidence	892	Polyol	0.7296 (0.032)	0.6753 (0.024)	0.6256 (0.027)	3.391E-02
Myristic Acid	Putative	11005	Fatty Acid	0.3578 (0.028)	0.4097 (0.017)	0.3600 (0.018)	1.210E-02
N-acetylneuraminic Acid	Putative	906	Monosaccharide	0.0271 (0.003)	0.0415 (0.003)	0.0275 (0.002)	4.575E-05
Normetanephrine	Putative	1237	Catecholamine	0.0321 (0.003)	0.0384 (0.002)	0.0293 (0.002)	1.200E-03
Octadecanoic Acid	High Confidence	5281	Fatty Acid	0.1018 (0.003)	0.0988 (0.004)	0.1006 (0.003)	6.718E-01
Oleic Acid	High Confidence	445639	Fatty Acid	0.0486(0.003)	0.0438 (0.004)	0.0435 (0.003)	1.294E-01
Palitoleic Acid	Putative	445638	Fatty Acid	0.0270 (0.002)	0.0262 (0.002)	0.0252 (0.001)	1.275E-01
Phenylalanine	High	6140	Amino Acid	0.2943 (0.012)	0.3433 (0.009)	0.2894 (0.012)	4.341E-

	Confidence						04
Phosphate	High Confidence	1061	Phosphate	3.8635(0.191)	3.1017 (0.225)	3.5684 (0.211)	3.362E-02
Phosphocreatinine	Putative	71214	Organic Acid	0.0934 (0.049)	0.0220 (0.008)	0.0229 (0.008)	1.698E-01
Polyol	Putative	N/A	Polyol	0.0854 (0.019)	0.0421 (0.005)	0.0358 (0.006)	2.965E-05
Polyol	Putative	N/A	Polyol	0.0467 (0.011)	0.0660 (0.007)	0.0408 (0.004)	2.468E-04
Polyol	Putative	N/A	Polyol	0.1930 (0.018)	0.2380 (0.011)	0.1981 (0.012)	1.349E-03
Polyol	Putative	N/A	Polyol	0.0530 (0.008)	0.0763 (0.007)	0.0446 (0.004)	3.424E-03
Polyol	Putative	N/A	Polyol	0.0103 (0.017)	0.0144 (0.007)	0.0092 (0.008)	2.243E-03
Polyol	Putative	N/A	Polyol	0.0244 (0.018)	0.0328 (0.022)	0.0208 (0.012)	1.392E-04
Proline	Putative	N/A	Amino Acid	0.0891 (0.101)	0.0562 (0.076)	0.0611 (0.084)	1.661E-01
Pyroglutamic Acid	High Confidence	7405	Amino Acid	0.1097 (0.003)	0.2151 (0.003)	0.1322 (0.001)	3.266E-04
Serine	Putative	5951	Amino Acid	2.5401 (0.001)	2.7785 (0.001)	2.4922 (0.001)	1.096E-02
Sugar/Polyol	Putative	N/A	Polyol	0.0430 (0.003)	0.0528 (0.003)	0.0400 (0.002)	4.543E-04
Threitol	Putative	169019	Polyol	0.2717 (0.021)	0.3315 (0.012)	0.2886 (0.015)	1.465E-03
Threonine	High Confidence	6288	Amino Acid	0.5469 (0.031)	0.6143 (0.021)	0.5335 (0.024)	1.119E-02
Tyrosine/Tyramine	Putative	6057/5610	Amino Acid	0.1421 (0.009)	0.1611 (0.007)	0.1300 (0.006)	7.593E-04
Valine	High Confidence	6287	Amino Acid	2.0377 (0.144)	2.4013 (0.099)	2.0180 (0.098)	4.694E-03

Table 2.S1 Key

Confidence: metabolite ID confidence - high confidence or putative (supposed)

CID Number: compound identification number (PubChem)

Values: average peak area ± standard error (arbitrary); n=6

P-value: determined by ANOVA

Table 2.S2. Significant Negative LC-MS Metabolites

Metabolite	m/z	Retention Time (s)	Confidence	CID Number	Chemical Class	Norm Average (±SE)	Hyp Average (±SE)	CoCl ₂ Average (±SE)	P-Value
(2s)-2,8-Diaminooctanoic Acid/ N-Dimethyl-Lysine	195. 1122	489.05	Putative	469369 85/1647 95	Amino Acid	2.90E-05 (2.07E-06)	3.88E-05 (5.62E-06)	1.43E-05 (4.04E-06)	0.0301 16939
1-hexadecyl-2-octadecyl-sn-glycero-3-phosphocholine	802. 5509	1181.04	Putative	247794 06	Phosphocholine	0.94E-04 (5.75E-06)	8.09E-04 (4.95E-06)	7.13E-04 (4.80E-06)	3.9310 5E-13
3-(Methylthio)propionic Acid/Dimethylsulfonioacetate	162. 9811	86.72	Putative	563/160 765	Fatty Acid	3.95E-05 (3.74E-06)	2.19E-05 (3.83E-06)	2.57E-05 (4.02E-06)	0.0137 00903
5,6-Dihydroxyindole-2-carboxylate	192. 0300	62.02	Putative	119405	Amino Acid	5.13E-04 (1.8E-04)	1.80E-04 (3.14E-05)	1.08E-04 (1.14E-05)	0.0273 02042
Amino Fatty Acid	443. 1567	54.78	Putative	N/A	Fatty Acid	1.19E-05 (2.96E-06)	3.29E-05 (5.49E-06)	8.05E-06 (2.34E-06)	0.0001 42736
Beta-(2-Naphthyl)-Alanine	282. 0740	747.70	Putative	185915	Amino Acid	3.04E-05 (5.06E-06)	1.44E-06 (3.60E-06)	2.28E-05 (4.31E-06)	0.0129 29445
Carbohydrates/Amino Acid	241. 0803	64.82	Putative	N/A	Carbohydrate/ Amino Acid	1.44E-04 (1.46E-05)	3.16E-04 (2.83E-05)	2.70E-04 (2.84E-05)	2.2654 1E-06
Diacylglycerol	719. 5245	1143.93	Putative	N/A	Diacylglycerol	1.80E-04 (1.09E-05)	1.40E-04 (1.24E-05)	7.61E-05 (7.95E-06)	4.6863 8E-09
Diacylglycerol	749. 5691	1177.72	Putative	N/A	Diacylglycerol	1.11E-04 (4.78E-06)	9.99E-05 (4.31E-06)	1.90E-04 (4.34E-06)	0.0001 15246
Diacylglycerol	707. 5856	1244.72	Putative	N/A	Diacylglycerol	5.81E-05 (1.25E-05)	2.51E-05 (1.35E-05)	1.93E-05 (1.41E-05)	1.2346 1E-07
Dodecanedioic acid	287. 1039	373.67	Putative	12736	Dicarboxylic Acid	2.58E-05 (4.80E-06)	3.26E-05 (5.69E-06)	9.25E-06 (2.88E-06)	0.0056 78595
Fatty Acid	221. 1527	913.36	Putative	N/A	Fatty Acid	6.77E-05 (5.85E-06)	6.99E-05 (4.65E-06)	8.85E-05 (5.77E-06)	0.0130 89381
Fatty Acid	193. 0853	746.04	Putative	N/A	Fatty Acid	6.96E-05 (1.15E-05)	5.42E-05 (7.17E-06)	7.95E-05 (8.93E-06)	0.0397 05082
Fatty Acid/Dicarboxylic Acid	287. 1039	373.67	Putative	N/A	Fatty Acid	2.58E-05 (4.98E-06)	3.26E-05 (5.69E-06)	9.25E-06 (2.88E-06)	0.0056 78595
Fatty Aldehyde	144. 0459	463.79	Putative	N/A	Fatty Aldehyde	3.81E-05 (4.02E-06)	4.93E-05 (6.42E-06)	6.96E-05 (5.39E-06)	1.5321 3E-05
Fatty Amides	516. 2137	43.93	Putative	N/A	Fatty Amide	2.90E-05 (4.88E-06)	8.23E-05 (8.78E-06)	4.47E-05 (8.21E-06)	3.4969 3E-06
Free Fatty Acid	287. 1039	373.67	Putative	N/A	Fatty Acid	2.58E-05 (4.98E-06)	3.26E-05 (5.69E-06)	9.25E-06 (2.88E-06)	0.0056 78595

Glycerophospholipid	802.5509	1181.04	Putative	N/A	Phospholipid	9.42E-04 (5.75E-06)	8.10E-04 (4.95E-06)	7.13E-04 (4.80E-06)	3.9310 5E-13
Hydroxyethylcysteine; Methionine sulfoxide	186.0214	364.24	Putative	119224/ 847	Amino Acid	4.56E-05 (7.34E-06)	2.69E-05 (5.07E-06)	1.11E-05 (2.99E-06)	7.4390 7E-05
IMP	347.0413	50.41	Putative	8582	Nucleotide	6.99E-05 (3.64E-06)	9.01E-05 (3.50E-06)	6.98E-05 (3.35E-06)	0.0001 94313
Indoxyl sulfate	327.9180	1416.71	Putative	10258	Indole	7.05E-05 (1.40E-06)	5.90E-05 (4.61E-06)	6.10E-05 (4.13E-06)	0.0207 79516
Keto-Acids; Dicarboxylic Acids; Fatty Acids	131.0343	92.42	Putative	N/A	Fatty Acid	3.38E-04 (2.65E-05)	5.13E-04 (5.51E-05)	2.50E-04 (3.17E-05)	0.0368 2816
L-phenylalanyl-L-proline / L-prolyl-L-phenylalanine	283.1077	829.54	Putative	406913 1/52260 97	Amino Acid	3.57E-05 (3.36E-06)	2.40E-05 (2.26E-06)	3.69E-05 (2.85E-06)	0.0007 1347
Monoacylglycerophosphate	545.1831	530.78	Putative	N/A	Monoacyl- glycerophosph ate	3.58E-05 (3.99E-06)	1.88E-05 (3.68E-06)	1.75E-05 (3.61E-06)	0.0011 69672
N-Acetyl-beta-D- glucosaminyllamine	277.0566	65.17	Putative	439454	Carbohydrate	2.75E-04 (3.14E-05)	6.50E-04 (6.41E-05)	5.40E-04 (6.30E-05)	0.0005 81226
Pantothenic Acid (Vitamin B5)	276.0620	95.68	Putative	6613	Vitamin	5.95E-05 (2.51E-06)	4.57E-05 (1.80E-06)	5.75E-05 (2.58E-06)	4.4425 4E-05
Phosphocholine	804.5671	1203.72	Putative	N/A	Phosphocholin e	6.58E-04 (9.49E-06)	6.00E-04 (1.48E-05)	6.50E-04 (1.30E-05)	0.0014 13567
Phosphocholine	802.5509	1181.04	Putative	N/A	Phosphocholin e	9.42E-04 (2.04E-05)	8.10E-04 (1.87E-05)	7.12E-04 (1.43E-05)	3.9310 5E-13
Phosphocholine	870.5366	1181.36	Putative	N/A	Phosphocholin e	3.79E-05 (5.75E-06)	4.22E-05 (4.95E-06)	2.53E-05 (4.80E-06)	0.0159 47378
Phosphocholine	774.5183	1156.14	Putative	N/A	Phosphocholin e	5.76E-04 (5.75E-06)	4.50E-04 (4.95E-06)	3.33E-04 (4.80E-06)	3.4082 E-13
Phosphocholine Derivative	792.5931	1225.06	Putative	N/A	Phosphocholin e	5.63E-05 (2.77E-06)	4.36E-05 (4.72E-06)	3.48E-05 (5.90E-06)	0.0017 60607
PS(16:0/18:0) or PS(18:0/16:0) (Glycerophosphocholines)	779.5543	1198.69	Putative	N/A	Phosphocholin e	5.97E-05 (2.42E-06)	4.71E-05 (3.74E-06)	6.15E-05 (2.58E-06)	0.0059 20676
S-(2-Hydroxyethyl)-N-acetyl-L- cysteine	228.0311	80.19	Putative	108009	Amino Acid	4.75E-05 (8.01E-06)	5.91E-05 (5.87E-06)	3.00E-06 (1.37E-06)	7.3138 6E-06
Sugar Alcohol	168.988	309.35	Putative	N/A	Polyol	1.28E-04 (1.96E-05)	6.73E-05 (9.74E-06)	1.23E-04 (4.38E-05)	0.0071 44813
Threonine-Aspartic Ester	279.0561	50.30	Putative	N/A	Amino Acid	1.66E-03 (1.14E-04)	2.36E-03 (9.73E-05)	1.65E-03 (6.56E-05)	1.6164 7E-05
Threonine-Aspartic Ester/ Lysine Nz-Carboxylic Acid	257.0747	49.59	Putative	N/A	Amino Acid	7.89E-04 (7.94E-05)	1.30E-03 (6.48E-05)	9.75E-04 (5.88E-05)	1.7984 1E-05
Vitamin B2 and Derivatives	421.	775.86	Putative	493570	Vitamin	1.07E-04	8.44E-05	7.33E-05	4.49E-

	1363					(1.91E-06)	(2.05E-06)	(2.17E-06)	10
Vitamin D2 and derivatives	443. 1567	54.78	Putative	3249	Vitamin	1.20E-05 (3.31E-06)	3.29E-05 (1.57E-06)	8.05E-06 (2.49E-06)	0.0001 42736
Vitamin D2 and derivatives	411. 1929	33.82	Putative	3249	Vitamin	1.90E-05 (2.96E-06)	3.68E-05 (5.49E-06)	2.20E-05 (2.34E-06)	3.2078 E-05
Xanthosine	341. 0256	50.73	Putative	64959	Nucleoside	2.70E-05 (2.07E-06)	3.59E-05 (1.98E-06)	2.75E-05 (9.64E-07)	0.0004 09292

Table 2.S2 Key

m/z: mass to charge ratio of the compound

Retention Time: time taken for analyte to reach the detector

Confidence: metabolite ID confidence - high confidence or putative (supposed)

CID Number: compound identification number (PubChem)

Values: average peak area ± standard error (arbitrary); n=6

P-value: determined by ANOVA

Table 2.S3. Significant Positive LC-MS Metabolites

Metabolite	m/z	Retention Time (s)	Confidence	CID Number	Chemical Class	Norm Average (\pm SE)	Hyp Average (\pm SE)	CoCl ₂ Average (\pm SE)	P Value
3-Amino-6-Hydroxy-Tyrosine	281.0 743	49.03	Putative	6917016	Amino Acid	1.95E-04 (1.75E-05)	2.76E-04 (1.94E-05)	2.05E-04 (1.61E-05)	0.002737 869
4-Oxoproline;5-Oxoproline (Pyroglutamic Acid)	130.0 495	48.62	Putative	7405	Amino Acid	8.00E-03 (2.77E-04)	9.64E-03 (2.95E-04)	7.74E-03 (2.43E-04)	6.4115 8E-06
6-O-Cyclohexylmethyl Guanine	316.1 368	59.01	Putative	4564	Amino Acid	3.04E-04 (2.42E-04)	4.56E-03 (2.50E-04)	3.57E-03 (2.38E-04)	7.04053E -05
Acetyltropine	258.0 650	86.15	Putative	1055936 9	Alkaloid	9.74E-05 *2.75E-06)	8.20E-05 (2.34E-06)	9.77E-05 (3.22E-06)	6.98711E -05
Adenine	136.0 613	44.55	Putative	190	Nucleobase	8.41E-06 (1.21E-06)	1.40E-05 (1.30E-06)	1.22E-05 (1.23E-06)	0.002447 362
Amino Acid	156.0 764	41.32	Putative	N/A	Amino Acid	4.87E-04 (1.11E-05)	4.94E-04 (1.01E-05)	3.59E-04 (9.80E-06)	7.49226E -14
Amino Acid	155.0 886	60.66	Putative	N/A	Amino Acid	2.75E-04 (7.17E-06)	2.26E-04 (9.76E-06)	2.60E-04 (6.12E-06)	0.000144 484
Amino Acid	261.9 879	437.97	Putative	N/A	Amino Acid	5.98E-05 (1.61E-06)	7.05E-05 (2.50E-06)	6.35E-05 (2.28E-06)	0.000632 701
Batilol	345.3 359	813.31	Putative	3681	Polyol	3.04E-05 (4.75E-06)	2.97E-05 (5.97E-06)	6.38E-05 (8.14E-06)	0.001093 749
Cysteine	190.0 896	305.68	Putative	5862	Amino Acid	2.52E-04 (1.92E-05)	2.23E-04 (1.54E-05)	1.04E-04 (9.16E-06)	2.1161E- 08
Diacylglycerol/30-hydroxy-triacontanoic Acid	559.4 317	868.66	Putative	N/A	Diacylglycerol	1.19E-04 (9.91E-06)	1.17E-04 (1.17E-05)	3.15E-05 (6.31E-06)	5.27324E -09
Fatty Acids Phosphoglycerols	605.5 497	1016.31	Putative	N/A	Fatty Acid	7.10E-06 (2.29E-06)	5.94E-06 (1.90E-06)	4.05E-05 (4.43E-06)	8.58507E -09
Glutathione Derived Polypeptide	308.0 912	47.39	Putative	N/A	Polypeptide	2.19E-04 (1.52E-05)	5.49E-05 (1.03E-05)	7.76E-05 (1.17E-05)	0.000849 227
Glutathione Derived Polypeptide	380.1 130	50.58	Putative	N/A	Polypeptide	1.24E-04 (4.31E-05)	4.56E-05 (1.36E-05)	8.97E-05 (1.54E-05)	7.75908E -05
Glycerophospholipid/Phosphocholines	476.3 131	873.72	Putative	N/A	Phospholipid/Phosphocholine	8.43E-05 (2.33E-06)	2.38E-06 (2.38E-06)	2.78E-06 (2.78E-06)	0.391180 913
Glycerophospholipid/Phosphocholines/Glycerophosphocholines	504.3 442	896.55	Putative	N/A	Phospholipid/Phosphocholine	6.07E-05 (1.08E-06)	1.65E-06 (1.65E-06)	2.03E-06 (2.03E-06)	0.397882 982

sphocholines									
Hydroxy Fatty Acids	299.1 825	599.65	Putative	N/A	Fatty Acid	2.78E-05 (2.39E-06)	9.15E-06 (1.99E-06)	1.36E-05 (2.11E-06)	1.59811E -07
Lactic Acid	113.0 205	47.16	Putative	612	Carboxylic Acid	1.66E-04 (8.01E-06)	1.02E-04 (9.57E-06)	1.36E-04 (9.70E-06)	4.35769E -06
L-Histidine	156.0 764	41.32	Putative	6274	Amino Acid	4.87E-04 (1.11E-05)	4.94E-04 (1.01E-05)	3.59E-04 (9.80E-06)	7.49226E -14
Methyltransferase	151.0 907	288.21	Putative	N/A	Transferase Enzyme	5.30E-05 (1.70E-05)	1.98E-04 (2.95E-05)	9.16E-04 (2.20E-05)	8.58165E -05
Pantothenic Acid (vitamin B5)	220.1 177	85.21	Putative	6613	Vitamin	1.33E-04 (4.34E-06)	1.10E-04 (3.78E-06)	1.28E-04 (4.84E-06)	0.000233 767
Phosphocholine	752.5 210	873.75	Putative	N/A	Phosphocholine	1.38E-04 (9.55E-06)	1.08E-04 (9.44E-06)	6.43E-05 (1.10E-05)	3.94702E -07
Phosphocholine	758.5 994	898.46	Putative	N/A	Phosphocholine	8.67E-04 (1.10E-05)	7.87E-04 (1.02E-05)	7.20E-04 (5.75E-06)	1.98675E -05
Phosphocholine	780.5 515	898.36	Putative	N/A	Phosphocholine	1.07E-04 (1.86E-06)	9.95E-04 (1.61E-06)	6.68E-05 (1.62E-06)	0.000148 579
Phosphocholine	788.6 177	954.22	Putative	N/A	Phosphocholine	6.45E-05 (6.38E-06)	6.05E-05 (5.43E-06)	9.13E-05 (7.62E-06)	0.000806 851
Phosphocholine	748.6 233	974.84	Putative	N/A	Phosphocholine	6.06E-05 (4.91E-06)	3.45E-05 (4.16E-06)	1.17E-04 (5.91E-06)	3.31267E -07
Phosphocholine and quinones	730.5 389	874.38	Putative	N/A	Phosphocholine	5.11E-04 (3.14E-05)	2.81E-05 (2.81E-05)	1.84E-05 (1.84E-05)	0.343481 52
Polypeptides; FAs; Alcohols/Polyols; Fatty alcohols	247.1 288	77.67	Putative	N/A	Polypeptide/Fatty Acid/Polyol	4.13E-05 (3.27E-06)	3.75E-05 (3.74E-06)	6.28E-05 (2.31E-06)	3.89061E -07
Sphingo basis and/or Fatty Acid's	303.3 084	719.32	Putative	N/A	Sphingobase/Fatt y Acid	2.75E-05 (3.02E-06)	2.15E-05 (3.51E-06)	4.08E-05 (3.43E-06)	0.005465 915
Sphingomyelin	675.5 444	863.40	Putative	N/A	Sphingolipid	1.73E-04 (1.07E-05)	1.60E-04 (1.13E-05)	1.21E-04 (8.36E-06)	2.47475E -06
Sphingomyelin	703.5 747	887.17	Putative	N/A	Sphingolipid	5.89E-05 (7.58E-06)	5.64E-05 (8.13E-06)	1.52E-04 (6.23E-06)	4.79351E -09
Tridecanoic Acid	299.1 825	599.65	Putative	12530	Fatty Acid	2.78E-05 (2.39E-06)	9.15E-06 (1.99E-06)	1.36E-05 (2.11E-06)	1.59811E -07

See Table 2.S2 Key for details

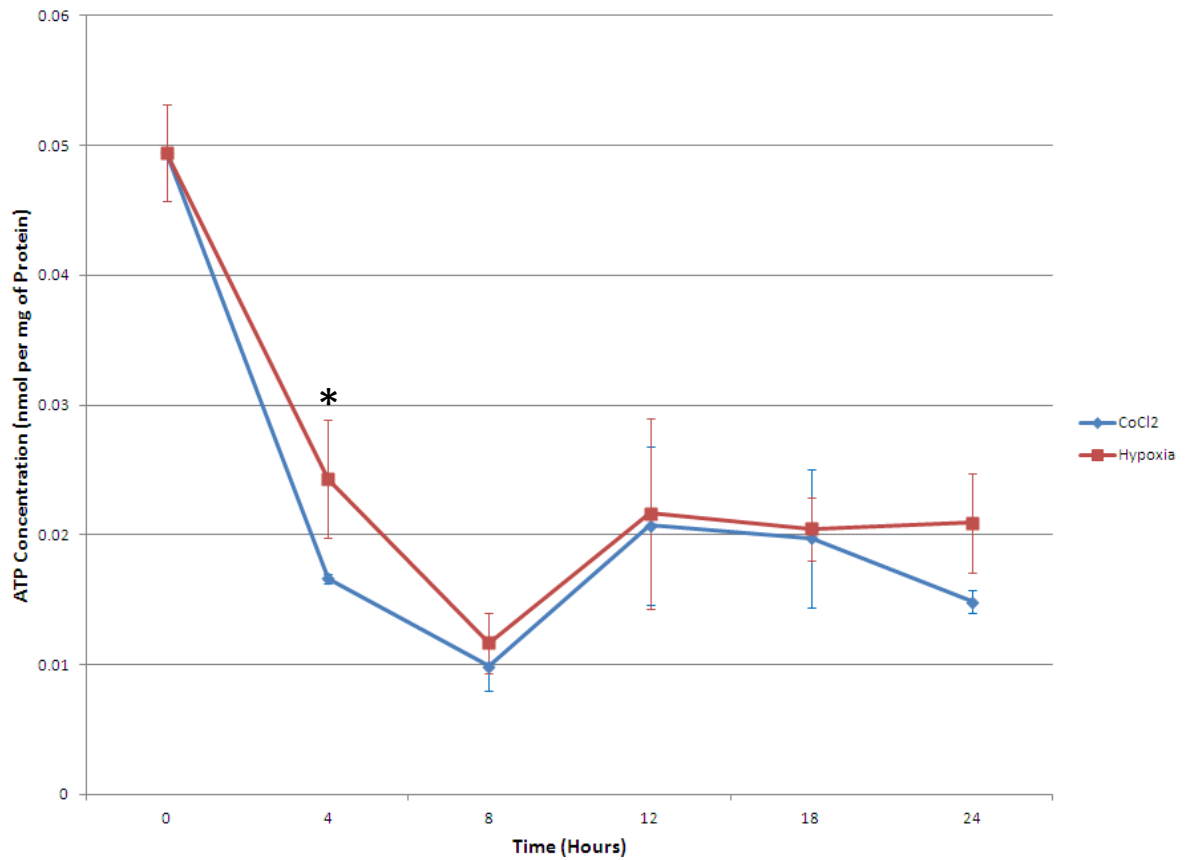


Figure 2.S1. ATP concentrations for hTERT cells during normoxia, hypoxia and CoCl₂ exposure at a range of time points. The blue line indicates the ATP concentrations for CoCl₂ exposure, the red line signifies the ATP concentrations for the hypoxic condition, and the standard errors are highlighted for each condition. The normoxic condition is found at time point zero, i.e. no condition exposure. The samples were normalised to total protein concentration to account for cell number variation. The asterix (*) denotes a significant result (mann-whitney; p<0.05).

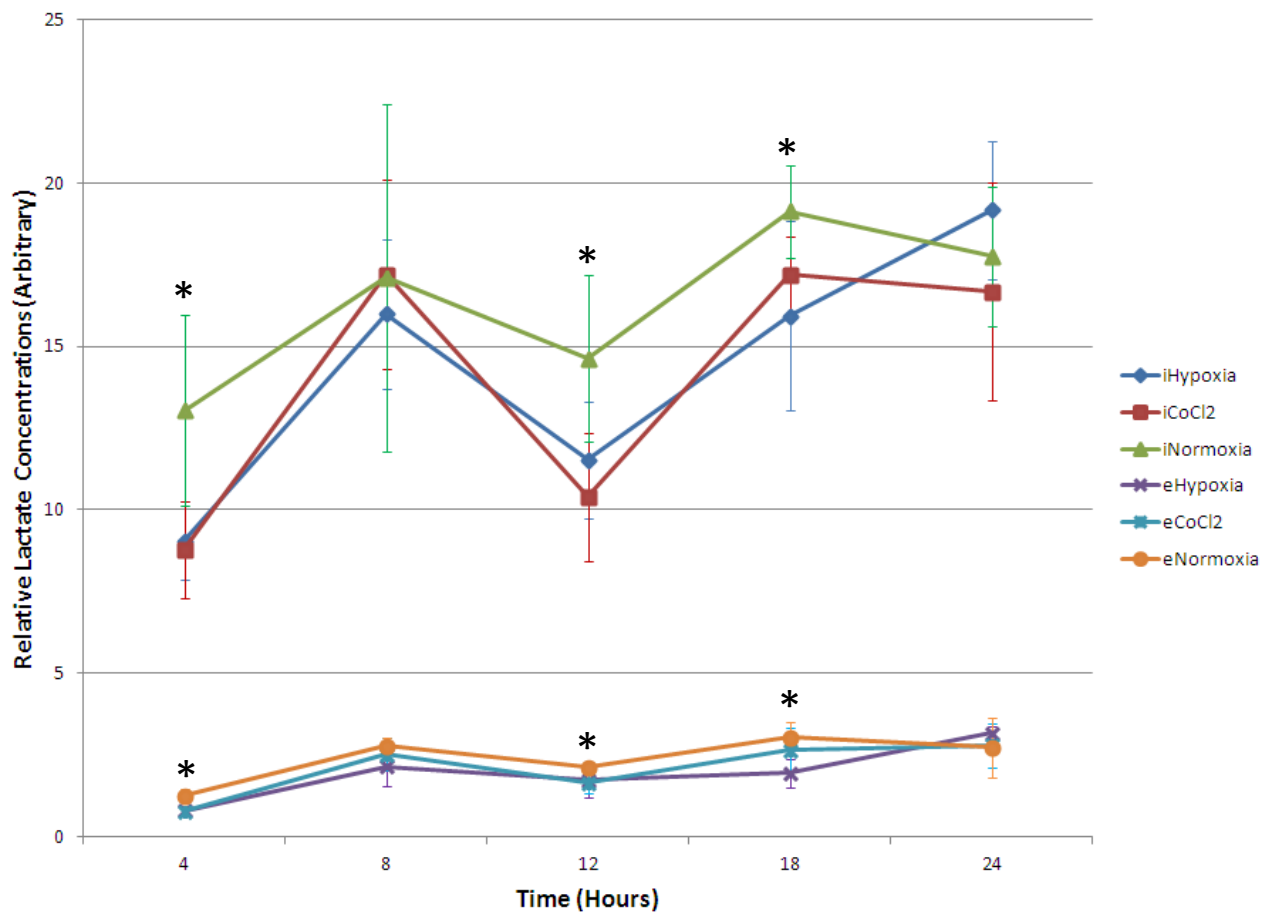
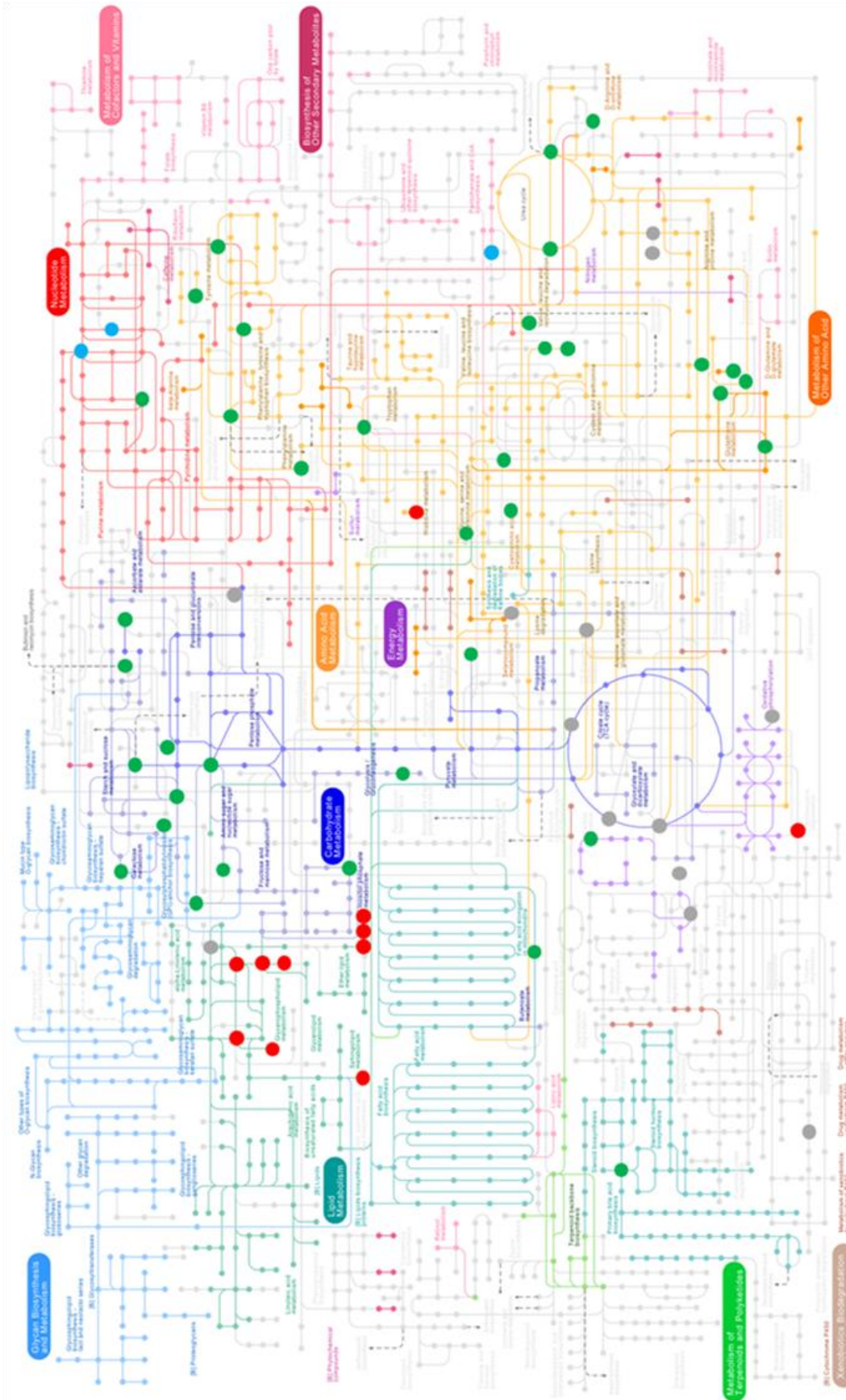


Figure 2.S2. Internal and external lactic acid concentrations for hTERT cells during normoxia, hypoxia and CoCl₂ exposure at a range of time points. In terms of external lactic acid, the purple line indicates the levels for hypoxia, the orange signifies values for normoxia and mid-blue denotes those for CoCl₂. For internal lactic acid, dark blue indicates hypoxia, dark red designates CoCl₂ and green symbolises normoxia. Data are mean \pm SE. This plot was composed through the data obtained in the GC-MS experiment from the metabolite fingerprint and footprint analyses. The asterisk (*) denotes a significant result (Kruskal-Wallis; $p < 0.05$). Lactic acid production is important under hypoxic conditions as it is one of the end products of glycolysis. It is noteworthy that cancer cells under hypoxic conditions produce more lactic acid than “normal cells” under hypoxic conditions.



- **CoCl₂ mimicking the hypoxic response**
- **CoCl₂ not mimicking the hypoxic response**
- **Off target effects of CoCl₂**
- **No hypoxic or CoCl₂ response**

Figure 2. S3. Please see the next page for the figure legend.

Figure 2.S3. KEGG map of human metabolism highlighting important metabolites in terms of the hypoxic response and CoCl₂ exposure. The green signifies where the CoCl₂ mimics the hypoxic response, the blue highlights where the CoCl₂ does not mimic the hypoxic response, red denotes off target effects of CoCl₂ and the grey represents where no hypoxic or CoCl₂ response was detected. It is apparent that the CoCl₂ has the ability to mimic the hypoxic response in carbohydrate and amino acid metabolism i.e. central metabolism. The vast majority of off target effects caused by the CoCl₂ are related to the metabolism of phospholipids as depicted by the cluster of red spots.

Chapter 3:

The phenotypic and metabolic effects of phosphodiesterase type 4D (PDE4D) knockdown in the oral squamous cell carcinoma (OSCC) cell line BicR16

The following chapter is to be submitted as a peer reviewed paper to Cancer Research before the end of 2012. Further experiments may also be included in this manuscript.

Royston Goodacre, Nalin Thakker, Ian Hampson and Lynne Hampson contributed through continuous advice and support throughout the project. William Allwood was involved in the operation of mass spectrometry and also various aspects of data analysis. Xun Xu aided with the data analysis. Thomas Walker and Gavin Batman provided support through the wet side of the project including the knockdown of the cell line and the Western blot of PDE4D, respectively.

3.1 Abstract

Phosphodiesterase type 4D (PDE4D) regulates the degradation of cyclic adenosine monophosphate (cAMP) which, in turn, regulates the expression of many genes through the transcription factor cAMP response element binding (CREB). Other transcription factors such as hypoxia inducible factor-1 (HIF-1) may interact with CREB causing further regulation. It is not clear whether PDE4D functions as a tumour suppressor gene (TSG) or an oncogene. The effect of PDE4D knockdown on cellular proliferation, migration, resistance to ionising radiation and central metabolism was investigated using the oral squamous cell carcinoma (OSCC) cell line, BicR16. MTT, clonogenic and scratch assays were used alongside gas chromatography-mass spectrometry (GC-MS). The knockdown caused an increase in proliferation, migration and radiation resistance suggesting the role of a TSG. Amino acids, cholesterol, fatty acids, carbohydrates and TCA intermediates were also altered. CREB was able to regulate gene expression dependently and independently of HIF-1.

3.2 Introduction

Oral squamous cell carcinoma (OSCC) currently accounts for ~3% of all cancers worldwide (Scully & Felix, 2006) with an abysmal 5 year survival rate of approximately 50%, which has remained constant for the past three decades (Park *et al.*, 2006). One reason for this poor prognosis is the late diagnosis of many patients (Liu *et al.*, 2009) with surgery and radiation the most effective treatment.

As with most complex diseases, OSCC onset is developed through a combination of natural (genomic) and environmental factors (Bookman *et al.*, 2011). Genomic factors involved in OSCC include: *p53* (Swaminathan *et al.*, 2012), *Cyclin Dependent Kinase 2A (CDKN2A)* – which encodes the proteins *p16^{INK4A}* and *p19^{ARF}* (Wu *et al.*, 1999) and *CyclinD1* (Baldwin *et al.*, 2005; Matta *et al.*, 2007).

PDE4D is a constituent of the phosphodiesterase (PDE) family of enzymes which is solely responsible for degrading cAMP (cyclic adenosine monophosphate) and cGMP (cyclic guanosine monophosphate) to 5'AMP

and 5'GMP, respectively (Ong *et al.*, 2009). cAMP and cGMP are nucleotides which operate as secondary messengers within the cell (Houslay & Adams, 2003) and are involved in gene expression, the cell cycle, cytoskeletal function, metabolism and proliferation (McCahill *et al.*, 2008). Due to the nature of PDE4Ds role within the cell, its regulation is tightly controlled through gene expression and post translational modifications (Houslay & Adams, 2003; Lugnier, 2006; McCahill *et al.*, 2008). There are nine isoforms of PDE4D which exist in various forms: long form (PDE4D 3, 4, 5, 7, 8 and 9); short form (PDE4D 1, 2 and 6) and in addition there are super-short and "dead-short" forms (Houslay & Adams, 2003; Houslay, Baillie & Maurice, 2007; Rahrmann *et al.*, 2009) which are all cAMP specific.

Research has shown that cancerous cells commonly exhibit depleted levels of cAMP in comparison to their non-cancerous counterparts (Marko *et al.*, 2000). This is a result of the relative activities of the enzymes involved in producing and degrading cAMP; adenylate cyclase (AC) and the PDE family, respectively (Weber, 2002). The activity of these enzymes is heavily dependent on the cell type and cellular location. Interestingly, this cell type dependency appears to also be a factor in the role of PDE4D in cancer. Marko and co-workers (2000) and Weber (2002) discovered these effects in lung cancer and hepatocellular carcinoma, respectively, suggesting the PDE enzymes to be oncogenes. However, more recently, Nancarrow *et al.* (2008) and Jarvinen *et al.* (2008) reported homozygous deletions (HDs) of PDE4D (5q12) in various head and neck squamous cell carcinomas (HNSCCs). This has also been observed in lung adenocarcinoma (Weir *et al.*, 2007) and this evidence suggests PDE4D to have tumor suppressor gene (TSG) qualities.

One downstream effect of cAMP, and hence PDE4D is the regulation of the transcription factor (TF) cAMP response element binding (CREB). Once phosphorylated via protein kinase A (PKA) (Abramovitch *et al.*, 2004), CREB is able to bind to the *cis* region CRE (CREB response element) and regulate the transcription of approximately 4000 genes (Suzuki *et al.*, 2009). This regulation is heavily dependent on the methylation state of the *cis* regions and the selective recruitment of cofactors (Zhang *et al.*, 2005). However, literature suggests that this process is intricate and may involve

other TFs such as hypoxia inducible factor-1 (HIF-1). HIF-1 is regulated through oxygen concentrations and is also profoundly associated with cancer. When activated under hypoxic conditions, HIF-1 binds to the hypoxia response element (HRE) and regulates transcription accordingly.

There are two models in the literature regarding the regulation of genes through HIF-1 and CREB, the HIF dependent regulation and the HIF independent regulation. The former was proposed by Firth and co-workers (1995) where HIF-1 cannot regulate gene expression exclusively and adjacent binding of other TFs such as CREB is necessary (Breit *et al.*, 2008). The latter model states that CREB can regulate gene expression, regardless of the involvement of the co-activator HIF-1 (O'Reilly *et al.*, 2006; Dimova *et al.*, 2007; Meyuhas *et al.*, 2008). In addition, CREB functions may be enhanced through hypoxia due to the augmented CREB phosphorylation from PKA (Dimova *et al.*, 2007) and the upregulation in transcription of CREB and the CREB binding protein (CBP) (Freeland *et al.*, 2001). Furthermore, the binding of CREB and HIF-1 to CRE and HRE are interchangeable (Dimova *et al.*, 2007; O'Reilly *et al.*, 2006) and both may simultaneously bind to a solitary HRE or CRE domain. This results in additional regulation of the gene (Abramovitch *et al.*, 2004).

Therefore, this study set out to investigate the effect of PDE4D knock down (KD) on the oral cancer cell line BicR16. Phenotypic alterations and central metabolism were the main focus since this may shed some light on the role of PDE4D in OSCC. In addition, inducing CREB (via PDE4D KD) and HIF-1 (through hypoxic exposure) was investigated to distinguish if any emergent properties may arise from these interactions.

3.3 Materials and Methods

3.3.1 Cell culture. BicR16 (oral squamous cell carcinoma) cell lines were obtained from INH (St. Mary's hospital, Manchester). Cells were cultured in DMEM (Invitrogen, Paisley, UK) supplemented with 10% FBS (Sigma Aldrich, Dorset, UK), 2% HEPES buffer (Sigma Aldrich, Dorset, UK), 1% L-glutamine (Sigma Aldrich, Dorset, UK) and 0.2% hydrocortisone. The cells were grown to a maximum of 70% confluence in a humidified incubator

at 37°C and 5% CO₂ before sub-culturing and re-seeding at $\sim 0.5 \times 10^6$ cells per T75 culture flask.

3.3.2 Control and target shRNAs. Mission shRNA (short hairpin ribose nucleic acid) DNA clones were purchased from Sigma-Aldrich (Dorset, UK) and used for transient and stable KD of PDE4D. A total of five pLKO.1 clones (TRCN0000048834 (834); TRCN0000048835 (835); TRCN0000236065 (065); TRCN0000236066 (066) and TRCN0000236067 (067)) and three controls (SHC001 (pure control vector), SHC002 (non-target control vector and SHC008 (β 2M control vector)) were purchased. The quantity of the shRNAs was increased through transformation and maxi-prep. An additional wild-type (WT) control was used which encompassed untreated cells.

3.3.3 Transformations, maxi-prep and quality assurance of shRNAs. *E. coli* XL1- competent cells were purchased from Stratagene (Agilent Technologies, Cheshire, UK) to increase the quantity of shRNAs and the protocol was conducted as per manufacturer's protocol. Subsequently, a maxi-prep (Qiagen, Crawley, UK) was undertaken to purify the plasmids and the methods were followed as described. The plasmids were run on a 1.5% agarose gel to check the plasmid size (Figure 3.S1) and to check for leakages of the maxi-prep (Figure 3.S2). The concentrations and purities were checked through Nanodrop® 1000 (Thermo Scientific, Wilmington, USA) analysis (Table 3.S1). All shRNAs were suitable for KD.

3.3.4 Puromycin kill curve for BicR16 cells. BicR16 cells were cultured as described previously. Cells were exposed to a range of puromycin concentrations (0 μ g/mL – 0.3 μ g/mL) for 192h (8d) and checked daily with regular medium changes for 480h (20d). A concentration of 0.08 μ g/mL was optimum and subsequently used (Figure 3.S3).

3.3.5 KD of PDE4D in BicR16 cells. Firstly, a transient KD was used to determine the most efficient shRNA plasmid(s) and to assess the effect of the control shRNAs on the PDE4D in BicR16 cells. Lipofectamine™ 2000 was purchased from Invitrogen (Paisley, UK) and the protocol followed as described for all KD and control shRNAs. mRNA was extracted using TRIzol® reagent (Life Technologies, Invitrogen, Paisley, UK) by following the manufacturer's protocol and analysed via qPCR as described. shRNAs 834

and 837 showed the greatest efficiency (Figure 3.S4); therefore they were used for the stable KD. No undesired effects were observed in the control samples.

For the stable KD, each shRNA was used to produce two polyclones and a set of monoclonal clones. Again, Lipofectamine™ 2000 was used and the protocol followed. TRIzol® was used to extract DNA, RNA and protein (as described) from all monoclonal clones and polyclones and assessed using qPCR, end point PCR and Western blot to gauge which clones possessed the most efficient KD.

3.3.6 Taqman design for qPCR. Taqman primers and probes were designed for isoform specific detection and quantification of PDE4D3, PDE4D4, PDE4D5, PDE4D6, PDE4D7, PDE4D8 and PDE4D9 and in addition, a Taqman assay which captures all PDE4D isoforms. Isoform specific designs for PDE4D1 and PDE4D2 were not possible as these are merely truncated forms of one or more of the other isoforms. All primers, probes and reagents were purchased from Applied Biosystems. 6-carboxyfluorescein (FAM) probes were used as the probes for the PDE4D design. The product numbers of the assays were: PDE4D3 (AJARAR – custom made); PDE4D4 (HS01588302 – pre-designed); PDE4D5 (HS01588303 – pre-designed); PDE4D6 (HS01572151 – pre-designed); PDE4D7 (AJHSNM3 – custom made); PDE4D8 (HS0093823 – pre-designed); PDE4D9 (HS01572149 – pre-designed) and all PDE4D isoforms (HS01579625 – pre-designed). The β -actin (4310886E) housekeeping Taqman assay using the VIC® probe was used for normalisation. All assays spanned an intron, ensuring that RNA only was detected.

3.3.7 Reverse-transcriptase PCR (RT-PCR). The mRNA was cleaned of any DNA contamination using DNase digest. First strand cDNA synthesis (RT-step) followed, where 20 μ L sample from the previous stage, 3 μ L of 50 μ M random decamers (RDs) and 2 μ L of dNTP mix (10mM) which was mixed and incubated at 70°C for 5min, followed by 3min on ice. The following was added to each 25 μ L sample: 7 μ L 5x RT buffer, 7 μ L dH₂O, 0.5 μ L of RNaseOUT™ (40U/ μ L) and SuperScript™ III RT (200 U/ μ L), totalling 40 μ L per cDNA sample. The sample was then incubated at 43°C for 1h and subsequently stored at -20°C until use.

3.3.8 Taqman gene expression assay for relative PDE4D quantification. The Taqman assay was performed on an Illumina®, Eco™ Real-Time PCR system (San Diego, CA, USA). Samples were loaded into 48 well plates and performed in triplicate. Each sample contained: 1µL cDNA, 1µL PDE4D Taqman, 1µL β-actin Taqman, 7µL RNase free water and 10µL of 10x Taqman reaction buffer (20µL total volume). To ensure the samples do not evaporate, an air tight cover was added to the plate.

3.3.9 Verification of shRNA insert through end point PCR. End point PCR was used to ensure that the shRNA vector had successfully incorporated into the genome and is being passed onto daughter cells. Primers were produced and procedures followed in accordance with Stamm *et al.* (2012). The primers were designed in the U6 promoter region of the pLKO.1 vector. The forward primer was 5' TGGACTATCATATGCTTACCGTAAC 3' and the reverse primer was 5' GTATGTCTGTTGCTATTATGTCTA 3' resulting in a 216 base pair product. The thermal cycle was as follows: 95°C for 3min, followed by 35 cycles of 95°C for 30s, annealing for 60°C for 30s, 72°C for 30s and finally 5min at 72°C.

3.3.10 Efficiency of the PDE4D KDs verified through Western blotting. The most efficient KDs as detected in the Taqman assays were verified to ensure the observed decrease in PDE4D mRNA was also reduced at the protein level. To do so, the KD, control, and WT cells were compared. Cells were cultured and harvested as described previously before resuspending the pellet in PBS at a concentration of 0.5×10^6 cells/10µL. An equal amount of LaemmLi buffer was added resulting in a final concentration of 0.5×10^6 cells/20µL. The samples were boiled/frozen (x3) and run on a 10% acrylamide running gel and 4% stacking gel. The gel was transferred to a PVDF (polyvinylidene fluoride) membrane before blocked and exposed to the PDE4D primary antibody (ab77080, Abcam, Cambridge, UK) at a 1:500 dilution. The membrane was then exposed to rabbit anti-mouse IgG HRP (Abcam, Cambridge, UK) at 1:2000 before using Amersham™ ECL™ Plus (GE Life Sciences, Buckinghamshire, UK) as described in the protocol for band detection. The GAPDH antibody (Abcam, Cambridge, UK) was then used as described by the manufacturer for normalisation.

3.3.11 MTT assay to assess cell proliferation. Monoclonal and polyclonal cell lines of the most efficient knockdowns (KDs) and controls alongside the parent cells were selected for analysis. A 1 in 3 series dilution of cells was used with cells ranging from 3000 cells to 1 cell per well in triplicate. The cells were grown for 12 days, with regular medium changes. The CellTiter 96® Aqueous One Solution Cell Proliferation Assay (Promega, Southampton, UK) was used as described in the protocol.

3.3.12 Clonogenic assay to assess radiation resistance. Methods were followed as described in Donne *et al.*, (2009). Cells of interest were subjected to either three Grays or five Grays of radiation (Faxitron, Lincolnshire, IL, USA) before sub-cultured into 96 well plates as described in the MTT assay. The cells were grown for 12 days with frequent medium changes and AQ96 solution was used to assess proliferation.

3.3.13 Scratch assay to assess migration. The cells of interest were analysed in triplicate. Six well plates were prepared by drawing a single straight line on the underside of the plates using a thin permanent marker. Cells were grown to 95-100% confluence in the six well plates before removing the medium and using sterile cotton buds to gently scratch half the cells away from each well, directly down the marker line. The remaining cells were washed in PBS and fresh warmed medium added before culturing the cells as normal. Each day, pictures of the cells were taken using a light microscope at x4 for 12 days.

3.3.14 Metabolic analysis of PDE4D KD using GC-MS. To ensure that the observed effects are a result of the PDE4D KD rather than another factor, a preliminary GC-MS analysis was designed. It is expected that the controls (monoclonal and polyclonal) and WT cells behave in a similar fashion, and dissimilarly to the KDs. In addition, the KD monoclonal and polyclonal cell lines should also act in an analogous manner. Therefore, the relevant samples were each grown to 75-80% confluency in five T150 flasks ($n=5$). The cells were harvested and quenched in -48°C MeOH before scraping the cells on ice. The cells were flash frozen in liquid nitrogen for 1 minute, vortexed for 30 seconds and thawed on ice (x4). Samples were then centrifuged at $3000\times g$ for 10 minutes and the supernatant retained. $100\mu\text{L}$ of internal standard 2 (IS2) solution was added to each sample (IS2 was prepared by diluting 2 mL of IS1 in

10mL of HPLC grade H₂O) before evaporation of the solvent using a speed vac and storage at -80°C until analysis. Internal standard 1 (IS1) was composed of 10mg succinic-*d*₄ acid, 10mg glycine-*d*₅ acid and 10mg malonic-*d*₂ acid in 10mL of HPLC grade H₂O. The samples were derivatisation immediately before analysis using methods described by Lenz and Wilson (2007). In brief, methoxylation was achieved utilising methoxyamine hydrochloride at 60°C for 30min and silylation through *N*-methyl-*N*-(trimethylsilyl)-trifluoroacetamide (MSTFA) at 60°C for 30min. An Agilent 6890 gas chromatograph coupled to a Leco Pegasus III TOF mass spectrometer with an Agilent 7893 autosampler was used and methods were followed as described in Begley *et al.* (2009).

Subsequently, a reduced GC-MS analysis was performed investigating the combined effects of PDE4D KD and hypoxia. A pure monoclonal sample and a KD monoclonal sample were chosen and cultured as described previously in 36x T150 flasks (18x pure and 18x KD) and grown to 75-80% confluence. Subsequently, 9x pure samples and 9x KD samples were exposed to hypoxic conditions at 1% oxygen, 5% CO₂ at 37°C for 8h (as this time exposure displays the hypoxic stress response). To ensure instant hypoxia exposure to the cells, the old medium was replaced with fresh, warmed hypoxic medium in these cell cultures. The remaining 18x samples were maintained in standard normoxic conditions; however, the medium was replaced with fresh normoxic medium. Following the 8h condition exposure cells were quenched, harvested, the metabolites extracted, derivatised and analysed via GC-MS using the methods described above.

3.3.15 Data processing and data analysis. Metabolites were assigned in concurrence with the Metabolomics Standards Initiative for Chemical Analysis (Sumner *et al.*, 2007). The methods of Begley *et al.* (2008) were followed to deconvolve the chromatograms in the LECO ChromaTOF software before using our in-house GC library and the Max Planck Institute Molecular Plant Physiology database (GMD) using a forward and reverse match score of 80%+ in addition to a retention index error of +/- 10.

The univariate and multivariate data analysis were performed in MATLAB 2010b and Microsoft Excel 2007. Principal components analysis (PCA) was utilised to assess variations in the classes in the GC-MS data. PCA is used to reduce the complexity of data whilst maintaining the variance through its interpretation using a small number of principal components (PCs). The ranksum test (non-parametric t-test: $p < 0.05$) was performed on the GC-MS data to provide significant values between the various classes.

3.4 Results

3.4.1 Stable KD of PDE4D in BicR16 cells. This resulted in a WT, two polyclones and numerous monoclones for each sample type. To ensure the plasmid had successfully incorporated into the genome end point PCR was performed (Figure 3.1).

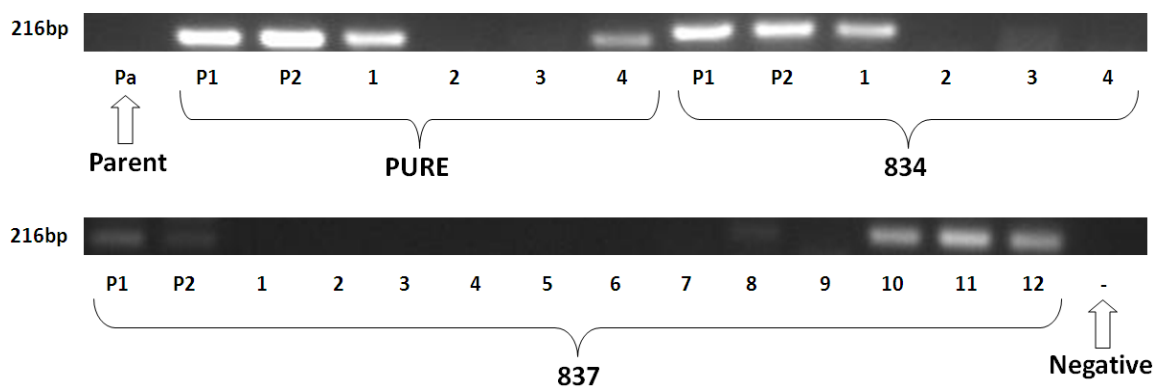


Figure.15 End Point PCR to Verify the Incorporation of the shRNA Containing pLKO.1 Vector into the BicR16 Genome. The wild type (parent) cell line and a negative control were included and are indicated in the figure. The pure samples (from left to right) comprise of polyclone 1, polyclone 2, monoclonal 1, monoclonal 2, monoclonal 3 and monoclonal 4 (all of which originate from different clones from the initial KD process. The same format can be transferred to the 834 knock down samples and the 837 knock down samples. The resulting positive product from these primers is 216 base pairs in length.

As expected, the WT and negative control did not result in a band. Pure monoclonal 1 and 4 were positive for the vector as were both polyclones. Bands can also be seen in KD 834 for both polyclones and monoclonal 1 and 3 (faint). KD 837 was positive for both polyclones and monoclonal 8 (weak), 10, 11 and 12. The graph in Figure 3.2 shows the

most efficient stable KDs of PDE4D. The expression of PDE4D in the KDs was reduced in comparison to those of the WT and pure samples. The greatest KDs were found in 834 polyclone 2 (62%), 837 polyclone 2 (63%) and 837 monoclones 11 (76%) and 12 (72%). For an unknown reason, the concentrations of PDE4D in the pure control samples are were greater than the parent cells.

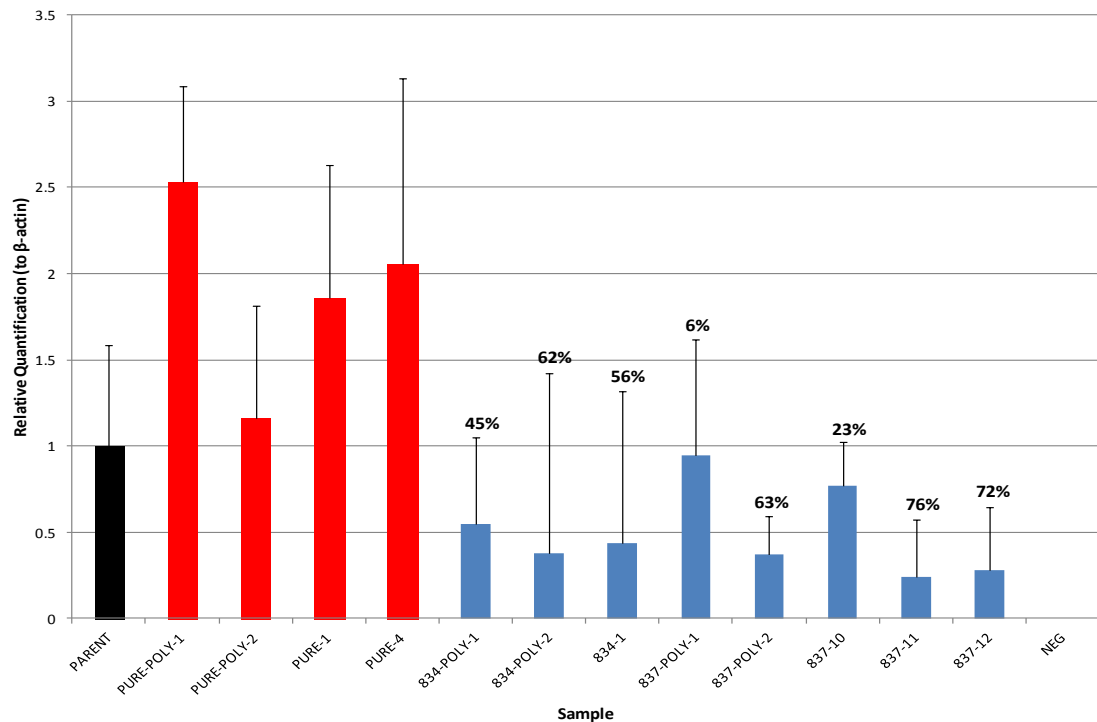


Figure 16 Relative Quantification of Gene Expression for total PDE4D in Stably Transfected BicR16 Cells. Black indicates the wild type, red signifies the control and blue the KD cell lines. Samples include (from left to right) the wild type (parent), pure polyclone 1, pure polyclone 2, pure monoclonal 1, pure monoclonal 4, 834 polyclone 1, 834 polyclone 2, 834 monoclonal 1, 837 polyclone 1, 837 polyclone 2, and 837 monoclonal 10-12 followed by the negative control for the qPCR experiment. The standard deviation is highlighted by the error bars (N=3) and the values above KD samples denote the KD efficiency in relation to the parent cells.

3.4.2 PDE4D KD increases proliferation, migration and ability to withstand radiation. The MTT assay was used to assess the effect of PDE4D KD on cell proliferation (Figure 3.3A). It is clear that the KD cells have a greater proliferation rate than the control and parent cells with an average increase of 31.3%. Pure polyclone 2 and monoclonal 1 have similar

proliferation rates to that of the WT (1.7-2), whereas pure polyclone 1 and monoclonal 4 are slightly reduced between ~1.4-1.5. All knockdown samples range from 2.3-3. The average standard deviation (SD) for all samples is 0.14.

Two clonogenic assays (three Grays or five Grays) were undertaken to assess the effects of the KD on the ability of the cells to withstand radiation therapy (Figure 3.3B and Figure 3.3C, respectively). The former resulted in the KD cells (with the exception of monoclonal 837-10) proliferating to a greater extent than the parent/control cells with an average increase of 56.8%. The resulting SD of all samples was 0.21. The latter assay resulted in a reduced proliferation rate in comparison to the former assay with an average absorbance of 1.29 and 0.39, respectively. A greater proliferation rate was still observed in the latter, with an average increase in proliferation in the KD cells of 23.0% and a general SD of 0.08. It is noteworthy, that KDs 837 polyclone 2 and 837 monoclonal 11 and 12 showed no increase in proliferation.

A scratch assay was undertaken to assess the KD effect on cell migration (Figure 3.S5). Similar behaviour was observed in the WT, pure monoclonal and pure polyclonal as was behaviour in the KD monoclonal and polyclonal. Up until the 4 day point, no migration was observed of any of the cell lines. At day 8 cells begin to migrate in the KD samples whereas the WT/controls show little sign of any migration. After 12 days the KD cells have considerably migrated to the right of the picture whereas the WT/controls show little signs of migration.

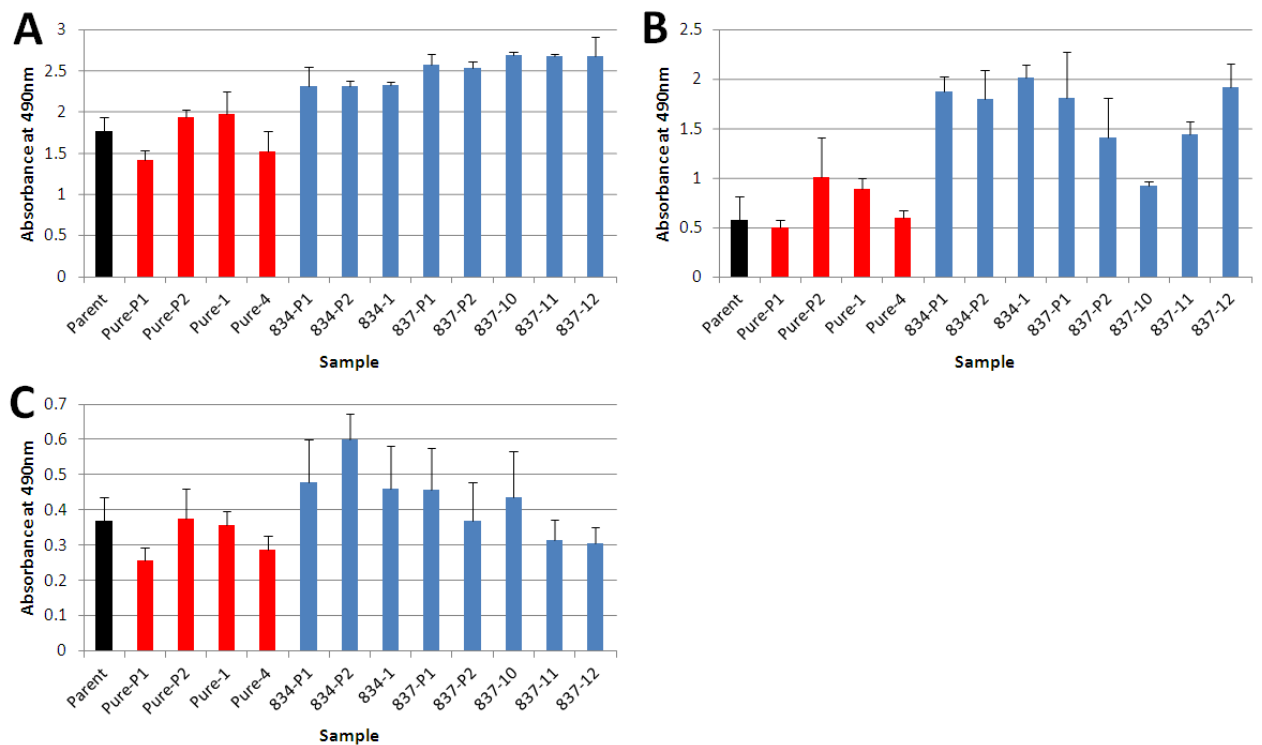


Figure 17 Phenotypic assays comparing stable PDE4D KDs with control and WT BicR16 cells. The parent cells are marked with the black bar, the red bars denote the pure samples and the blue bars signify the knock down cells. The P's immediately prior to the number in the sample names represent the polyclones and those where the P is absent are the monoclonal samples. The numbers in the sample names denote the sample number. The bars are means and the error bars display standard deviation from triplicate measurements. These results were not significant (Mann Whitney; $p < 0.05$). **(A) Proliferation of BicR16 cells (MTT Assay).** The MTT assay functions through determining the number of viable cells by measuring the activity of enzymes that reduce MTT which may then be quantified by measuring the absorbance at 490nm (y-axis). **Clonogenic assays - proliferation of BicR16 Cells Following Exposure to three Grays (B) and five Grays (C) of Radiation.** Cells were exposed to three Grays or five Grays of radiation and allowed to proliferate for 12 days before using the MTT assay to assay the number of viable cells.

3.4.3 PDE4D KD causes a metabolic reconfiguration. A preliminary GC-MS experiment was adopted in order to address a number of points as discussed later. The PCA displayed in Figure 3.4A shows clear separation between the WT/control and the KD samples across PC1, positioned on the negative and positive, respectively. The pure monoclonal and polyclone samples are clustering neatly together alongside the WT

samples. The KD monoclones and polyclones are clustering closely and are distant from the WT and pure samples.

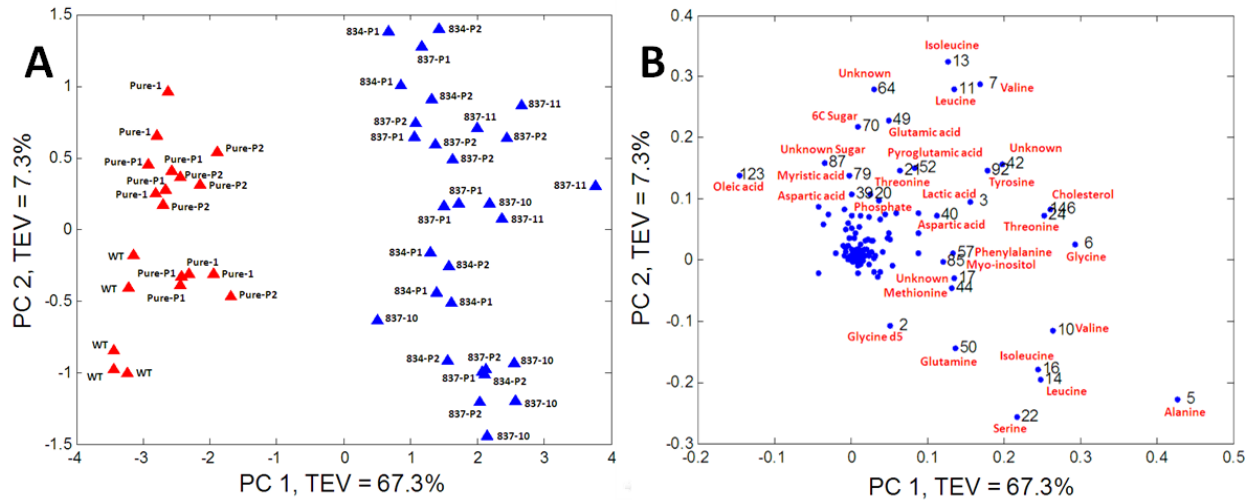


Figure 18 Preliminary GC-MS PCA scores and loadings plots. A) PCA scores plot highlighting separation of the WT/controls and the PDE4D KD Samples. The red triangles denote the wild type (WT) and pure control vectors (Pure) and the blue triangles signify the KD samples (834 and 837). The P1 and P2 highlight the polyclones one and two respectively, and those samples where 'P' is absent are monoclones. Samples were aligned using QCs across the GC-MS run and one sample from each class was repeated a total of three times to assess instrument variation. This PCA plot was produced in MATLAB and shows PC1 vs PC2 explaining 67.3% and 7.3% of the variance respectively. **B) PCA loadings plot explaining the origin of separation of the PCA scores plot.** Loadings plot showing PC1 vs. PC2 for the preliminary GC-MS experiment on the PDE4D KD. Each blue spot represents a metabolite from the GC-MS data, and those deviating furthest from the centre (0, 0) point are imposing the greatest effect on the separation seen in the PCA. The numbers are associated with the metabolite number and only these spots which are distant from the centre are annotated. As with the numbers, the red labels depict the metabolite identification and again, are only annotated when the spots are distant from the centre and having a significant effect on the separation.

Figure 3.4B exhibits a loadings plot which depicts which metabolites are causing the separation in the PCA. The WT/control samples are gravitated to the negative of PC1 as a result of oleic acid and to a lesser degree, aspartic acid, myristic acid and an unknown sugar. The KD samples are attracted to the positive of PC1 predominantly due to alanine, glycine, valine, leucine, Isoleucine, serine, threonine, tyrosine, an unknown, myo-inositol, phenylalanine and cholesterol and to a lesser extent, glutamine, methionine, another unknown metabolite and lactic acid.

3.4.4 The combined effects of CREB and HIF-1 on central metabolism. Now that the KD samples had been established, the KD and control cells were exposed to a hypoxic or normoxic environment for 8h before assessing central metabolism through GC-MS. The resulting PCA is shown in Figure 3.5A. Clear separation of the hypoxic and normoxic conditions is observed, chiefly through PC1 but also to some extent, across PC2. The former is situated on the negative of PC1 and mainly on the positive of PC2 whereas the latter is located on the positive of PC1 and predominantly on the negative of PC2. There is also a degree of separation between the KD and control cells under their respective conditions. This separation is clearer under normoxia as there is some extent of overlapping of the KD and pure samples during hypoxia.

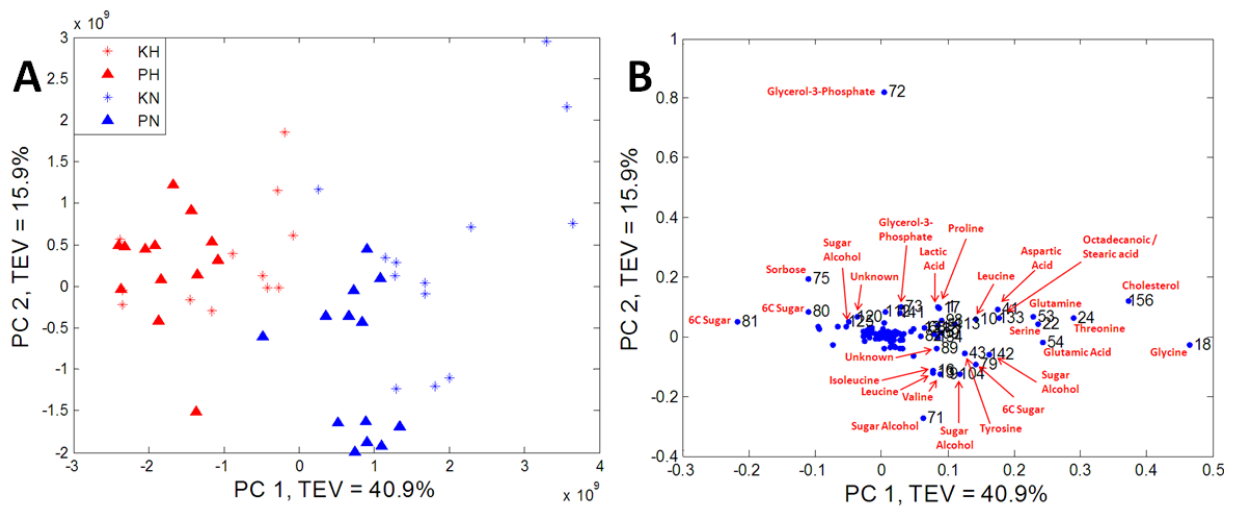


Figure 19 Full GC-MS PCA scores and loadings plots. A) PCA scores plot showing separation of the PDE4D KD and control cells under hypoxia or normoxia. The key in the top left corner depicts the sample types where the KD and pure (control) samples are represented by "K" and "P" respectively and the hypoxic and normoxic environments are coded by the "H" and "N" respectively. Hence, the red stars signify the KD/hypoxic samples, the red triangles the pure/hypoxia, the blue stars represent the KD/normoxia and the blue triangles the pure/normoxia samples. The plot was produced in MATLAB and shows PC1 vs. PC2 explaining 40.9% and 15.9% of the variance respectively. **B) PCA loadings plot explaining the origin of separation of the PCA scores plot.** Loadings plot showing PC1 vs. PC2 for the full GC-MS experiment on the PDE4D KD and hypoxic/normoxia environments. Please refer to Figure 3.4B for further details.

The loadings plot (Figure 3.5B) highlights the origin of variance seen in the PCA. Separation across PC1 can be attributed to 6-carbon sugars (x3), sorbose, proline, polyols (x3), aspartic acid (x2), leucine, isoleucine, glycine, threonine, glutamic acid, serine, glutamine, tyrosine, cholesterol, octadecanoic acid/stearic acid and an unknown metabolite. Metabolites causing variation across PC2 are glycerol-3-phosphate, sorbose, cholesterol, isoleucine, leucine, valine, a polyol, aspartic acid, tyrosine and a 6-carbon sugar.

From the significant metabolites highlighted in the loadings plot, the univariate analyses (data not shown) revealed that 39% (9/23) are affected solely from hypoxia where the KD has no effect. This had the greatest effect on the data set. 30% (7/23) was affected by both hypoxia and the KD and

13% (3/23) was affected by the KD only. Miscellaneous accounted for 17% (4/23).

Those metabolites which are influenced by the combination of KD and hypoxia (36/156) include polyols (glycerol, threitol, inositol derivatives (x2)), amino acids (glutamic acid derivatives (x3), proline), sugars (tagatose/fructose/sorbose, xylose), glycolysis intermediates (pyruvic acid), vitamin B6, urea and several unknown metabolites. Generally, hypoxia causes an upregulation of these metabolites and of which, the KD causes a further reduction (67%) or increase (33%). Alternatively, hypoxia may cause a decrease in the metabolite with the KD further attributing the same effects as above.

The metabolites affected only by hypoxia (39/156) included amino acids (methionine, phenylalanine, serine, isoleucine, leucine, tyramine, tyrosine, valine), polyols (mannitol/sorbitol/dulcitol, rabinol), fatty acids (octadecanoic acid/stearic acid, oleic acid/elaidic acid), ketone bodies (4-methyl-2-oxovaleric acid), carbohydrates (mannose/glucose/galactose, mannose/glucose, sorbose, theonic acid, fructose), TCA/glycolysis intermediates (fructose, succinic acid), organic acids (acetic acid, creatine) and unknown metabolites. The KD was found to have no significant effect on these metabolites. Hypoxia exposure resulted in an increase in metabolite concentration in 75% and a decrease in the remaining 25%.

The KD controlled the metabolite concentrations of 12/156 metabolites irrespective of hypoxia. These included glycerol-3-phosphate, cholesterol, TCA associates (citric acid, malic acid, 3-ureidopropionic acid), amino acids (glycine, aspartic acid), butanoic acid and unknowns. These were found in elevated concentrations in the KD compared to the controls.

3.5 Discussion

There is current debate regarding the role of PDE4D in cancer. There is compelling evidence for its role as a TSG and an oncogene. Here we provide insight into the role of PDE4D in OSCC.

The phenotypic assays exhibited enhanced proliferation and migration when PDE4D expression was decreased. This is in concurrence

with the role of PDE4D as a TSG in HNSCCs (Jarvinen *et al.*, 2008; Nancarrow *et al.*, 2008; Gu *et al.*, 2010; Wu *et al.*, 2011). Conversely, there is an abundance of literature labelling PDE4D as an oncogene including in: prostate cancer (Rahrmann *et al.*, 2009), lung cancer (Pullamsetti *et al.*, 2012) and even the HNSCC adenoid cystic carcinoma (Patel *et al.*, 2006). These inconsistencies lead one to believe that the PDE4D gene is able to operate as a TSG or an oncogene depending on context such as cell type and environment. Such paradoxical genes have been presented previously such as RUNX (Runt-related transcription factor) (Blyth *et al.*, 2005).

PDE4D KD also resulted in increased radiation resistance. To our knowledge this is the first evidence relating this gene to radiation sensitivity in OSCC cells. Conversely, non-specific PDE4 inhibition has previously been reported to increase radiation sensitivity in brain tumors (Goldhoff *et al.*, 2008) and haematological malignancies (Lerner *et al.*, 2006). However, PDE4D is known to be an oncogene in these cells which may explain the varying response.

The preliminary GC-MS experiment successfully addressed a number of key issues which were necessary before undertaking the later GC-MS experiment. Firstly, the WT cells behaved in a similar manner to the control cells implying that no undesired effects were brought about from the transfection procedure. Secondly, the monoclonal and polyclonal for the control and KD samples behaved analogously. This signifies that the random shRNA integration is unlikely to have had adverse effects on the cells. These precautions were adhered to throughout including during the phenotypic assays and the KD procedure.

The initial GC-MS data demonstrated clear separation of the WT/controls and the KDs, chiefly as a result of increased amino acid and cholesterol concentrations in the latter and fatty acid production in the former. Since the KD raised the proliferation and migration of the cells, the increase in amino acids may be the result of uptake/synthesis of biomass by the cell to produce daughter cells (Vander Heiden *et al.*, 2009; Shlomi *et al.*, 2011). In addition, cholesterol was also increased in the KD cells. This is fundamental in cell growth and division as it is necessary for plasma membrane synthesis and also, the cholesterol biosynthesis pathway

provides the cell with essential compounds for this process (Fernández *et al.*, 2005). Oleic acid was also found to be increased in concentration in the KD cells and has previously been linked with proliferation and migration in rat vascular smooth muscle cells (Zhang *et al.*, 2007) and breast cancer cells (Soto-Guzman *et al.*, 2010). Subsequently, the second GC-MS experiment introduced the influence of hypoxia on the KD. It is evident that hypoxia is having a greater effect on central metabolism than the KD, not only in terms of the number of metabolites effected, but also due to the extent of alteration.

The lack of distinction between the pure and KD samples under hypoxia is attributed by the differences between the relative metabolite concentrations. Conversely, the differences between the pure and KD samples under normoxia are greater which explains the more defined separation under this condition. For instance, tyrosine, glutamic acid and pyruvic acid all exhibit larger variations between the pure and KD samples under normoxia compared to hypoxia. Furthermore, some metabolites are displaying significant changes in all conditions except between the KD and pure samples under hypoxia. For example, sorbose is influencing the PCA plot and is affected by hypoxia and the KD under normoxia only (i.e., the KD does not have an effect under hypoxia). Moreover, the KD and the hypoxic environment effect a number of metabolites in the same manner (i.e., both increase the concentration of the metabolite) whereas, in other cases they appear to have opposite functions (i.e., one increases and one decreases the concentration). The latter cases may have impacted the PCA by contributing to the merging of these two classes.

Metabolites which were affected by a combination of KD and hypoxia constitute the second largest group. This metabolic reconfiguration is predominantly due to the regulation of the TFs HIF-1 and CREB, which may be working independently (Dimova *et al.*, 2007) or dependently (Firth *et al.*, 1995). The metabolites behave in an intricate fashion with hypoxia and the KD having varying effects on each entity. Depending on the hypoxic/normoxic state, the KD may cause a significant upregulation for one condition and the opposite for the other condition, implying that some interaction is occurring between the two TFs. For example, this behaviour

was found for the inositol derivatives where under normoxic conditions, the KD caused a downregulation of the metabolite, whereas, under hypoxic conditions, the KD caused an upregulation of the metabolite. Hence, the regulation by these two interacting TFs is not trivial and other factors may be influencing the regulation of genes such as the availability of the cofactors (Breit, 2008) and potentially the involvement of other TFs.

However, the majority of these metabolites were found in greatest concentration in one of the hypoxic conditions. This inherently consists of the HIF-1 TF. Hereon, the CREB TF may cause an upregulation or downregulation of genes in a gene dependent manner, either the former, which results in the greatest (further) concentration of metabolite in the hypoxic, KD condition, or predominantly the latter resulting in the pure, hypoxic condition with the greatest concentration. Alternatively, when hypoxia causes a downregulation of the metabolite, the KD can still impose supplementary affects by up-regulating or down-regulating genes further. As discussed previously, the hypoxic state has some input into the role of CREB.

The hypoxia only associated changes in metabolites were the largest group further suggesting that hypoxia was regulating metabolism more than the KD. As the KD was found to have no significant effect on these metabolites, only HIF-1 resulted in any alterations. Many of these were related to amino acids, fatty acids, sugars and TCA/glycolysis intermediates, the vast majority of which were found in elevated concentrations during hypoxia. These elements are essential for daughter cell production (Tennant *et al.*, 2009) and it has previously been demonstrated that hypoxia causes an upregulation of proliferation through enhancing c-Myc (Gordan *et al.*, 2007). These data were also in line with our previous work investigating hypoxia on hTERT cells (Wilcock *et al.*, 2012).

Although considerably smaller, a third group consisting of metabolites which were significantly altered by the KD only were observed. The preliminary GC-MS data are consistent with this. For example, cholesterol, glycine and aspartic acid (alongside others) increased in metabolite concentration for the KD in both experiments. This is a partially a consequence of CREB, which is able to regulate transcription independent

of HIF-1, as a similar increase was observed in the hypoxic and normoxic environments. Hence, CREB can function independently to HIF-1, although this does not disprove any theories (Firth et al., 1995) of CREB requiring other TFs not investigated here.

3.6 Concluding Remarks

The role of PDE4D in cancer is paradoxical in terms of its TSG or oncogene status. Here we provide evidence of its role as a TSG in OSCC; a reduction in expression caused elevated proliferation and migration. Furthermore, this diminished expression of PDE4D resulted in elevated resistance to substantial levels of radiation which may be a significant finding relating to the treatment of OSCC. In addition, PDE4D appears to be involved with central metabolism, particularly that of amino acids, cholesterol and fatty acids which may be coupled with the effect on cellular proliferation and migration. Finally, the combination of PDE4D KD and hypoxia caused a substantial central metabolic reconfiguration, where CREB was able to regulate transcription, independently of HIF-1.

3.7 Acknowledgements

We would like to thank Dr Susan Greenwood for the use of her hypoxic chamber. JWA and YX were funded by Cancer Research UK and the Wolfson Foundation within the Clinical Research Infrastructure Scheme. YX funding was also contributed to by CPI. PW, RG and CLW wish to thank BBSRC for financial support of The Manchester Centre for Integrative Systems Biology (BBC0082191). GB was supported by the Margaret Pritchard Memorial Fund which was awarded by the Humane Research Trust. TW was funded by the RL Gardner request fund by the pennine acute hospital charity. Work in the Gynaecological Research Laboratories was also supported by donations from the Caring Cancer Trust, The Cancer Prevention Research Trust and United-in-Cancer

3.8 References

- Abramovitch, R. Tavor, E. Jacob-Hirsch, J. Zeira, E. Amariglio, N. Pappo, O. Rechavi, G. Galun, E. and Honigman, A. (2004). A Pivotal Role of Cyclic AMP-Responsive Element Binding Protein in Tumor Progression. *Cancer Research*, **64**:1338-1346.
- Baldwin, C. Garnis, C. Zhang, L. Rosin, M. P. and Lam, W. L. (2005). Multiple Microalterations Detected at High Frequency in Oral Cancer. *Cancer Research*, **65**:7561-7567.
- Begley, P. Francis-McIntyre, S. Dunn, W. B. Broadhurst, D. I. Halsall, A. Tseng, A. Knowles, J. HUSERMET Consortium, Goodacre, R. and Kell, D. B. (2009). Development and performance of a gas chromatography-time-of-flight mass spectrometry analysis for large-scale nontargeted metabolomic studies of human serum. *Analytical Chemistry*, **81**:7038-7046.
- Blyth, K. Cameron, E. R. and Neil, J. C. (2005). The RUNX genes: Gain of Loss of Function in Cancer. *Nature Reviews*, **5**:376-387.
- Bookman, E. B. McAllister, K. Gillanders, E. Wanke, K. Balshaw, D. Rutter, J. Reedy, J. Shaughnessy, D. Agurs-Collins, T. Paltoo, D. Atienza, A. Bierut, L. Kraft, P. Fallin, M. D. Perera, F. Turkheimer, E. Boardman, J. Marazita, M. L. Rappaport, S. M. Boerwinkle, E. Suomi, S. J. Caporaso, N. E. Hertz-Picciotto, I. Jacobson, K. C. Lowe, W. L. Goldman, L. R. Duggal, P. Gunnar, M. R. Manolio, T. A. Green, E. D. Olster, D. H. and Birnbaum, L. S. for the NIH G × E (2011). Gene-Environment Interplay in Common Complex Diseases: Forging an Integrative Model – Recommendations From an NIH Workshop. *Genetic Epidemiology*, **35**:217-225.
- Breit, J. F. Ault-Ziel, K. Al-Mehdi, AB. and Gillespie, M. N. (2008). Nuclear protein-induced bending and flexing of the hypoxic response element of the rat vascular endothelial growth factor promoter. *The FASEB Journal*, **22**:19-29.

Donne, A, J. Hampson, L. He, X, T. Day, P, J, R. Salway, F. Rothera, M, P. Homer, J, J. Hampson, I, N. (2009). Potential risk factors associated with the use of cidofovir to treat benign human papillomavirus-related disease. *Antiviral Therapy*, **14**:939-952.

Dimova, E, Y. Jakubowska, M, M. and Kietzmann, T. (2007). CREB binding to the hypoxia-inducible factor-1 responsive elements in the plasminogen activator inhibitor-1 promoter mediates the glucagon effect. *Journal of Thrombosis and Haemostasis*, **98**:296-303.

Fernández, C. Martín, M. Gómez-Coronado, D. and Lasunción, M, A. (2005). Effects of distal cholesterol biosynthesis inhibitors on cell proliferation and cell cycle progression. *Journal of Lipid Research*, **46**:920-929.

Firth, J, D. Ebert, B, L. and Ratcliffe, P, J. (1995). Hypoxic Regulation of Lactate Dehydrogenase A. Interactions between hypoxia-inducible factor 1 and cAMP response elements. *The Journal of Biological Chemistry*, **270**:21021-21027.

Freeland, K. Boxerb, L, M. Latchman, D, S. (2001). The cyclic AMP response element in the Bcl-2 promoter confers inducibility by hypoxia in neuronal cells. *Molecular Brain Research*, **92**:98-106.

Goldhoff, P. Warrington, N, M. Limbrick Jr. D, D. Hope, A. Woerner, B, M. Jackson, E. Perry, A. Piwnica-Worms, D. and Rubin, J, B. (2008). Targeted inhibition of cyclic AMP phosphodiesterase-4 promotes brain tumor regression. *Clinical Cancer Research*, **14**:7717-7725.

Gordan, J, D. Bertout, J, A. Hu, C, J. Diehl, J, A. and Simon, M, C. (2009). HIF-2 α promotes hypoxic cell proliferation by enhancing c-Myc transcriptional activity. *Cancer Cell*, **11**:335-347.

Gu, J. Ajani, J, A. Hawk, E, T. Ye, Y. Lee, J, H. Bhutani, M, S. Hofstetter, W, L. Swisher, S, G. Wang, K, K. and Wu, X. (2010). Genome-Wide Catalogue of Chromosomal Aberrations in Barrett's Esophagus and Esophageal Adenocarcinoma: A High-Density Single Nucleotide Polymorphism Array Analysis. *Cancer Prevention Research*, **3**:1176-1186.

Houslay, M, D. and Adams, D, R. (2003). PDE4 cAMP phosphodiesterases : modular enzymes that orchestrate signalling cross-talk, desensitization and compartmentalization. *Biochemical Journal*, **370**:1-18.

Houslay, M, D. Baillie, G, S. and Maurice, D, H. (2007). cAMP specific phosphodiesterase-4 enzymes in the cardiovascular system: a molecular toolbox for generating compartmentalised cAMP signalling. *Circulation Research*, **100**:950-966.

Jarvinen, AK. Autio, R. Kilpinen, S. Saarela, M. Leivo, I. Grenman, R. Makitie, A, A. and Monni, O. (2008). High-Resolution Copy Number and Gene Expression Microarray Analyses of Head and Neck Squamous Cell Carcinoma Cell Lines of Tongue and Larynx. *Genes, Chromosomes & Cancer*, **47**:500-509.

Lenz, E, M. and Wilson, I, D. (2007). Analytical strategies in metabolomics. *Journal of Proteome Research*. **6**:443-458.

Lerner, A. and Epstein, P, M. (2006). Cyclic nucleotide phosphodiesterase as targets for treatment of haematological malignancies. *Biochemical Journal*, **393**:21-41.

Liu, HS. Lu, HH. Lui, MT. Yu, EH. Shen, W. Chen, YP. Chang, KW. And Tu, HF. (2009). Detection of copy number amplification of cyclin D1 (CCND1) and cortactin (CTTN) in oral carcinoma and oral brushed samples from areca chewers. *Oral oncology*, **12**:1032-1036.

Lugnier, C. (2006). Cyclic nucleotide phosphodiesterase (PDE) superfamily: A new target for the development of specific therapeutic agents. *Pharmacology & Therapeutics*, **109**:366-398.

- Marko, D. Pahlke, G. Merz, KH, and Eisenbrand, G. (2000). Cyclic 3', 5'-Nucleotide Phosphodiesterases: Potential Targets for Anticancer Therapy. *Chemical Research in Toxicology*, **13**:944-948.
- Matta, A. Bahadur, S. Duggal, R. Gupta, S, D. and Ralhan, R. (2007). Over-expression of 14-3-3zeta is an early event in oral cancer. *BMC Cancer*, **7**, 169.
- McCahill, A, C. Huston, E. Li, X. and Houslay, M, D. (2008). PDE4 Associates with Different Scaffolding Proteins: Modulating Interactions as Treatment for Certain Diseases' *IN* Klussmann, E. Scott, J. (eds.) *Protein-Protein Interactions as New Drug Targets*, **186**:125-166.
- Meyuhas, R. Pikarsky, E. Tavor, E. Klar, A. Abramovitch, R. Hochman, J. Lago, T, G. and Honigman, A. (2008). A Key Role for Cyclic AMP-Responsive Element Binding Protein in Hypoxia-Mediated Activation of the Angiogenesis Factor CCN1(CYR61) in Tumor Cell. *Molecular Cancer Research*, **6**:1397-1409.
- Nancarrow, D, J. Handoko, H, Y. Smithers, M. Gotley, D, C. Drew, P, A. Watson, D, I. Clouston, A, D. Hayward, N, K. and Whiteman, D, C. (2008). Genome-Wide Copy Number Analysis in Esophageal Adenocarcinoma Using High-Density Single-Nucleotide. *Cancer Research*, **68**:4163-4172.
- Ong, W, K. Gribble, F, M. Reimann, F. Lynch, M, J. Houslay, M, D. Baillie, G, S. Furman, B, L. and Pyne, N, J. (2009). The role of the PDE4D cAMP phosphodiesterase in the regulation of glucagon-like peptide-1 release. *British Journal of Pharmacology*, **157**:633-644.
- O'Reilly, S, M. Leonard, M, O. Kieran, N. Comerford, K, M. Cummins, E. Pouliot, M. Lee, S, B and Taylor, C, T. (2006). Hypoxia induces epithelial amphiregulin gene expression in a CREB-dependent manner. *American Journal of Cell Physiology*, **290**:592-600.

Park, S. Ku, Y. K. Seo, M. J. Kim, D. Y. Yeon, J. E. Lee, K. M. Jeong, S.C. Yoon, W. K. Harn, C. H. and Kim, H. M. (2006). Principal component analysis and discriminant analysis (PCA–DA) for discriminating profiles of terminal restriction fragment length polymorphism (T-RFLP) in soil bacterial communities. *Soil Biology and Biochemistry*, **38**:2344-2349.

Patel, K. J. Pambuccian, S. E. Ondrey, F. G. Adams, G. L. and Gaffney, P. M. (2006). Genes associated with early development, apoptosis and cell cycle regulation define a gene expression profile of adenoid cystic carcinoma. *Oral Oncology*, **42**:994-1004.

Pullamsetti, S.S. Banat, G.A. Schmall, A. Szibor, M. Pomagruk, D.Hänze, J. Kolosionek, E. Wilhelm, J. Braun, T. Grimminger, F. Seeger, W. Schermuly, R.T. and Savai, R. (2012). Phosphodiesterase-4 promotes proliferation and angiogenesis of lung cancer by crosstalk with HIF. *Oncogene*, **1-14**:10.1038/onc.2012.136.

Rahrmann, E. P. Collier, L. S. Knutson, T. P. Doyal, M. E. Kuslak, S. L. Green, L. E. Malinowski, R. L. Roethe, L. Akagi, K. Waknitz, M. Huang, W. Largaespada, D. A. and Marker, P. C. (2009). Identification of PDE4D as a Proliferation Promoting Factor in Prostate Cancer Using a Sleeping Beauty Transposon-Based Somatic Mutagenesis Screen. *Cancer Research*, **69**:4388-4397.

Scully, C. and Felix, D. H. (2006). Oral Medicine — Update for the dental practitioner Oral Cancer. *British Dental Journal*, **200**:13-17.

Shlomi, T. Benyamini, T. Gottlieb, E. Sharan, R. Ruppin, E. (2011). Genome-Scale Metabolic Modeling Elucidates the Role of Proliferative Adaptation in Causing the Warburg Effect. *PLoS Computational Biology*, **7**:e1002018. doi:10.1371/journal.pcbi.1002018.

Soto-Guzman, A. Navarro-Tito, N. Castro-Sanchez, L. Martinez-Orozco, R. and Salazar, E. P. (2010). Oleic acid promotes MMP-9 secretion and invasion of breast cancer cells. *Clinical Experimental Metastasis*, **27**:505-515.

Stamm, S. Smith, C. and Lührmann, R. (2012). *Alternative Pre-mRNA Splicing: Theory and Protocols*. John Wiley & Sons.

Sumner, L, W. Amberg, A. Barrett, D. Beger, R. Beale, M, H. Daykin, C, A. Fan, T, WM. Fiehn, O. Goodacre, R. Griffin, J, L. Hardy, N. Higashi, R. Kopka, J. Lindon, J, C. Lane, A, N. Marriott, P. Nicholls, A, W. Reilly, M, D. and Viant M. (2007). Proposed minimum reporting standards for chemical analysis: Chemical Analysis Working Group (CAWG) Metabolomics Standards Initiative (MSI). *Metabolomics*, **3**:211-221.

Suzuki, M. Shinohara, F. Endo, M. Sugazaki, M. Echigo, S. and Rikiishi, H. (2009). Zebularine suppresses the apoptotic potential of 5-Xuorouracil via cAMP/PKA/CREB pathway against human oral squamous cell carcinoma cells. *Cancer Chemotherapy Pharmacology*, **64**:223-232.

Swaminathan, U. Joshua, E. Rao, U, K. and Ranganathan, K. (2012). Expression of p53 and CyclinD1 in oral squamous cell carcinoma and normal mucosa: An immunohistochemical study. *Journal of Oral and Maxillofacial Pathology*, **16**:172-177.

Tennant, D, A. Durán, R, V. Boulahbel, H and Gottlieb, E. (2009). Metabolic transformation in cancer. *Carcinogenesis*, **30**:1269-1280.

Vander Heiden, M, G. Cantley, L, C. Thompson, C, B. (2009). Understanding the Warburg Effect: The Metabolic Requirements of Cell Proliferation. *Science*, **324**:1029-1033.

Weber, G. (2002). Reciprocal regulation: recognition of pattern of gene expression in cancer cells. *Advanced Enzyme Regulation*, **42**:83-100.

Weir, B, A. Woo, M, S. Getz G, Perner, S. Ding, L. Beroukhir, R. Lin, W, M. Province, M, A. Kraja, A. Johnson, L, A. Shah, K. Sato, M. Thomas, R, K. Barletta, J, A. Borecki, I, B. Broderick, S, B. Chang, A, C. Chiang, D, Y. Chirieac, L, R. Cho, J. Fujii, Y. Gazdar, A, F. Giordano, T. Greulich, H. Hanna, M. Johnson, B, E. Kris, M, G. Lash, A. Lin, L. Lindeman, N. Mardis, E, R. McPherson, J, D. Minna, J, D. Morgan, M, B. Nadel, M. Orringer, M, B. Osborne, J, R. Ozenberger, B. Ramos, A, H. Robinson, J. Roth, J, A. Rusch, V. Sasaki, H. Shepherd, F. Sougnez, C. Spitz, M, R. Tsao, MS. Twomey, D. Verhaak, R, G, W. Weinstock, G, M. Wheeler, D, A. Winckler, W. Yoshizawa, A. Yu, S. Zakowski, M, F. Zhang, Q. Beer, D, G. Wistuba, I, I. Watson, M, A. Garraway, L, A. Ladanyi, M. Travis, W, D. Pao, W. Rubin, M, A. Gabriel, S, B. Gibbs, R, A. Varmus, H, A. Wilson, R, K. Lander, E, S. and Meyerson, M. (2007). Characterizing the cancer genome in lung adenocarcinoma. *Nature*, **450**:893-898.

Wilcock, P. Allwood, J, W. Correa, E. Vaughan, A, A. Batman, G. Wedge, D, C. Hampson, L. Hampson, I, N. Thakker, N. Goodacre, R. (2012). A metabolomics investigation into the suitability of cobalt chloride as a substitute for hypoxia in eukaryotic cells. *PLoS One*. Submission pending.

Wu, C. Hu, Z. He, Z. Jia, W. Wang, F. Zhou, Y. Liu, Z. Zhan, O. Liu, Y. Yu, D. Zhai, K. Chang, J. Qiao, Y. Jin, G. Liu, Z. Shen, Y. Guo, C. Fu, J. Miao, X. Tan, W. Shen, H. Ke, Y. Zeng, Y. Wu, T. and Lin, D. (2011). Genome-wide association study identifies three new susceptibility loci for esophageal squamous-cell carcinoma in Chinese populations. *Nature Genetics*, **43**:679-684.

Wu, CL. Loz, L. McKown, S. Sloan, P. Read, AP. Holland, S. Scully, C. Paterson, I. Tavassoli, M. and Thakker, N. (1999). DNA studies underestimate the major role of CDKN2A inactivation in oral and oropharyngeal squamous cell carcinomas. *Genes Chromosomes Cancer*, **52**:16-25.

Zhang, X. Odom, D, T. Koo, SH. Conkright, M, D. Canettieri, G. Best, J. Chen, H. Jenner, R. Herbolzheimer, E. Kadam, S. Ecker, J, R. Emerson, B. Hogenesch, J, B. Unterman, T. Young, R, A. and Montminy, M. (2005). Genome-wide analysis of cAMP-response element binding protein occupancy, phosphorylation, and target gene activation in human tissues', *Proceedings of the National Academy of Science of the USA*, 102:4459-4464.

Zhang, Y. Liu, C. Zhu, L. Jiang, X. Chen, X. Qi, X. Liang, X. Jin, S. Zhang, P. Li, Q. Wang, D. Liu, X. Zeng, K. Zhang, J. Xiang, Y. and Zhang, CY (2007). PGC-1 α inhibits oleic acid induced proliferation and migration of rat vascular smooth muscle cells. *PLoS One*, 2:e1137. Doi:10.1371/journal.pone.0001137.

3.9 Supplementary Information

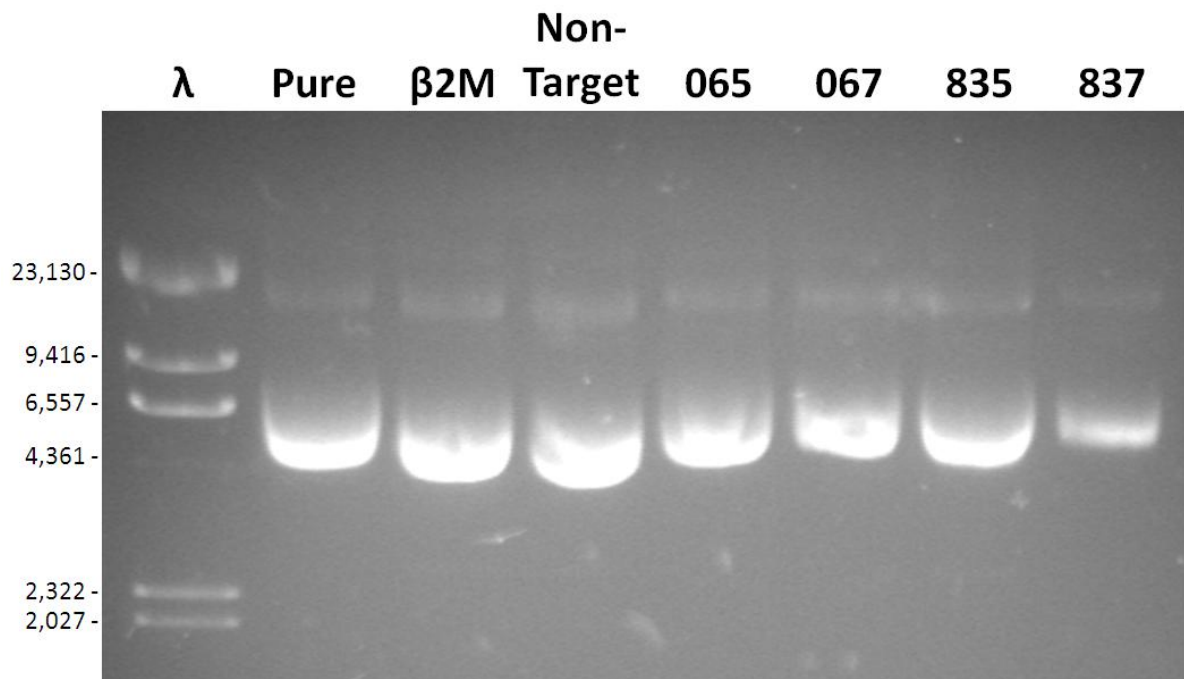


Figure 3.S1. Gel Displaying Eluted Plasmids Following Transformation in XL1-Blue Cells. The wells contain (from left to right); (1) lambda ladder, (2) pure control vector, (3) B2M shRNA vector, (4) non-target control, (5) shRNA 065, (6) shRNA 067, (7) shRNA 835 and (8) shRNA 837. The lambda ladder base pair number is indicated on the left of the gel.

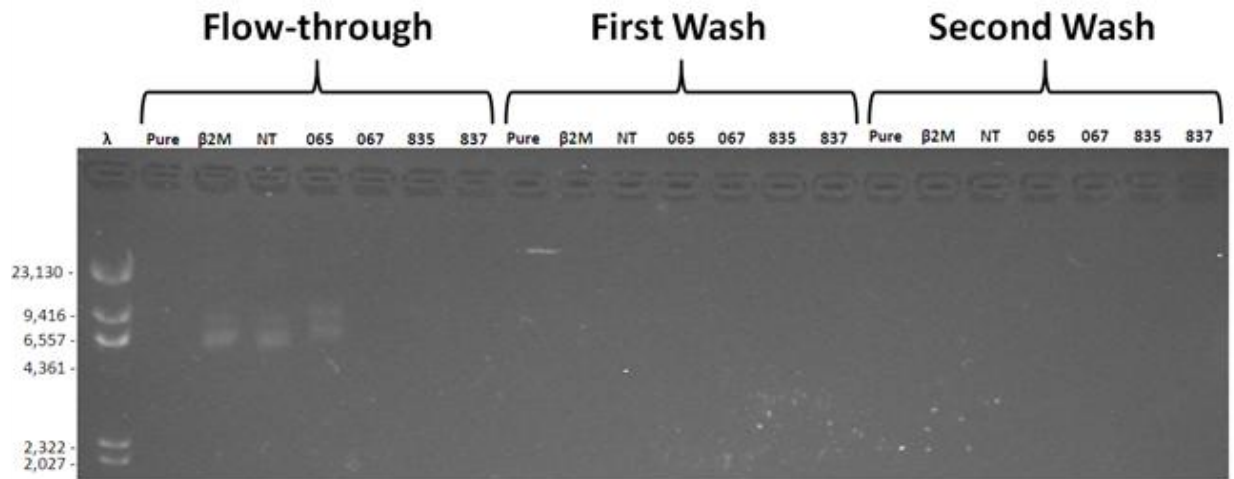


Figure 3.S2. Fraction analysis at various stages during the maxi prep. There are three stages of analysis (which are labelled above) and each sample; pure, B2M, non-target, 065, 067, 835 and 837 were assessed for each. On the left of the gel is a lambda ladder and immediately indicated to the left of this is the base pair number.

Sample	Sample Concentration (ng/μL)	DNA/RNA Purity (A260/A280)	Nucleic Acid Purity (A260/A230)
Pure	800	1.8	1.95
NT	950.9	1.78	1.94
B2M	821.4	1.64	1.82
065	761.6	1.76	1.95
067	671.9	1.88	2.06
834	872.8	1.81	2.02
837	217.1	1.93	2.07

Table 3.S1. Sample concentrations and contaminations of the eluted shRNAs from the maxi prep derived from the Nanodrop®. DNA concentrations and contamination levels were determined using the Nanodrop® for pure, non-target, B2M, shRNA 065, shRNA 067, shRNA 834 and shRNA 837 as a single measurement. For each sample stated on the left, there is a sample concentration (ng/ μ L), a DNA/RNA purity value (A260/A280) and a nucleic acid purity value (A260/A230). As stated in the Nanodrop® 1000 manual, an acceptable value for A260/A280 is ~1.8 for DNA and significantly lower values may signify potential contamination of protein, phenol or other contaminants. The A260/A230 values are generally within the region of 1.8-2.2 and significantly lower values may indicate the presence of co-eluted contaminants.

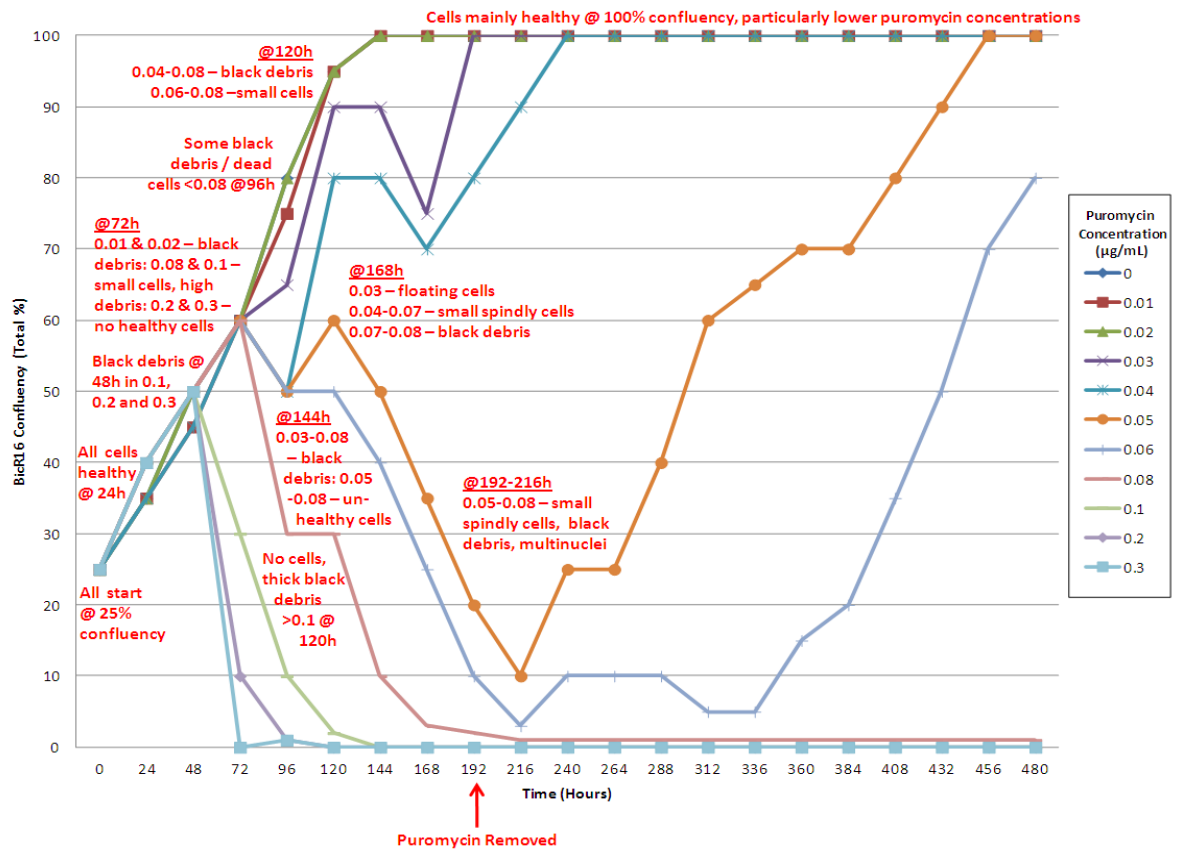


Figure 3.S3. Kill curve of BicR16 cells subjected to a range of puromycin. BicR16 cells were subjected to a range of puromycin concentrations to establish the most efficient concentration. Cells were exposed to 0µg/mL, 0.01µg/mL, 0.02µg/mL, 0.03µg/mL, 0.04µg/mL, 0.05µg/mL, 0.06µg/mL, 0.08µg/mL, 0.1µg/mL, 0.2µg/mL and 0.3µg/mL of puromycin for 480h (20 days) and assessed daily. The key on the right depicts the puromycin concentrations and associated line/marker patterns whilst the red text outlines the situation. The healthy BicR16 cells (dark blue line) were consistently healthy and at 100% confluency from 144h. The 0.01µg/mL (dark red) and 0.02µg/mL (dark green) concentrations initially grew healthily until 72-96h when debris/black matter was observed. However, from here on in, the cells recovered and grew to 100% confluency from 144h. At the 0.03µg/mL (purple) and 0.04µg/mL (mid-blue) concentrations, black matter /debris was visible between 96-144h which was more evident in the more concentrated sample. At 168h the 0.03µg/mL sample contains some floating cells, but recovers from here and eventually reaches confluency whereas the 0.04µg/mL includes some small spindly cells and recovers except during the 264-284 period where non-adherent cells were observed. However, from 312h, the cells appear healthy. The concentrations 0.05µg/mL (orange), 0.06µg/mL (aqua) and 0.08µg/mL (pink) appear healthy until 72-96h when debris, dead cells and small cells become apparent, especially in the greater concentrations. At 0.05µg/mL and 0.06µg/mL, the cells deteriorate with further debris, dead cells and small cells and the addition of multi-nuclei and spindly cells, until they eventually fully recover and begin to proliferate normally from 336h and 384h, respectively. Only unhealthy cells were observed at the 0.08µg/mL from 72h with similar phenotypes to that described for the immediately lower concentrations only more exaggerated. The number of cells dramatically decreases until 312h, where later, only one adherent cell can be observed in each field of view. The cells exposed to greater extreme concentrations of 0.1µg/mL (light green), 0.2µg/mL (light purple) and 0.3µg/mL (light blue) appear healthy for 24h, before debris is clear at 48h and from here on, cells become increasingly unhealthy and more scarce until no cells were visible and only thick black debris was seen.

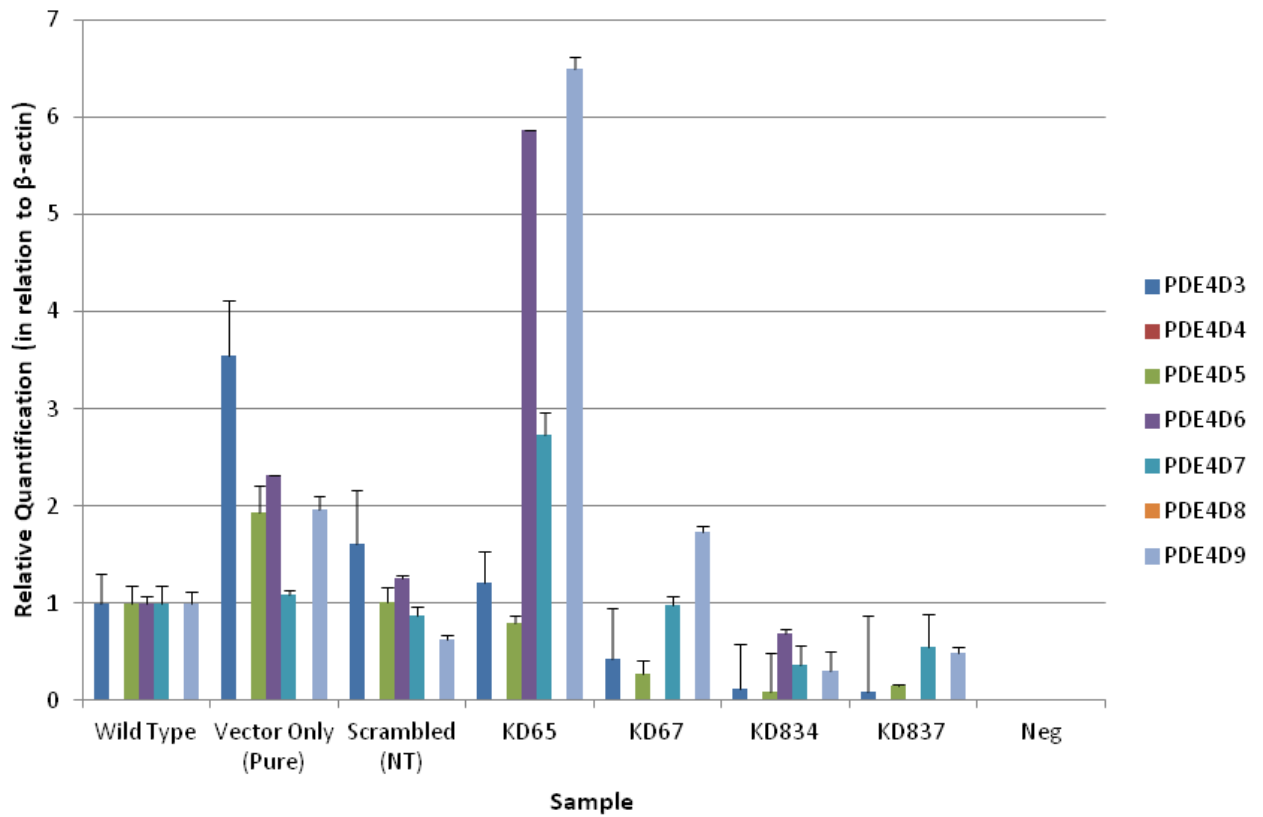


Figure 3.S4. Relative Gene Expression Levels of PDE4D3-PDE4D9 in BicR16 Cells Subsequent to Transient KD. Cells were transfected and the relative expression of seven PDE4Ds were assessed using qPCR and using β -actin as the reference gene. The wild type indicates the non-transfected cells, the vector only signifies the pure vector containing no shRNA within the plasmid, the scrambled denotes the non-target shRNA (NT) and the following four samples designate the KD samples of 065, 067, 834 and 837. The PDE4D isoforms are colour coded and referenced in the key on the right of the chart. The error bars show the SD of values from triplicate.

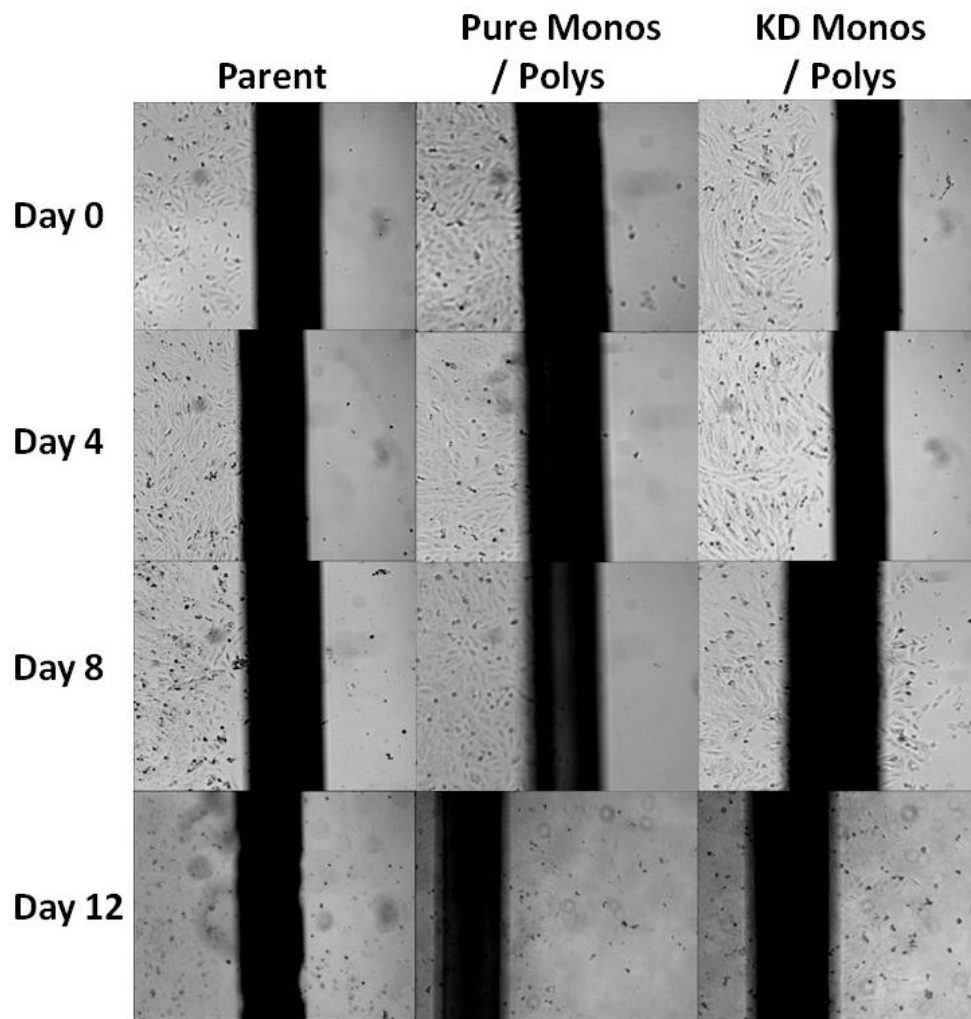


Figure 3.S5. Scratch Assay of Parent, Pure Controls and KD Cells over 12 Days. The same cell lines used in the previous phenotypic assays were assessed using a scratch assay by growing to 95-100% confluency, removing half of the cells at a specified line and allowed to migrate for 12 days and taking pictures on a daily basis. The figure is a summary showing pictures of the cells every four days for the WT, pure polys/monoclones and KD polys/monos.

Chapter 4:

Kinetic model of cellular metabolism and the affects of Hypoxia Inducible Factor 1 (HIF-1)

Subsequent to a substantial amount of work, the following chapter is to be submitted as a peer reviewed paper before the end of 2012.

Royston Goodacre, Nalin Thakker and Pedro Mendes contributed through continuous advice and support throughout the project.

4.1 Abstract

Central metabolism is profoundly associated with cancer initiation and progression. This is in part due to the hypoxic environment in which cancer cells are subjected to as a direct result of the transcription factor hypoxia inducible factor-1 (HIF-1). To aid in the understanding of central metabolism, a model consisting of glycolysis/TCA/glutaminolysis under normoxic and hypoxic conditions was produced; partially through the amalgamation of two established models from the literature, the addition of new reactions and parameters and new metabolite concentrations originating from GC-MS data. COPASI was utilised to do this. The model was validated using experimental data from the literature and steady state and flux analyses. Subsequently, sensitivity analysis and a reduction in external glucose and glutamine were mimicked and the alterations in hypoxic and normoxic metabolism analysed. Variations in the states' behaviour were observed when glucose and glutamine inputs were altered. Furthermore, vCSII, vGS, vPGK and vGII were identified as potential therapeutic targets which may affect metabolism in hypoxia only. However, certain validation methods proved unsuccessful and hence the model requires further work before attempting the analyses again.

4.2 Introduction

It is now widely accepted that cellular metabolism is heavily involved in the initiation and progression of many cancers. One contributing feature is the transcription factor Hypoxia Inducible Factor - 1 (HIF-1) which is known to regulate a host of genes involved with central metabolism in an attempt to alleviate pressure brought about through a hypoxic environment (Bartrons & Caro, 2007). Many cancers, particularly the centre of large tumorous growths, experience a significant lack of oxygen due to the inability of the vascular system in delivering an adequate supply of nutrients. In effect, this increase in HIF-1 causes a metabolic switch from oxidative phosphorylation, the regular mode of synthesising energy, to glycolysis. This metabolic shift is also known as the Warburg effect (Warburg, 1930; 1956; 1965; Warburg *et al.*, 1924 and Warburg *et al.*, 1927) and a paradoxical situation arises, in

terms of energy production. Oxidative phosphorylation is a much more efficient means of producing energy compared to glycolysis, producing ~30 and two ATP molecules per glucose molecule, respectively. Therefore, since cancer cells rapidly grow and proliferate in comparison to their healthy counterpart, they need to consume greater quantities of energy.

The HIF-1 transcription factor is comprised of two subunits; a beta subunit which is constitutively expressed and an alpha subunit which is heavily regulated through local oxygen concentrations (Minchenko *et al.*, 2002). Under normoxic conditions HIF-1 α is hydroxylated by an enzyme called prolyl hydroxylase (PHD) (Ke and Costa, 2006) which results in poly-ubiquitination of the molecule by the pVHL (von Hippel-Lindau gene product) and subsequent degradation by the 26S proteasome. Conversely, under hypoxic conditions, the PHD is inhibited due to the lack of oxygen and so the cascade of events is prevented and HIF-1 α concentrations elevate.

Due to the complexity of the hypoxic system within eukaryotic cells, the construction of a mathematical model would be valuable in an attempt to further understand metabolic behaviour under the varying states of normoxia and hypoxia. Such models potentially have the ability to elucidate therapeutic targets in cancer treatment, highlight potential biomarkers and provide more general information such as quantifying the rate limitation and sensitivity of the model. Hornberg and co-workers (2006) provide a useful review on kinetic models of cancer whilst highlighting the important aspects of utilising systems biology for investigating such a complex disease. Nevertheless, the production of mathematical models is a challenging prospect due to the immense quantity and interaction of genes, RNA, proteins and molecules, particularly in higher organisms such as *Homo sapiens*. Utilising simpler organisms such as *Saccharomyces cerevisiae* (brewing yeast) is a common occurrence to reduce model complexity; however, the behaviour of such models does not always directly correlate with those from higher organisms. Cancer is by definition a multi-cellular disorder which creates further complexity, thus to model the system accurately, interaction between cells must be accounted for in conjunction with natural cellular processes such as apoptosis. Hence, a delicate balance is needed between complexity and realism.

The production of complex mathematical models is made possible through the development of high-throughput experimental instrumentation such as microarray and gas chromatography-mass spectrometry (GC-MS)/liquid chromatography-mass spectrometry (GC-MS) procedures which may also be subsequently used to verify the models' predictions.

Consequently, a mathematical model was produced using COPASI (COmplex PAthway SImulator) to elucidate variations between hypoxic and normoxic behaviour in eukaryotic cells. The model was constructed through the amalgamation of two published models; a glycogenolysis model (Lambeth & Kushmerick, 2002) and a TCA and energy regulation model (Nazaret *et al.*, 2009), with the addition of glutaminolysis reactions. It is noteworthy that this task is not trivial and considerations are necessary, such as which reactions/metabolites should be removed/added, which linking reactions should be used to connect to two models and assumptions which are necessary for the amalgamated model. The aims of the model are to elucidate variations between the hypoxic and normoxic states through varying the carbon sources glucose and glutamine and assessing the sensitivity of the model to determine potential therapeutic targets.

4.3 Materials & Methods

4.3.1 Constructing the model. The model was constructed in COPASI 4.8.35 (download for free at www.COPASI.org) through the combination of two published models, namely, a model of glycogenolysis by Lambeth & Kushmerick (2002) and a TCA and energy regulation model from Nazaret and co-workers (2009). A number of reactions and metabolites were eradicated including glycogen and glucose-1-phosphate and their associated reactions as they were redundant in this model. A number of metabolites and reactions were added, most notably the reactions for glutaminolysis as an input into the TCA cycle, which is known to be utilised in cancer cell metabolism (Scott *et al.*, 2011). Figure 4.1 exhibits a schematic of the model that was generated beginning with the glucose input into glycolysis on the left through to lactate or alternatively, from pyruvate, which may enter the TCA cycle in the mitochondria through to citrate or oxaloacetic acid (OAA).

As discussed previously, there is also an input into the TCA cycle from glutaminolysis on the right of the model using alpha-ketoglutaric acid (α -KG) as an entry point. The TCA cycle has been simplified, comprising of just three components (citrate, OAA and α -KG). The energetic production/degradation and transport to/from the cytoplasm into the mitochondria of the cell are scattered amongst the schematic.

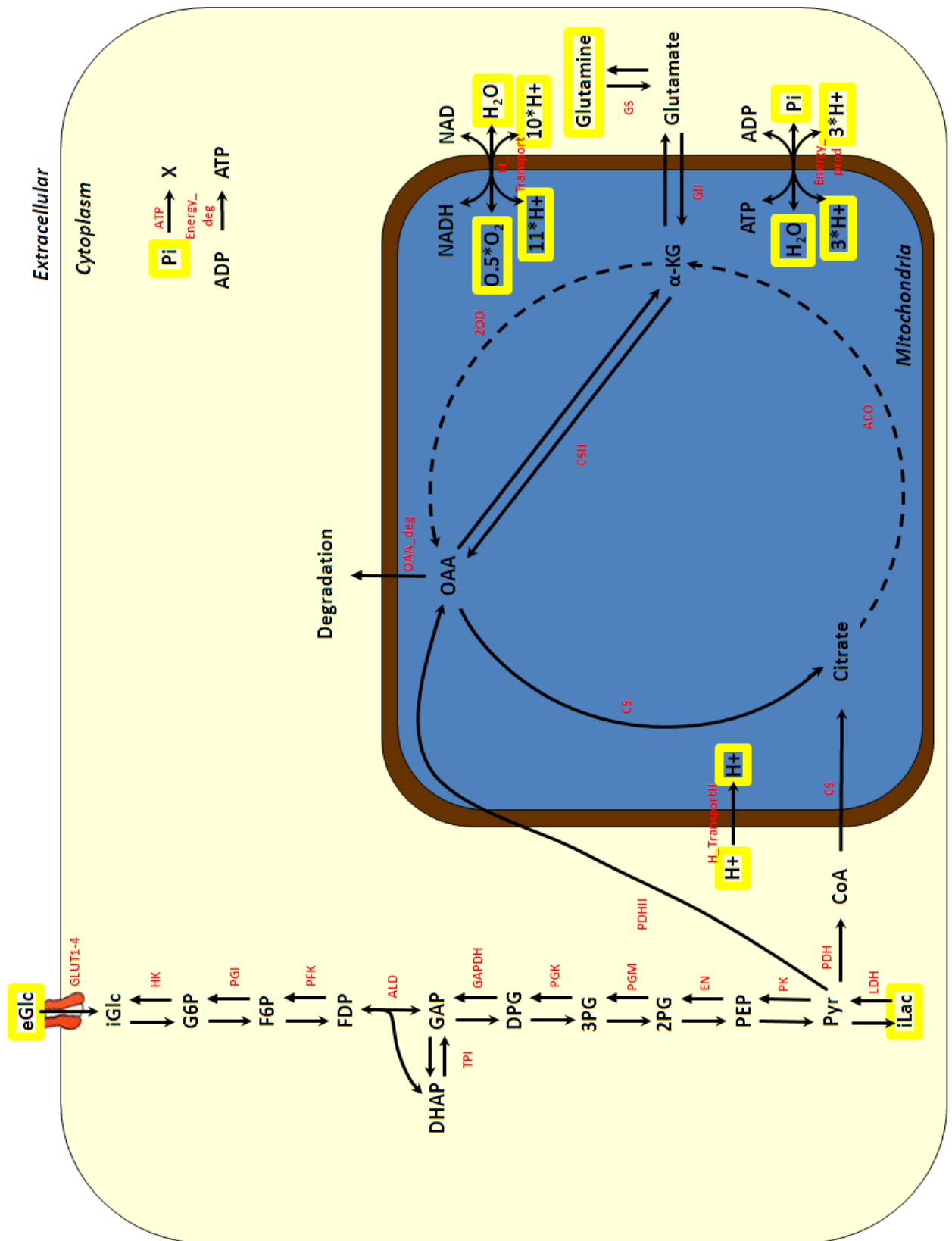


Figure 20 Schematic of the mathematical model comprising of glycolysis, the TCA cycle, glutaminolysis and cell energetics. The black labels indicate the metabolites of the system, the arrows denote the reaction and their associated direction, the red labels highlight the enzymes involved in the specific reactions and the yellow boxes specify the metabolites which are of a fixed concentration as they are end points of reactions. Tables of metabolites and initial concentrations (Table 4.1), reactions (Table 4.2) and parameters (Table 4.3) are shown below.

Table 4.1 Metabolites and initial concentrations

Metabolite	Compartment	Type	Initial Concentration (mmol/l)	Origin
Alpha-ketoglutarate (a-KG)	Mitochondria	Reactions	0.225	Nazaret <i>et al.</i> (2009)
Acetyl-CoA	Mitochondria	Reactions	0.063	Nazaret <i>et al.</i> (2009)
Adenosine diphosphate (ADP)	Mitochondria	Assignment	0.624	Nazaret <i>et al.</i> (2009)
Adenosine monophosphate (AMP)	Cytoplasm	Reactions	2.00×10^{-5}	Lambeth & Kushmerick (2002)
Adenosine triphosphate (ATP)	Mitochondria	Reactions	3.536	Nazaret <i>et al.</i> (2009)
Citrate	Mitochondria	Reactions	0.44	Nazaret <i>et al.</i> (2009)
Creatine (Cr)	Cytoplasm	Reactions	5.333	Lambeth & Kushmerick (2002)
Dihydroxyacetone phosphate (DHAP)	Cytoplasm	Reactions	0.0764	Lambeth & Kushmerick (2002)
Diphosphoglycerate (DPG)	Cytoplasm	Reactions	0.065	Lambeth & Kushmerick (2002)
External Glucose (eGlc)	Extracellular	Fixed	1	Lambeth & Kushmerick (2002)
Fructose-6-phosphate (F6P)	Cytoplasm	Reactions	0.228	Lambeth & Kushmerick (2002)

Fructose diphosphate (FDP)	Cytoplasm	Reactions	0.0723	Lambeth & Kushmerick (2002)
Glucose-6-Phosphate (G6P)	Cytoplasm	Reactions	0.75	Lambeth & Kushmerick (2002)
Glyceraldehyde Phosphate (GAP)	Cytoplasm	Reactions	0.0355	Lambeth & Kushmerick (2002)
Glutamate	Cytoplasm	Reactions	0.1	Lambeth & Kushmerick (2002)
Glutamine	Cytoplasm	Fixed	0.025001	Parameter Estimation
H ⁺	Cytoplasm	Fixed	1	Nazaret <i>et al.</i> (2009)
H ⁺	Mitochondria	Fixed	1	Nazaret <i>et al.</i> , (2009)
H ₂ O	Mitochondria	Fixed	1	Nazaret <i>et al.</i> , (2009)
Internal Glucose (iGlc)	Cytoplasm	Reactions	1	Lambeth & Kushmerick (2002)
Internal Lactate (iLac)	Cytoplasm	Reactions	1.3	Lambeth & Kushmerick (2002)
NAD(+)	Mitochondria	Reactions	0.856	Nazaret <i>et al.</i> (2009)
NADH	Mitochondria	Assignment	0.214	Nazaret et al., 2009
O ₂	Mitochondria	Fixed	0.39	Nazaret <i>et al.</i> , 2009

Oxalacetic acid (OAA)	Mitochondria	Reactions	0.005	Nazaret <i>et al.</i> , 2009
2-phospho-glycerate (P2G)	Cytoplasm	Reactions	0.005	Lambeth & Kushmerick, 2002
3-phospho-glycerate (P3G)	Cytoplasm	Reactions	0.052	Lambeth & Kushmerick, 2002
Phosphocreatine (PCr)	Cytoplasm	Reactions	34.67	Lambeth & Kushmerick, 2002
Phosphoenolpyruvic acid (PEP)	Cytoplasm	Reactions	0.01	Lambeth & Kushmerick, 2002
Phosphate (Pi)	Mitochondria	Fixed	2.44	Nazaret <i>et al.</i> , 2009
Pyruvate	Mitochondria	Reactions	0.154	Nazaret <i>et al.</i> , 2009

Table 4.2 Model Reactions

Name	Reaction	Rate Law
vPDH	Pyruvate + NAD(+) -> acetyl-CoA + NADH	Mass action (irreversible)
vCS	OAA + acetyl-CoA -> Citrate	Mass action (irreversible)
vACO	Citrate + NAD(+) -> a-KG + NADH	Mass action (irreversible)
v2OD	a-KG + ADP + 2 * NAD(+) -> OAA + ATP + 2 * NADH	function_4_v5
vCSII	OAA = a-KG	function_4_v6
vPDHII	Pyruvate + ATP -> OAA + ADP	Mass action (irreversible)
vOAA_deg	OAA ->	Mass action (irreversible)
vresp	NADH + 0.5 * O2 + 11 * H+{Mitochondria} -> NAD(+) + H2O + 10 * H+{Cytoplasm}	function_4_vresp
vATP	ADP + Pi + 3 * H+{Cytoplasm} = ATP + H2O + 3 * H+{Mitochondria}	function_4_vATP
vleak	H+{Cytoplasm} -> H+{Mitochondria}	function_4_vleak

vPGI	$G6P = F6P$	Rate Law for vPGI
vPFK	$ATP + F6P = ADP + FDP; AMP$	Rate Law for vPFK
vALD	$FDP = DHAP + GAP$	Rate Law for vALD
vTPI	$GAP = DHAP$	Rate Law for vTPI
vGAPDH	$Pi + GAP + NAD(+) = NADH + DPG$	Rate Law for vGAPDH
vPGK	$ADP + DPG = ATP + P3G$	Rate Law for vPGK
vPGM	$P3G = P2G$	Rate Law for vPGM
vEN	$P2G = PEP$	Rate Law for vEN
vPK	$ADP + PEP = ATP + Pyruvate$	Rate Law for vPK
vLDH	$NADH + Pyruvate = iLac + NAD(+)$	Rate Law for vLDH
vCK	$ATP + Cr = ADP + PCr$	Rate Law for vCK
vADK	$ATP + AMP = 2 * ADP$	Rate Law for vADK
vATPase	$ATP = ADP + Pi$	Rate Law for vATPase

vFOUT iLac = eLac

Rate Law for vFOUT

vHK Pi + iGlc = G6P

Rate Law for vHK

vGLUT eGlc = iGlc

Rate Law for vGLUT

vGII Glutamate = a-KG

Rate Law for vGII

vGS Glutamate = Glutamine

Rate Law for vGS

Table 4.3 Parameter Values of the Model

Initial values of global quantities:

ATPcrit	3.89302
At	4.16
C	6.75E-06
DeltaGtransport	1.74E+07
DeltaPsi	150
DeltaPsim	150
Faraday constant	96485
JANT	0.190484
JATP	0.0941811
Jleak	0.0639
Jresp	0.120822
K	2
Kapp	4.40E-09
Nt	1.07
gas constant	8314
absolute temperature	298
a	0.1
b	0.004
kANT	0.05387
kATP	131.9
kleak	0.000426
kresp	2.5

Reaction parameters:

vPDH	
k1	0.152 l/(mmol*s)

vCS	
k1	57.142 l/(mmol*s)

vACO	
k1	0.053 l/(mmol*s)

v2OD	
At	-> At (mmol/l)
	0.082361
k5	l ² /(mmol ² *s)

vCSII	
Keq	0.3975 1
k6	0.0032 1/s

vPDHII	
	0.04
k1	l/(mmol*s)

vOAA_deg	
k1	3.6 1/s

vresp	
Jresp	-> Jresp (?)

vATP	
JATP	-> JATP (?)

vleak	
Jleak	-> Jleak (?)

vPGI	
Vbpgi_3	0.88 ?
Kpgig6p_3	0.48 mmol/l
Kpgif6p_3	0.119 mmol/l

vPFK	
Vfpfk_4	0.056 ?
Kpfkatp_4	0.08 mmol/l
Kpfkf6p_4	0.18 mmol/l
Lo_4	13 ?
en_4	0.01 1
Kpfkamp_4	0.06 mmol/l
Kpfkiatp_4	0.08 mmol/l
KpfkatpT_4	0.25 mmol/l
Kpfkf6pT_4	20 mmol/l
KpfkfdpT_4	4.2 mmol/l
KpfkadpT_4	2.71 mmol/l
dn_4	0.01 1
Kpfkfdp_4	4.2 mmol/l
Kpfkadp_4	2.71 mmol/l

vALD	
Vfald_5	0.104 ?
Kaldfdp_5	0.5 mmol/l
Kaldgap_5	1 mmol/l
Kalddhap_5	2 mmol/l

vTPI	
Vftpi_6	12 ?
Ktpigap_6	0.32 mmol/l
Ktpidhap_6	0.61 mmol/l

vGAPDH	
Vfgad_7	1.65 ?
	0.0025
Kgapdhgap_7	mmol/l
Kgapdhnad_7	0.09 mmol/l
Kgapdhip_7	0.29 mmol/l
	0.0008
Kgapdh13dpg_7	mmol/l
	0.0033
Kgapdhnad_7	mmol/l

vPGK	
Vbpgk_8	1.12 ?
Kpgk3pg_8	1.2 mmol/l
Kpgkatp_8	0.35 mmol/l
Kpgkadp_8	0.083 mmol/l
	0.0019
Kpgk13dpg_8	mmol/l

vPGM	
Vfpgm_9	1.12 ?
Kpgm3pg_9	0.2 mmol/l
Kpgm2pg_9	0.014 mmol/l

vEN	
Vfen_10	0.192 ?
Ken2pg_10	0.1 mmol/l
Kenpep_10	0.37 mmol/l

vPK	
Vfpk_11	1.44 ?
Kpkpep_11	0.08 mmol/l
Kpkadp_11	0.3 mmol/l
Kpkpyr_11	7.05 mmol/l
Kpkatp_11	1.13 mmol/l

vLDH	
Vfldh_12	1.92 ?
Kldhpyr_12	0.335 mmol/l
	0.002167
Kldhndh_12	mmol/l
Kldhlac_12	17.17 mmol/l
Kldhnd_12	0.849 mmol/l

vCK	
VrevCK_13	0.5 ?
Kckiatp_13	3.5 mmol/l
Kckcr_13	3.8 mmol/l
KeqCK_13	233 ?
Kckiadp_13	0.135 mmol/l
KckPCr_13	1.11 mmol/l
KckIPCr_13	3.9 mmol/l

vADK	
Vfadk_14	0.88 ?
Kadkatp_14	0.27 mmol/l
Kadkamp_14	0.32 mmol/l
Kadkadp_14	0.00035 ?

vATPase	
k_15	0.075 ?

vFOUT	
kout_16	0.2 ?

vHK	
VmGLK	226.452 ?
SUMAXP	4.1 ?
KeqAK	0.45 ?
KeqGLK	3800 ?
KmGLKATP	0.15 ?
KmGLKGLCi	0.08 mmol/l
KmGLKG6P	30 mmol/l
KmGLKADP	0.23 ?

vGLUT	
VmGLT	97.264 ?
KeqGLT	11
	1.1918
KmGLTGLCo	mmol/l
	1.1918
KmGLTGLCi	mmol/l

vGII	
VmGII	0.1 ?
KmGIIIGlutamate	0.1 mmol/l
KeqGII	0.1 1
KmGIIaKG	50 mmol/l

vGS	
VmVS	0.1 ?
KmVSIGlutamine	0.9 mmol/l
KeqVS	0.1 1
KmVSIGlutamate	1.4 mmol/l

4.3.2 Rate laws of the model. The vast majority of the rate laws incorporated into the model were acquired from Nazaret *et al.* (2009) or Lambeth & Kushmerick (2002). vGLUT and vHK originate from Teusink (2000) (please refer to papers for details). Additional rate laws for vGS and vGII were composed and are shown in the supplementary information. Parameters for these were found in the literature or estimated as described below.

4.3.3 Model assumptions. When constructing a model, it is vital to assess the assumptions which have been made. Since no model is perfect, all models possess assumptions; in the case of this model they have been segregated into two categories; inherited assumptions from the Nazaret or Lambeth models and additional assumptions.

There are three considerations in terms of the inherited assumptions. Firstly, the model has been simplified and hence there are numerous reversible reactions which are represented as irreversible reactions. In addition, there are also mass action kinetics which implies simple rate laws, however, steady state is still obtainable (Nazaret *et al.*, 2009). Secondly, there are many activators and inhibitors absent from the model, again in an attempt to retain the models simplicity (Lambeth and Kushmerick, 2002). Finally, cationic bound species are generalised to have the same affinities for the enzyme and therefore is assumed to have constant pH, Mg^{2+} concentration etc (Lambeth and Kushmerick, 2002).

Furthermore, there are two additional assumptions which are specific to this fused model. Although all parameters originated from human samples, they are not derived from the same tissue types and so it is assumed that these parameters are universal across varying tissues. Also, HIF-1 regulation of genes, mRNA and proteins is an elaborate process and hence, this has been simplified with the aim of maintaining accuracy of the mathematical model and its predictability precision.

4.3.4 Parameter estimation. The parameter estimation function in COPASI was used to estimate the values of nine unknown parameters (Table 4.4). Condor-COPASI was adopted to take advantage of high throughput computing (Kent *et al.*, 2012). All algorithms available in COPASI were each tested five times and the best values obtained were compared

using the sum of squares (objective function value) to establish which algorithm was most successful in terms of this model. Parameters were estimated by fitting to steady state concentrations of the model which are exhibited in Table 4.4. Boundaries were set: $0 \leq \text{parameter value} \leq \text{infinity}$ with a start value of 10 for each parameter.

Table 4.4 Parameters and values used in the parameter estimation function.

The table on the left depicts the unknown parameters which are to be estimated, where the code within the brackets indicates the reaction from which the parameter originates and the subsequent code denotes the specific parameter. These are parameters belonging to the rate laws, except the final parameter which signifies the initial concentration for glutamine. The tables on the right indicate steady state values which are used in the algorithm for fitting the unknown parameters.

Parameter	Parameter	Value	Parameter	Value
(vGII).KmGIIaKG	a-KG	0.225	H+	1
(vGII).KmGIIIGlutamate	acetyl-CoA	0.063	H+	1
(vGII).KeqGII	ADP	0.624	H ₂ O	1
(vGII).VmGII	ATP	3.536	iGlc	1
(vGS).KeqVS	Citrate	0.44	iLac	1.3
(vGS).KmVSGlutamate	DHAP	0.07	NAD(+)	0.856
(vGS).KmVSGlutamine	DPG	0.065	NADH	0.214
(vGS).VmVS	eGlc	1	O ₂	0.39
[Glutaine]_0	F6P	0.2	OAA	0.005
	FDP	0.07	P2G	0.005
	G6P	0.75	P3G	0.05
	GAP	0.03	PEP	0.01
	Glutamate	0.1	Pi	2.44
	Glutamine	0.025001	Pyruvate	0.154

4.3.5 Model optimisation. Once the parameters had been estimated, the next stage was to optimise the model using the same set of steady state parameters as shown in Table 4.4 and altering all V_{\max} and unknown K_m

values. As with the parameter estimation, Condor-COPASI was utilised and all algorithms were repeated five times, again the most efficient determined through the sum of squares values. Adjacent to this, a further parameter estimation was undertaken, but rather than using the initial parameter values, random start values were assigned for the parameters. This aids in determining if there is more than one steady state for the model.

4.3.6 Production of the hypoxic state. The model produced thus far represents cell metabolism under a normoxic state. This model was saved and then modified to represent a hypoxic state which was achieved through the use of GC-MS experimental data (Wilcock *et al.*, 2012). The hypoxic model was optimised as described above, by fitting the V_{max} s and unknown K_m 's to new steady state concentrations which are displayed in Table 4.5. As this GC-MS data is semi-quantitative, the initial concentrations from the normoxic state were proportionally increased/decreased as calculated from the normoxic and hypoxic experimental data.

Table 26 Steady state concentrations used to create a hypoxic state in the model. Highlighted in the table are the metabolites (labelled on the left) of which the steady state concentrations were modified from the normoxic levels (middle column) to the hypoxic levels (right column).

Metabolite	Steady State	
	Concentration <u>Normoxia</u>	Concentration <u>Hypoxia</u>
Citrate	0.44	0.62742
F6P	0.2	0.13717
G6P	0.75	1.49725
Internal Glucose	1	1.48009
Glutamine	0.025001	0.01834
Lactate	1.3	0.90271
Phosphate	2.44	2.12728
Pyruvate	0.154	0.18415

4.3.7 Model validation using initial concentrations vs. steady state concentrations and comparing V_{\max} values. The aim of the optimisation of the model is to attain steady state values which are the same, or as close as possible, to the initial concentrations for each of the metabolites for both the normoxic and hypoxic modes. In addition, two optimisations were adopted for each mode, one using a predetermined V_{\max} value and the second using random start values for each V_{\max} parameter within each reaction. These V_{\max} values were then compared which is indicative of the model having more than a sole solution if varying V_{\max} 's are observed.

4.3.8 Model validation through flux and steady state analyses and comparison of experimental data and data from the literature. First, the model was validated through a comparison of the steady state concentrations and fluxes under the normoxic and hypoxic states. If the model was to mimic the hypoxic response accurately, the steady state concentrations and fluxes would be greater through glycolysis in the hypoxic condition in comparison to the normoxic state as a result of the transcription factor HIF-1. In addition, alterations may also be observed in terms of the TCA cycle and energy regulation between the states. The steady state concentrations and fluxes were acquired through the steady state function in COPASI using the initial conditions as described previously.

To validate the model further, experimental data were obtained from the literature and compared to the model following a perturbation according to Lu *et al.*, (2008). In this study the authors induced PDK-3 expression in HeLa cells. PDK inhibits PDH which was found to increase lactic acid production, particularly under hypoxic conditions. Therefore, PDH activity was reduced in the normoxic and hypoxic models; 0% (wild-type), 25%, 50%, 75%, 90% and 100% by the relative reduction of the k_1 parameter of the vPDH reaction. The production of lactic acid was assessed through the flux of vLDH.

Wigfield and co-workers (2008) reduced the expression of PDK in an HNSCC cell line, which in turn increases the expression of PDH. This resulted in a decrease in pyruvate production was observed under hypoxic conditions. To imitate this behaviour, the PDH activity was increased to

100% (wild-type), 250%, 500%, 750%, 900% and 1000% through the relative increase in the k_1 parameter of the v_{PDH} reaction. Pyruvate production was then assessed by the flux through the v_{PK} reaction,

LDH-A deficient adenocarcinoma cell lines were produced by Seth *et al.* (2011) and subsequent assessment for lactate and ATP production. This enzyme is responsible for the interconversion of pyruvate to lactate. The authors found a decrease in lactic acid production when LDH-A was reduced. This was imitated in the model through the reduction of LDH activity in both model states by; 0% (wild-type), 25%, 50%, 75%, 90% and 100% through the relative reduction of the V_{ldh_12} parameter of the v_{LDH} reaction. The production of lactic acid was assessed as described above.

The same authors also assessed ATP production of the cells following LDH activity reduction. Under hypoxic conditions, ATP concentrations were reduced whereas under normoxic conditions there was found to be no change. This was modelled as described above and ATP concentrations were assessed at steady state concentrations.

4.3.9 Fluctuation of external glucose, glutamine and sensitivity analysis. Once the models were created, optimised and validated they were compared to assess any variations between the hypoxic and normoxic states. First, external glucose (eGlc) was altered to 0, 0.1, 0.5, 1 (original concentration), 10, 100 and 1000mmol/l. As eGlc is a fixed metabolite, the initial concentration was altered in COPASI which does not change over time. The concentration of all metabolites were analysed over the change in eGlc and the normoxic and hypoxic conditions compared. Line plots were plotted for metabolites comparing the two states.

A similar independent experiment was undertaken altering the concentration of glutamine (also fixed). Concentrations used were 0, 0.01, 0.025001 (original concentration), 0.1, 1, 10 and 100mmol/l and the data analysed as described above.

A sensitivity analysis was performed using the sensitivity analysis task in COPASI. The sensitivities were based on steady state concentrations for all parameters in the model. The most significant parameters for the hypoxic and normoxic models were plotted on a bar chart highlighting the

sensitivity. In addition, the steady state concentrations which are altered by the alterations in the parameters were also analysed but are not shown.

4.4 Results and Discussion

4.4.1 Time course of the models post optimisation. Figures 4.2A and 4.2C exhibit the behaviour of the metabolites over the initial 100s for normoxia and hypoxia, respectively. These plots are generally homogenous between the normoxic and hypoxic models as only large variations in concentration are observed due to the scaling. For example, ATP (turquoise) reaches steady state quickly with only small variations in behaviour between the two models. However, variations in metabolite behaviour were apparent in glutamate (light purple) and α -KG (green). There is a rapid decrease in glutamate from $\sim 73\text{mmol/l}$ to $2 \times 10^{-2}\text{mmol/l}$ which takes the normoxic and hypoxic models 1s and 3s, respectively. This implies that the glutamine is being heavily used as a carbon source in both models to initiate metabolism. In the normoxia model, α -KG fluctuates in concentration between 0.23mmol/l to 0.53mmol/l over the 100s whereas in the hypoxia model, there is an initial, rapid increase from 0.23mmol/l to 12.58mmol/l after 3s, followed by a decrease to 1.74mmol/l after 100s.

Since the 100s plots display limited information due to the scaling, the behaviour of those metabolites in lower concentration were plotted over 0.3s for normoxia and hypoxia (Figures 4.2B and 4.2D, respectively). This highlighted the distinct behaviour of the two models. The rapid decrease in glutamate (light purple) is observable in the normoxic model but not in the hypoxic model. NAD(+) (purple) increases in the normoxic model from 0.86mmol/l to 1.04mmol/l whereas the hypoxic model shows an initial increase and subsequent decrease to 0.63mmol/l after 0.3s. Similar behaviour was also observed in P3G (pale pink). ADP rapidly decreased 20-fold during normoxia in 0.003s whilst in the hypoxic model, decreased gradually to $\sim 20\%$ over 0.282s. During normoxia, α -KG (green) remained stable at approximately 0.23mmol/l whereas there was a rapid increase during hypoxia to 2.22 after 0.3s and still increasing. Pyruvate (light blue) and NADH (medium blue) both decreased ~ 10 -fold in the normoxia model

and increased ~3-fold in the hypoxia model. Conversely, numerous metabolites behaved homogenously between the models including internal glucose (iGlc) (green), G6P (orange), F6P (purple), citrate (dark orange) and acetyl CoA (dark blue).

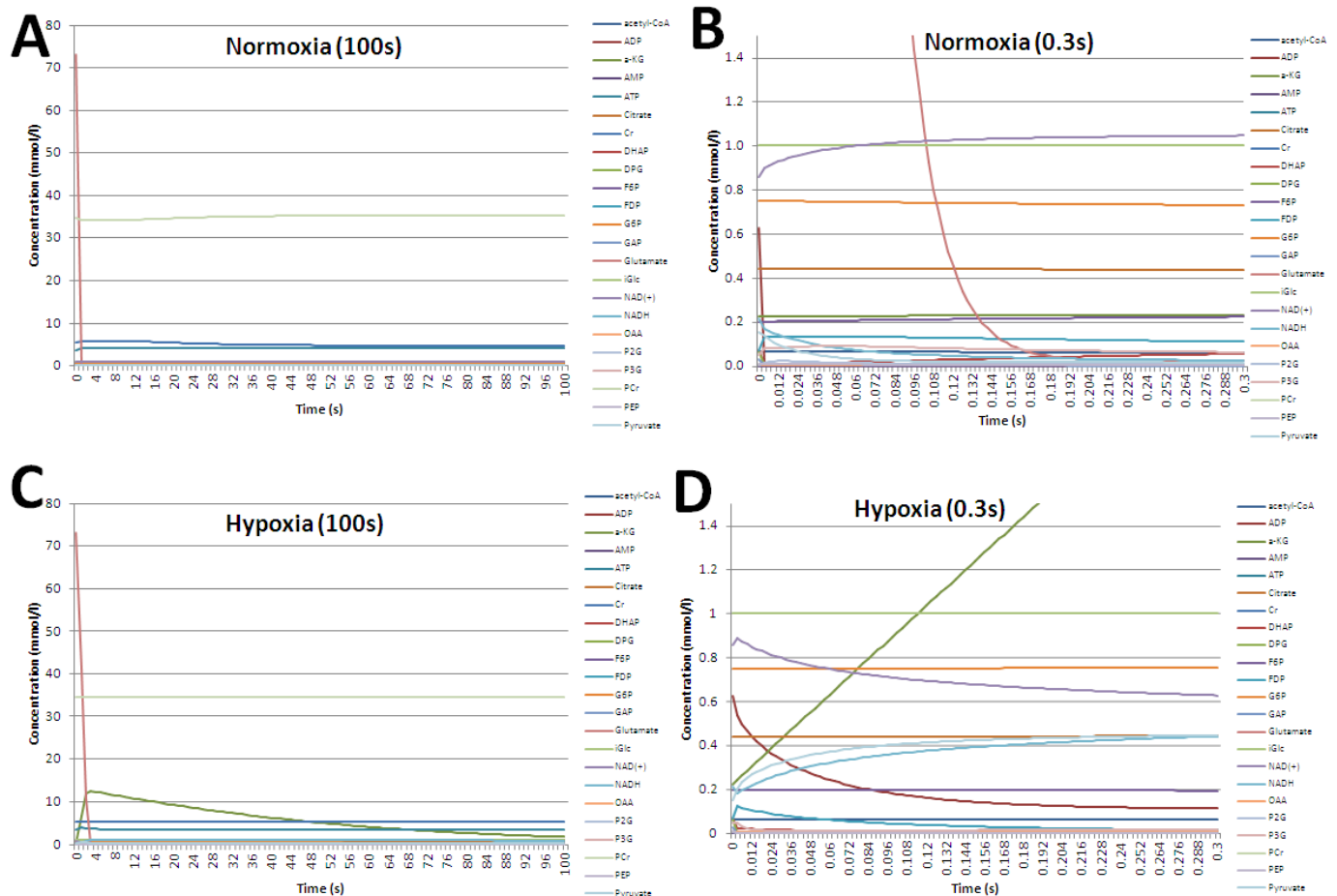


Figure 21 Time course of the models. Metabolite concentrations for the normoxic and hypoxic models where time is measured in seconds, the concentration is in mmol/l and the legend on the right of each plot highlights the metabolite identifications. The behaviour was assessed over the initial 100s for normoxia (A) and hypoxia (C). In addition, the scaling of the plots was altered to highlight the behaviour over the initial 0.3s for normoxia (B) and hypoxia (D).

4.4.2 Optimisation – regular start values vs. random start values.

Optimisation was completed by altering all V_{\max} 's and unknown K_m 's for normoxia and hypoxia (Table 4.6). Ten repeats were used in total for each model, five using the regular start values from the model and five using random start values. The best model was then chosen using the sum of least squares and the new parameters from the random start and regular start values were compared. The normoxia and hypoxia models resulted in 9/20 (45%) and 9/20 (45%) of the parameters within the same order of magnitude, respectively. This indicates that the model has more than one solution and requires further/more accurate parameters from the literature (which are unavailable). If there was only a sole solution, all of the parameters from the random and regular start values would be identical.

Table 4.6 Comparison of parameter estimation values from regular start values and random start values for the normoxic and hypoxic models. The 20 parameters used in optimising the models are shown on the left, where the reaction is displayed in the brackets and the subsequent parameter for that reaction thereafter.

Parameter Estimated	Normoxia		Hypoxia	
	Parameter Value (mmol) (Regular Start Values)	Parameter Value (mmol) (Random Start Values)	Parameter Value (mmol) (Regular Start Values)	Parameter Value (mmol) (Random Start Values)
(vGS).VmVS	4114.87	0.00	9.65	10994.80
(vGII).VmGII	7.01×10^{-5}	11089.00	0.86	0.00
(vGLUT).VmGLT	45596.00	670.83	18580.50	100000.00
(vHK).VmGLK	0.46	0.47	0.072	0.07
(vADK).Vfadh_14	924.37	15885.80	20147.30	3101.89
(vCK).VrevCK_13	4953.23	25677.00	0.15	0.17
(vLDH).Vfldh_12	12.69	12.59	1.00E-06	1.00E-06
(vPK).Vfpk_11	10197.20	12583.30	172.97	155.47
(vEN).Vfen_10	18317.20	97492.40	2005.66	196.45
(vPGM).Vfpgm_9	5.42	4.85	65881.30	35062.60
(vPGK).Vbpgk_8	31.72	1.56	1.53	0.05
(vGAPDH).Vfgad_7	169.74	73417.30	6.75	825.23
(vTPI).Vftpi_6	13.24	26306.40	27.68	2361.88
(vALD).Vfald_5	53999.50	99534.00	5160.33	7358.12
(vPFK).Vfpfk_4	12.20	13.45	2.74	2.82
(vPGI).Vbpgi_3	0.84	0.47	0.023	0.02
(vGII).KmGIIaKG	324.90	999.89	9.20	1000.00
(vGII).KmGIIIGlutamate	10.12	493.16	2.57	1.45
(vGS).KmVSGlutamate	34.58	974.95	0.048	356.87
(vGS).KmVSGlutamine	81.71	933.89	25.27	7.23

4.4.3 Comparison of initial concentrations and steady state concentrations. The optimisation's aim is to attain steady state concentrations as close as possible to the initial concentrations by changing the parameters shown in Table 4.6 (Table 4.7). The number of metabolites showing initial and steady state concentrations in the same order of magnitude (or metabolites which are within close proximity e.g. iGlc for normoxia) were 13/23 (57%) (normoxia) and 11/23 (48%) (hypoxia).

Table ii Modelling of initial and steady state concentrations of metabolites.

Initial and steady state concentrations were compared for 31 metabolites. Those highlighted in yellow depict fixed metabolites.

Species	Normoxia		Hypoxia	
	Initial Concentration (mmol/l)	Steady State Concentration (mmol/l)	Initial Concentration (mmol/l)	Steady State Concentration (mmol/l)
acetyl-CoA	0.06	0.06	0.06	0.017
ADP	0.62	2.78E-03	0.62	0.81
a-KG	0.23	0.28	0.23	0.71
AMP	2.00E-05	8.39E-07	2.00E-05	0.09
ATP	3.54	4.16	3.54	3.35
Citrate	0.44	0.04	0.63	0.45
Cr	5.33	5.38	5.33	39.30
DHAP	0.07	0.07	0.07	0.00
DPG	0.07	1.64E-03	0.07	1.89E-06
eGlc	1.00	1.00	1.00	1.00
F6P	0.20	0.22	0.14	0.12
FDP	0.07	0.07	0.07	8.36E-05
G6P	0.75	0.66	1.50	1.14
GAP	0.03	1.14E-04	0.03	1.72E-05
Glutamate	73.17	0.02	73.17	0.02
Glutamine	0.25	0.25	0.18	0.18
H+{Cytoplasm}	1.00	1.00	1.00	1.00
H+{Mitochondria}	1.00	1.00	1.00	1.00
H2O	1.00	1.00	1.00	1.00
iGlc	1.00	1.00	1.48	1.00
iLac	1.30	1.30	0.90	0.90
NAD(+)	0.86	1.05	0.86	0.40
NADH	0.21	0.02	0.21	0.67
O2	0.39	0.39	0.39	0.39
OAA	5.0E-03	6.66E-04	5.0E-03	0.01
P2G	5.0E-03	6.34E-03	5.0E-03	1.29E-04
P3G	0.05	0.05	0.05	8.0E-04
PCr	34.67	34.62	34.67	0.70
PEP	0.01	0.00	0.01	6.32E-05
Pi	2.44	2.44	2.13	2.13
Pyruvate	0.15	0.01	0.18	0.16

With supplementary experimental data and further model tweaking through optimisation and validation, these figures could be improved. In addition, due to the construction of this hypoxic model, it could be enhanced through the acquirement of more experimental variations between the normoxic and hypoxic states.

Table 4.7 also provides details of how the modelled conditions vary prior to perturbation. In terms of energy regulation, steady state ADP concentrations increased ~300 fold and AMP increased from 8.40×10^{-7} mmol/l to 2.00×10^{-5} mmol/l under hypoxia. ATP levels reduced approximately 20% which may partially account for the increase in the adenosine mono- and di- phosphates. This is logical since the switch from oxidative phosphorylation to glycolysis under hypoxia is a less efficient method of producing ATP (Lunt and Vander Heiden, 2011). There is also an increase in NADH and an associated decrease in NAD(+). This is a result of an increase in flux through the TCA cycle under hypoxic conditions in the model. This is supported with an increase in metabolite concentrations and flux associated with the TCA cycle/glutaminolysis where citrate, α -KG and OAA were elevated in concentration by 10 fold, 3.5 fold and 15 fold, respectively.

The model did not behave as expected in terms of glycolysis with reduced concentrations (except G6P) and fluxes under hypoxia. These were expected to increase during hypoxia from the upregulation from HIF-1 (Frezza & Gottlieb, 2009). However, this evidence relates to hypoxia in oncology and this model was produced using non-cancerous cell line metabolic data. Scott and co-workers (2011) showed that hypoxic effects are much more prominent in cancer cells which is one plausible explanation as to the unexpected behaviour of the model.

4.4.4 Model Validation. Numerous methods were used to validate the model. Firstly, partial validation was attempted through the evaluation of flux through both the models. As discussed previously, it is expected that HIF-1 would cause an increase in flux through glycolysis (Frezza & Gottlieb, 2009). However, the hypoxic model actually reduced the flux through glycolysis as displayed in Table 4.8.

There is a consistent 88% reduction in flux between normoxia and hypoxia throughout glycolysis. During the early stages of the pathway (vGLUT, vALD, vHK, vPFK and vPGI) there is a constant flux in normoxia (0.252mmol/s) and hypoxia (0.030mmol/s). This flux doubles (in both states) after the vALD reaction and remains constant once more in the latter stages of glycolysis (vPGK, vPGM, vPK, vEN, and vGAPDH), obviously maintaining the 88% variation between the conditions.

This suggests that the model is not mimicking hypoxic behaviour and further work is necessary. For example, the reduction in glucose uptake by GLUT (vGLUT) is inaccurate. The expression of GLUT is usually increased through HIF-1 causing an upregulation of glucose uptake under hypoxia (Bartrons & Caro, 2007). In addition, vHK flux is decreased when this has also been found to be increased under hypoxia (Frezza & Gottlieb, 2009). Hence, the model is not reflecting the behaviour of genuine hypoxia.

In relation, lactate production should also be increased during hypoxia (Valenza *et al.*, 2005); however, there is actually a reduction in flux to lactate production from 0.245 to 2.99×10^{-5} mmol/s. The GC-MS data on which the hypoxic model is based displayed this behaviour and this is the reason for this reduction in lactate production.

The anaplerotic input of glutamine into the TCA (vGII) increases in hypoxia with an associated 23% reduction in concentration and increased flux from 1.34×10^{-7} to 1.52×10^{-2} mmol/s. Such behaviour has been observed not only in cancer cells, but also to a lesser degree in their healthy counterparts (Scott *et al.*, 2011). There is also a 4-fold increase in flux from pyruvate into the TCA cycle to acetyl-CoA (vPDH) further supporting this process. However, this is not usually observed under hypoxia due to the HIF-1 stimulation of pyruvate dehydrogenase kinase (PDK) which reduces the flux between glycolysis and the TCA (Kim *et al.*, 2006). Pyruvate also has an entry point into the TCA cycle via vPDHII where there is ~10 fold increase in flux.

Table 4.8. Comparison of normoxic and hypoxic fluxes. Fluxes of the models were compared for 27 reactions from glycolysis, TCA cycle, glutaminolysis and energy regulation. Those highlighted in yellow are associated with increased flux through hypoxia.

Reaction ID	Reaction	Flux (mmol/s)	
		Normoxia	Hypoxia
v2OD	a-KG + ADP + 2 * NAD(+) -> OAA + ATP + 2 * NADH	7.140x10 ⁻⁵	0.019
vACO	Citrate + NAD(+) -> a-KG + NADH	0.002	0.009
vADK	ATP + AMP = 2 * ADP	-1.380x10 ⁻¹⁶	3.790x10 ⁻¹⁷
vALD	FDP = DHAP + GAP	0.126	0.015
vATP	ADP + Pi + 3 * H+{Cyto} = ATP + H2O + 3 * H+{Mito}	-0.064	0.207
vATPase	ATP = ADP + Pi	0.312	0.251
vCK	ATP + Cr = ADP + PCr	-1.070x10 ⁻¹⁰	5.410x10 ⁻¹³
vCS	OAA + acetyl-CoA -> Citrate	0.002	0.009
vCSII	OAA = a-KG	-0.002	-0.006
vEN	P2G = PEP	0.252	0.030
vGAPDH	Pi + GAP + NAD(+) = NADH + DPG	0.252	0.030
vGII	Glutamate = a-KG	1.340x10 ⁻⁷	0.015
vGLUT	eGlc = iGlc	0.126	0.015
vGS	Glutamate = Glutamine	-1.340x10 ⁻⁷	-0.015
vHK	Pi + iGlc = G6P	0.126	0.015
vLDH	NADH + Pyruvate = iLac + NAD(+)	0.24	2.990x10 ⁻⁰⁵
vleak	H+{Cytoplasm} -> H+{Mitochondria}	0.064	0.072
vOAA_de g	OAA ->	0.002	0.036
vPDH	Pyruvate + NAD(+) -> acetyl-CoA + NADH	0.002	0.009
vPDHII	Pyruvate + ATP -> OAA + ADP	0.002	0.020
vPFK	ATP + F6P = ADP + FDP; AMP	0.126	0.015
vPGI	G6P = F6P	0.126	0.015
vPGK	ADP + DPG = ATP + P3G	0.252	0.030
vPGM	P3G = P2G	0.252	0.030
vPK	ADP + PEP = ATP + Pyruvate	0.252	0.0303
vresp	NADH + 0.5 * O2 + 11 * H+{Mito} -> NAD(+) + H2O + 10 * H+{Cyto}	0.009	0.087
vTPI	GAP = DHAP	-0.126	-0.015

In addition to the general assessment of metabolite concentrations and reaction fluxes, literature were used to validate the behaviour of the model. Studies of changes in PDK (which de-activates PDH) and LDH-A expression were impersonated using the models and the behaviour assessed.

Induced PDK-3 expression in HeLa cells was performed by Lu and co-workers (2008) and subsequent analysis of various aspects. PDK is responsible for the phosphorylation and hence inhibition of PDH, which in turn regulates the conversion of acetyl-CoA to pyruvate. The inactivation of PDH causes a switch from oxidative phosphorylation to glycolysis which causes an increase in lactic acid production. The increased expression of PDK and hence reduction in PDH caused an increase in lactic acid, particularly under hypoxic conditions. To part-validate the model, PDH activity was reduced 25%, 50%, 75%, 90% and 100% and lactate production assessed (Figure 4.3A). In concordance, the model found a PDH activity-dependant increase of lactic acid during hypoxia. No change in lactic acid production was found in the normoxic model, even at 100% PDH knockdown. Hence, the model was able to mimic the experimental data under hypoxic conditions.

Wigfield *et al.* (2008) reduced expression of PDK-1 in a HNSCC cell line and assessed the effect on pyruvate production. The knockdown of PDK-1 resulted in an increase in PDH and subsequent reduced levels of pyruvate under hypoxic conditions. This was emulated in the model by increasing PDH activity 250%, 500%, 750%, 900% and 1000% (Figure 4.3B). Pyruvate production was not affected by the change in PDH activity in the model. The model was unable to replicate the experimental data in this fashion.

Finally, Seth and co-workers (2011) generated LDH-A deficient adenocarcinoma cell lines and assessed ATP and lactate production. LDH-A is the enzyme involved in the interconversion of pyruvate to lactate. The experimental data showed that the knockdown had no effect on ATP during hypoxia and caused a decrease under normoxic conditions. Figure 4.3C shows the model output for LDH activity which was reduced 25%, 50%, 75%, 90% and 100%. ATP concentrations reduced 24% under normoxic conditions with complete reduction in LDH activity. Aside from this there was no change in ATP concentrations. The model therefore predicts the ATP outcome correctly, although, only with extreme reduction in the LDH activity.

In terms of lactic acid production, Seth and colleagues (2008) found a decrease in lactic acid production following a deduction in LDH activity.

Figure 4.3D displays the output from the model where LDH was reduced as described above. There is a LDH activity-dependant reduction in lactate under normoxic and hypoxic conditions, except for the behaviour at 75% reduction and hypoxia where there is an uncharacteristic rise. Thus, the model is able to predict the behaviour of lactic acid following a reduction in LDH activity.

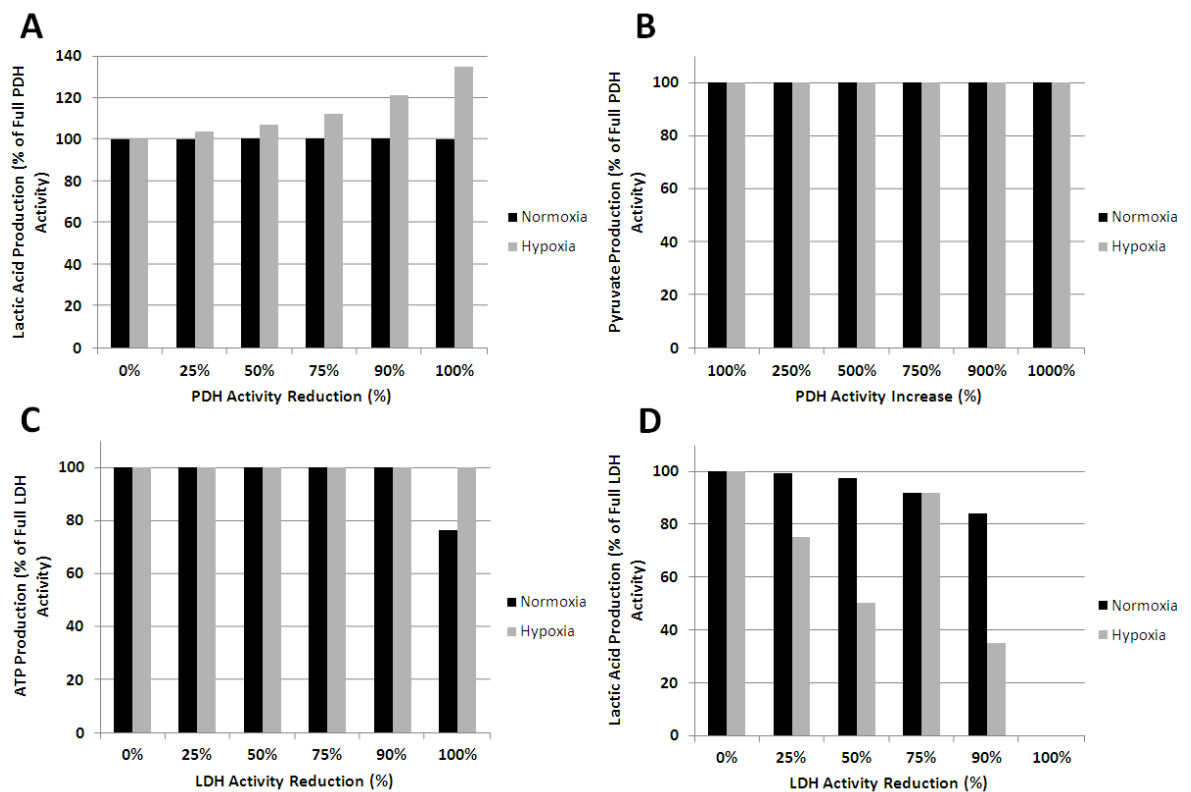


Figure 23 Model validation using behavioural aspects from the literature. PDH and LDH relative activities were reduced by 0% (wild-type expression), 25%, 50% 75%, 90% and 100% in the normoxic and hypoxic models (Figures A, B and D). Relative PDH activity was increased 100% (wild-type), 250%, 500%, 750%, 900% and 1000% in the normoxic and hypoxic models (Figure D). The effects on lactic acid, pyruvate and ATP were then assessed and compared with the literature. (A) The effects of PDH knockdown on lactic acid production (compared with Lu *et al.*, 2008). (B) The effects of PDH increase on pyruvate production (compared with Wigfield *et al.*, 2008). (C) The effects of LDH knockdown on ATP production (compared with Seth *et al.*, 2011). (D) The effects of LDH knockdown on lactic acid production during normoxia (compared with Seth *et al.*, 2008).

4.4.5 The predicted effects from altering external glucose concentrations on cellular metabolism. Central metabolism is revised

when eukaryotic cells are subjected to a hypoxic environment. This is of importance in oncology, since many tumors display hypoxic characteristics. Therefore, it is vital to understand the varying behaviours of hypoxia and normoxia to prevent cancer progression and enhance treatment. Since cellular behaviour is extremely complex, modelling central metabolism may aid in understanding the phenomena. Glucose uptake and carbon metabolism is known to be altered under hypoxia and so the model was used to assess how external glucose (eGlc) concentration effects metabolism. Figure 4.4 displays how nine interesting metabolites change with varying external glucose concentrations.

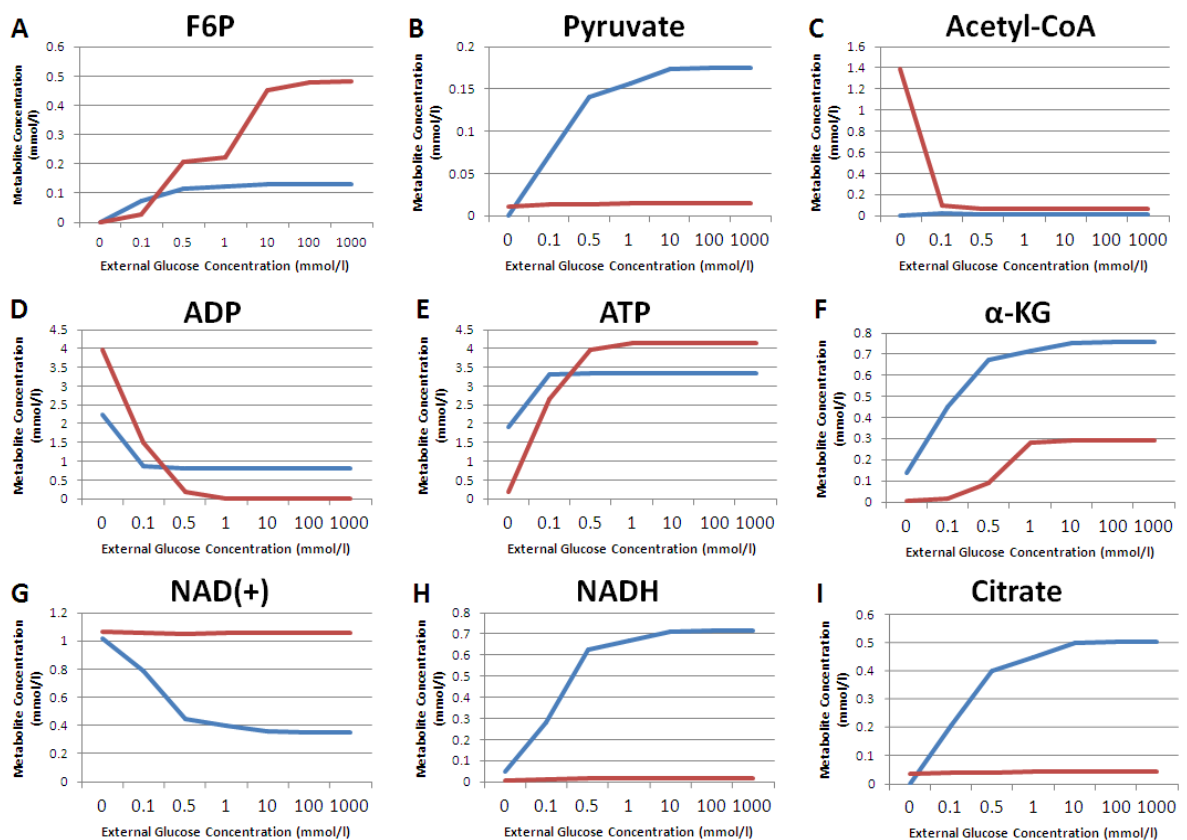


Figure 24. The predicted effects of altering external glucose concentration on central metabolism under normoxia and hypoxia. External glucose was altered to 0mmol/l, 0.1mmol/l, 0.5mmol/l, 1mmol/l, 10mmol/l, 100mmol/l and 1000mmol/l in the model and the effects on metabolism assessed. The red lines highlight normoxia and the blue lines hypoxia. Data are shown for the most interesting metabolites: **(A)** F6P; **(B)** pyruvate; **(C)** acetyl-CoA; **(D)** ADP; **(E)** ATP; **(F)** α -KG; **(G)** NAD(+); **(H)** NADH and **(I)** citrate.

In terms of glycolysis, the uptake of glucose into the cell from GLUT was efficient enough to attain an equal concentration of glucose internally and externally under both hypoxia and normoxia (data not shown). G6P and F6P (Figure 4.4A) displayed an increase in concentration as eGlc was elevated with greater levels found under normoxia. The remainder of the glycolytic pathway up until pyruvate displayed similar behaviour where an increase in eGlc caused an increase in metabolite concentration and flux through the pathway. However, hypoxia actually caused a decrease in glycolytic metabolite concentrations and flux and hence the model does not reflect true behaviour in this respect.

Figure 4.4B shows the behaviour of pyruvate where there is only a 29% increase under normoxia but a 1.3×10^6 -fold augmentation under hypoxia between 0 and 1000mmol/l eGlc. This increase in pyruvate causes a 30% increase in vLDH (the conversion of pyruvate to lactate) flux under hypoxia which is also observed in reality (Valenza *et al.*, 2005).

Acetyl-CoA is displayed in Figure 4.4C and shows a relatively large reduction under normoxia from 1.4 to 0.1mmol/l between 0-0.1mmol/l of eGlc before reaching a steady state. Conversely, under hypoxia, there is a small increase between 0 and 0.1mmol/l of eGlc before reaching a plateau at around a 75% lower concentration than normoxia.

The TCA cycle intermediates α -KG (Figure 4.4F) and OAA (data not shown) behave similarly. There is a positive relationship between eGlc and metabolite concentrations before approaching steady state at ~ 1 mmol/l eGlc. The concentration under hypoxia is consistently greater than under normoxia as is the flux. Citrate (Figure 4.4I) also displays a strong positive relationship with eGlc under hypoxia with an increase from 4×10^{-7} mmol/l to 0.5mmol/l, whereas normoxia shows only a 29% increase. Hence, the model is predicting an increase in TCA flux under hypoxia. In addition, the increase in eGlc and hence carbon input into the system is more prominent in the TCA cycle under hypoxia. However, this may not be reflective of reality as the flux from glucose into the TCA cycle through pyruvate to acetyl-CoA is inhibited through PDK and hence PDH under hypoxia as described previously.

Energy regulation is also of importance under hypoxic conditions and this was assessed through the production of ATP and NADH. As expected, the increase in eGlc led to a reduction of AMP (data not shown) and ADP (Figure 4.4D) and subsequent increase in ATP (Figure 4.4E). A 23x and 1.75x increase in ATP levels were observed under normoxia and hypoxia respectively due to the increase eGlc. This is a direct result of increased flux through the pathways and hence ATP production. NAD(+) and NADH behaviour with varying eGlc concentrations can be seen in Figures 4.4G and 4.4H, respectively. During normoxia, only relatively minute changes were observed in NAD(+) and NADH with increasing eGlc. Conversely, the hypoxic condition saw a large decrease in NAD(+) of 66% and an increase in NADH of ~1400% between 0mmol/l and 1000mmol/l eGlc. This is a direct result of the increase in flux through the TCA cycle under hypoxia which is occurring in the model. The TCA cycle generates the majority of the NADH from NAD(+) through vACO (citrate to α -KG) and v2OD (α -KG to OAA) but there is also a contribution from vPDH (pyruvate to acetyl-CoA) and vGAPDH (GAP to DPG).

4.4.6 The predicted effects from altering glutamine concentrations on cellular metabolism. Glutamine is an amino acid which eukaryotic cells use as energy source and is believed to be the preferred source for cancer cells (DeBerardinis *et al.*, 2008). Glutaminolysis is a pathway which involves conversion of glutamine to glutamate where it can then enter the TCA cycle via α -KG. The behaviour of the model was assessed after altering the concentration of glutamine in the system. Analysis of the TCA cycle, glycolysis and energy regulation was undertaken under hypoxic and normoxic conditions (Figure 4.5).

The concentration of glutamate was similar to the initial glutamine concentration for both model states. OAA (Figure 4.5F) concentrations did not change under normoxia but a large increase in hypoxia from 0.164mmol/l at 0mmol/l glutamine to 320.1mmol/l at 100mmol/l glutamine was observed. α -KG (data not shown) behaved homogeneously to OAA with a similar increase under hypoxia. Figure 4.5I shows citrate concentrations, where similarly, there was no change under normoxia, but an elevation under hypoxia with a maximum of around 0.64mmol/l at 1mmol/l glutamine.

Under normoxia, this value was consistently around 15-fold the lower. Hence, there is an upregulation of the TCA cycle under hypoxia but not under normoxia with increasing concentrations of glutamine.

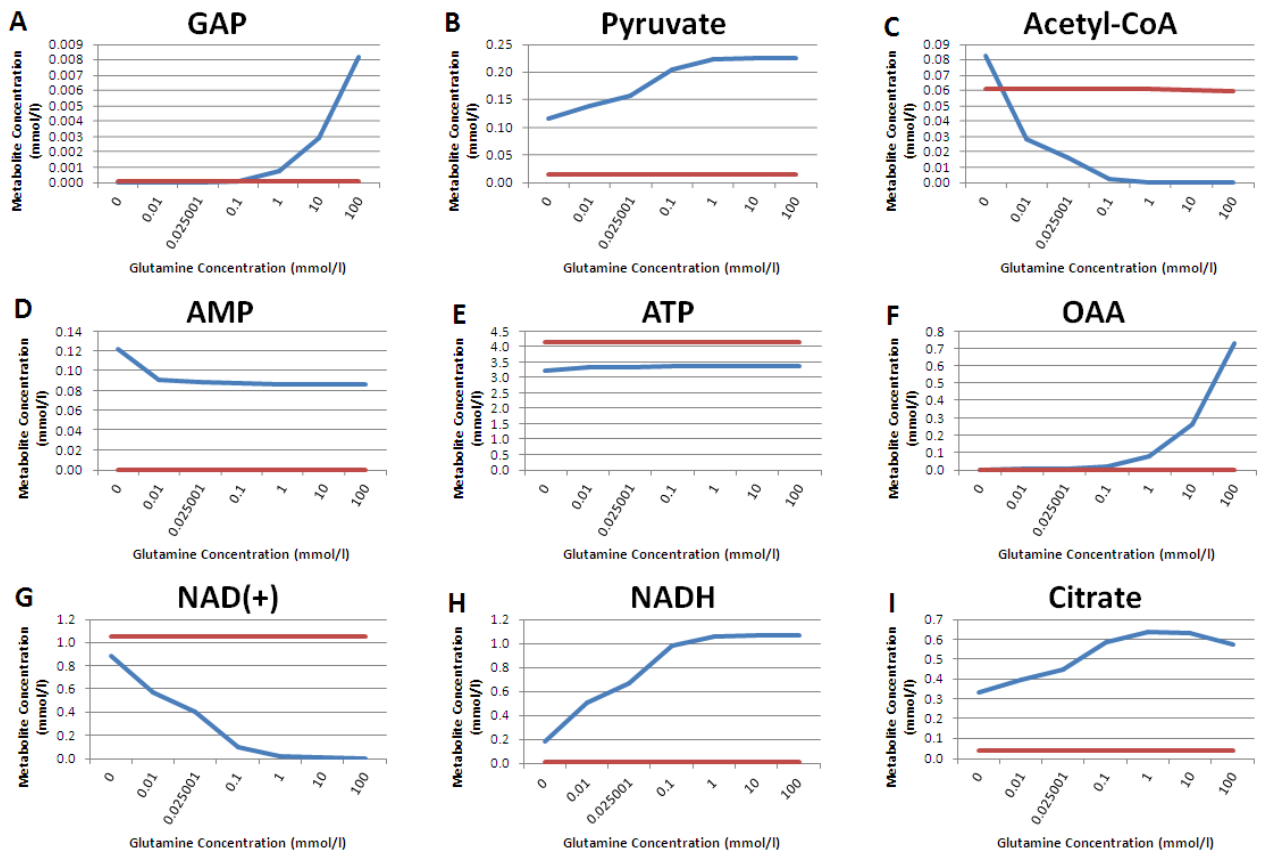


Figure 25. The model predicted effects of altering glutamine concentration on central metabolism under normoxia and hypoxia. Glutamine was altered to 0mmol/l, 0.01mmol/l, 0.025001mmol/l, 0.1mmol/l, 1mmol/l, 10mmol/l and 100mmol/l in the model and the effects on metabolism assessed. The red lines highlight normoxia and the blue lines hypoxia. Data are shown for the most interesting metabolites: **(A)** GAP; **(B)** pyruvate; **(C)** acetyl-CoA; **(D)** AMP; **(E)** ATP; **(F)** OAA; **(G)** NAD(+); **(H)** NADH and **(I)** citrate.

In terms of glycolysis intermediates, a number of metabolites were found in elevated concentrations in hypoxia; increasing with glutamine concentrations. For example, Figure 4.5A shows how GAP increases with amplified glutamine concentrations under hypoxia. This was similar for DHAP and FDP and to a lesser extent F6P and G6P. P2G, P3G and PEP were found unchanged under both states. Pyruvate (Figure 4.5B) also positively correlates with glutamine concentration under hypoxia, with no alterations under normoxia. It is therefore apparent that there is an increase

in glycolytic activity under hypoxic conditions when increasing glutamine intake into cellular metabolism. There is no direct link within the model from the TCA cycle into glycolysis as vPDH (pyruvate to acetyl-CoA) is an irreversible reaction (although in reality, glutamine can eventually be converted into pyruvate via malate (Baggetto, 1992)). Hence, this relationship between increased glutamine and glycolytic activity in the hypoxic model is indirect.

Changes in glutamine concentrations did not affect acetyl-CoA concentrations under normoxia (Figure 4.5C). However, under hypoxia, there was a dramatic reduction from 0.08 to 1.10×10^{-4} mmol/l between 0 and 1 mmol/l glutamine.

NAD(+) and NADH are graphically displayed in Figures 4.5G and 4.5H, respectively. In the hypoxic model, the increase in glutamine from 0 to 100 mmol/l caused a reduction in the former and an elevation in the latter by 650-fold and 6-fold, respectively. No change was observed in the normoxic model. As discussed previously, this is a result of an increase in flux through the TCA cycle from the enhanced anaplerotic input of glutamine.

AMP (Figure 4.5D) and ATP (Figure 4.5E) displayed no glutamine dependent changes under normoxia. However, the hypoxic state was found to have a 14% decrease in AMP and a 4% increase in ATP when glutamine was elevated from 0 to 100 mmol/l. This was a direct result of the increase in flux through the TCA cycle and more specifically, v2OD (α -KG to OAA) which involves the production of ATP.

4.4.7 Sensitivity analysis to determine potential target intermediates. A sensitivity analysis is a method for establishing the degree of change in a set of variables when a particular parameter is changed. In this instance, all model parameters were fluctuated and the modified steady state concentrations assessed for change. It is valuable to understand the sensitivity of a model to perturbations and also to what degree the sensitivity is distributed. In metabolic models such as this, sensitivity analysis can aid in predicting the effects of perturbations and hence highlight potential therapeutic targets for drug design or metabolic engineering.

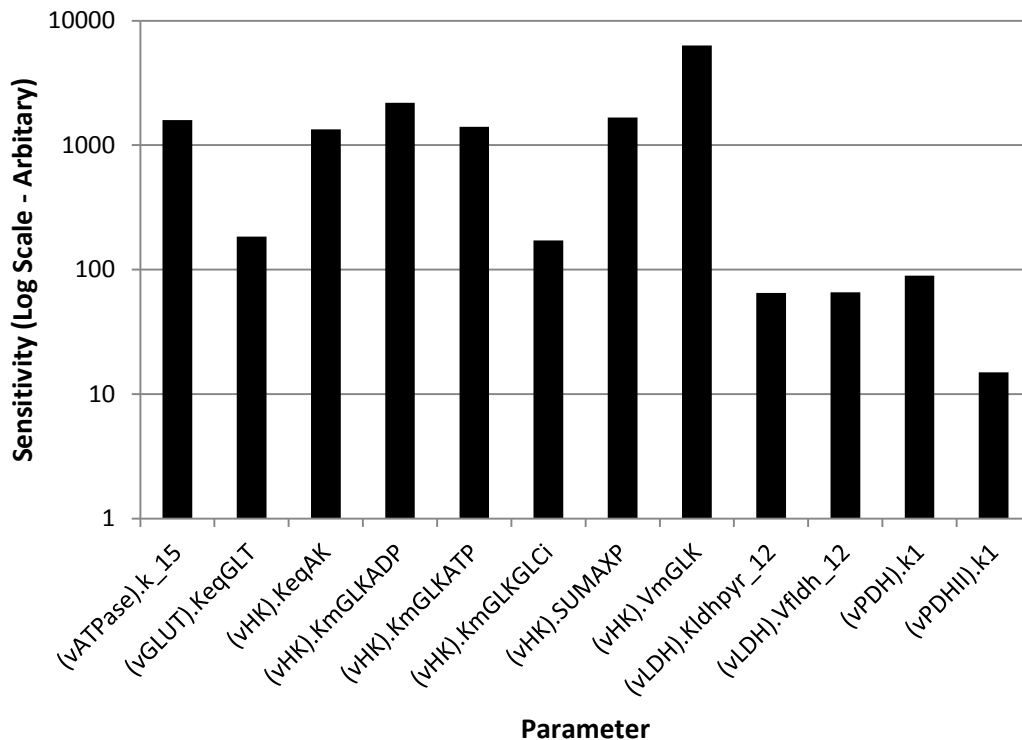


Figure 26. Sensitivity analysis of the normoxic model. The 12 most significant parameters derived from the sensitivity analysis of the normoxic model. The parameters are signified on the x-axis and the extent of sensitivity is highlighted on the y-axis (log scale and arbitrary values). In terms of parameters, the bracketed text depicts the reaction and the subsequent text emphasises the specific parameter.

Figure 4.6 and 4.7 show the most significant parameters in terms of sensitivity for the normoxic and hypoxic models, respectively. The former resulted in 12 parameters which when perturbed, caused major alterations in the steady state concentrations of the model metabolites. These parameters originate from the reactions vATPase (x1), vGLUT (x1), vHK (x6), vLDH (x2), vPDH (x1) and vPDHII (x1). Elevating the values of (vGLUT).KeqGLT, (vHK).KeqAK, (vHK).KmGLKADP, (vHK).VmGLK, (vLDH).Kldhpyr_12, (vPDH).k1 and (vPDHII).k1a all caused similar effects and increased many glycolysis intermediates including FDP, GAP, DPG, P3G, P2G and PEP whilst decreasing AMP and ADP levels. Conversely, increasing the values of (vATPase).k_15, (vLDH).Vfldh_12, (vHK).SUMAXP, (vHK).KmGLKATP, (vHK).KmGLKGLCi resulted in the opposite effects with a decrease in

glycolytic metabolites and an increase in ADP and AMP. The greater the sensitivity of the parameter as depicted on the graph, the larger the effect on the metabolites.

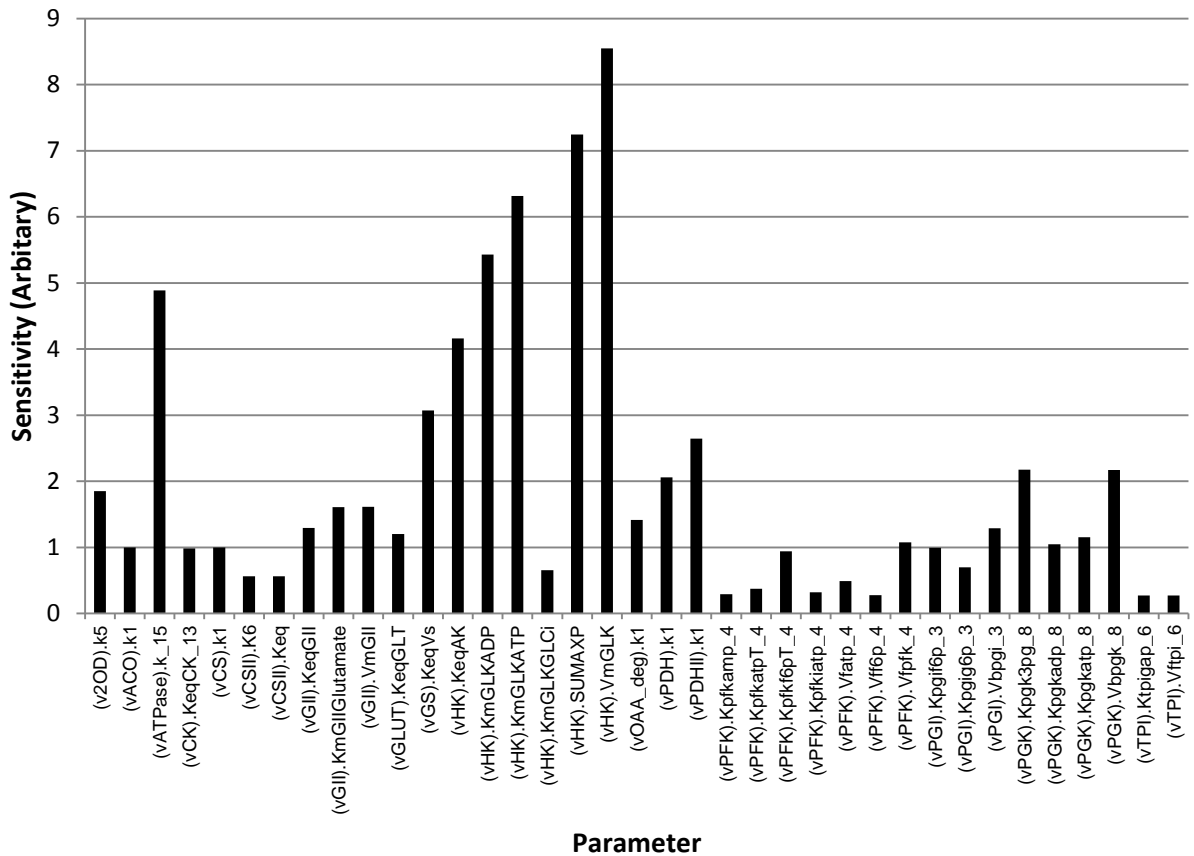


Figure 27. Sensitivity analysis of the hypoxic model. The 37 most significant parameters derived from the sensitivity analysis of the hypoxic model. The parameters are signified on the x-axis and the extent of sensitivity is highlighted on the y-axis (arbitrary values). In terms of parameters, the bracketed text depicts the reaction and the subsequent text emphasises the specific parameter.

The hypoxic sensitivity analysis is more complex as the distribution of sensitivity is greater than the normoxia model. This included 37 significant parameters from v2OD (x1), vACO (x1), vATPase (x1), vCK (x1), vCS (x1), vCSII (x2), vGII (x3), vGLUT (x1), vGS (x1), vHK (x6), vOAA_deg (x1), vPDH (x1), vPDHII (x1), vPFK (x7), vPGI (x3), vPGK (x4), vTPI (x2). The parameters discussed above in terms of elevating glycolysis intermediates in normoxia all have the same effects here with the exception of (vLDH).Kldhpyr_12 which was found to have no effect and (vPDHII).k1a which decreased glycolytic intermediates in the hypoxic model. In addition,

(vCSII).Keq, (vPGK).Kpgkadb_8, (vGII).KeqGII caused an increase in glycolysis intermediates. A reduction was seen in glycolytic metabolites when the parameters; (vCSII).K6, (vPGK).Vbpgk_8, (vATPase).k_15, (vHK).SUMAXP, (vHK).KmGLKATP, (vGLUT).KeqGLT, (vGII).VmGII and (vGS).KeqVs were increased.

Alterations in the parameters of the normoxic model did not produce any effect on the TCA cycle. However the hypoxic model was found to have increased concentrations of TCA intermediates when (vPDH).k1, (vHK).VmGLK and (vATPase).k_15 were individually increased. The opposite effects were observed when (v2OD).k5, (vACO).k1, (vOAA_deg).k1 and (vPDHII).k1 were elevated.

Therefore, since tumorous cells are hypoxic, it may be plausible to target reactions of the glycolytic pathway/TCA cycle which are likely to affect only the hypoxic cells. Reactions highlighted from this model include vCSII, vGS, vPGK and vGII as these are likely to disrupt metabolism of the hypoxic model whilst minimising the effect under normoxia. However, the model validation has highlighted that further work is required to ensure the behaviour of the model accurately impersonates reality.

4.5 Concluding Remarks

Caution should be taken when analysing the predicted outcomes from the model, due to the behaviour and validation displaying its inaccuracies. Improvements of the model are necessary including increasing the experimental data, using data from cancerous cell lines and further optimisation and validation. The more kinetic parameters obtained experimentally, the more accurate the models predictions will be. In addition, the experimental data to create the hypoxic model requires increasing and to be more accurate. However, the model has discovered a number of potential therapeutic targets where behaviour varies between hypoxia and normoxia. A reduction in external glucose and glutamine found variations in behaviour between the two conditions and may also aid in the understanding of how a cell behaves under hypoxic stress.

4.6 References

Baggetto, L, G. (1992). Deviant energetic metabolism of glycolytic cancer cells. *Biochimie*, **74**: 959-974.

Bartrons, R. and Caro, J. (2007). Hypoxia, glucose metabolism and the Warburg's effect. *Journal of Bioenergetics and Biomembranes*, **39**: 223-229.

DeBerardinis, R, J. Sayed, N. Ditsworth, D. and Thompson, C, B. (2008). Brick by brick: metabolism and tumor cell growth. *Current Opinion in Genetics & Development*, **18**: 54-61.

Frezza, C. and Gottlieb, E. (2009). Mitochondria in cancer: Not just innocent bystanders. *Seminars in Cancer Biology*, **19**: 4-11.

Hornberg, J, J. Bruggemana, F, J. Westerhoff, H, V. and Lankelma, J. (2006). Cancer: A Systems Biology disease. *BioSystems*, **83**: 81-90.

Ke, Q. and Costa, M. (2006). Hypoxia-Inducible Factor-1 (HIF-1). *Molecular Pharmacology*, **70**: 1469-1480.

Kent, E. Hoops, S. and Mendes, P. (2012). Condor-COPASI: high-throughput computing for biochemical networks. *BMC Systems Biology*, **6**: 91.

Kim, J, W. Tchernyshyov, I. Semenza, G, L. and Dang, C, V. (2006). HIF-1-mediated expression of pyruvate dehydrogenase kinase: a metabolic switch required for cellular adaptation to hypoxia. *Cell Metabolism*, **3**: 177-185.

Lambeth, M, J. and Kushmerick, M, J. (2002). A Computational Model for Glycogenolysis in Skeletal Muscle. *Annals of Biomedical Engineering*, **30**: 808-827.

Lu, CW. Lin, SC. Chen, KF. Lai, YY. and Tsai, SJ. (2008). Induction of Pyruvate Dehydrogenase Kinase-3 by Hypoxia-inducible Factor-1 Promotes Metabolic Switch and Drug Resistance. *The Journal of Biological Chemistry*, **283**: 28106-28114.

Lunt, S, Y. and Vander Heiden, M, G. (2011). Aerobic Glycolysis: Meeting the Metabolic Requirements of Cell Proliferation. *Annual Review of Cell and Developmental Biology*, **27**: 441-464.

Minchenko, A. Leshchinsky, I. Opentanova, I. Sang, N. Srinivas, V. Armstead, V. and Caro, J. (2002). Hypoxia-inducible Factor-1-mediated Expression of the 6-Phosphofructo-2-kinase/fructose-2,6-bisphosphatase-3 (PFKFB3) Gene. *Journal of Biological Chemistry*, **277**: 6183-6187.

Nazaret, C. Heiske, M. Thurley, K. Mazat, JP. (2009). Mitochondrial energetic metabolism: A simplified model of TCA cycle with ATP production. *Journal of Theoretical Biology*, **258**: 455-464.

Seth, P. Grant, A. Tang, J. Vinogradov, E. Wang, X. Lenkinski, R. and Sukhatme, R, P. (2011). On-target Inhibition of Tumor Fermentative Glycolysis as Visualized by Hyperpolarized Pyruvate. *Neoplasia*, **13**: 60-71.

Scott, D, A. Richardson, A, D. Filipp, F, V. Knutzen, C, A. Chiang, G, C. Ronai, Z, A. Osterman, A, L. and Smith, J, W. (2011). Comparative Metabolic Flux Profiling of Melanoma Cell Lines. *BEYOND THE WARBURG EFFECT. The Journal of Biochemistry*, **286**: 42626-42634.

Teusink, B. Passarge, J. Reijenga, C, A. Esgalhado, E. van der Weijden C, C. Schepper, M. Walsh, M, C. Bakker, B, M. van Dam, K. Westerhoff, H, V. and Snoep, J, L. (2000). Can yeast glycolysis be understood in terms of in vitro kinetics of the constituent enzymes? Testing biochemistry. *European Journal of Biochemistry*, **267**: 5313-5329.

Valenza, F. Aletti, G. Fossali, T. Chevallard, G. Sacconi, F. Irace, M. and Gattinoni, L. (2005). Lactate as a marker of energy failure in critically ill patients: hypothesis. *Critical Care*, **9**: 588-593.

Warburg, O. Posener, K. and Negelein, E, U. (1924). On metabolism of tumors. *Biochemical Magazine*, **152**: 319-344.

Warburg, O. Wind, F, and Negelein, E. (1927). The metabolism of tumors in the body. *The Journal of General Physiology*, **8**: 519-530.

Warburg, O. (1930). The metabolism of tumours. Constable: London.

Warburg, O. (1956). On the origin of cancer cells. *Science*, **123**: 309-314.

Warburg, O. (1965). On respiratory impairment in cancer cells. *Science*, **124**: 269-270.

Wigfield, S, M. Winter, S, C. Giatromanolaki, A. Taylor, J. Koukourakis, ML. and Harris, AL. (2008). PDK-1 regulates lactate production in hypoxia and is associated with poor prognosis in head and neck squamous cancer. *British Journal of Cancer*, **98**: 1975-1984.

Wilcock, P. Allwood, J, W. Correa, E. Vaughan, A, A. Batman, G. Wedge, D, C. Hampson, L. Hampson, I, N. Thakker, N. Goodacre, R. (2012). A metabolomics investigation into the suitability of cobalt chloride as a substitute for hypoxia in eukaryotic cells. *PLoS One*, Submission pending.

4.7 Supplementary Information

$\frac{d([AMP] \cdot V_{Cytoplasm})}{dt}$	= -Rate Law for vADK"(Vfadc_14(vADK), [ATP], [AMP], Kadkatp_14(vADK), Kadkamp_14(vADK), Kadkadv_14(vADK), [ADP], V _{Cytoplasm})
$\frac{d([G6P] \cdot V_{Cytoplasm})}{dt}$	= -V _{Cytoplasm} *Rate Law for vPGI"(Vbpgl_3(vPGI), Kpgl6p_3(vPGI), Kpgf6p_3(vPGI), [G6P], [F6P], V _{Cytoplasm}) +Rate Law for vHK"(VmGLK(vHK), [G6P], SUMAXP(vHK), [P], KeqAK(vHK), KeqGLK(vHK), [Glc], KmGLKATP(vHK), KmGLKGLC(vHK), KmGLKG6P(vHK), KmGLKADP(vHK), V _{Cytoplasm})
$\frac{d([F6P] \cdot V_{Cytoplasm})}{dt}$	= +V _{Cytoplasm} *Rate Law for vPGI"(Vbpgl_3(vPGI), Kpgl6p_3(vPGI), Kpgf6p_3(vPGI), [G6P], [F6P], V _{Cytoplasm}) -Rate Law for vPFK"(Vfprk_4(vPFK), [ATP], [F6P], Kprkatp_4(vPFK), Kprkf6p_4(vPFK), Lo_4(vPFK), en_4(vPFK), [AMP], Kprkmp_4(vPFK), Kprkfatp_4(vPFK), KprkfatT_4(vPFK), Kprkf6pT_4(vPFK), [FDP], KprkfdpT_4(vPFK), [ADP], Kprkadt_4(vPFK), dn_4(vPFK), Kprkfdp_4(vPFK), Kprkadv_4(vPFK), V _{Cytoplasm})
$\frac{d([FDP] \cdot V_{Cytoplasm})}{dt}$	= +Rate Law for vPFK"(Vfprk_4(vPFK), [ATP], [F6P], Kprkatp_4(vPFK), Kprkf6p_4(vPFK), Lo_4(vPFK), en_4(vPFK), [AMP], Kprkmp_4(vPFK), Kprkfatp_4(vPFK), KprkfatT_4(vPFK), Kprkf6pT_4(vPFK), [FDP], KprkfdpT_4(vPFK), [ADP], Kprkadt_4(vPFK), dn_4(vPFK), Kprkfdp_4(vPFK), Kprkadv_4(vPFK), V _{Cytoplasm}) -V _{Cytoplasm} *Rate Law for vALD"(Vfald_5(vALD), [FDP], Kaldfdp_5(vALD), Kaldgap_5(vALD), Kaldhdp_5(vALD), [DHAP], [GAP], V _{Cytoplasm})
$\frac{d([DHAP] \cdot V_{Cytoplasm})}{dt}$	= +V _{Cytoplasm} *Rate Law for vALD"(Vfald_5(vALD), [FDP], Kaldfdp_5(vALD), Kaldgap_5(vALD), Kaldhdp_5(vALD), [DHAP], [GAP], V _{Cytoplasm}) +V _{Cytoplasm} *Rate Law for vTPI"(Vftpl_6(vTPI), [GAP], Ktpgap_6(vTPI), Ktpdhdp_6(vTPI), [DHAP], V _{Cytoplasm})
$\frac{d([GAP] \cdot V_{Cytoplasm})}{dt}$	= +V _{Cytoplasm} *Rate Law for vALD"(Vfald_5(vALD), [FDP], Kaldfdp_5(vALD), Kaldgap_5(vALD), Kaldhdp_5(vALD), [DHAP], [GAP], V _{Cytoplasm}) -V _{Cytoplasm} *Rate Law for vTPI"(Vftpl_6(vTPI), [GAP], Ktpgap_6(vTPI), Ktpdhdp_6(vTPI), [DHAP], V _{Cytoplasm}) -Rate Law for vGAPDH"(Vfgad_7(vGAPDH), [DPG], [NADH], Kgapdhgap_7(vGAPDH), Kgapdhnad_7(vGAPDH), Kgapdhpl_7(vGAPDH), [GAP], [NAD(+)], [P], Kgapdh13dpg_7(vGAPDH), Kgapdhnadh_7(vGAPDH), V _{Cytoplasm})
$\frac{d([DPG] \cdot V_{Cytoplasm})}{dt}$	= +Rate Law for vGAPDH"(Vfgad_7(vGAPDH), [DPG], [NADH], Kgapdhgap_7(vGAPDH), Kgapdhnad_7(vGAPDH), Kgapdhpl_7(vGAPDH), [GAP], [NAD(+)], [P], Kgapdh13dpg_7(vGAPDH), Kgapdhnadh_7(vGAPDH), V _{Cytoplasm}) -Rate Law for vPGK"(Vbpgk_8(vPGK), [ADP], [DPG], Kpgk3pg_8(vPGK), Kpgkatp_8(vPGK), [ATP], [P3G], Kpgkadv_8(vPGK), Kpgk13dpg_8(vPGK), V _{Cytoplasm})
$\frac{d([P3G] \cdot V_{Cytoplasm})}{dt}$	= +Rate Law for vPGK"(Vbpgk_8(vPGK), [ADP], [DPG], Kpgk3pg_8(vPGK), Kpgkatp_8(vPGK), [ATP], [P3G], Kpgkadv_8(vPGK), Kpgk13dpg_8(vPGK), V _{Cytoplasm}) -V _{Cytoplasm} *Rate Law for vPGM"(Vfpgm_9(vPGM), [P3G], Kpgm3pg_9(vPGM), Kpgm2pg_9(vPGM), [P2G], V _{Cytoplasm})
$\frac{d([P2G] \cdot V_{Cytoplasm})}{dt}$	= +V _{Cytoplasm} *Rate Law for vPGM"(Vfpgm_9(vPGM), [P3G], Kpgm3pg_9(vPGM), Kpgm2pg_9(vPGM), [P2G], V _{Cytoplasm}) -V _{Cytoplasm} *Rate Law for vEN"(vfen_10(vEN), [P2G], Ken2pg_10(vEN), Kenpep_10(vEN), [PEP], V _{Cytoplasm})
$\frac{d([PEP] \cdot V_{Cytoplasm})}{dt}$	= +V _{Cytoplasm} *Rate Law for vEN"(vfen_10(vEN), [P2G], Ken2pg_10(vEN), Kenpep_10(vEN), [PEP], V _{Cytoplasm}) -Rate Law for vPK"(Vfprk_11(vPK), [PEP], [ADP], Kpkpep_11(vPK), Kpkadv_11(vPK), Kpkpyr_11(vPK), Kpkatp_11(vPK), [Pyruvate], [ATP], V _{Cytoplasm})
$\frac{d([Cr] \cdot V_{Cytoplasm})}{dt}$	= -Rate Law for vCK"(Vrevck_13(vCK), [ATP], [Cr], Kckiatp_13(vCK), Kckcr_13(vCK), KeqCK_13(vCK), Kckadv_13(vCK), Kckpcr_13(vCK), [ADP], [PCr], Kckpcr_13(vCK), V _{Cytoplasm})
$\frac{d([Glc] \cdot V_{Cytoplasm})}{dt}$	= -Rate Law for vHK"(VmGLK(vHK), [G6P], SUMAXP(vHK), [P], KeqAK(vHK), KeqGLK(vHK), [Glc], KmGLKATP(vHK), KmGLKGLC(vHK), KmGLKG6P(vHK), KmGLKADP(vHK), V _{Cytoplasm}) +Rate Law for vGLUT"(VmGLT(vGLUT), [eGlc], [Glc], KeqGLT(vGLUT), KmGLTGLCo(vGLUT), KmGLTGLC(vGLUT), V _{Cytoplasm})
$\frac{d([Glutamate] \cdot V_{Cytoplasm})}{dt}$	= -Rate Law for vGII"(VmGII(vGII), KmGII(Glutamate(vGII), [Glutamate], [a-KG], KeqGII(vGII), KmGIIakG(vGII), V _{Cytoplasm}) -V _{Cytoplasm} *Rate Law for vGS"(VmVSG(vGS), KmVSG(Glutamine(vGS), [Glutamate], [Glutamine], KeqVSG(vGS), KmVSG(Glutamate(vGS), V _{Cytoplasm})

$$\begin{aligned}
 &= At \cdot [ATP] \\
 \frac{d([ATP] \cdot \%Mitochondria)}{dt} &= -\text{"Rate Law for vPFK"}(vfbfk_4(vPFK), [ATP], [F6P], Kpfkatp_4(vPFK), Kpfkfp_4(vPFK), Lo_4(vPFK), en_4(vPFK), [AMP], Kofkamp_4(vPFK), Kofklatp_4(vPFK), KofklatpT_4(vPFK), KofkfpT_4(vPFK), [FDP], KofkfpdT_4(vPFK), [ADP], KofkadtT_4(vPFK), dn_4(vPFK), Kofkfdp_4(vPFK), Kofkfdp_4(vPFK), \%Cytoplasm) \\
 &\quad + \text{"Rate Law for vPGK"}(vbpk_8(vPGK), [ADP], [DPG], Kpgk3pg_8(vPGK), Kpgkatp_8(vPGK), [ATP], [P3G], Kpgkadp_8(vPGK), Kpgk13dp_8(vPGK), \%Cytoplasm) \\
 &\quad + \text{"Rate Law for vPK"}(vfbk_11(vPK), [PEP], [ADP], Kpkpep_11(vPK), Kpkadp_11(vPK), Kpkpyr_11(vPK), Kpkatp_11(vPK), [Pyruvate], [ATP], \%Cytoplasm) \\
 &\quad - \text{"Rate Law for vCK"}(vrevCK_13(vCK), [ATP], [C], Kcklatp_13(vCK), Kckcr_13(vCK), KeqCK_13(vCK), Kckadp_13(vCK), Kckpcr_13(vCK), [ADP], [PC], Kckpcr_13(vCK), \%Cytoplasm) \\
 &\quad - \text{"Rate Law for vADK"}(vfadk_14(vADK), [ATP], [AMP], Kackatp_14(vADK), Kackamp_14(vADK), Kackadp_14(vADK), [ADP], \%Cytoplasm) \\
 &\quad - \text{"Mitochondria - Rate Law for vATPase"}(K_15(vATPase), [ATP], \%Cytoplasm) \\
 &\quad + \text{"Mitochondria - function_4_v5"}([ATP], At, [a-KG], [NAD(+)], k5(v200)) \\
 &\quad - \text{"Mitochondria - k1(vPDH)} \cdot [Pyruvate] \cdot [ATP] \\
 &\quad + \text{function_4_vATP}(\text{JATP}, \%Mitochondria) \\
 \frac{d([NAD(+)] \cdot \%Mitochondria)}{dt} &= - \text{"Mitochondria - k1(vPDH)} \cdot [Pyruvate] \cdot [NAD(+)] \\
 &\quad - \text{"Rate Law for vGAPDH"}(vfgad_7(vGAPDH), [DPG], [NADH], Kgapdhgap_7(vGAPDH), Kgapdhnad_7(vGAPDH), Kgapdhp_7(vGAPDH), [GAP], [NAD(+)], [P], Kgapdh13dp_7(vGAPDH), Kgapdhnad_7(vGAPDH), \%Cytoplasm) \\
 &\quad + \text{"Rate Law for vLDH"}(vldh_12(vLDH), [Pyruvate], [NADH], Kldhpyr_12(vLDH), Kldhnadh_12(vLDH), Kldhac_12(vLDH), Kldhnad_12(vLDH), [Lac], [NAD(+)], \%Cytoplasm) \\
 &\quad - \text{"Mitochondria - k1(vACO)} \cdot [Citrate] \cdot [NAD(+)] \\
 &\quad - 2 \cdot \text{"Mitochondria - function_4_v5"}([ATP], At, [a-KG], [NAD(+)], k5(v200)) \\
 &\quad + \text{function_4_vresp}(\text{Jresp}, \%Mitochondria) \\
 [NADH] &= Nt - [NAD(+)] \\
 \frac{d([acetyl-CoA] \cdot \%Mitochondria)}{dt} &= + \text{"Mitochondria - k1(vPDH)} \cdot [Pyruvate] \cdot [NAD(+)] \\
 &\quad - \text{"Mitochondria - k1(vCS)} \cdot [OAA] \cdot [acetyl-CoA] \\
 \frac{d([a-KG] \cdot \%Mitochondria)}{dt} &= + \text{"Mitochondria - k1(vACO)} \cdot [Citrate] \cdot [NAD(+)] \\
 &\quad + \text{"Rate Law for vGII"}(vmgII(vGII), KmGII(Glutamate(vGII), [Glutamate], [a-KG], KeqGII(vGII), KmGIIaKG(vGII), \%Cytoplasm) \\
 &\quad - \text{"Mitochondria - function_4_v5"}([ATP], At, [a-KG], [NAD(+)], k5(v200)) \\
 &\quad + \text{"Mitochondria - function_4_v6"}([a-KG], Keq(vCSII), [OAA], k6(vCSII)) \\
 \frac{d([Citrate] \cdot \%Mitochondria)}{dt} &= + \text{"Mitochondria - k1(vCS)} \cdot [OAA] \cdot [acetyl-CoA] \\
 &\quad - \text{"Mitochondria - k1(vACO)} \cdot [Citrate] \cdot [NAD(+)] \\
 \frac{d([OAA] \cdot \%Mitochondria)}{dt} &= - \text{"Mitochondria - k1(vCS)} \cdot [OAA] \cdot [acetyl-CoA] \\
 &\quad + \text{"Mitochondria - function_4_v5"}([ATP], At, [a-KG], [NAD(+)], k5(v200)) \\
 &\quad - \text{"Mitochondria - function_4_v6"}([a-KG], Keq(vCSII), [OAA], k6(vCSII)) \\
 &\quad + \text{"Mitochondria - k1(vPDH)} \cdot [Pyruvate] \cdot [ATP] \\
 &\quad - \text{"Mitochondria - k1(vOAA_deg)} \cdot [OAA] \\
 \frac{d([Pyruvate] \cdot \%Mitochondria)}{dt} &= - \text{"Mitochondria - k1(vPDH)} \cdot [Pyruvate] \cdot [NAD(+)] \\
 &\quad + \text{"Rate Law for vPK"}(vfbk_11(vPK), [PEP], [ADP], Kpkpep_11(vPK), Kpkadp_11(vPK), Kpkpyr_11(vPK), Kpkatp_11(vPK), [Pyruvate], [ATP], \%Cytoplasm) \\
 &\quad - \text{"Rate Law for vLDH"}(vldh_12(vLDH), [Pyruvate], [NADH], Kldhpyr_12(vLDH), Kldhnadh_12(vLDH), Kldhac_12(vLDH), Kldhnad_12(vLDH), [Lac], [NAD(+)], \%Cytoplasm) \\
 &\quad - \text{"Mitochondria - k1(vPDH)} \cdot [Pyruvate] \cdot [ATP] \\
 \frac{d\Delta\text{Psi}}{dt} &= \frac{10 \cdot \text{Jresp} - 3 \cdot \text{JATP} - \text{Jleak} - \text{JANT}}{C} \\
 \text{ATPcrit} &= \frac{At}{-3 \cdot \Delta\text{PsiGransport}} \\
 &= \frac{1 + e^{\frac{\text{"gas constant"} \cdot \text{"absolute temperature"}}{Kapp \cdot [P]}}}{-3 \cdot \Delta\text{PsiGransport}} \\
 \Delta\text{PsiGransport} &= 1.2 \cdot \text{"Faraday constant"} \cdot \Delta\text{Psi} \\
 \text{JANT} &= \text{KANT} \cdot [\text{ATP}] \\
 \text{JATP} &= \text{kATP} \cdot \left(\frac{2}{1 + e^{\frac{\text{"gas constant"} \cdot \text{"absolute temperature"}}{Kapp \cdot [P]}}} - 1 \right) \\
 \text{Jleak} &= \text{Kleak} \cdot \Delta\text{Psi} \\
 \text{Jresp} &= \frac{\text{Kresp} \cdot Nt - [NAD(+)]}{K + Nt - [NAD(+)]} \\
 &= \frac{1}{1 + e^{\frac{\text{"gas constant"} \cdot \text{"absolute temperature"}}{Kapp \cdot [P]}}} \cdot (\Delta\text{Psi} - \Delta\text{Psiim})
 \end{aligned}$$

Additional rate laws of the model

v_{VS}

$$(i) \quad \frac{\frac{V_{mVS}}{K_{mVS\text{Glutamine}}} \cdot \left(\text{Glutamine} - \frac{\text{Glutamate}}{K_{eqVS}} \right)}{1 + \frac{\text{Glutamine}}{K_{mVS\text{Glutamine}}} + \frac{\text{Glutamate}}{K_{mVS\text{Glutamate}}}}$$

Where: $V_{mVS} = V_{\max}$ of VS; $K_{mVS\text{Glutamine}} = K_m$ of glutamine for VS; Glutamine=initial glutamine concentration; Glutamate=initial glutamate concentration; K_{eqVS} =equilibrium constant of VS; $K_{mVS\text{Glutamate}} = K_m$ of glutamate for VS.

v_{GII}

$$(ii) \quad \frac{\frac{V_{mGII}}{K_{mGII\text{Glutamate}}} \cdot \left(\text{Glutamate} - \frac{aKG}{K_{eqGII}} \right)}{1 + \frac{\text{Glutamate}}{K_{mGII\text{Glutamate}}} + \frac{aKG}{K_{mGIIaKG}}}$$

Where: $V_{mGII} = V_{\max}$ of GII; $K_{mGII\text{Glutamate}} = K_m$ of glutamate for GII; Glutamate=initial glutamate concentration; aKG=initial α -KG concentration; K_{eqGII} =equilibrium constant of GII; $K_{mGIIaKG} = K_m$ of α -KG for GII.

Chapter 5:

General Discussion and

Conclusions

5.1 General Discussion

Cancer is a disorder characterised by uncontrollable growth of abnormal cells and comprises of more than 200 forms. The onset and development of cancer is attributed to a large set of genetic and environmental factors resulting in a complex disease (Johnson and Todd, 2000; Kato *et al.*, 2006). For this reason, cancer may be difficult to diagnose and treat and therefore a deep understanding of the interacting factors is needed. One notoriously difficult form of the cancer is OSCC which is becoming increasingly common and has a poor 5 year survival rate.

The role of the gene PDE4D and the inclusion of hypoxia were investigated on the issue of OSCC. Regardless of the research and funds invested into this disease over the past three decades, the five year survival rate has remained constant at approximately 50% (Park *et al.*, 2009). Due to its complex nature, OSCC involves many genomic and environmental factors (Bookman *et al.*, 2011) and recent reports suggest that PDE4D may be inclusive in OSCC (Fushimia *et al.*, 2008) and other HNSCC (Jarvinen *et al.*, 2008; Nancarrow *et al.*, 2008). Although, the exact role of PDE4D appears to be context specific (i.e., has varying roles depending on the cell type), there is conflicting evidence suggesting PDE4D to be a TSG and an oncogene. The former role has been described in OTSCC/LSCC (Jarvinen *et al.*, 2008), EAC (Nancarrow *et al.*, 2008; Gu *et al.*, 2010), lung adenocarcinoma (Weir *et al.*, 2007) and ESCC (Wu *et al.*, 2011); whereas the latter has been expressed in lung cancer (Marko *et al.*, 2000; Pullamsetti *et al.*, 2012), hepatocellular carcinoma (Weber, 2002), prostate cancer (Rahrmann *et al.*, 2009) and the HNSCC adenoid cystic carcinoma (Patel *et al.*, 2006).

Prior to this study, the exact functionality and advantages of PDE4D functioning in OSCC was unknown. One known function of PDE4D in all cells is the downstream regulation of the TF CREB via cAMP and PKA (Abramovitch *et al.*,

2004; Suzuki *et al.*, 2009b). Potentially, CREB has the ability to function in the presence and/or absence of other TF such as HIF-1. HIF-1 is regulated through oxygen concentrations within cells which obviously has major implications in cellular oncology as discussed previously.

Additionally, in tangent with the hypoxia work, it is commonly accepted that CoCl_2 has the ability to mimic hypoxic conditions under a normoxic environment (An *et al.*, 1998; Guo *et al.*, 2006). It is a regular feature for investigators to adopt this approach when studying cells and hypoxia; however, the supplementary off-target effects which may be brought about by the CoCl_2 are commonly overlooked. It is imperative to take note of these effects when analysing such data, as CoCl_2 is a potent substance, even at relatively low concentrations (μM).

In relation to the varying oxygen aspect of the project, a hypoxic mathematical model is useful when investigating the metabolic behaviour of cells under normoxic and hypoxic conditions. Such models may enlighten on the behaviour under the various conditions and highlight potential therapeutic targets, biomarkers and provide insight into the rate limitation of the model (Hornberg *et al.*, 2006).

Hence, there were three main aspects to the project:

- investigate the efficiency of CoCl_2 as a hypoxic mimic and address, if any, off-target effects which are brought about by this substance which are not associated with the hypoxic response (chapter 2)
- explore the role of PDE4D (and complementary effects of hypoxia) on OSCC, specifically focussing on central metabolism and phenotypic alterations of the cells (chapter 3)
- the construction of a metabolic, mathematical model of hypoxia and normoxia, with model optimisation, validation and analysis using its predictive capabilities (chapter 4)

First and foremost, it was determined that CoCl_2 was able to function as a hypoxic mimic in the human Keratinocyte cell line hTERT in terms of central metabolism. However, the CoCl_2 concentration of $100\mu\text{M}$ was not sufficient to induce a hypoxic response in central metabolism to the same levels to those observed in the metabolome of cells cultured in 1% oxygen concentrations. In addition, off-target effects were observed in secondary metabolism including that of lipid and fatty acid alterations. The overall outcome of this study was to avoid the use of CoCl_2 wherever possible and if this simulation is necessary, then extra care should be adopted when analysing the data.

Subsequently, the role of PDE4D in OSCC was assessed in terms of central metabolism and phenotypic behaviour. In accordance with Fushimia *et al.*, (2008), Jarvinen and co-workers (2008) and Nancarrow and colleagues (2008), PDE4D was found to function as a TSG in the OSCC cell line BicR16. A KD in PDE4D expression resulted in an elevation in proliferation and migration compared to the WT/ control samples. The GC-MS analysis of the metabolome clearly distinguished between the groups predominantly as a consequence of the increase in amino acid and cholesterol synthesis in the KD cells and a

reduction in fatty acid production in the WT/control samples. Hence, central metabolism was consistently altered in the mono and poly KD cells.

The combined effects of the PDE4D KD and hypoxia was then analysed to assess, if any, emergent properties which have arisen from the co-activation of CREB and HIF-1. Although CoCl_2 was able to mimic hypoxia in terms of central metabolism; the off-target effects in secondary metabolism established that a genuine hypoxic environment should be used. The individual and combined effects of CREB (PDE4D KD) and HIF-1 (hypoxia) caused metabolic reconfigurations in terms of central metabolism. It was also clear that CREB was able to function independently of HIF-1; however, interaction between the two TFs was evident in the data.

Table 5.1 Summary of central metabolite alterations subsequent to PDE4D KD, hypoxia exposure, combined KD and hypoxia exposure and CoCl₂ exposure. The arrows signify an increase (↑) or decrease (↓) in concentration from the non-treated condition and a blank represents no significant change in the metabolite/metabolite not detected or identified. The KD and hypoxia column displays two arrows, the first of which depicts the influence of the KD and the second the effect if hypoxia. Where 'H' and 'N' are highlighted here indicates where behaviour was varied between hypoxia (H) and normoxia.

Metabolite	PDE4D KD	Hypoxia	KD and Hypoxia	CoCl ₂
Acetic Acid		↑		
Alanine	↑			
Arginine/Citrulline		↑		
Aspartic Acid	↑	↓		↓
Bishydroxybutanoic Acid			↑ and ↑	
Butanoic Acid	↑			
Cholesterol	↑	↓		↓
Citric Acid	↑	↓		↓
Creatinine		↑		
Cuminaldehyde/Adenine		↑		
Cysteine	↑			↓
Fructose		↑		
Fumaric Acid/Maleic Acid		↑		
Glutamic Acid/Glutamine	↑	↓	↓ and ↑	↓
Glycerolaldehyde		↓		
Glycerol		↓	↓ and ↑	
Glycerol-3-phosphate	↑			
Glycine	↑			

Metabolite	PDE4D KD	Hypoxia	KD and Hypoxia	CoCl ₂
Myo-inositol	↓	↓		↓
Myristic Acid		↑		
N-acetylneuraminic Acid		↑		
Normetanephrine				↓
Octadecanoic/Stearic Acid		↑		
Oleic Acid/Elaidic Acid	↓	↓		
Phenylalanine	↑	↓		
Phosphate	↑	↓		↓
Phosphocreatinine		↓		↓
Proline			↑ and ↑	
Propanedioic (Malonic) Acid			↓ and ↑	
Pyridoxine/Pyridoxal			↓ and ↑	
Pyroglutamic Acid	↑	↑		↑
Pyruvic Acid			↑(H), ↓(N) and ↑	
Ribitol		↑		
Scyllo-inositol/Myo-inositol			↑(N), ↓(H) and ↑	
Serine	↑	↓		
Sorbose		↑		

Hexonic Acid		↑		
Hexadecanoic (Palmitic) Acid		↑		
Hypotaurine	↑			
Isoleucine	↑	↑		
Lactic Acid	↑	↓		↓
Leucine	↑	↑		
Malic Acid	↑	↓		
Mannitol/Sorbitol/Dulcitol		↑		
Manose/Allose/Glucose/Gallatose		↑		
Mannose/Glucose/Galactose		↓		
Methionine	↑	↓		
Methylovaleric Acid		↑		

Succinic Acid		↑		
Tagatose/Fructose/Sorbose			↑(H), ↓(N) and ↑	
Threitol		↑		↑
Threonic Acid		↑		
Threonine	↑	↑		
Tyramine		↑		↓
Tyrosine	↑	↓		↓
Urea			↑ and ↑	
Ureidopropionic Acid	↑			
Valine	↑	↓		
Xylose		↑		

Table 5.1 summarises the central metabolic changes seen under the various conditions including the combined effects of the KD and hypoxia. Although a number of the blanks in the table are a result of no significant changes in the metabolite concentration, many are due to the metabolite not been detected or identified. This will be improved upon in the future through enhanced targeted GC-MS/LC-MS methods.

Finally, the mathematical models were constructed for hypoxic and normoxic environments in order to compare and contrast to aid in further understanding. The model was in-part produced using data obtained from the original CoCl_2 mimicking experiment. This lead to an inaccurate hypoxic model as validation determined that glycolysis was not upregulated in hypoxia as expected. This is partially due to lack of experimental data which was fed into the model. In addition, hypoxic characteristics are more prominent in cancer cells and non-malignant cells were utilised here. Therefore, the collection of cancerous hypoxic experimental data would be advantageous.

This project has made a significant contribution to the scientific community in terms of PDE4D, HIF-1, CoCl_2 ability to mimic hypoxia and a hypoxic mathematical model. However, without time constraints, improvements and developments could be made in many of these areas.

In terms of the CoCl_2 and hypoxia work, although important findings were made, experimental design may have been improved. Firstly, the 8h time point appears to behave in a peculiar fashion which is diverse from the remaining time points. This is the result of either a significant biological process which is occurring at this time or a potential anomaly time point. Due to the experimental design, the three conditions at each specific time point (i.e. 8h) were cultured and harvested simultaneously. This was due to experimental constraints (e.g. lack of incubator space) and the impractical task of harvesting 96 flasks consecutively. To investigate the origin of the misbehaving 8h time point, this experiment could be repeated in full to assess if the same results are obtained

once more, although this would be an extremely lengthy duplication. Alternatively, the 8h time point only could be repeated, however, due to variations in medium, FBS, the number of culture passages etc, this may give rise to further issues, and so the former suggestion would be more effective. Perhaps a compromise would be to re-run 0h, 4h, 8h and 12h.

In addition, it was obvious that the 100 μ M CoCl₂ does not induce the same hypoxic response as 1% oxygen levels at the associated time points. This CoCl₂ concentration was derived from the literature through assessing a range of articles and, slightly over-cautiously, arriving at a value which was deemed appropriate. It is now evident however, that this value would have been more efficient if elevated, but it would be vital not to jeopardise the health of the cells under investigation. To determine the value of CoCl₂ which should have been adopted, varying concentrations of CoCl₂ should have been used and various analyses undertaken. Firstly, growth curves of the cells to ensure that the cells are in as good health as possible. In conjunction with this, a Western blot/ELISA should be used to assess the levels of HIF-1 α which can then be compared to 1% oxygen under the same exposure time. That said, even at low concentrations of CoCl₂, many undesired off-target effects were seen.

Further improvement is possible through the development of GC-MS/LC-MS methods. Although this is time consuming and expensive, it is worth developing such techniques in terms of data processing and expanding the associated libraries to improve metabolite ID and confidence. This will strengthen the biological aspects and provide more metabolic information of the studies. It would also be useful to improve mass accuracy, sensitivity and dynamic range of the instruments which will be possible in the foreseeable future.

The investigation on PDE4D revealed some important findings in terms of central metabolism and phenotypic behaviour in the OSCC cell line BicR16. However, the role of PDE4D requires further exploration which can be

approached via various means. One such study is currently underway as we are utilising an expression microarray to assess variations in WT/controls and PDE4D KDs. The CRE region is found in approximately 4000 genes which are ultimately affected by the expression of PDE4D (Suzuki *et al.*, 2009). Hence, it is likely that the transcription expression will vary significantly between the conditions and may provide further information as to what this gene controls and its significance (as a TSG or oncogene) in cancer.

Another possibility is to assess the effects of PDE4D on secondary metabolism using LC-MS. This will highlight changes in lipids, fatty acids, amino acids, nucleotides, vitamins, polyols and carbohydrates and may provide further insight into the role of PDE4D in OSCC.

In related terms, further analyses could be performed on the GC-MS data obtained for the PDE4D KD to attain greater confidence in the data analysis. This ensures that similar outcomes result from the varying algorithms and techniques. Potential methods include clustergrams, heat maps of metabolites, partial least squares (PLS) and canonical correlation analysis (CCA). Moreover, as discussed above, an improvement in GC-MS and LC-MS methods would also advance data sets such as these.

Knockdown of PDE4D was relatively efficient, with the most efficient knockdown by 76% of WT/control as assessed by qPCR. What this information fails to notify us is which isoforms of PDE4D have been affected the greatest, as specific isoforms are known to behave differently within the cell. To gauge the knockdown on specific isoforms, qPCR could be adopted using isoform specific primers/probes or alternatively, the use of the expression microarray could be used which has the capacity of analysing isoform specific alterations.

Mathematical models can always be improved in one respect or another and this hypoxia model is no exception. First, although all the parameters originate

from *Homo sapiens*, the tissue types range which is likely to have an overall effect on the model. Ideally, all parameters should derive from the same species and the equivalent cell type; however, more often than not this is not possible. Second, the production of the hypoxic mathematical model was a revision of the normoxic model through alterations in steady state concentrations. This was based on the data I obtained in the hypoxia and CoCl_2 . However, since all metabolites were not detected/confidently identified in GC-MS and/or LC-MS, the model was based on just eight new steady state concentrations. Although this functioned effectively, a more accurate model could be produced if more hypoxia steady state values were obtained. Since these values are absent from the literature, the most effective means would be to advance the GC-MS and LC-MS platforms and use a less systems based approach for those metabolites which are unattainable from these platforms.

Furthermore, enzyme kinetics data is vital in the production of mathematical models. Parameters which arise from such experiments vary dramatically from species to species and even tissue to tissue. It can also be time-consuming in acquiring enzyme kinetics information which results in a lack of data in the literature which can be used for modelling. Therefore, when constructing models, it is common practice to utilise parameters originating from other tissues and even varying species. This causes further inaccuracies which was the case in these models.

Additionally, once the hypoxia model was maximally optimised, incorporation of the PDE4D system may be an option to aid in the understanding of the complementary effects of PDE4D and hypoxia. However, this model would be significantly more complex than the original model since there would be four separate states and the incorporation of further metabolites would be advantageous.

5.2 Concluding Remarks

PDE4D operates as a TSG in the OSCC cell line BicR16, which may be potentially enhanced when coupled with the hypoxic response. This was investigated using a genuine hypoxic environment, rather than using a hypoxic mimic such as CoCl_2 as profound off-target effects were observed under CoCl_2 exposure, which are unrelated to the hypoxic response. The genuine hypoxic response was emulated through the production of a mathematical model which was able to predict metabolic behaviour qualitatively and can be used in future for its predictive capabilities.

5.3 References

Abramovitch, R. Tavor, E. Jacob-Hirsch, J. Zeira, E. Amariglio, N. Pappo, O. Rechavi, G. Galun, E. and Honigman, A. (2004). A Pivotal Role of Cyclic AMP-Responsive Element Binding Protein in Tumor Progression. *Cancer Research*, **64**: 1338-1346.

An, W, G. Kanekal, M. Simon, M, C. Maltepe, E. Blagosklonny, M, V. and Meckers, L, M. (1998). Stabilization of wild-type p53 by hypoxia-inducible factor 1alpha. *Nature*, **392**: 405-408.

Bookman, E, B. McAllister, K. Gillanders, E. Wanke, K. Balshaw, D. Rutter, J. Reedy, J. Shaughnessy, D. Agurs-Collins, T. Paltoo, D. Atienza, A. Bierut, L. Kraft, P. Fallin, M, D. Perera, F. Turkheimer, E. Boardman, J. Marazita, M, L. Rappaport, S, M. Boerwinkle, E. Suomi, S, J. Caporaso, N, E. Hertz-Picciotto, I. Jacobson, K, C. Lowe, W, L. Goldman, L, R. Duggal, P. Gunnar, M, R. Manolio, T, A. Green, E, D. Olster, D, H. and Birnbaum, L, S. for the NIH G x E (2011). Gene-Environment Interplay in Common Complex Diseases: Forging an Integrative Model - Recommendations From an NIH Workshop. *Genetic Epidemiology*, **35**: 217-225.

Fushimia, K. Uzawaa, K. Ishigamia, T. Yamamotof, N. Kawatab, T. Shibaharaf, T. Itob, H. Mizoe, J. Tsujie, H. Tanzawaa, H. (2008). Susceptible genes and molecular pathways related to heavy ion irradiation in oral squamous cell carcinoma cells. *Radiotherapy and Oncology*, **89**: 237-244.

Gu, J. Ajani, J, A. Hawk, E, T. Ye, Y. Lee, J, H. Bhutani, M, S. Hofstetter, W, L. Swisher, S, G. Wang, K, K. and Wu, X. (2010). Genome-Wide Catalogue of Chromosomal Aberrations in Barrett's Esophagus and Esophageal Adenocarcinoma: A High-Density Single Nucleotide Polymorphism Array Analysis. *Cancer Prevention Research*, **3**: 1176-1186.

Guo, M. Song, LP. Jiang, Y. Liu, W. Yu, Y. and Chen, GQ. (2006). Hypoxia-mimetic agents desferrioxamine and cobalt chloride induce leukemic cell apoptosis through different hypoxia-inducible factor-1 α independent mechanisms. *Apoptosis*. **11**: 67-77.

Hornberg, J, J. Bruggemana, F, J. Westerhoff, H, V. and Lankelma, J. (2006). Cancer: A Systems Biology disease. *BioSystems*, **83**: 81-90.

Jarvinen, AK. Autio, R. Kilpinen, S. Saarela, M. Leivo, I. Grenman, R. Makitie, A, A. and Monni, O. (2008). High-Resolution Copy Number and Gene Expression Microarray Analyses of Head and Neck Squamous Cell Carcinoma Cell Lines of Tongue and Larynx. *Genes, Chromosomes & Cancer*, **47**: 500-509.

Johnson, G, C, L. and Todd, J, A. (2000). Strategies in complex disease mapping. *Current Opinion in Genetics & Development*, **10**: 330-334.

Kato, K. Hara, A. Kuno, T. Mori, H. Yamashita, T. Toida, M. and Shibata, T. (2006). Aberrant promoter hypermethylation of p16 and MGMT genes in oral squamous cell carcinomas and the surrounding normal mucosa. *Journal of Cancer Research and Clinical Oncology*, **132**: 735-743.

Marko, D. Pahlke, G. Merz, KH, and Eisenbrand, G. (2000). Cyclic 3', 5'-Nucleotide Phosphodiesterases: Potential Targets for Anticancer Therapy. *Chemical Research in Toxicology*, **13**: 944-948.

Nancarrow, D, J. Handoko, H, Y. Smithers, M. Gotley, D, C. Drew, P, A. Watson, D, I. Clouston, A, D. Hayward, N, K. and Whiteman, D, C. (2008). Genome-Wide Copy Number Analysis in Esophageal Adenocarcinoma Using High-Density Single-Nucleotide. *Cancer Research*, **68**: 4163-4172.

Park, N, J. Zhou, H. Elashoff, D. Henson, B, S. Kastratovic, D, A. Abemayor, E. and Wong, D, T. (2009). Salivary microRNA: Discovery, Characterization, and Clinical Utility for Oral Cancer Detection. *Clinical Cancer Research*, **15**: 5473-5477.

Patel, K, J. Pambuccian, S, E. Ondrey, F, G. Adams, G, L. and Gaffney, P, M. (2006). Genes associated with early development, apoptosis and cell cycle regulation define a gene expression profile of adenoid cystic carcinoma. *Oral Oncology*, **42**: 994-1004.

Pullamsetti, SS. Banat, GA. Schmall, A. Szibor, M. Pomagruk, D.Hänze, J. Kolosionek,E. Wilhelm, J. Braun, T. Grimminger, F. Seeger, W. Schermuly, RT. and Savai, R. (2012). Phosphodiesterase-4 promotes proliferation and angiogenesis of lung cancer by crosstalk with HIF. *Oncogene*, **1-14**: 10.1038/onc.2012.136

Rahrmann, E, P. Collier, L, S. Knutson, T, P. Doyal, M, E. Kuslak, S, L. Green, L, E. Malinowski, R, L. Roethe, L. Akagi, K. Waknitz, M. Huang, W. Largaespada, D, A. and Marker, P, C. (2009). Identification of PDE4D as a Proliferation Promoting Factor in Prostate Cancer Using a Sleeping Beauty Transposon-Based Somatic Mutagenesis Screen. *Cancer Research*, **69**: 4388-4397.

Suzuki, M. Shinohara, F. Endo, M. Sugazaki, M. Echigo, S. and Rikiishi, H. (2009). Zebularine suppresses the apoptotic potential of 5-Xuorouracil via cAMP/PKA/CREB pathway against human oral squamous cell carcinoma cells. *Cancer Chemotherapy Pharmacology*, (2009b), **64**: 223-232.

Weir, B, A. Woo, M, S. Getz G, Perner, S. Ding, L. Beroukhim, R. Lin, W, M. Province, M, A. Kraja, A. Johnson, L, A. Shah, K. Sato, M. Thomas, R, K. Barletta, J, A. Borecki, I, B. Broderick, S, B. Chang, A, C. Chiang, D, Y. Chirieac, L, R. Cho, J. Fujii, Y. Gazdar, A, F. Giordano, T. Greulich, H. Hanna, M. Johnson, B, E. Kris, M, G. Lash, A. Lin, L. Lindeman, N. Mardis, E, R. McPherson, J, D. Minna, J, D. Morgan, M, B. Nadel, M. Orringer, M, B. Osborne, J, R. Ozenberger, B. Ramos, A, H. Robinson, J. Roth, J, A. Rusch, V. Sasaki, H. Shepherd, F. Sougnez, C. Spitz, M, R. Tsao, MS. Twomey, D. Verhaak, R, G, W. Weinstock, G, M. Wheeler, D, A. Winckler, W. Yoshizawa, A. Yu, S. Zakowski, M, F. Zhang, Q. Beer, D, G. Wistuba, I, I. Watson, M, A. Garraway¹, L, A. Ladanyi, M. Travis, W, D. Pao, W. Rubin, M, A. Gabriel, S, B. Gibbs, R, A. Varmus, H, A. Wilson, R, K. Lander, E, S. and Meyerson, M. (2007). Characterizing the cancer genome in lung adenocarcinoma. *Nature*, **450**: 893-898.

Weber, G. (2002). Reciprocal regulation: recognition of pattern of gene expression in cancer cells. *Advanced Enzyme Regulation*, **42**: 83-100.

Wu, C. Hu, Z. He, Z. Jia, W. Wang, F. Zhou, Y. Liu, Z. Zhan, O. Liu, Y. Yu, D. Zhai, K. Chang, J. Qiao, Y. Jin, G. Liu, Z. Shen, Y. Guo, C. Fu, J. Miao, X. Tan, W. Shen, H. Ke, Y. Zeng, Y. Wu, T. and Lin, D. (2011). Genome-wide association study identifies three new susceptibility loci for esophageal squamous-cell carcinoma in Chinese populations. *Nature Genetics*, **43**: 679-684.